To the Graduate Council:

I am submitting herewith a thesis written by David Michael Carden entitled "Light Attenuation and Transparency in Eutrophic Boone Reservoir." I have examined the final copy of this thesis for form and content and recommend that it be accepted in partial fulfillment of the requirements for the degree of Master of Science, with a major in Environmental Engineering.

R. Bruce Robinson,
Major Professor

We have read this thesis
and recommend its acceptance:

Accepted for the Council:

Vice Provost
and Dean of The Graduate School

STATEMENT OF PERMISSION TO USE

In presenting this thesis in partial fulfillment of the requirements for a Master's degree at The University of Tennessee, Knoxville, I agree that the Library shall make it available to borrowers under rules of the Library. Brief quotations from this thesis are allowable without special permission, provided that accurate acknowledgment of the source is made.

Permission for extensive quotation from or reproduction of this thesis may be granted by my major professor, or in his absence, by the Head of the Interlibrary Services when, in the opinion of either, the proposed use of the material is for scholarly purposes. Any copying or use of the material in this thesis for financial gain shall not be allowed without my written permission.

Signature David M. Carden

Date March 5, 1986

LIGHT ATTENUATION AND TRANSPARENCY IN EUTROPHIC BOONE RESERVOIR

A Thesis

Presented for the

Master of Engineering

Degree

The University of Tennessee, Knoxville

David Michael Carden

March 1986

ACKNOWLEDGMENTS

I hereby gratefully acknowledge the assistance of my major professor, Dr. R. Bruce Robinson, whose encouragement, criticism, and consultation were invaluable in the preparation of this thesis. Acknowledgments are also given to Dr. Greg D. Reed and Dr. Bruce A. Tschantz whose review and comment were particularly beneficial. I also acknowledge the encouragement and consultation by Dr. Russ Brown of Tennessee Technological University whose experience in light attenuation and algal modeling was very helpful.

ABSTRACT

An evaluation is presented of the factors controlling light attention and algal production in Boone Reservoir, a eutrophic reservoir located in upper east Tennessee. The study upon which this evaluation is based was conducted by TVA during the spring and summer of 1984. The basic equation for the attenuation of light underwater is the Beer-Lambert equation which expresses light attenuation as an exponential decay function:

$$\frac{I_z}{I_o} = e^{-K_d z}$$

where I_z = irradiance at depth z (energy/m^2/s)

I_o = irradiance just below water surface (energy/m^2/s)

K_d = total light attenuation coefficient for vertical downward irradiance (1/m)

z = depth (m)

To determine the influence of variance light attenuating substances (algae, sediment, dissolved color, etc.) on the transparency of Boone Reservoir, the coefficient K_d can be partitioned in terms of the light attenuating substances present. Two approaches are used to partition K_d values. The first involves linear regression of K_d and measured concentrations of chlorophyll a and algal

cell populations. The second approach utilizes relationships which express apparent optical properties (e.g. K_d) as functions of the inherent scattering and absorption coefficients (a and b, respectively). Regression of values of a and b against corresponding concentrations of light attenuating substances will permit an evaluation of the fractional contribution of each substance to a and b and hence to K_d. Statistical evaluation of each partitioning method showed that the first method (direct linear regression of K_d versus chlorophyll a) provided the best results for Boone Reservoir.

The value of partitioning the coefficient K_d is that it allows a determination of which substances control the transparency of a reservoir. This will provide guidance to reservoir management strategies directed at improving the aesthetic quality of a reservoir. By partitioning the light attenuation coefficients obtained on Boone Reservoir it was shown that algae are a major factor controlling the transparency of the reservoir with the fractional light attenuation by algae generally greater than 50 percent.

The quantification of the light attenuation by algae may also be useful as an input parameter in methematical models of algal production. Plans are currently under consideration to implement tertiary nutrient removal for

the municipal wastewater dischargers to Boone Reservoir as a means of reducing the eutrophic state and excessive algal growth problems. The application of algal models should provide a cost effective means of evaluating the benefits derived from reservoir management strategies such as tertiary nutrient removal before funds are invested in implementation of such strategies.

Due to the significant role of algae in light transparency reductions in Boone Reservoir and other algal related water quality problems, an evaluation was also conducted of the photosynthetic response of the reservoir algal population to light. This was done primarily in an attempt to provide the light response variables (e.g. light-saturated production rate and the irradiance at which the photosynthetic rate is maximum) for use in algal production modeling. Limited success was achieved, however, in defining these variables due to inconsistencies in field measurements of algal production. These inconsistencies may have been due to the use of depth integrated samples in measurements of algal production.

TABLE OF CONTENTS

LIST OF TABLES

TABLE PAGE

TABLE PAGE

LIST OF FIGURES

CHAPTER 1

INTRODUCTION

1.1 Thesis

The evaluation of sunlight attenuation in water and the attendent effects upon transparency and phytoplankton productivity is of major importance in the management and protection of water quality in lakes and reservoirs. Currently many lakes and reservoirs are suffering from beneficial use impairments due to the detrimental effects of cultural eutrophication caused by nutrient enrichment by manmade processes. These detrimental effects are often manifested by excessive phytoplankton (i.e. algae) blooms and severe transparency reductions. Excessive algal growth can adversely affect water quality through increases in organic loadings to the metalimmion and hypolimmion caused by death and settling of algal cells. This may result in dissolved oxygen reduction by aerobic bacterial activity in the middle and lower depths which in turn can affect the assimilation capacity of the reservoir, the habitats of aquatic biota, and the quality of reservoir releases. Other algal associated problems include taste and odor problems for water supplies, interference with industrial uses of the affected water, reductions in water transparency, and impairment of recreational benefits.

Because of the severity of the problems associated with cultural eutrophication, environmental engineers are often charged with the task of development of mitigative solutions such as nonpoint source nutrient controls for agricultural areas or advanced wastewater treatment for point source discharges. These solutions are usually, however, very costly and the public sector will require convincing proof of the benefits of such alternatives before providing funds for their implementation.

Mathematical models provide a logical and cost effective means of assessing the benefits of nutrient control strategies. Since algal population reduction is many times aimed at improving the aesthetic quality of reservoir transparency, accurate models of light attenuation with depth and the fractional contribution of various attenuating substances (e.g. algae, dissolved color, turbidity, etc.) are essential. By establishing the fractional contributions of each major light absorbing or scattering substance, the effects of a reduction in any one of these substances can be predicted. It is possible that significant reductions in algal populations will not result in large improvements in reservoir transparency because of a dominant attenuation effect by some other substance such as dissolved color or inanimate suspended solids. In these cases, the use of

light attenuation modeling would predict such attenuation relationships and the use of advanced wastewater treatment might no longer be considered as a cost effective alternative.

The effects of reservoir management strategies (e.g. nutrient control) on the reduction in algal populations may be predicted through the use of algal growth models. Since light is a necessary requirement for the photosynthetic growth of algae, algal models must account for the amount of light absorbed by algal cells and the efficiency with which light is converted to photosynthetic products.

In this thesis various mathematical models will be used to evaluate the factors affecting light with depth in Boone Reservoir, a eutropic reservoir operated by the Tennessee Valley Authority. The response of algal growth to light will also be investigated. Boone Reservoir is currently suffering from high transparency reduction and water quality impairments related to excessive algal growth. Such an evaluation should serve a useful purpose as public and regulatory pressure is currently being placed upon municipal dischargers to the reservoir to install tertiary wastewater treatment in an attempt to reduce algal populations.

Light attenuation and algal response formulations alone will not provide a complete answer to the question of whether or not tertiary wastewater treatment will be effective in improving the transparency and reducing algal population in Boone Reservoir. They will, however, provide necessary components for more detailed reservior computer models which should be able to answer this question. These computer models generally include many sub-models including hydrodynamic formulations, nutrient and organic fluxes, biochemical oxygen demands, as well as light attenuation and algal response models. Many reservoir computer models have often, for lack of better information, made oversimplified assumptions in obtaining the light attenuation and algal response coefficients which are used in the models or have relied upon values obtained in the literature. The determination of these model coefficients by the fitting of models to actual field data however provides a far superior technique. In this thesis, available field data will be used to determine the model coefficients which best describe the light attenuation and algal response characteristics in Boone Reservoir. Once determined, these coefficients may be used in detailed computer models to provide results which can be viewed with more confidence.

1.2 Scope

To achieve the objectives of this thesis a three phase process will be used. First a detailed literature review will be presented which discusses factors affecting light attenuation and transparency in water; mathematical models for simulating light penetration and evaluating light extinction coefficients; and the influences of light conditions on phytoplankton productivity. Second, using information obtained from the literature review, relationships defining the attenuation of solar radiation with depth will be developed using light measurements made on Boone Reservoir during 1984. The light extinction coefficients which are derived will then be partitioned into various attenuation components including background attenuation by water, scattering and absorption by algae and their degradation products, and scattering and absorption by nonbiological particulates and the dissolved compounds in water. Finally, the applicability of various light-productivity models in simulating measured algal photosynthetic rates in Boone Reservoir will be investigated using the light attenuation coefficients calculated for algae and mathematical models obtained from the literature review.

1.3 Background

Boone Reservoir is formed by Boone Dam which is located on the South Fork Holston River in Sullivan County of upper East Tennessee. The Tennessee Valley Authority (TVA) operates the reservoir primarily for the purpose of flood control, hydroelectric power generation, and recreation. The reservoir consists of two distinct arms, one formed by impoundment of the South Fork Holston River and the other by impoundment of the Watauga River. The reservoir extends approximately 17.4 miles on the South Fork Holston River and 15.3 miles on the Watauga River for a total length of 32.7 miles. The maximum depth of the reservoir is 120 feet at normal summer pool and 96 feet at normal winter pool. Mean depth of the reservoir is 44 feet at normal summer pool and 39 feet at normal winter pool. The total storage volume of the reservoir is 193,500 acre-feet.

Water quality in Boone Reservoir is affected by nutrient and organic loadings from both point and non-point sources. Point source loadings consist mainly of the municipal secondary wastewater treatment plant effluents for the cities of Bristol, Johnson City, Elizabethton and Bluff City and the industrial effluent of the North American Rayon Company in Elizabethton. Nonpoint source loadings, although not well documented at the present time, are expected to be significant due to the extent of

agricultural and urban development in the reservoir drainage area and the hilly topography. It has also been proposed that failing septic tanks along the Boone Reservoir shoreline may contribute significant loads of nutrients and organics to the reservoir. Extensive algal blooms generally occur during the late spring and summer months possibly due to the high nutrient loadings to the reservoir. These algal blooms significantly impair the transparency of the reservoir and impart a pea green color to the water. Secchi disc depths of less than one meter are common during the algal growing season.

Algal settling and decomposition also results in metalimnetic dissolved oxygen depletion at various locations in the reservoir. When the reservoir is thermally stratified, dead algal cells will settle until they encounter colder, denser water in the metalimmion. At this point their settling rate is significantly reduced and aerobic decomposition results in reduction or total depletion of dissolved oxygen.

Multivariate trophic state analyese by TVA and EPA (30) have classified Boone Reservoir as being a eutrophic reservoir. In these analyses, trophic state index values (TSI values) are derived for a series of geographically and hydraulically similar reservoirs based on chlorophyll, total phosphorus, total nitrogen and bioavailable inorganic

carbon levels. The reservoirs are then ranked from most eutrophic to least eutrophic (i.e. oligotrophic). Based on the analyses of eleven TVA reservoirs located on tributaries to the Tennessee River, Boone Reservoir was ranked as the most eutrophic.

The study upon which this report is based was initiated in May 1984 and extended through August 1984. Light penetration, secchi disc depth, turbidity, light beam transmission, chlorophyll a, pheophytin, phytoplankton productivity, and insitu algal fluorescence were measured at several locations within the reservoir over the four month period. Measurements of total solar radiation were also obtained in conjunction with the above measurements.

It should be noted that the data presented in this report were not collected specifically for the purposes of conducting the data analyses and interpretations described in the following sections. These data rather constitute only one part of an intensive monitoring effort which was designed by TVA to obtain information for guiding reservoir management decisions concerning Boone Reservoir.

CHAPTER 2

LITERATURE REVIEW

The following literature review presents and discusses the important concepts and theories of light attenuation and phytoplankton modeling. The information presented in this section will provide the basis for the analyses of field data collected on Boone Reservoir and the development of mathematical models for predicting light attenuation and algal production in the reservoir. The literature review will begin with a discussion of the factors which determine the intensity and wavelength of sunlight reaching the surface of a reservoir. A discussion of the units of measurement for solar energy will follow thus providing a starting point for a discussion of the quantitative prediction of sunlight attenuation under water. Next, the factors affecting sunlight attenuation in reservoirs will be discussed and mathematical models for the prediction of light attenuation and the relative contributions of attenuating substances will be presented and evaluated. Finally, a discussion of the effects of light on the growth and production of algae will be presented and various light-productivity models will be evaluated.

2.1 Incident Solar Radiation

Solar radiation is of major importance to the dynamics of lake and reservoir ecosystems. Energy supplied by solar radiation is the primary driving force for metabolic activities within a lake (39). It has been reported (10) that each square meter of water surface may be illuminated by as much as one kilowatt of solar power. By photosynthesis, solar energy is transformed into potential chemical energy either autochthonously (within the lake) or allochthonously (outside the lake and brought into the lake in the form of organic matter). The absorption of solar energy by a lake and subsequent conversion to heat also has a major influence on thermal stratification and circulation patterns within a lake which in turn have a direct influence on nutrient cycling, distribution of dissolved oxygen and other gases, and the habitats of aquatic biota (39). Typical summer heat incomes to lakes have been reported as 30,010 cal/cm^2 for Crater Lake in Oregon and 42,300 cal/cm^2 for Lake Michigan (23). For these reasons the optical properties of lakes are important parameters which should be subject to reservoir management and/or regulatory controls (39).

Sunlight should be considered as a portion of the radiant energy of the electromagnetic spectrum which is divided into units of wavelength and frequency. At one

end of the electromagnetic spectrum are cosmic rays with short wavelengths and high frequency at the other end are radio and power transmission waves of low frequency and long wavelength. Solar energy extends from wavelengths of 100 nanometers (nm) to greater than 3000 nm and includes ultraviolet to infrared radiation (39). The portion of the solar spectrum which is useful in photosynthesis extends from 400 to 700 nm and is termed Photosynthetically Available Radiation or PAR (21). The PAR spectrum also includes all wavelengths of visible light (39). Figure 1 is a typical representation of solar flux as it is received extraterrestrially above the earth's atmosphere. Also shown in Figure 1 is the solar flux at ground level after selective atmospheric absorption has altered its wavelength characteristics.

Light energy involves the radiation of pulses of electromagnetic energy termed photons or quanta (39). The energy of a photon is proportional to frequency and inversely proportional to wavelength in accordance with Planck's Law which is:

$$\varepsilon = h\gamma = hc/\lambda \qquad (1)$$

where ε = energy of photon

h = Planck's constant,

$= 6.62 \times 10^{-27}$ erg - second

λ = frequency of radiation, cycles/sec

λ = wavelength, length units

c = speed of light, length/time

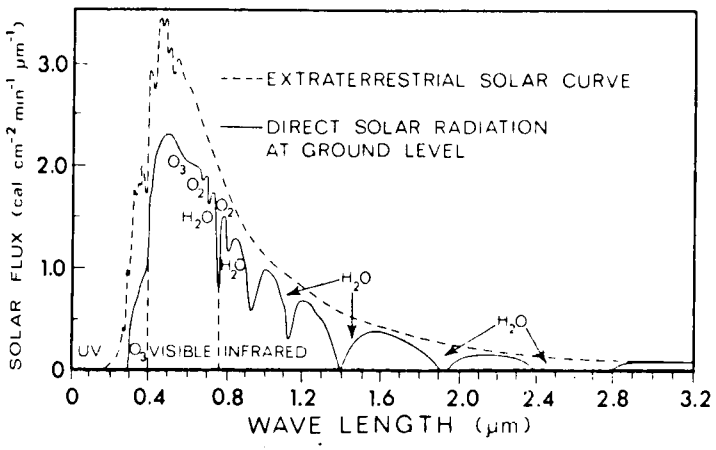

Figure 1. Extraterrestrial Solar Flux and that at the Surface of the Earth with Major Absorption Bands from Atmospheric O_2, O_3, and Water Vapor (After Wetzel, R.G., Limnology, W. B. Saunders Company, 1975).

As light travels through the earth's atmosphere, its spectral characteristics are altered dramatically by the processes of absorption and scattering. Ultraviolet energy is strongly absorbed by ozone and oxygen and infrared by water vapor, ozone, and carbon dioxide (see Figure 1). Absorption of light by atoms and molecules results due to the resonation of the electrons of the atoms and molecules at definite frequencies which correspond to the energy state of the quanta or photon. In the collision of an electron and a photon, the electron gains the quantum of energy lost by the photon (39). Scattering of radiant energy results in an increased probability of absorption by increasing the pathlength which a photon must traverse. Moisture in the atmosphere results in increased levels of scattering. Also, scattering and absorption of solar radiation can be influenced strongly at regional levels by both industrial and urban derived air pollutants (39). In addition to scattering and absorption, geographical latitude and time of the year also influence the quantity of incident solar radiation as shown in Figure 2.

Now that the factors influencing the intensity of solar radiation reaching the surface of a lake or reservoir have been presented, the next logical step in assessing the influences of solar radiation on a reservoir

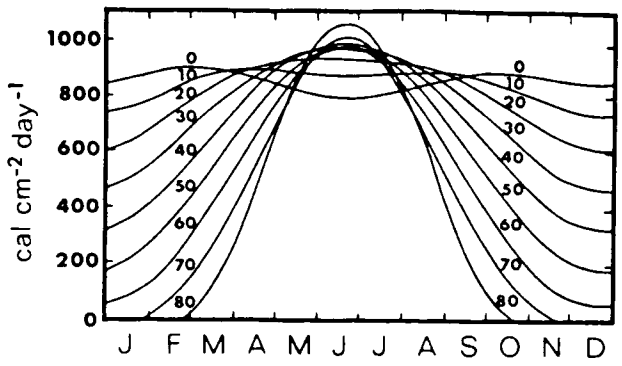

Figure 2. Daily Totals of Undepleted Solar Radiation Received on a Horizontal Surface for Different Geographical Latitudes as a Function of the Time of Year for a Solar Constant* of 1.94 cal/cm^2/min (After Wetzel, R.G., Limnology, W. B. Saunders Company, 1975).

*Solar constant is the amount of direct solar energy per unit of time from the sun, incident on a surface outside the atmosphere perpendicular to the rays of the sun at an average distance of the earth from the sun.

is to describe the factors affecting solar radiation under water and the modeling of light attenuation with depth. Prior to this discussion, however, it is necessary to present the units of measurement of solar radiation, for these units will be used consistently throughout the remainder of this report.

2.2 Units of Measurement for Incident and Underwater Solar Radiation

Solar radiation is measured in irradiance units which express the solar energy flux as energy/area/time or quanta/area/time. Using energy units irradiance is most often expressed as microwatts/cm^2 which is equivalent to 1 x 10^{-6} joules/s/cm^2 (39). The total energy irradiance within a given wavelength region is expressed by the integral (9):

$$I_w = \int_{\lambda_1}^{\lambda_2} I(\lambda)\,d\lambda \qquad (2)$$

where I_w = total energy irradiance of wavelength region from λ_1 to λ_2

$I(\lambda)$ = energy irradiance of a specific wavelength of light

In the measurement of photosynthetically available light (PAR), it is often desirable to measure solar radiation in quanta units rather than energy units since

photosynthesis is a quantum process with photosynthetic response related to the number of quanta impinging upon algal receptor systems (29). Using quanta units, irradiance is most often expressed as einsteins/cm^2/s. The unit "einstein" is synonomous with the term "mole" in chemical terminology. Thus one einstein contains Avogadro's number of quanta, i.e. one einstein is equivalent to 6.02×10^{23} quanta (39). Since many instruments measure energy irradiance rather than quanta irradiance, it is desirable to have conversion factors between the two types of units. The general relationship between quanta and energy irradiance for a monochromatic beam of light (29) is

$$I_Q/I_W = \lambda/hc \qquad (3)$$

where I_Q = quanta irradiance

I_W = energy irradiance

λ = wavelength of monochromatic light

h = Planck's constant

$= 6.62 \times 10^{-27}$ erg-sec

$= 6.62 \times 10^{-34}$ joules-sec

c = speed of light (length/time)

For a given wavelength region (e.g. the PAR region between 400 and 700 nm) the relationship between quanta and energy is defined by the integral (29):

$$I_Q = \int_{\lambda_1}^{\lambda_2} I_W(\lambda) \times \frac{\lambda}{hc} \times d\lambda \qquad (4)$$

where all terms are as defined previously.

Thus for a range of wavelengths the ratio I_Q/I_W, often called the Q/W ratio, is not necessarily constant but varies with variations in the spectral distribution of irradiance (29).

Morel and Smith (29) showed that for the incident solar radiation above the water surface, the Q/W ratio varies very little with changing spectral distribution. A Q/W ratio for the 400 to 700 nm region was given as 2.77×10^{18} quanta/sec/watt ± 0.58%. Below the water surface the Q/W ratio is rapidly modified by the absorption and scattering of the water and its dissolved components. Moral and Smith also found that Q/W for the 400 to 700 nm region varies ± 10% about the value 2.5×10^{18} quanta/sec/watt for waters with a wide range of optical properties. Bannister (1) states that 1 einstein/m^2/day of PAR corresponds to approximately 2.76×10^{18} quanta/joule. The upper and lower limits to the Q/W ratio for natural waters has been shown to depend primarily on the absorption properties of water and of chlorophyll a (29).

2.3 Attenuation of Solar Radiation Underwater

Solar radiation incident upon the surface of a lake or reservoir is modified by several processes as it penetrates into the underwater environment. Vertical

penetration of light into water is attenuated by three primary processes including reflectance from the water surface, scattering, and absorption (9). The amount of solar radiation which is reflected from the water surface is dependent upon the angle of incidence of the solar radiation, the cloud cover, and the physical and textural properties of the water surface (e.g. turbulence of the water surface, ice cover, etc.) (39). Estimates of the amount of solar radiation reflected upwards from the surface of a lake have been reported as 5 to 10% of the incident irradiance (10,39).

As sunlight penetrates down into a water body, its intensity is diminished and its spectral quality is altered as a result of absorption and scattering by various components of the aquatic medium. These attenuating components have been described as the water itself, dissolved yellow (humic) substances, the phytoplankton (live algal cells and decomposition products), and non-living particulate matter (5,19,21). In clear shallow lakes, the lake bottom may also serve to absorb or scatter sunlight (34). Apart from the small amount of light scattered back out of the water, attenuation of light is entirely due to absorption since this is the only process which actually removes light by conversion to heat or biochemical potential energy (21). The role of

scattering in light attenuation is to intensify the attenuation of light with depth by increasing the path-length of photons which subsequently increases the probability of absorption (22).

The light attenuation properties of the water itself have been characterized from spectral irradiance measurements in either distilled water or extremely clear natural waters such as Crater Lake, Oregon or the Sargasso Sea. Data reported by Duntley (10) and Wetzel (39) for distilled water indicate that the shorter wavelengths of light have the greatest transmittance (i.e. least absorbance) with the peak transmittance occurring near 480 nm in the blue region. Measurements made by Smith and Tyler (33) in Crater Lake indicate that the maximum transmittance with depth occurred for 420 nm wavelength light. Measurements by Larson (15) in Crater Lake also found that blue light had the greatest penetration. The greatest absorbance of light is reported to occur at the longest wavelengths of light with the maximum absorption in the red region (greater than 600 nm) (23,33). This high absorption of red (and infrared) wavelengths of light is common to all waters regardless of the optical clarity and has important effects on the heating of a water body. Absorption of the red and infrared wavelengths is near 100% complete within the first few meters of water even

for the clearest waters, thus red light does not penetrate very far (23,39).

The presence of dissolved humic compounds in water shifts the wavelength absorption selectivity and reduces the transmission of light. Duntley (10) reports that dissolved humic substances shift the maximum transmission of light from the blue wavelengths to the green wavelengths (near 520 nm). Data reported by James and Birge for several lakes stained with organic color indicate that absorption increases with decreasing wavelengths with greatest absorption in the ultraviolet, blue and green wavelengths (less than 600 nm) and least in the red region (39).

Light attenuation by phytoplankton is a result of the capture of photons by chlorophyll a or other accessory pigments and subsequent conversion to biochemical potential energy. Algae, by selective absorption of various wavelengths of light, are often the major determinants of their own light environment (9). The spectral absorption properties of algae shows large variations seasonally and among different species (5,9,12). These variations in spectral absorption properties are due primarily to three factors: (1) Varying composition of accessory pigments (i.e. pigments other than chlorophyll a); (2) variations in cell size and pigment concentration;

and (3) variations in the age of the algal culture (37). Chlorophyll a, the major photosynthetic pigment, has two major absorption peaks in the PAR wavelength region; these are approximately 440 nm in the blue region and 670 nm in the red region (21). Accessory pigments such as cartenoids also have peak absorbance in the blue region of the PAR spectrum. Varying concentrations of cartenoids in different algal species results in variations in absorption spectra for the blue wavelength region (400 - 520 nm) and differences in light attenuation characteristics (5). Since variation in the dominant species of algae in a lake occur seasonally, variations in light attenuation by absorbance may occur with changes of season. Dubinsky reported variations in the light penetration in Lake Kinneret in Israel due to the seasonal shift in the dominant algal species from the green algae Chlorophyta to the dinoflagellate Peridinium (9). The effect of cell size on light absorbance has been reported to be inversely related (5). Thus for a given amount of an absorbing pigment, absorbance will decrease with increasing cell size. This is principally due to the "packaging effect" which means that if a given amount of chlorophyll is packaged into smaller cells, it will absorb more light because more chlorophyll surface area is exposed to the light source. The effect of algal

culture age on light absorbance is related to the presence of pheopigments which are degradation products of photosynthetic pigments. These pheopigments absorb light almost in the same manner as active chlorophyll a and are present in variable amounts according to the age of the algal culture (21,37). The older the age of the culture the greater will be the concentration of pheopigments due to death and decomposition of algal cells.

The absorbance of light by inanimate particulates is not well understood but has been shown to increase with decreasing wavelength (21). Measurements by Kirk in the turbid waters of Lake Burley Griffin and Lake George in Australia showed that the particulate fraction, which included a small amount of phytoplankton, absorbed more strongly than the soluble fraction at all wavelengths with increasing absorbance with decreasing wavelength (21).

As stated previously, scattering of light intensifies the attenuation of light with depth by increasing the probability of light absorption. When a photon is scattered as a result of collision with a particle in water it diverges from its original path. As a result of repeated scattering, photons are made to follow a zig-zag trajectory with an increase in pathlength in passing through a given water depth and an increase in the

probability of capture by one of the absorbing components of the system (22). The light field formed by this multiple scattering of photons is termed diffuse light (39). The angular distribution of solar flux underwater is termed the radiance distribution (10,19,22). The radiance distribution defines the proportion of radiant energy impinging upon a receptor at various angles. In a non-scattering medium (e.g. a turbidity-free clear spring fed reservoir) the radiance distribution remains virtually constant with depth although decreases in radiant energy will occur due to absorption by dissolved substances and water (19). Small changes in radiance distribution even in completely turbidity-free waters may occur, however, due to scattering at the molecular level (4). In a scattering medium the radiance distribution of sunlight entering at the surface begins to change and become progressively more diffuse with depth. At a certain depth, the distribution of light will take on a fixed form called the Asymptotic Radiance Distribution (10,19,20,22,33). The asymptotic radiance distribution is dependent only upon the characteristics of the water mass including the optical properties of the absorbing and scattering materials in the water (10,19). It is independent of the solar altitude and prevailing sky conditions and is invariant with further increases

in depth unless optically different water is encountered (19). Measurements of the underwater radiance distribution have shown that the peak radiance occurs at an angle of 0° measured from the vertical once the asymptotic radiance distribution has been reached (10,33).

Scattering of light underwater is due to the presence of suspended matter (i.e. algal and non-algal turbidity) and the water itself. Light scattering in pure water free of dissolved and particulate matter is due to scattering by water molecules. Molecular scattering is Rayleighian in nature with the intensity of scattering inversely proportional to wavelength to the fourth power (10,39). Thus the shorter wavelengths of light will be scattered the greatest. For this reason clean, clear natural waters such as Crater Lake have a deep blue appearance; for it is blue light that is absorbed the least and scattered the most by pure water. The blue light scattered upward emerges from the lake as reflected light giving the water a blue color.

The presence of suspended solids in water results in increased scattering of light. Different researchers have reported varying results concerning the dependence of scattering on wavelength. Duntley (10) reports that scattering in natural waters is due to particles which are large compared to the wavelengths of light and is

thus virtually independent of wavelength. Wetzel (39), however, reports that scattering by suspended material is dependent on wavelength with scattering of longer wavelengths being predominant. Hard-water lakes with high suspensions of $CaCO_3$ were reported to scatter light predominantly in the blue-green region and those rich in suspended organic materials were reported to scatter yellow light (39). Measurements by Bricaud (5) on live algal cultures revealed that scattering by phytoplankton is strongly variable from species to species and exhibits scattering spectra which are approximately inverse to absorption spectra (i.e. the wavelengths of absorption maxima correspond to scattering minima and vice versa).

In summary, light attenuation in reservoirs can be related to the light absorption and scattering properties of various substances including algae, suspended organic and inorganic matter, dissolved color, and the water itself. Following a brief discussion of the instrumentation available for the measurement of solar radiation, various modeling approaches for predicting light attenuation and the fractional contribution of various attenuating substances to the overall light diminution in a reservoir will be presented.

2.4 Instrumentation for Measurement of Solar Radiation

Various instruments are available for the measurement of solar radiation in the ambient environment and underwater. Solar pyrheliometers are used to measure the total incident solar flux usually in units of $cal/cm^2/min$. Total solar radiation readings from a pyrheliometer may be converted to photosynthetically available radiation (PAR) by assuming PAR to be approximately 46% of the total radiation (37).

Three major instruments used for measuring the penetration of solar energy into the underwater environment are the secchi disc, the irradiameter, and the spectroradiometer. The secchi disc developed in 1866 by Professor P. A. Secchi was the first experimental instrument used to assess the transparency of a body of water (38). A secchi disc reading is made by lowering the secchi disc (a black and white disc) on the shaded side of a boat to the depth at which it first disappears--this is the secchi disc depth. The secchi disc depth gives an approximate value of the transparency of a lake and is a function of the reflection of light from the disc surface (39).

Measurements of underwater irradiation can be made using an irradiameter which measures the spectral response over a set wavelength interval (usually the PAR region

of 400 to 700 nm) or by a spectroradiometer which measures the separate spectral responses for a series of small wavelength intervals or for specific wavelengths (4,9,18,28,33). Each of these instruments may measure quantum response (quanta/s/cm^2) or energy response (microwatts/cm^2).

Irradiameters are of two major types: scalar collectors and cosine collectors. Cosine collector irradiameters consist of flat plate sensors which collect light in proportion to the cosine of the angle of incidence (18,33). Thus the cosine collector irradiameter measures only the vertical component of the incident or diffuse radiation. Cosine collectors are available with sensors facing upward for measuring only the downward attenuation of light or with sensors facing upward and downward for measuring both vertically incident light and the vertical light reflected upward from the lower depths (18). Figure 3a illustrates two of the types of cosine collector sensors. Scalar irradiance is defined as the total underwater light received by a receptor system, such as that received by an algal cell from all angles and is a measure of the optimum radiant energy available for photosynthesis. Scalar irradiance is measured by a scalar irradiameter which usually consists of a spherical translucent collector which collects light from all directions (4). Figure 3b provides an illustration of a scalar irradiameter.

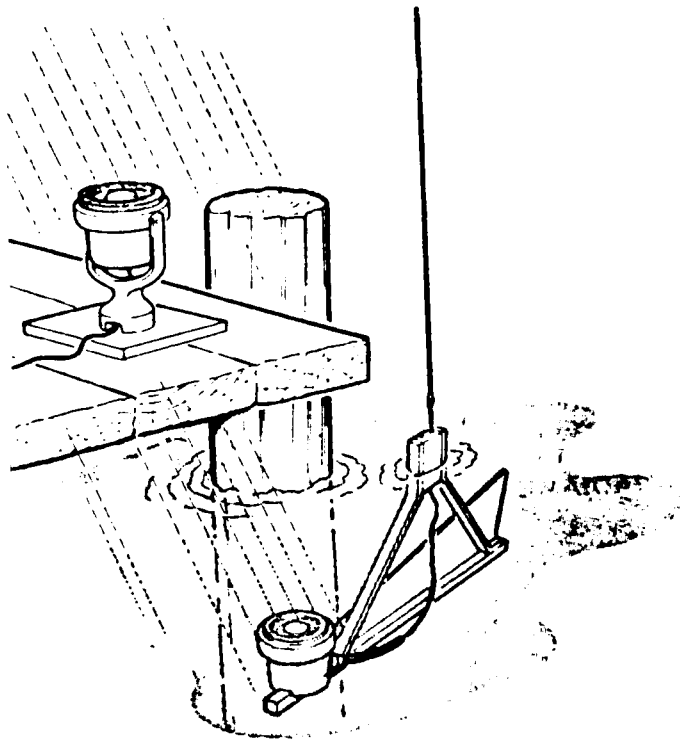

(a) Cosine collector for measuring vertical downward irradiance (10)

Figure 3. Illustrations of Underwater Irradiameters for Measuring Vertical and Scalar Irradiance

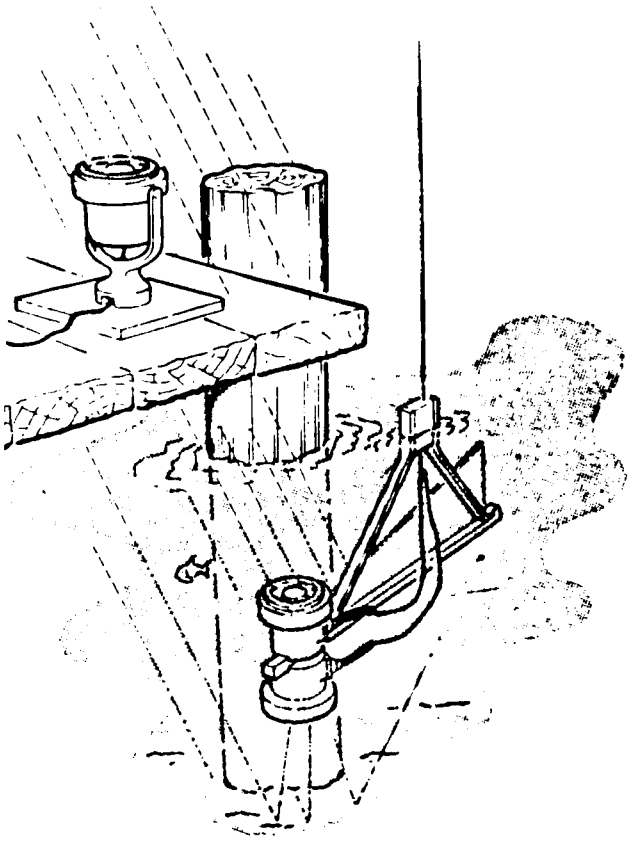

(b) Cosine collector for measuring vertical downward and vertical reflected irradiance (10)

Figure 3 (continued)

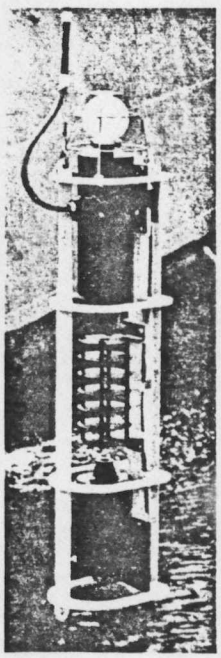

(c) Scalar irradiameter with spherical collector at top of instrument for measurement of scalar irradiance (from Duntley (6))

Figure 3 (continued)

The spectroradiometer is similar to the irradiameter except it measures individual responses at particular wavelengths or wavebands rather than the total response for the entire PAR wavelength region. Uses of the spectroradiometer have been described by Tyler (33) and Dubinsky (9). Some cosine collector irradiameters are capable fo being equipped with colored light filters so that they measure the response of various wavebands within the PAR region (18). The measured response using these light filters, however, covers much broader wavelength regions (e.g. 400 to 475 nm with a blue filter, 475 to 600 nm with a green filter, and 600 to 700 nm with a red filter) than the narrow banded or wavelength specific response of the spectroradiometer.

2.5 Estimation and Modeling of the Optical Properties of Water

In this section, mathematical models for providing quantitative estimates of light attenuation with depth will be presented. These models will be used later in the data analyses section of this report to model the light attenuation in Boone Reservoir and to determine what factors should be controlled to improve the transparency of the reservoir. Also the methods presented herein for estimating the fractional absorption of light

by algae will be used in the development of light-productivity models for the reservoir.

The attenuation of light underwater is best described by the Beer-Lambert equation which expresses light attenuation as an exponential decay function (9,19,39):

$$I_z = I_o e^{-Kz} \qquad (5)$$

where I_z = the irradiance at depth z (quanta/m^2/s or energy/m^2/s as I_z)

K = vertical attenuation coefficient (m^{-1})

z = depth (m).

This equation can be applied to attenuation of downward irradiance or upward (i.e. reflected) irradiance (19). The equation is, however, imperfect for natural waters. This imperfection arises because the equation assumes that the incoming light beams are parallel, that the medium absorbs light but does not scatter it, and that the light is monochromatic (9). None of these assumptions are true, however, for sunlight in natural waters. Nevertheless, the equation does, however, provide a good approximation of light attenuation in natural waters. Kirk (19) reported that in the upper layer of water the attenuation of downward or upward irradiance with depth is approximately, but not exactly, exponential since the angular distribution is changing in this region. Once

the fixed form asymptotic radiance distribution has been established, the attenuation of light with depth is, however, exactly exponential.

The attenuation coefficient in the Beer-Lambert equation is often determined as the vertical attenuation coefficient for downward irradiance, K_d. K_d is commonly measured as an average value over the euphotic zone depth which is defined as the depth at which downward irradiance is reduced to 1% of the irradiance just below the surface (19). A commonly accepted rule-of-thumb is that significant algal production does not occur below the euphotic zone depth. Another depth at which K_d is commonly obtained is at the middle of the euphotic zone which is defined as the depth at which the downward irradiance has been reduced to 10% of the irradiance just below the surface. Kirk (19) reports that the asymptotic radiance distribution is generally established before the depth of the midpoint of the euphotic zone and completely established at the euphotic zone depth.

In order to accurately model light attenuation with depth, it is important that a good estimate of the vertical attenuation coefficient, K_d, be obtained. K_d may be estimated directly from underwater irradiance measurement by rewriting the Beer-Lambert equation as:

$$\ln (I_o / I_z) = K_d z \qquad (6)$$

The value of K_d may now be evaluated by linear regression of ln (I_o / I_z) versus depth (10). K_d evaluated in this manner is often expressed with units of ln/m rather than 1/m to indicate that it is taken as the slope of a semi-log plot. The value of K_d will vary at different times during the day primarily due to changes in solar elevation. For comparable estimates of attenuation coefficients, underwater irradiance should be measured on sunny days near solar noon, because near solar noon attenuation coefficients change most slowly with time (27).

Secchi disc depths may be used to obtain an approximation of the value of K_d (6,16,25). This is done by assuming that the secchi depth corresponds to a constant percentage of light attenuation, usually 10 to 30% (29). K_d may then be calculated as:

$$K_d = \frac{-\ln (I_z / I_o)}{z} \qquad (7)$$

$$= \frac{-\ln (\text{constant})}{\text{secchi depth}}$$

Gulliver and Stefan (16) found that light attenuation in Lake Calhoun, Minnesota could be estimated by assuming that secchi depths corresponded to 15% light attenuation thus:

$$K_d = \frac{-\ln (0.15)}{\text{secchi depth}} = \frac{1.90}{\text{secchi depth}} \qquad (8)$$

Lorenzen (27) assumed tht secchi disc depth was related to 20% light attenuation. Brown (6) reported that the extinction coefficients for Fort Loudon Lake, Tennessee and Lake Erie could both be approximated as 1/secchi depth which corresponds to approximately 37% light attenuation. Because of the wide variability in the relationships between secchi depth and K_d, the use of underwater irradiance readings in determining K_d should provide better and more reliable results.

The value of K_d may also be estimated in some cases through use of turbidity measurements. Measurements reported by Brown (6) for several lakes and reservoirs showed relationships of the form K_d = C x Turbidity where C varied between 0.15 and 0.50. These large variations in the relationship between turbidity and K_d are not unexpected because light attenuation is a complex process involving absorption, scattering, reflection, and refraction (6).

For effective modeling of light penetration in a lake or reservoir, relationships should be established between the various absorbing and scattering components (e.g. phytoplankton, dissolved color, suspended solids, and the water itself) and the extinction coefficient, K_d. Establishment of these relationships will allow computation of the relative contribution of each light

attenuating substance to the overall attenuation of light. This partitioning of light attenuation components has significant value in lake and reservoir management programs concerned with improvements in light transparency (12). Knowledge of the fractional absorption of light by algae is also important in phytoplankton productivity models (37).

Two approaches which have been used to partition the light extinction coefficient, K_d, into its various attenuating components are described briefly below. The first approach involves regression analysis of the light extinction coefficient against the various attenuating components (1,9,12,16,25,27,37). The second approach is a more rigorous, mechanistic approach which involves establishing the relationships between the various attenuating components and the inherent properties of a water (i.e. those optical properties which do not depend on the radiance distribution of sunlight). The inherent optical properties are then used to estimate the apparent properties of the water (i.e. properties which depend on the radiance distribution and depth such as irradiance, and K_d) (5,10,19,20,22,25).

The linear regression partitioning method is most often expressed as (1,9,12,16,25,27,37):

$$K_d = K_c \times C + K_w \qquad (9)$$

where K_d = vertical extinction coefficient for downward irradiance (m^{-1})

K_c = average spectral attenuation coefficient by phytoplankton (m^2 / mg chlorophyll a)

C = concentration of chlorophyll a (mg/m^3)

K_w = average spectral attenuation coefficient of water and its non-phytoplankton components (m^{-1})

This method is applicable only if samples for chlorophyll analyses are collected at the same depths and time at which K_d is calculated. To determine K_c and K_w, the values of K_d are plotted against chlorophyll concentration, C. The slope of this plot is equivalent to K_c and the y-intercept is equivalent to K_w. Various values of K_c and K_w reported in the literature using this method and the location where each was measured are given in Table 1. It should be noted that the coefficients determined in Lake Constance (37) using scalar irradiance measurements were not substantially different from the other values which were obtained using cosine collector irradiameters.

Measurements by Dubinsky (9) in Lake Kinneret, Israel show that K_c is very dependent on the wavelength of measurement with values ranging from 0.005 m^{-1} for the most penetrating wavelength (560 nm) to 0.012 m^{-1} for the wavelengths near the absorption maxima for

TABLE 1

Estimates of K_c and K_w for the PAR Region at Various Lakes

Location	Reference	K_c (m^2/mgChl a)	K_w (m^{-1})	n	r^2
Lake Minnetonka, Minnesota (Halsted Bay)	27	0.022 ± 0.005	0.68 ± 0.35	9	0.93
Port Hacking Estuary, Australia	27	0.021	0.10	73	0.58
Lake Calhoun, Minnesota	16	0.030	0.60	-	-
Lake Kinneret, Israel	9	0.0067 ± 0.0008	0.49 ± 0.076	43	0.66
Mean Estimate for Several Lakes	1	0.016	-	-	-
Lake Constance, West Germany	37	0.015*	0.27	-	0.90

*Measurements made using a scalar irradiameter.

chlorophyll (450 nm and 650 nm). Despite this dependency on wavelength, measurements of irradiance for the entire PAR waveband should adequately define the relationship between the chlorophyll and the attenuation of PAR with depth (9,27). Use of uncorrected chlorophyll concentrations (i.e. uncorrected for the presence of pheophytin, see Standard Methods (34) in the estimation of K_c may lead to falsely high values for the attenuation of light due to algal cells because pheophytin (a degradation production of chlorophyll) absorbs at near the same wavelengths as chlorophyll a (37). Since pheopigments do not collect light for photosynthesis, their light interception should be added to background attenuation which is accounted for by K_w. Tilzer provided a method for separating the attenuation due to pheopigments from K_c and adding it to K_w; this method is given as (37):

$$K_w = K'_w + K_c C \quad (1 - p) = K'_w + K_p \qquad (10)$$

where K_w = background light attenuation coefficient due to non-phytoplankton components and pheophytin (m^{-1})

K'_w = background light attenuation coefficient due to non-phytoplankton components only (m^{-1})

C = uncorrected chlorophyll a concentration, includes pheopigments

p = C'/C where C' is the concentration of chlorophyll a only (corrected for pheopigments) and C is as defined above.

K_p = light attenuation coefficient due to pheopigments (m^{-1})

$= K_c C (1 - p)$

Other factors affecting the values of K_c and K_w are season, algal cell size, and variations in dissolved and suspended non-algal matter. The variations in dominant algal species with season may result in seasonal variations in K_c for the same location (9). The seasonal variations with species are probably due to differences in accessory pigments such as carotenoids (5). K_c has also been shown to be inversely related to cell size (5,9). Megard (27) reports that for measurements made in Lake Minnetonka, Minnesota, the value of K_w was much more variable than K_c when compared with other lakes. This greater variability was attributed to differences in the concentrations of dissolved organic (humic) materials.

The second approach for the partitioning of the vertical attenuation coefficients involves the establishment of relationships between the inherent and apparent

optical properties of a water body. Inherent optical properties are those whose value at a given point are independent of changes in the angular distribution of radiant flux (radiance distribution) (19). These properties include the absorption coefficient, a, the scattering coefficient, b, the beam attenuation coefficient, c (where c = a + b), and the volume scattering function $\beta(\theta)$. These parameters are defined in terms of the behavior of a collimated (i.e. parallel) beam of monochromatic light perpendicularly incident on a thin layer of the water in question rather than in terms of the diffuse light field that actually exists in a lake or reservoir (10,19). Because inherent optical properties are properties belonging to the water itself, they may be measured in the laboratory using water samples taken from the water body in question (19). The attenuation of a collimated beam of light may be defined in terms of the inherent optical properties using the Beer-Lambert equation (10):

$$I_z = I_o e^{-cz} \qquad (11)$$

where I_o = initial unattenauted irradiance of beam of collimated light (energy/s/m^2)

I_z = residual irradiance of the beam at a distance or depth z (energy/s/m^2)

c = beam attenuation coefficient (m^{-1})

$c = a + b$

a = absorption coefficient (m^{-1})

b = total scattering coefficient (m^{-1})

The volume scattering function, $\beta(\theta)$, specifies the proportion of light scattered at various angular intervals for a beam of perpendicularly incident collimated light (10,22). Measurement of the inherent properties a and b have been described by Kirk (20,21) and Bricaud (5). Measurement of the volume scattering function is described by Duntley (10).

Apparent properties are those whose value at a given point is not independent of changes in the radiance distribution (19). These properties include insitu irradiance, the vertical attenuation coefficient for irradiance, and the reflectance (i.e. the ratio of upward to downward irradiance). The apparent properties must be measured insitu within the water body itself (19). It is the apparent properties of a lake or reservoir which directly determine its transparency and photosynthetic productivity.

To determine the effects of various light attenuating substances on the light field of a water body, the relationships between the apparent optical properties and the inherent optical properties must first be determined. Next, relationships must be developed relating the

inherent optical properties to concentrations of various light attenuating materials (e.g. phytoplankton, non-algal suspended solids, dissolved humic substances) (12). Once these relationships have been established, the effects of a change in one of the attenuating materials (e.g. a seasonal algal bloom or an increase in suspended solids due to highway construction) on the transparency of a lake may be estimated.

For a completely non-scattering medium the inherent absorption coefficient for a collimated beam of light, a, may be related to the vertical attenuation coefficient for downward irradiance by the expression (19):

$$K_d = \frac{a}{\cos \theta} \qquad (12)$$

where a = inherent absorption coefficient (m^{-1})

θ = angle of light beam within the water measured from zenith position (e.g. for zenith sun θ = 0 degrees, for the setting sun θ = 90 degrees)

For a scattering medium, the relationships between the inherent absorption and scattering coefficients and the corresponding coefficients for a diffuse light field become more complex due to multiple scattering and change in the radiance distribution with depth (19).

The absorption coefficient for diffuse light

consists of a downward component, a_d, which is the proportion of the downward light stream which is absorbed, and an upward component, a_u, which is the proportion of the upward (i.e. reflected) light stream which is absorbed (19). To obtain the diffuse absorption coefficient for a particular depth, the radiance distribution at that depth must be known. Given the radiance distribution and the inherent absorption coefficient the diffuse absorption coefficients, a_d and a_u, for a specified depth may be computed using the average cosine of the radiance distribution as follows (19):

$$a_d = \frac{a}{\bar{\mu}_d} \quad ; \quad a_u = \frac{a}{\bar{\mu}_u} \tag{13}$$

where a_d and a_u = diffuse absorption coefficients for downward and upward light streams (m^{-1})

a = inherent absorption coefficient (m^{-1})

$\bar{\mu}_d$ and $\bar{\mu}_u$ = average cosines for downward and upward irradiance

Kirk (19) reports the average cosines may be estimated from scalar irradiance measurements as:

$$\bar{\mu}_d = \frac{I_d}{I_{sd}} \text{ and } \bar{\mu}_u = \frac{I_u}{I_{su}} \tag{14}$$

where I_d and I_u = downward and upward irradiance (measured by cosine collector)

I_{sd} and I_{su} = lower and upward hemispherical components of scalar irradiance

The coefficient of scattering for a diffuse light field is called the backscattering coefficient and is defined as b_b. It consists of a downward scattering coefficient, b_{bd}, which is the proportion of the downward light stream which is scattered back upward, and an upward scattering coefficient, b_{bu}, which is the proportion of the upward (i.e. reflected) light stream which is scattered back downward (5,19,20,22). The total backscattering coefficient is equal to the sum of b_{bd} and b_{bu}. The correlation between the inherent scattering coefficient, b, and the diffuse scattering coefficient, b_b, is much more complex than that between the inherent absorption coefficient and the diffuse absorption coefficient. The relationship between b and b_b must be derived using the volume scattering funciton, $\beta(\theta)$, and the radiance distribution for the depth at which b_b is to be obtained (19,22). This type of calculation becomes very complex because the volume scattering function and the radiance distribution are parameters which are not easily measured in the field. Calculation of b_b also requires that the flux of scattered light for each angular interval of the volume scattering

function be computed for each angular interval of incident flux of the radiance distribution (22). This type of computation involves an iterative solution which is only feasible through use of a computer. Kirk (22) calculated values of b_b for various values of b using volume scattering function and radiance distribution data obtained by other researchers at different locations. It would be desirable, however, to use actual radiance distribution and volume scattering data measured from the water body in question when making such a computation. Once values of b_b and a_d have been computed for the diffuse light field, the vertical attenuation coefficient for downward irradiance may be computed as (19):

$$K_d = a_d + b_{bd} - b_{bu} R \tag{15}$$

$$R = b_{bd}/(a_u + b_{bu} + K_u) \tag{16}$$

where K_d, a_d, a_u, b_{bd}, and b_{bu} are as defined previously

R = reflectance = K_u/K_d

K_u = vertical attenuation coefficient for upward irradiance (m^{-1})

One of the major problems in the use of inherent optical properties to estimate apparent optical properties is that the volume scattering function, $\beta(\theta)$, and the

radiance distribution must be measured or assumed. These types of measurements are not routinely made in the field and require special instrumentation (22). Therefore use of this method would probably require that radiance distribution and volume scattering function data be obtained from the literature for measurements made at some other location. Duntley (10) reports that there is a strong similarity in shape between volume scattering functions for measurements made by different researchers in waters of differing optical properties. Therefore, the use of an assumed volume scattering function may not result in significant errors. The radiance distribution is, however, more variable with differing optical properties (22). Assumed radiance distribution data should be from waters of similar optical properties (22).

Kirk (19) avoided the problem of having to assume a radiance distribution by using a Monte Carlo computer modeling technique to simulate the underwater radiance distributions for various values of a and b and an assumed volume scattering function. This simulation was conducted by tracing the individual fates of 10^6 photons. Values of the inherent absorption, scattering, and beam attenuation coefficients (a, b, and c, respectively) were used in the simulation to specify the probability of a photon traversing a particular pathlength before interacting

with some component of the medium. The cumulative probability of being scattered or absorbed at any distance up to P was given by:

$$1 - e^{-cp} = \text{probability} \qquad (17)$$

where c = beam attenuation coefficient

P = pathlength

A random number, between 0 and 1 was generated to specify probability and the corresponding pathlength was given as:

$$P = -(1/c)\ \ln\ (1 - r) \qquad (18)$$

where r = the random number probability

This computation fixed the pathlength. After computation of the pathlength, additional random numbers were generated and used in the above pathlength equation with values of a and b replacing the beam coefficient c. If the pathlength obtained using the absorption coefficient was less than that obtained using the scattering coefficient and the beam attenuation coefficient, then the photon was said to be absorbed. Likewise if the scattering pathlength was the least then the photon was scattered. The angle of scattering was determined by an assumed volume scattering function. If a photon was absorbed, a new photon was introduced. If a photon was scattered, its trajectory was followed until it was absorbed or

scattered out of the water. The calculation was repeated using various wavelength specific values of the absorption and scattering coefficients to simulate the penetration of the whole PAR waveband. The number of photons of all wavelengths passing up and down a series of depth markers, along with their angular distribution, was recorded. From this data, irradiance, scalar irradiance, reflectance, average cosines, and the radiance distribution at 5 degree intervals was calculated. It was then possible to determine relationships between K_d and the inherent optical properties.

The importance of the simulations by Kirk was that generalized relationships were developed for calculating the apparent properties at a given optical depth (e.g. the euphotic zone depth, or midpoint of the euphotic zone) (19). From the computer simulation, it was determined that for water with a given volume scattering function the relationships between the average cosine, reflectance, and K_d were fixed for specified values of optical depth and b/a. Using these fixed relationships the equation for K_d at the midpoint of the euphotic zone was specified as:

$$K_d\ (z_m\ ) = (a^2 + 0.256\ ab)^{0.5} \qquad (19)$$

Results of the Monte Carlo study by Kirk also provided relationships for estimating values of the

inherent properties a and b using insitu measurements of reflectance and the vertical attenuation coefficient for net downward irradiance (i.e. the difference between downward and upward vertical irradiance) (20).

Comparisons by Kirk (19) of K_d values calculated by the Monte Carlo procedure using values of a and b for various Australian lakes showed good correlations with values calculated from insitu measurements. Effler (12) analyzed the applicability of Kirk's relationship using field data obtained on Onondaga Lake in New York. It was found that the K_d values computed by the equation for K_d at the midpoint of the euphotic zone (i.e. the above equation) were very close to K_d values observed in the field.

Effler took the relationships developed by Kirk one step further and analyzed the relative contributions of various attenuating substances to the overall light attenuation (12). Using measured values of reflectance and net downward irradiance, the inherent absorption and scattering coefficients were estimated by Kirk's relationships (20). The absorption and scattering coefficients were then partitioned into various components (i.e. water, phytoplankton, dissolved color, calcium carbonate, pheopigments) by linear regression of the concentrations of the attenuating substances on a and b. The fractional

contribution of each component to the vertical attenuation of downward irradiance was then determined using the K_d equation developed by Kirk for the midpoint of the euphotic zone (19).

Comparison of the two methods available for partitioning of the light attenuation coefficient reveals some important concerns. While the second method of partitioning in terms of apparent and inherent optical properties yields coefficients which define the fundamental attenuation processes of absorption and scattering, it suffers from complexity. This method is based upon field measurements which are complex and difficult to obtain (i.e. the radiance distribution and volume scattering function). Simplifications of the method by Kirk (19,20) are only applicable if the water body under investigation is optically similar to that used by Kirk in his modeling studies. The first method of regression of K_d on the concentration of attenuating substance, however, should be applicable for any water body and is much simpler to use. While it will not obtain coefficients which segregate the processes of absorption and scattering, it does define the fractional contribution of various attenuating substances to the overall attenuation of light. From an engineering viewpoint this would be of most concern because reservoir management programs are often directed at

improving the reservoir transparency by controlling the levels of attenuating substances. Knowledge of which substance is controlling the transparency of the reservoir will provide reservoir management programs with the direction in which their efforts should be focused.

Up to this point, the discussion has been focused primarily on assessing what environmental factors affect light attenuation and on quantifying the degree of light attenuation given field measurements of these factors. This will allow an evaluation of the light climate in Boone Reservoir and permit the development of mathematical models which can be used to predict changes in the reservoir transparency given changes in the concentrations of attenuating substances. In the next section the effects of light on algal productivity and growth will be discussed.

2.6 Light and Algal Productivity Modeling

In this section, the relationships between light and algal productivity and growth will be discussed and various algal models will be evaluated. Other factors influencing algal dynamics will also be presented (i.e. adaptive state, nutrients, carbon) but the emphasis will be on the response of algae to light. The information presented will be used in the Results and Data Analyses

section of this report to evaluate the response of algae in Boone Reservoir to light related variables. This will allow the development of light-productivity relationships specific to Boone Reservoir which can in turn be used in reservoir computer models to evaluate the effects of nutrient management strategies on algal dynamics.

The discussion will begin with an overview of the uses of algal models and a presentation of a few examples of actual cases where algal models were applied to provide needed information. Next, the factors which affect algal production and growth, including environmental variables and parameters specific to the algae themselves, will be presented. Various mathematical models for predicting the influence of light on algal productivity will then be presented and evaluated. Finally the general theory for modeling of algal dynamics including all environmental influences (nutrients, carbon, light, etc.) and all loss processes (death, respiration, grazing) will be presented and discussed.

2.6.1 Uses of algal models

It is often desirable to model the production and growth of algal biomass in a reservoir as a function of various environmental variables (light, nutrients, temperature, cell losses to settling and grazing, etc.). The

development and calibration of an algal model will provide a means of predicting the consequences of a change in a particular variable such as a reduction in nutrient concentrations on the rate of algal photosynthesis and growth. Such a prediction may be beneficial and necessary for regulatory agencies, municipalities, and other groups concerned with the management or restoration of reservoir water quality and prevention of beneficial use impairment. When expensive alternatives for reservoir management (e.g. tertiary wastewater treatment) are considered, a mathematical model can provide inexpensive information on the probable success or failure of reservoir management techniques. A few example cases of the uses of algal models are described below.

Through the application of a phytoplankton growth model Gullivar and Stefan (16) were able to predict the effects of artificial reservoir destratification on algal population. It was shown that destratification during the algal growing season resulted in an upwelling of nutrients from the sediments and as much as a three-fold increase in phytoplankton density. Field (12,14) developed an algal productivity model for hypereutrophic Onondaga Lake in New York which was then used to guide lake restoration decisions. Megard (26) developed a similar model for describing the phytoplankton dynamics in Lake

Minnetonka, Minnesota, also a eutrophic reservoir. Brown et al. (7,8) used algal models to predict the effects of waste discharges on various TVA reservoirs thus providing important information for guiding reservoir management decisions.

2.6.2 Factors affecting algal production and growth

Primary productivity of algae is a measure of the inorganic carbon uptake or the oxygen production by algae during photosynthesis (34,39). It is generally expressed as a rate with units of mass of carbon fixed or oxygen produced/volume/time or as mass of carbon fixed or oxygen produced/area/time for the rate averaged over depth and time (27). Incident light and the factors affecting its attenuation with depth are of major importance in phytoplankton production and growth. Light provides the energy in the photosynthetic process for the production of ATP (adenosine triphosphate) and reducing power in the form of $NADPH_2$ (reduced nicotinamide adenine dinucleotide phosphate). The synthesis of cellular material (carbohydrates, glucose, cellulose, starches, amino acids, etc.) from carbon dioxide requires the stored energy available from ATP and the "reducing power" of $NADPH_2$. In addition, ATP provides the energy necessary for cellular active transport, respiration and other energy consuming processes vital to the algal cell (15).

The growth and photosynthetic production of algae in lakes and reservoirs is a function of several environmental variables (1,2,31) including:

(1) Incident light, I_o;

(2) Intensity of light absorption by the water and its nonphytoplankton components (expressed as K_w);

(3) Mixed layer depth;

(4) Sedimentation of algal cells;

(5) Consumption of algae by zooplankton and other primary consumers;

(6) Nutrient levels; and

(7) Temperature

In addition species specific or adaptive parameters (i.e. a parameter that varies with time in any particular species due to variations in environmental variables or physiological conditions of the algae) of the algae themselves affect growth and production (1,2); these include:

(1) Intensity of light absorption by chlorophyll and photosynthetic algal pigments (expressed as $K_c C$);

(2) Intensity of light which saturates photosynthetic pigments; and

(3) Efficiency with which light absorbed by photoplankton generates photosynthetic products (i.e. reduced carbon)

The influence of light on algal production is determined primarily by the incident light intensity and by the values of K_w and K_c which are components of the overall light attenuation coefficient (K_d) due to, respectively, the background attenuation by water and its nonphotosynthetic components and to the species specific attenuation of light by algae (1). Variations in these factors will determine the number of quanta that are available to an algal cell for photosynthetic production and growth. As discussed previously (see Section 2.3), the algal light attenuation coefficient K_c may vary with algal species and with the age of the algal culture and K_w may vary in response to changes in turbidity, dissolved color, and phytoplankton degradation products.

Two other light related variables which affect photosynthetic production and growth are the efficiency of generation of photosynthetic products from absorbed light and the intensity of light which saturates photosynthesis (1,2). Both factors are species specific and vary with adaptive changes resulting from changes in environmental conditions or physiological conditions (1,2,24,3). An example of an adaptive change in the efficiency of generation of photosynthetic products is the reduction of carbon incorporation during nutrient limited conditions (1,36). When the growth rate of algae

is restricted by nutrient supply, algae must depress photosynthetic carbon incorporation to maintain balanced growth. An example of an adaptive change in the photosynthetic saturation light intensity (i.e. that light intensity above which photosynthetic production ceases to increase or begins to decline due to photoinhibition) is light-shade adaptation caused by algal self shading or other changes in the underwater light climate (1,37). A light limited algal cell cannot benefit from producing the enzymatic machinery necessary for a high light saturated rate; therefore it will begin to process a smaller number of photosynthetic enzymes per unit of chlorophyll (2). This maximizes the photosynthetic production per unit of cellular carbon invested in the photosynthetic apparatus.

The effect of temperature on algal growth and production is due primarily to the effects of temperature on biochemical reaction rates (31). In the photosynthetic process there are two principal reactions (14). The first reaction is the temperature independent photochemical process in which light energy is absorbed and subsequently transferred into chemical form (e.g. ATP). The second reaction involves the reduction of carbon dioxide through temperature dependent enzyme catalyzed reactions. At high light levels (i.e. near light saturation conditions) the

second reaction controls the rate of photosynthesis (14). The effects of temperature are primarily due to the effects on enzyme molecule characteristics and integrity (31).

Variations in growth limiting nutrients may also significantly affect algal production and growth rates. Phosphorus and nitrogen are generally the two primary growth limiting nutrients with phosphorus limitations being most predominant. There is some evidence that more than half of the lakes in the U.S. east of the Rockies are phosphorus limited (31). Carbon must also be treated as a nutrient and not simply as a source of energy (24,31). Carbon limitation occurs when high cell densities result in rapid removal of carbon dioxide from solution during periods of intense photosynthesis (24). Under these conditions, the rate of carbon uptake is controlled by the rate at which atmospheric CO_2 is dissolved into solution. Micro-nutrients (i.e. essential metals, sulfur) may also be limiting under certain conditions particularly in oligotrophic (low productivity) lakes and reservoirs.

The mixed surface layer depth of a lake and the settling velocity of the algae also affect the density of algal cells in the euphotic zone (which may or may not be deeper than the mixed layer depth). The settling of algal cells out of the mixed layer represents a net

loss in production and growth unless the buoyant capabilities of the cells are such that they can rise back up into the mixed layer (2,40). In some instances these factors may be the primary influence on the sustenance of cell populations of certain algal species. Diatoms, which are characterized by high silica content in their outer shells, have a high cell weight compared with other algal cells and thus sink rapidly in quiesent waters. Diatoms thus need high mixed layer turbulence (resulting in slower sinking rates) and rapid cell division rates to produce cell population expansions (24).

Consumption of algae by predation (i.e. grazing) also affects algal productivity and growth through reductions in cell population densities. Zooplankton and other filter feeding aquatic organisms are the major algal grazers in aquatic systems (31). The amount of phytoplankton biomass consumed by zooplankton has been reported (31) to be a function of both the amount of algae grazed and the digestive efficiency of the zooplankton.

Now that the factors affecting algal production and growth have been defined, mathematical models which express the influences of these factors should be described. From an engineering viewpoint these models are of the most importance for they will allow quantitative predictions of the effects of controlling one or more of the

algal response variables (e.g. nutrient control). In the next two sections (2.6.3 and 2.6.4), various mathematical models for predicting the response of algae to light and other environmental variables and to algal adaptive changes will be discussed.

2.6.3 Light-productivity models

As a first step in the development of a general dynamic model for the growth of algal biomass, mathematical relationships must be obtained to describe the effects of light, light related parameters (i.e. K_c, K_w, etc.) and crop density on the gross photosynthetic production rate (1). Gross photosynthetic production refers to the total amount of oxygen produced or carbon assimilated during the photosynthetic period (24). It differs from the net photosynthetic rate which includes losses due to respiration.

The instantaneous volumetric rate of gross photosynthesis may be expressed generally as (1,2,14):

$$P(I) = P_{max} F(I) \qquad (20)$$

where $P(I)$ = instantaneous volumetric rate of gross photosynthesis at light intensity I (mass C assimilated or oxygen produced per unit volume per unit time)

P_{max} = Maximum volumetric gross photosynthetic rate at optimal or light saturating conditions (same units as above)

F(I) = Photosynthetic rate reduction term which accounts for non-optimal light conditions; equal to 1.0 for optimum light conditions (unitless)

The effects of nonoptimal light conditions (F(I)) may be expressed mathematically through light curve equations (2,14,15,17). Light curves describe the characteristic dependence of the instantaneous rate of photosynthesis on incident light. Two types of light curves are possible: (1) those that exhibit photoinhibition at high light; and (2) those that do not. Photoinhibition occurs when light levels are so high that they become damaging to the algal cell and result in a reduction in photosynthetic production rate. Figure 4 shows generalized representations of these two types of light curves.

Several relationships have been proposed to describe the shape of the light curve, most of which are empirically based (14,15). Studies by Bannister (1,3), Jassby and Platt (17), and Field and Effler (13,14) have found that the light curve relationship most appropriate for describing experimental data is that of a nonrectangular hyperbola which can be expressed as:

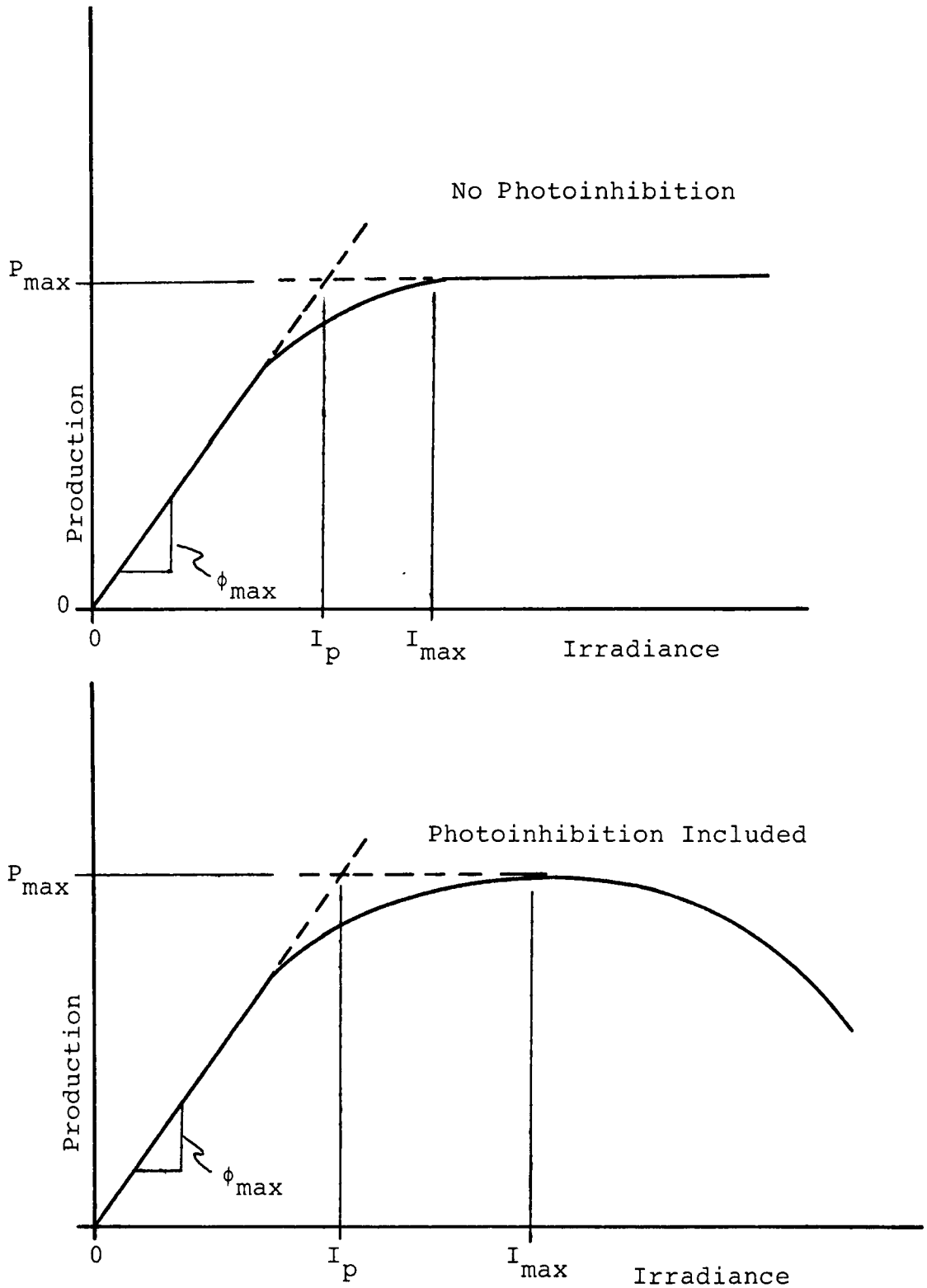

Figure 4. Generalized Representations of Light Curves With and Without Photoinhibition.

$$F(I) = \frac{I}{(I_p^{\,m} + I^m)^{1/m}} \qquad (21)$$

where I = Incident light irradiance

I_p = Light irradiance at which the photosynthetic rate is 70 to 80 percent of the light saturated maximum rate. Defined as the irradiance at the junction of the initial slope of the light curve and $P/P_{max} = 1.0$.

m = A shape parameter that describes the abruptness of the transition from the low light region (where P and I are proportional) to the high light region (where $P = P_{max}$).

Using this equation, the gross photosynthetic rate may be expressed as:

$$P(I) = P_{max} \frac{I}{(I_p^{\,m} + I^m)^{1/m}} \qquad (22)$$

(all terms as defined previously)

Field and Effler (13) have found that the use of an "m" value of 2.0 originally proposed by E. L. Smith (32) was most appropriate for describing the P versus I characteristics of Onondaga Lake in New York. Bannister (3) and Jassby and Platt (17), however, found that an "m" value of 2.5 was most appropriate.

One disadvantage of Equation 21 and 22, however, is that they do not take account of rate reductions due to photoinhibition. Field studies by Tilzer (37) and Megard (26) have shown photoinhibition is common in the upper one or two meters of the euphotic zone where high light intensities occur. The effects of photoinhibition on the profiles of photosynthetic rate with depth are illustrated in Figure 5. As light attenuation increases with depth, the effects of photoinhibition lessen until the light intensity reaches optimum saturating conditions. At this optimum light intensity, the photosynthetic rate reaches a maximum, P_{max}. Below the depth of optimum saturating light, the photosynthetic rate will decrease due to light limitation until total light extinction results in a photosynthetic rate of zero or until the lake bottom is reached. To take account of photoinhibition Steele (35) used an exponential light curve equation that can be expressed as:

$$F(I) = (I/I_{max})e^{1-(I/I_{max})} \qquad (23)$$

where I_{max} = light intensity which saturates photosynthesis

(all other terms as defined previously)

This equation is one of the most commonly used of all light curve equations and has been applied in some

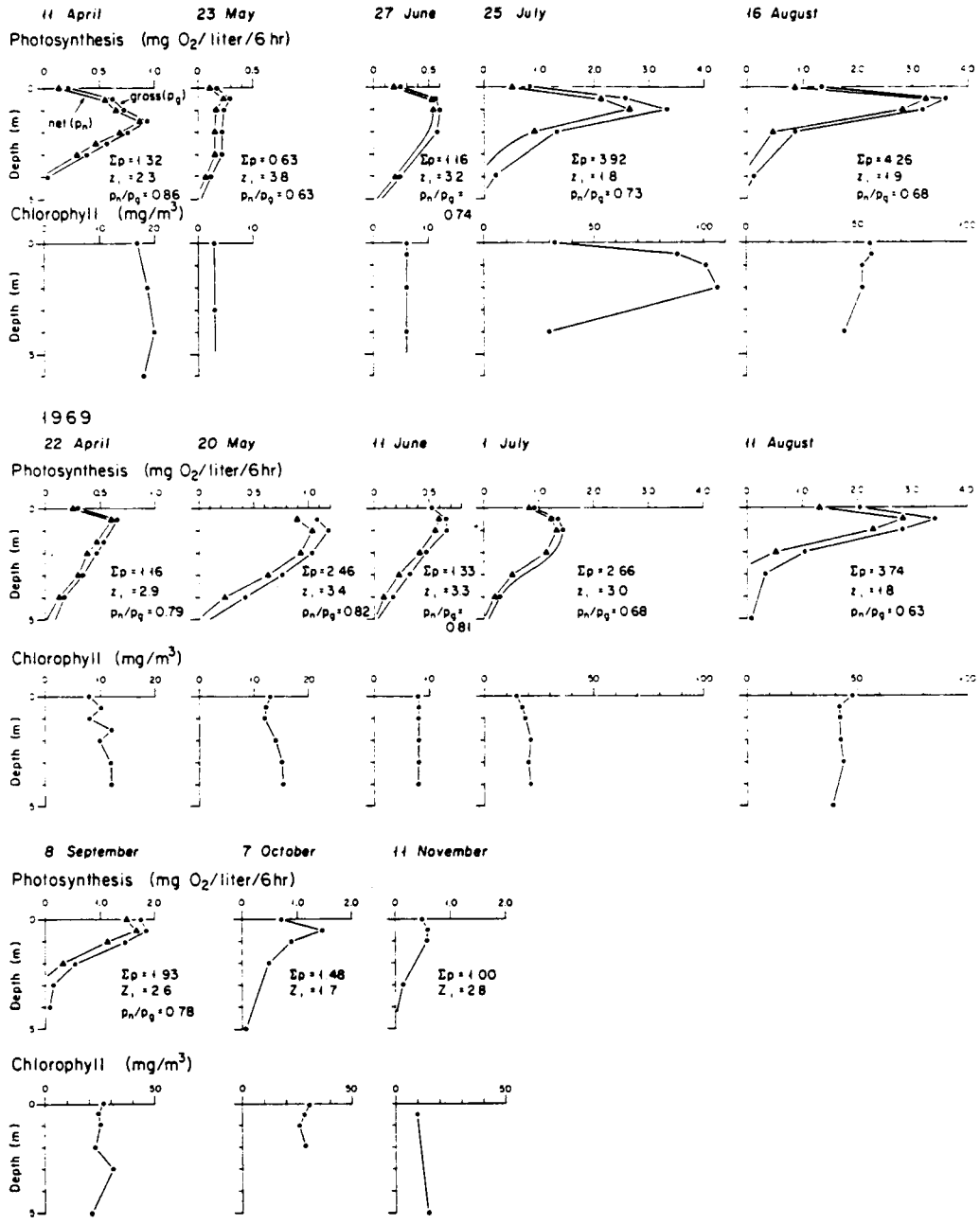

Figure 5. Profiles of Gross and Net Photosynthesis and Chlorophyll a Concentrations in Lake Minnetonka, Minnesota (After Megard (26))

cases to systems which did not demonstrate photoinhibition (17). Platt (17) also developed a light curve equation which considered photoinhibition; this equation is given as:

$$F(I) = \frac{I(1 - I/4I_p)}{I_p} \qquad (24)$$

(all terms as previously defined)

The choice of light curve equation depends solely on which gives the best description of algal response for the water body in question. Before choosing between an equation which includes photoinhibition or one that does not it is recommended that field measurements of productivity be obtained under various ambient sunlight conditions to determine the frequency of occurrence of photoinhibition.

One of the major problems with the light productivity relationships as given above is that the algal related parameters P_{max}, I_p and I_{max} are not always constant but vary with temperature, algal crop density (expressed as chlorophyll a), and the adaptive state of the algae (1). Thus difficulties may occur in applying the above equations, in which the parameters were determined for one set of field conditions, to field conditions at another time. The term P_{max} increases with increasing algal crop density (i.e. increasing chlorophyll a concentration).

The influence of algal crop density on P_{max} may be reduced or eliminated by expressing P_{max} on a unit chlorophyll a basis (i.e. dividing P_{max} by chlorophyll a concentration). Expressing P_{max} in this manner defines the "maximum assimilation number" which is most often designated as γ_{max} (1,14). Using the maximum assimilation number the equation for gross productivity may be written as:

$$\gamma(I) = \gamma_{max} F(I) \qquad (25)$$

where $\gamma(I)$ = The production rate per unit chlorophyll a at light intensity I; mass carbon fixed or oxygen produced per mass chlorophyll a per time; equivalent to P(I)/Chl a.

γ_{max} = Maximum assimilation number; same units as above; equivalent to P_{max}/Chl a.

F(I) = Light curve functions, unitless.

Although γ_{max} should not vary significantly with changes in chlorophyll a, it does vary with temperature and adaptive changes (1,2,14). The effects of temperature on γ_{max} have frequently been characterized by an Arrhenius-type formulation (14):

$$\gamma_{max}(T) = \gamma_{max}(20°C)\,\theta^{(T-20)} \qquad (26)$$

where γ_{max} (20°C) = Maximum assimilation number at 20°C (mg C or O_2/mg Chl a/time)

θ = A constant

T = Actual temperature, degrees C

The effects of temperature on the saturation light intensity parameters I_p and I_{max} have been shown to be coupled to changes in P_{max} (14). Bannister has shown that adaptive changes resulting in variations in algal growth rate also result in adaptive changes in I_p and I_{max} with subsequent variations in P_{max} (2).

Bannister (1,2,3) states that the use of the maximum quantum yield of photosynthesis in weak light, ϕ_{max}, instead of P_{max} provides a much more constant and fundamental productivity equation. ϕ_{max} is determined from the slope of the P versus I curve at low illumination (see Figure 4, page 63). It has long been recognized by plant physiologists that ϕ_{max} is independent of temperature (1). ϕ_{max} is associated with reaction 1 of the photosynthetic process which is the temperature independent photochemical process of light absorption and the subsequent transfer of the energy into chemical forms (14). It has also been shown that ϕ_{max} is less sensitive to the adaptive stage of algae (1,14). Bannister (1) rewrote the equation for gross productivity using the light curve equation of E. L. Smith and the maximum quantum

yield of photosynthesis. This was done by considering an optically thin layer of algal suspension of depth dz and an area of one square meter.

From the differential from of the Beer-Lambert equation, the instantaneous rate of light absorption by algae in the layer is:

$$dI_a = -dI = K_c C I dz \quad (27)$$

where dI_a = Light absorbed by algae (einsteins absorbed/m^2/day)

K_c = Attenuation coefficient by chlorophyll (m^2/mg Chl a)

z = Depth (m)

I = Incident light (einsteins/m^2/day)

C = Chlorophyll a (mg/m^3)

The instantaneous rate of photosynthesis for the layer dz using Smith's equation is:

$$Pdz\,(gC/m^2/day) = P_{max} \frac{I}{(I_p^{\,2} + I^2)^{1/2}} dz \quad (28)$$

(all terms as defined previously)

or expressed in moles of carbon,

$$\frac{Pdz}{12}\,(\text{moles C}/m^2/\text{day}) = \frac{P_{max}}{12} \frac{I}{(I_p^{\,2} + I^2)^{1/2}} dz \quad (29)$$

(dividing by 12 converts mass C to moles C)

The quantum yield may be expressed as:

$$\phi = \frac{Pdz/12}{dI_a} = \frac{P_{max}}{12\ K_c C\ (I_p^{\ 2} + I^2)^{1/2}} \tag{30}$$

The quantum yield will reach a maximum in weak light (i.e. when I becomes small compared to I_p); thus if I becomes small it can be eliminated from the above equation to yield:

$$\phi_{max} = \frac{P_{max}}{12\ K_c C\ I_p} \tag{31}$$

or

$$P_{max} = \phi_{max}\ 12\ K_c C\ I_p \tag{32}$$

Thus the gross productivity rate may now be expressed as:

$$P = \phi_{max}\ 12\ K_c C\ I_p \left(\frac{I}{I_p^{\ 2} + I^2}\right)^{1/2} \tag{33}$$

Of greater interest to the engineer concerned with the control of algal productivity and densities in a lake or reservoir is the daily integral rate of photosynthesis rather than the instantaneous volumetric production rate. Daily integral rate is obtained by integration of the instantaneous volumetric rate over depth and time of the photosynthetic period (i.e. the time of daylight) (1,26,27). It gives a better idea of the total daily

productivity of a lake or reservoir because it is the total daily productivity beneath a unit area of water surface. Vollenweider derived an equation for daily integral productivity using the Smith light curve equation (Equation 21 with m = 2) and assuming that the Beer-Lambert equation applies (1). Vollenweider showed that integration over depth and time gives an equation for daily productivity of the following form:

$$\pi = P_{max}\ \lambda/K_d \int_{-1/2}^{+1/2} \sinh^{-1}(I_o/I_p)\,dt' \qquad (34)$$

where π = Daily integral production ($gC/M^z/day$)

λ = Time in days between sunrise and sunset

$t' = t/\lambda$ = A dimensionless time such that t' is -1/2 at sunrise, zero at noon, and +1/2 at sunset

K_d = Total light extinction coefficient (ln/m)

I_o = Incident solar radiation just below surface of lake (some units as I_p)

Bannister (1) expressed the above equation in terms of the maximum quantum yield as follows:

$$\pi(gC/m^2/day) = \frac{12\phi_{max}\ I_p K_c C\lambda}{K_c C + K_w} \int_{-\frac{1}{2}}^{+\frac{1}{2}} \sinh^{-1}(I_o/I_p)\,dt' \qquad (35)$$

Bannister also simplified the above equation and defined a new term, Ψ, which is the unsurpassable upper limit to daily integral production which would be realized if all incident light was absorbed by phytoplankton. This would occur if the fractional absorbance by algae (i.e. $K_c C/(K_c C + K_w)$ were equal to unity, hence may be derived from Equation 34 as (1):

$$\Psi = 12\phi_{max} I_p \lambda \int_{-\frac{1}{2}}^{+\frac{1}{2}} \sinh^{-1}(I_o/I_p)dt' \qquad (36)$$

where Ψ = Maximum upper limit of daily integral photosynthesis ($mgC/m^2/day$)

Equation 34 may now be rewritten in a simplified form as:

$$\pi = \Psi \frac{K_c C}{K_c C + K_w} \qquad (37)$$

Another relationship for determining daily integral productivity has been described by Megard (26,27) as:

$$\pi = Z' P_{max} \qquad (38)$$

where π = Daily integral photosynthetic rate (mgC or $mgO_2/m^2/day$)

Z' = The average depth where the light intensity begins to be saturating for photosynthesis.

Defined as the depth where subsurface light is reduced to 50% of the intensity at the onset of saturation (m)

P_{max} = The photosynthetic rate at the depth of optimal illumination (mgC or $mgO_2/m^3/day$).

Daily integral production expressed by the above equation is set equal to the area of a rectangle with one side equal to the maximum daily volumetric rate, P_{max}, and the other side equal to the depth, Z'. Megard (27) also rearranged Equation 37 to yield an equation identical to that proposed by Bannister. By assuming the Beer-Lambert equation to apply, the equation was rewritten as:

$$\pi = \frac{\ln(I_o/I_{z'})}{K_d} P_{max} \quad (39)$$

where $I_{z'}$ = illuminance at depth Z' (irradiance units)

(all other terms as defined previously)

The above equation is further rewritten to obtain:

$$\pi = \frac{\ln(I_o/I_{z'})}{K_w + K_c C} P_{max} \quad (40)$$

or

$$\pi = \frac{\ln(I_o/I_{z'})}{K_c C} \frac{K_c C}{K_w + K_c C} P_{max} \quad (41)$$

Now if the fractional absorption by algae were to approach an upper limit of 1.0, then π would equal Ψ thus:

$$\Psi = \frac{\ln(I_o/I_z,)P_{max}}{K_c C} \quad (42)$$

Equation 40 may now be rewritten as:

$$\pi = \Psi \frac{K_c C}{K_w + K_c C} \quad (43)$$

which is exactly identical to Bannister's production equation (Equation 36).

Now that several relationships have been given for calculating algal production as a function of light intensity, light related parameters, and crop density, the question arises "how does one determine the variables and parameters in the equations so that they can be used to predict algal production?" The principal parameters involved in the light-productivity equations are I_p, I_{max}, ϕ_{max}, Z', Ψ, P_{max}, and γ_{max}. Two approaches may be used to determine these values, including:

(1) Obtaining values from the literature which have been determined experimentally by others.

(2) Obtaining values by fitting the production equations to experimental data (gross photosynthetic rates, chlorophyll a, I_o, I_z, etc.) measured in the field or in the laboratory for the water body in question.

EPA (31) has reported values for saturated light intensity (I_p and I_{max}) and maximum specific growth rate

for various species of algae. Maximum specific growth rate, G, may be converted to maximum assimilation number, γ, by the following relationship (14):

$$G_{max} = \frac{\gamma_{max}}{\Theta} \tag{44}$$

where G = Maximum specific growth rate ($time^{-1}$)

γ = Maximum specific assimilation number (mgC/mg Chl a/time)

θ = Weight ratio of cellular carbon to chlorophyll a (mgC/mg Chl a). Reported values range from 60 to 160 mgC/mg Chl a (14).

Values of I_{max} and γ_{max} have also been reported by Lehman et al. (24). Bannister (1) states that the use of a ϕ_{max} value of 0.06 moles C/einstein absorbed will be correct to within a factor of 1.5 or less for most if not all lakes. Experimental data by Field and Effler (14) reported a ϕ_{max} value of 0.07 moles C/einstein absorbed.

Although approximate values for rate constants may be available in the literature, there is obvious merit in determining the actual values which apply to the water body in question. These values are generally obtained by statistically fitting field or laboratory observations to the desired productivity equation. Field and Effler (14) and Jassby and Platt (17) describe a statistical

curve-fitting method which generates values by solving for a minimum error sum of squares. Megard (27) presented a method for evaluating Ψ, the upper limit to daily integral production, by expressing the Bannister equation in a Michaelis-Menten format:

$$\pi = \Psi \frac{C}{(K_w/K_c) + C} \qquad (45)$$

(all terms as defined previously)

The quotient K_w/K_c is analogous to a half-saturation constant and gives the chlorophyll a concentration at which the daily integral rate is equal to 0.5 Ψ. Equation 44 was then written in a form similar to the Lineweaver-Burk equation in enzyme kinetics:

$$1/\pi = 1/\Psi + [(K_w/K_c)/\Psi](1/c) \qquad (46)$$

By plotting $1/\pi$ versus $1/C$, Megard was able to evaluate Ψ as the reciprocal of the y-intercept.

The light-productivity equations presented in this section will not constitute a complete algal dynamic theory for three reasons (2):

(1) They consider only the effects of light conditions on productivity and do not include the influences of limiting nutrients and carbon conditions.

(2) They do not consider loss processes such as respiration, settling, death, and consumption by other microorganisms and filter feeders.

(3) The photoplankton parameters in the equations are not constant but rather undergo adaptive changes.

In the next section it will be shown how a complete algal dynamic model can be developed by inclusion of relationships for loss processes, nutrient limitations, and adaptive changes.

2.6.4 Phytoplankton dynamics models

The basic approach to simulating phytoplankton growth in many models is based upon the following expression (31):

$$\frac{dC}{dt} = (G - D)C = \mu C \qquad (47)$$

where μ = Instantaneous growth rate (day^{-1})

G = Specific growth rate (day^{-1})

= γ/θ (i.e. assimilation number divided by ratio of carbon to chlorophyll)

D = Specific loss rate (day^{-1})

C = Measure of phytoplankton biomass concentration generally expressed as mg Chl a/m^3

The specific growth rate G may be expressed generally by the expression (14,2,40):

$$G = \frac{\gamma_{max}}{\theta} F(I)\ F(N) + E \qquad (48)$$

where γ_{max} = Maximum assimilation number (mg C/mg chl a/day)

θ = Ratio of carbon to chlorophyll a (mg C/mg Chl a)

F(I) = Rate reduction term accounting for non-optimal light conditions (unitless)

F(N) = Rate reduction term accounting for non-optimal nutrient conditions (unitless)

E = Exogenous input (day^{-1})

The specific loss rate of phytoplankton may be expressed as (2,14,31,40):

$$D = R_p + R_g + v/d + M \qquad (49)$$

where R_p = The rate of respiration (day^{-1})

R_g = Grazing rate (i.e. rate of consumption by zooplankton and filter feeders, day^{-1})

v/d = Loss rate due to settling, v is the settling rate of phytoplankton, d is the depth of the wind mixed isothermal surface layer (day^{-1})

M = Mortality or death rate (day^{-1})

Thus the instantaneous growth rate for phytoplankton may be expressed as:

$$\mu = \frac{\gamma_{max}}{\theta} F(I)\ F(N) + E - (R_p + R_g + v/d + M) \qquad (50)$$

The rate reduction term due to nutrient limitation F(N) is most often expressed by a Michaelis-Menten relationship as (14,31):

$$F(N) = \frac{[S]}{K_s + [S]} \qquad (51)$$

where [S] = The concentration of a critical (potentially limiting) nutrient for phytoplankton growth (mass/volume)

K_s = The half saturation constant for phytoplankton growth (i.e. the concentration at which F(N) = 0.5; mass/volume)

Under nutrient saturated conditions when [S] is much greater than K_s, F(N) approaches a value of 1.0. Thus the growth rate of algae is unaffected by increased supplies of nutrients and is affected only by nutrient limiting conditions. Bannister (2,3) suggests that a criterion for nutrient saturation of at least 100 times the half-saturation constant (K_s) be used for phytoplankton growth. Wofsy (40) suggested a criteria of inorganic N > 2 μmole/L and inorganic P > 0.15 μmole/L for nutrient saturation. Various values of the nutrient half saturation constant for phosphorus, nitrogen, silicon, and carbon for various algal species have been reported by Lehman, et al. (24) and EPA (31).

One deficiency of the Michaelis-Menten approach in predicting the effects of nutrient limitation is that it fails to account for the effects of luxury nutrient uptake and storage on growth rate (31). Luxury uptake occurs when there is an excess at some time of a particular nutrient. The nutrient is then stored and used when there is a deficiency of that nutrient. This phenomena is likely to result in overestimation of the impact of short-term transient nutrient deficiencies and a lag in long-term deficiency impacts if the Michaelis-Menten approach is used (31).

Lehman et al. (24) recognized this deficiency of the Michaelis-Menten approach and developed a model which included the effects of nutrient uptake and storage. This model was based on the concept that each algal population may be characterized by a limiting nutrient store capacity (Q_m) and the maximal rates of nutrient uptake diminish as internal nutrient stores (Q) approach the maximal limiting quantity. Nutrient uptake rates were stated to be at a maximum when cell nutrient contents equal a minimum value (k_q) below which cell division cannot proceed. The equation for nutrient uptake rate was given as:

$$u = [(Q_m - Q)/(Q_m - k_q)]\ u_{max}\ S/(K_s + S) \qquad (52)$$

where u = Nutrient uptake velocity by algae (μmoles/cell/hr)

u_{max} = Maximum nutrient uptake velocity (same units as above)

Q = Quantity of nutrient in cell (μmoles/cell)

Q_m = Maximum nutrient storage capacity of cell (μmoles/cell)

k_q = Minimum cell nutrient content below which cell division cannot proceed (μmoles/cell)

S = External nutrient concentration (μmole/L)

K_s = Nutrient half saturation constant for phytoplankton growth (μmole/L)

The nutrient dependence (ND) on cell growth rate was given by:

$$ND = (Q - k_q)/Q \tag{53}$$

(all terms as defined previously)

The effects of nutrient dependence on growth rate was given by:

$$\mu_{cell} = (\mu_{cell})_{max} (T) \times ND \tag{54}$$

where μ_{cell} = The specific cell division rate, day^{-1} (Lehman used number of cells as a biomass growth indicator rather than mg Chl a as in all previous equations in this section).

$(\mu_{cell})_{max}$ (T) = The maximum cell division rate, day^{-1}, at temperature T

ND = Nutrient dependence factor (unitless)

The Lehman et al. model thus recognizes nutrient uptake rates as fractions of both internal and external nutrient levels but maintains that cell growth (expressed in terms of cell division rate) is dependent only on internal concentrations. This allows modeling of situations in which dissolved phosphorus and nitrogen disappear (through rapid algal uptake) following artificial enrichment of a lake, but produce long-term growth effects on the algae that absorb them.

Lehman et al. (24) treated carbon uptake in a manner similar to nutrient uptake and developed separate equations for carbon uptake (i.e. photosynthetic production rate) and growth rate (defined in terms of cell division rate). The equation for carbon uptake was given as:

$$P(I,C) = [(C_m - C)/(C_m - C_o)]P(I) \qquad (55)$$

where P(I) = Carbon fixation rate at light intensity I (mg $C/m^3/day$)

C_m = Maximum carbon store capacity (μmoles/cell)

C_o = Growth limiting carbon content (μmole/cell)

C = Carbon content of cell (μmole/cell)

This equation allows for end-product inhibition when carbon stores become too great. This end product inhibition is often manifested by depressed afternoon carbon fixation rates following periods of intense carbon fixation. The effect of carbon dependence (CD) on growth rate was expressed as:

$$CD = (C - C_o)/C \tag{56}$$

The combined effects of nutrient and carbon dependence on growth rate was expressed as:

$$\mu_{cell} = (\mu_{cell})_{max} (T) \times ND \times CD \tag{57}$$

(all terms as defined previously)

Specific values for Q_m, k_q, u_{max}, C_m, and C_o were also tabulated for various algal species (24).

Exogenous input to the euphotic zone may occur from several processes including inflow from other streams or reservoirs, reintroduction of algae (which have previously settled) by the buoyancy mechanisms of the cells, diffusive vertical transport from the lower layers, and advective vertical transport from the lower layers (16,40). Gulliver and Stefan (16) developed an algal model which included diffusive and advective transport to the euphotic zone which was considered as a completely mixed layer. In this model the diffusive transport of

algae to the surface mixed layer from the hypolimnion was governed by the equation:

$$J_{CD} = D_z \frac{dc}{dz} \tag{58}$$

where J_{CD} = The diffusive transport of algae (which have previously settled out of the mixed layer) back into the mixed layer ($M/L^2/T$)

D_z = Vertical eddy diffusion coefficient (L^2/T)

$\frac{dC}{dz}$ = Algal concentration gradient (M/L^4)

The transport was described as being vertically upward (into the mixed surface layer) rather than downward towards the sediments because of weak vertical temperature gradients and strong algal concentration gradients in the hypolimnion with the highest concentrations being at the lower depths. Diffusive transport within the surface mixed layer was equal to zero because in this layer dC/dz is zero.

The Gulliver and Stefan model (16) also had an advective transport component. This was added to describe the upward transport resulting from the installation of a compressed air bubbling device which was being used in the modeled reservoir to test the effects of destratification. The effect of the air bubble plume was to entrain and transport water from the deeper parts of the

lake to the surface. The advective transport was modeled as:

$$J_{CM} = f_m C \tag{59}$$

where J_{CM} = Advective transport of algae into mixed surface layer ($M/L^3/T$)

f_m = A constant representing the fraction of the phytoplankton concentration which is entrained and carried upward (T^{-1})

C = Phytoplankton concentration at any particular depth (M/L^3)

The rate of increase in algal biomass including all losses, inputs, and growth was modeled by Gulliver and Stefan (16) by dividing the subject lake into a series of layers of depth, Δz, and using the following expression:

$$\frac{dCi}{dt} = C_i\left(G - R_p - \frac{V}{\Delta z}\right) + C_{i-1}\frac{V}{\Delta z} + J_{CD} - J_{CM} \tag{60}$$

where C_i = Algal biomass in layer i (M/L^3)

C_{i-1} = Algal biomass in adjacent layer above layer i

G = Specific growth rate (T^{-1})

R_p = Respiration rate (T^{-1})

V = Algal settling velocity (L/T)

Δz = Thickness of each layer

t = Time

(J_{CD}, J_{CM} are as defined previously)

Zooplankton grazing was not considered in the model because it was said not to be significant for the lake studies. Boundary conditions for the model were zero fluxes across the water surface and zero diffusive flux of phytoplankton at the bed of the lake (16).

Reductions in algal biomass due to cell sinkage are modeled generally as v/d (i.e. algal settling velocity divided by mixed layer depth). Algal settling involves several complex processes including vertical turbulence effects, vertical density distribution, and the physiological state of the different species of phytoplankton (31). In regard to the physiological effects on settling, three points are worth noting (31):

(1) The generation of gelatinous sheaths by phytoplankton affects settling. This sheath may occur as adaptive change.

(2) The settling velocity of nutrient rich cells is somewhat lower than that of nutrient deficient cells.

(3) The phytoplankton settling velocity may be zero or cells may be sufficiently buoyant to move upward in the water column.

The losses of cellular carbon due to respiration are generally modeled as the parameter R_p. Respiration rate is not constant but varies with light levels, carbon stores, and temperature (16,24,17). Jassby and Platt (17)

provided an equation for correcting the respiration rate for influences of light:

$$(R_p)_{light} = r \frac{\gamma(I)}{\Theta} + R_p^B \quad (61)$$

where $(R_p)_{light}$ = The respiration rate in sunlight (day^{-1})

$\gamma(I)$ = Assimilation number at light intensity, I (mg C/mg Chl a/day)

Θ = Ratio of carbon to chlorophyll (mg C/mg Chl a)

r = A constant fraction of the recent photosynthate which is respired in addition to the basal respiration level R_p^B

R_p^B = Basal rate of respiration which is constant throughout the day (day^{-1})

Jassby and Platt, however, did not give specific values for the constant r.

The effect of carbon stores and temperature on respiration rate has been given by Lehman et al. (24) as:

$$R_p = (R_p)_{max} (C/C_m)^{0.67} \exp [2.3(T - T_{opt})/(T_{11} - T_{opt})] \quad (62)$$

where $(R_p)_{max}$ = The maximum respiration rate obtained at $T = T_{opt}$

C = Cell carbon content (μmole/cell)

C_m = Maximum carbon store capacity (μmole/cell)

T = Water temperature

T_{opt} = Optimum water temperature for algal growth

T_{11} = Lower limit of water temperature for algal growth

Lehman et al. also present published values of $(R_p)_{max}$ for various algal species. Gulliver and Stefan (16) have also presented an Arrhenius type relationship to show the effects of temperature on respiration rate:

$$R_p = R_p(20°C)^{T-20} \tag{63}$$

where $R_p(20°C)$ = Respiration rate at 20°C

= 0.1 day^{-1} (obtained from literature)

= 1.06

T = Water temperature (°C)

Phytoplankton loss due to grazing by zooplankton and other herbivores (R_g) is a complex process and only a rough approximation of the process can be modeled (31). The phytoplankton represent a food source for the herbivores and phytoplankton blooms are often associated

with succeeding blooms of herbivorous zooplankton (31). Bannister (2) developed a graphical method for evaluation of R_g based on the assumption that herbivorous consumers behave in such a manner as to maximize their daily harvest of phytoplankton carbon. Another relationship for computing phytoplankton grazing rate has been reported by EPA (31) in a Michaelis-Menten equation form:

$$R_g = C_g Z \frac{P}{K_{mp} + P} \tag{64}$$

where C_g = Grazing rate of herbivorous zooplankton (Liter/day/mg zooplankton carbon)

Z = Zooplankton carbon concentration (mg/L)

K_{mp} = Half-saturation constant for zooplankton grazing on algae (mg/L)

P = Algae concentration (mg/L)

EPA (31) has reported algal grazing rates for several different species of zooplankton.

The physiological death rate (M) of algae is often considered to be insignificant in algal dynamics modeling. It has been reported that natural mortality of actively dividing marine diatom populations is less than 1% of either daily production or grazing rates (24). However, under extreme suboptimal conditions physiological death becomes significant. The longer a population remains at these conditions the greater the mortality effects

become until some maximum fraction M_{max} of the population dies each day (32). Lehman et al. reports that the mortality rate under suboptimal conditions may be expressed as (32):

$$M = M_{max} [1 - \exp (-k\ SG)] \quad (65)$$

where M = Mortality rate (day^{-1})

M_{max} = Maximum mortality rate (day^{-1})

SG = Number of days at suboptimal conditions

k = (ln 2) divided by the number of days at suboptimal conditions until M reaches half of M_{max}

Lehman, however, did not give any typical values for M_{max}.

Mathematical relationships have now been defined for each loss, input, or growth process in the algal growth rate equation (Equation 49) and the effects of suboptimal light and nutrient conditions have been defined. However, for the algal dynamic theory to be complete, the effects of adaptive changes on the algal parameters must be considered. Bannister (2) provided a detailed evaluation of the effects of adaptation. In this evaluation the adaptive changes in I_p (the photosynthetic light saturation intensity), θ (the carbon to chlorophyll a ratio) and R_p (the rate of respiration) were shown to

be related to changes in growth rate. The relationships between growth rate and adaptive variations were obtained from experimental data in which the algal species Chlorella pyrenoidosa was grown turbidostatically (constant K_w) under nutrient saturated conditions in continuous light ranging from saturating to very weak light. The growth rate varied in relation to the changes in light intensity. The adaptive relationships were presented graphically by Bannister.

One of the major problems with the algal dynamics models discussed in this section is that they describe many complex processes and thus contain several rate coefficients (e.g. half-saturation constants, settling rates, grazing rates, death rates, etc.). This creates a problem in modeling because measurement of each coefficient in the field or in the laboratory would be time consuming and costly. These values are thus often obtained from the experimental work of others described in the literature. This may lead to substantial errors if the coefficients chosen are from water bodies which contain algal populations of dissimilar species, different adaptive state, or which respond to environmental variables in a substantially different manner. Nevertheless, if care is taken in choosing algal parameters from the literature or if many of the parameters are measured for the reservoir

under consideration, these algal models should provide good predictive results for the assessment of reservoir management strategies.

2.7 Summary

This literature review has presented the concepts and mathematical models for evaluating the influence of environmental variables on the attenuation of light in lakes and reservoirs and also on algal productivity and growth. Two models were presented for the evaluation of factors affecting light attenuation, one relies on the regression of the vertical light extinction coefficient, K_d, on the concentrations of various attenuating substances. The other method, however, describes light attenuation in terms of the fundamental processes which cause light attenuation; absorption and scattering. Once the coefficients of absorption and scattering have been defined, regression analyses can be used to determine the influence of concentrations of various attenuating substances on these coefficients and hence on K_d. Although the second method is desirable to use because it expresses light attenuation as functions of the two fundamental attenuation variables, absorption and scattering, it is based upon complex and difficult to obtain field measurements (i.e. radiance distributions, volume scattering

function). Kirk (19,20) utilized computer simulations to simplify this method to an easily useable format, however, his simplifications were based on assumed radiance distributions and volume scattering functions which may not be applicable to the water body under investigation. The first method, however, relies only upon simple regression analyses and thus does not suffer from the complexities of the latter method. The first method does not separate attenuation into absorption and scattering components but rather gives the fraction of the total attenuation due to various attenuating substances. From an engineering viewpoint, this method should be able to provide the necessary information about light attenuation. Generally one is most interested in what fraction of the total decrease in light penetration is due to particular substance and what increases in transparency would occur if reductions in this substance were to occur rather than what percentage of attenuation is due to absorption or to scattering. Thus, the first method should provide all the necessary information. In addition the first method can be used to provide a value for K_c (the attenuation coefficient due to algae) which is a necessary variable for some algal production models.

Light-productivity models were described which predict the influence of light on algal photosynthetic

rates and hence on biomass growth rate. These models were of two types, those that include photoinhibition at high light and those that do not. In deciding which of these to use for predictive purposes, one should obtain field measurements of productivity at various times of the year to determine the frequency of occurance of photoinhibited production (i.e. rates at surface layer less than rates at deeper depths).

These light-productivity models, however, define algal production rates only in terms of light conditions and do not include the effects of loss processes (e.g. respiration, settling, grazing, death), nutrients, carbon, or adaptive changes on algal growth. Several models were presented which account for these other factors and thus constitute models of algal dynamics. One of the major problems with models of algal dynamics is that they generally contain many rate coefficients (e.g. half-saturation constants of nutrient uptake, settling rates, respiration rates, death rates, grazing rates, etc.) which add to the complexity of the models. These constants must either be measured for the water body in question or must be obtained from the literature. Because of the expense that would be required for actual laboratory or field measurements of each constant, values obtained from the literature are often used. This could result

in modeling errors if the literature values used are from a dissimilar reservoir. Nevertheless, algal dynamics models should provide useful predictive information for assessing the benefits derived from various reservoir management strategies.

In the following sections, the information presented in this literature review will be used to determine the major influences on light attenuation in Boone Reservoir. It has been suspected that algae are the major factor controlling light attenuation, these analyses will thus be used to quantitatively define the fractional attenuation due to algae. Also by using the light attenuation relationships derived and actual field measurements of production, the response of algae to light will be modeled. This will provide needed information for more detailed reservoir computer models or algal dynamics models which can in turn be used to predict algal biomass reductions resulting from nutrient control strategies.

Prior to the evaluation of light attenuation and algal productivity in Boone Reservoir, a brief summary will be given of the sample collection methods and field and laboratory analyses techniques used during the water quality surveys on Boone Reservoir.

CHAPTER 3

METHODS

Measurements of underwater irradiance, secchi disc depth, turbidity, light transmission, algal fluorescence, chlorophyll a, pheophytin, photosynthetic productivity, and enumeration of algal species were made once each month on Boone Reservoir during May through August, 1984. All data collection was performed by the Tennessee Valley Authority, Division of Services and Field Operation. The author, who is an employee of the above organization, was involved in the planning and implementation of each data collection activity. Laboratory analyses were performed by the Tennessee Valley Authority, Laboratory Branch.

Table 2 and Figure 6 specify the location of each monitoring station and the type of measurements conducted at each station. Stations were selected to adequately define spatial variations in water quality throughout the reservoir.

Underwater irradiance was measured using a KAHLSICO Underwater Irradiameter (Model No. 268WA310). This instrument measured irradiance in microwatts/cm^2 for the PAR waveband of 400 to 700 nm and included both ambient (deck cell) and underwater photosensors. Each

TABLE 2

Boone Reservoir Water Quality Study--Field and Laboratory Analyses Conducted

Station	Map ID No.	Underwater Irradiance	Secchi Depth	Turbidity and Transmissivity, Fluorescence	Chlorophyll a,b,c and Pheophytin	Primary Productivity
SFHRM 19.0	1	X	X	X	X	X
SFHRM 22.4	2	X	X	X	X	X
SFHRM 25.0	3	X	X	X		
SFHRM 26.2	4	X	X	X	X	X
SFHRM 28.3	5	X	X	X		
SFHRM 30.8	6	X	X	X	X	X
SFHRM 32.4	7	X	X			
WRM 2.0	8	X	X	X	X	X
WRM 3.0	9	X	X	X		
WRM 6.0	10	X	X	X	X	X
WRM 8.4	11	X	X	X		
WRM 10.95	12	X	X	X	X	X
WRM 13.0	13	X	X	X		

Figure 6. Boone Lake Area Map

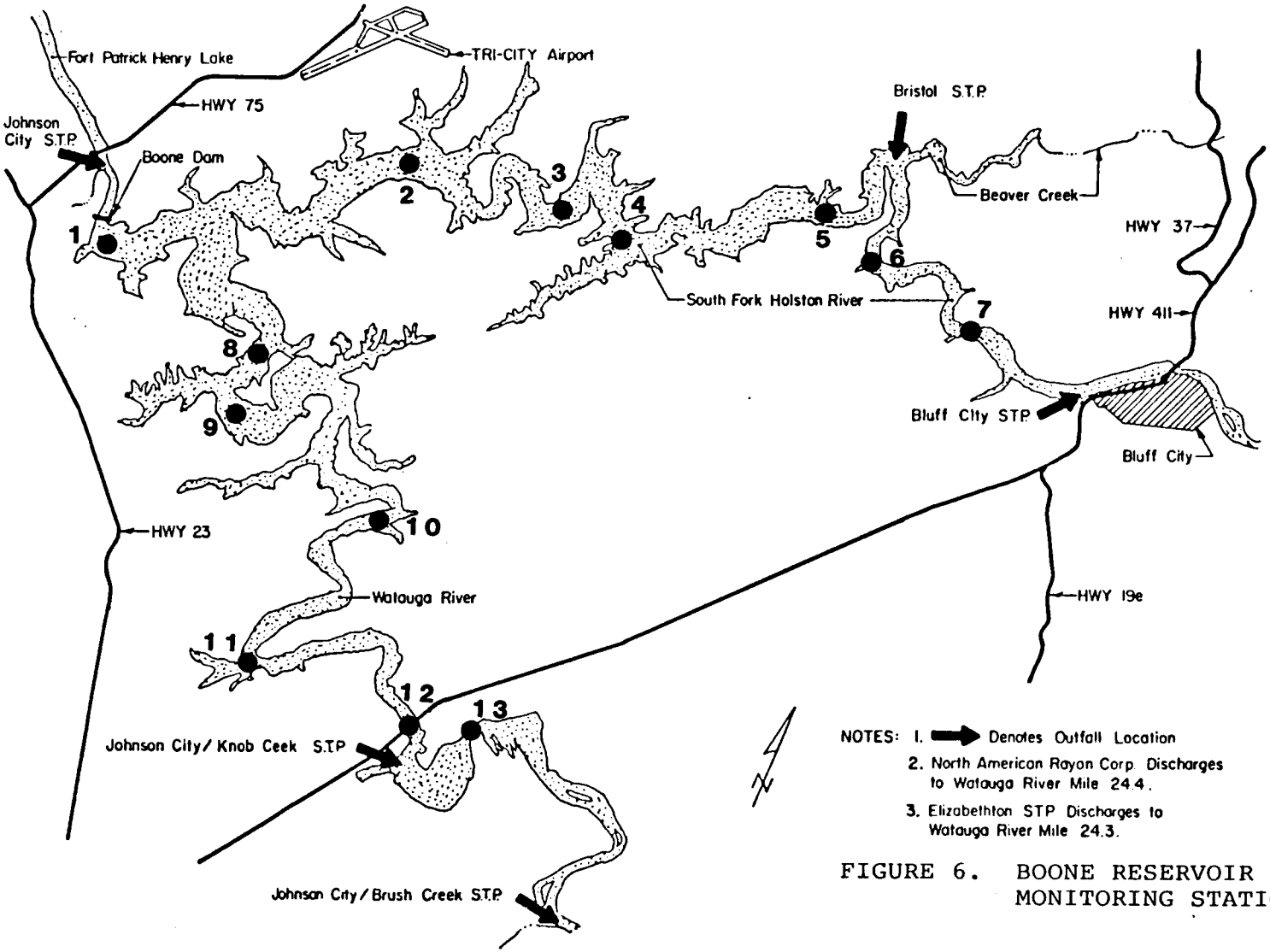

FIGURE 6. BOONE RESERVOIR MONITORING STATIONS

photosensor was furnished with a Lambert cosine corrector plate which accepted light in proportion to the cosine of the angle of incidence. The underwater photosensor was lowered to the desired depth and a reading of underwater irradiance was taken. Simultaneously, an ambient light reading was taken. Measurements were made at depths of 0.3 meters, 1 meter, and then at one meter increments down to a depth of 12 meters.

Turbidity and light transmission (i.e. transmissivity) were measured insitu through use of a Montedoro-Whitney Model TMU-1B Field Nephelometer-Transmissiometer. The transmissometer function of instrument measured the percent transmission of a light beam through a fixed path length while the nephelometer function measured the light scattered at a 90 degree angle (i.e. the turbidity). Insitu measurements of turbidity and transmissivity were made at the same depths as underwater irradiance.

Algal fluorescence was measured insitu using a Turner Designs Model 10-005 Field Fluorometer. The instrument was present to sense the fluorescence of chlorophyll a. This was done through the proper selection of fluorometer excitation lamp and emission, excitation and reference filters. The excitation lamp used was a F4T5 blue lamp. The excitation, emission, and reference filters used were of color specification 5-60, 2-64, and

3-66, respectively. The use of these lamps and filter combinations allowed the measurement of chlorophyll a fluorescence at optimum sensitivity.

Chlorophyll a and pheophytin were measured in the laboratory for samples collected as depth integrated composites from surface to 3 meters, and as discrete samples at 6 meters. Samples of the surface to 3 meter composite depth were collected and analyzed in duplicate. Chlorophyll and pheophytin analyses were performed in accordance with Standard Methods (34).

Phytoplankton photosynthetic productivity (i.e. primary productivity) was measured using the carbon 14 method. The analyses were conducted using surface to 3 meter depth integrated samples. The composite sample water was placed into light (transparent) and dark (completely sealed from light entry) bottles and dosed with radioactive sodium bicarbonate solution which had an activity of 1.0 μCi/L. The sample bottles were then placed underwater and incubated at various depths for four hours near solar noon. For each primary productivity analysis, two dark bottles and three light bottles were incubated at 0.5 meters, three bottles were incubated at 1.0 meter, two light bottles were incubated at 2.0 meters, and two light bottles and two dark bottles were incubated at 3.0 meters. Alkalinity and pH measurements

were made from a surface to 3 meter depth integrated sample for each primary productivity sampling station. These alkalinity and pH measurements were used to calculate the concentrations of dissolved inorganic carbon available for photosynthesis. Following incubation, the contents of each incubation bottle was filtered through a 0.45 micron filter to remove all algal cells. The activity of the assimilated radioactive carbon present on each filter was then measured in the laboratory. The volumetric primary production was then determined as mgC/m^3 for each incubation depth. The production rates at each station were then integrated over the depth of the euphotic zone to obtain the rate per unit surface area (mgC/m^2). To obtain the daily integral rate of photosynthesis, each production rate per unit surface area was multiplied by the ratio of the total solar energy during the incubation period to the total solar energy from sunrise to sunset. This ratio was determined by use of a solar pyrheliometer which was set up near the sampling stations. This resulted in the photosynthetic production rate expressed as $mgC/m^2/day$.

Samples for algal enumeration were collected as depth integrated composites of the surface to 3 meters depth. From each sample the algal groups present were identified along with the number of cells in each group and the number of genera in each group.

CHAPTER 4

RESULTS AND DATA ANALYSES

The results of underwater irradiance, algal fluorescence, chlorophyll a, turbidity and algal enumeration measurements are presented in Appendices I to IV. Results of algal production measurements are given later in this chapter. The following discussion presents an analysis of these results including an evaluation of the light attenuation factors in Boone Reservoir and their influence upon algal productivity.

The analyses will begin with an evaluation of the total light extinction coefficient, K_d, at various locations within the reservoir. This coefficient will then be partitioned into various attenuation components to determine which substance or substances present in the reservoir are controlling light attenuation with depth. Finally using field measurements of algal production rate and derived attenuation coefficients, the applicability of various light-productivity models will be evaluated.

These evaluations should provide needed information for the assessment of future reservoir management strategies for Boone Reservoir. These assessments may involve the use of reservoir computer models which contain algal dynamics components. The data analyses and

interpretations provided herein should facilitate the assessment of reservoir management strategies by providing actual values of necessary modeling coefficients and by pointing out areas where additional data is required.

4.1 Light Attenuation

4.1.1 Evaluation of K_d

The results of underwater irradiance measurements and secchi disc depths are presented in Appendix I. Irradiance measurements are given only down to the depth of the euphotic zone which is defined as the depth of approximately 1% available light. Presentation of the results of deeper readings would be of little use as light attenuation is nearly complete at the depth of the euphotic zone.

The coefficient of extinction for downward irradiance, K_d, was computed from the Beer-Lambert equation

$$I_z = I_o \, e^{-K_d z} \qquad \text{(Equation 5)}$$

$$\text{or } \ln(I_o/I_z) = K_d z \qquad \text{(Equation 6)}$$

K_d was determined from the field data as the slope of the linear regression of $\ln(I_o/I_z)$ versus depth. K_d calculated in this manner represents the average value for the

euphotic zone depth. Thus if the optical properties vary with depth in the euphotic zone (i.e. variations in attenuation coefficient with depth), the calculated value will be the average of the various K_d values which exist in the euphotic depth.

K_d was computed from field data in two manners. First, the regression was performed using the entire euphotic zone depth starting at the air-water interface. Since no values of irradiance were made immediately below the air-water interface, values for I_o had to be calculated from the ambient (above water) irradiance measurements and assuming a 10% water surface reflectance. Thus I_o was calculated as:

$$I_o = I_{ambient} \times 0.90 \qquad (66)$$

The obvious source of error using this method is that reflectance from the water surface is hard to predict and will vary with the angular height of the sun (i.e. it varies with time of day). The reflectance value of 10% is a commonly reported average value for water surface reflectance (10,39). Values of I_o were computed for each measurement depth and used with the underwater irradiance I_z for that depth to compute $\ln(I_o/I_z)$. Values for z equaled the depth from the water surface to the depth of measurement of I_z.

The second method for computing K_d also involved linear regression of $\ln(I_o/I_z)$ versus depth, however, the depth of the water column down to the first underwater irradiance measurement (i.e. the first 0.3 meters) was neglected. The light measurement at 0.3 meters was taken as I_o and values of $\ln(I_o/I_z)$ were computed with reference to this irradiance value. Values of I_o were assumed to vary with time in proportion to variations in ambient sunlight. Thus the value of I_o used to calculate $\ln(I_o/I_z)$ was:

$$I_o = \frac{I_{\text{ambient at time of measurement of } I_z}}{I_{\text{ambient at time of measurement of } I_{0.3m}}} \times I_{0.3m} \quad (67)$$

The depth z was equivalent to the measurement depth less 0.3 meters.

The results of K_d computations are given in Table 3. Also shown in this table are values of the correlation coefficient (r^2) for $\ln(I_o/I_z)$ versus depth, z. Figure 7 illustrates the fit of the exponential Beer-Lambert equation to the field data for various locations and months. The high correlations between $\ln(I_o/I_z)$ and depth, z, signify the exponential nature of the decreases in irradiance with depth observed in the field. These high r^2 values also indicate that in most cases greater than 99% of the observed variability in $\ln(I_o/I_z)$ was due

TABLE 3

Vertical Light Extinction Coefficients for Downward Irradiance, K_d (ln/m), Computed from Field Measurements--Methods 1 and 2--Boone Reservoir, May to August, 1984

Station	May				June				July				August			
	Method 1	r^2	Method 2	r^2	Method 1	r^2	Method 2	r^2	Method 1	r^2	Method 2	r^2	Method 1	r^2	Method 2	r^2
SFHRM 19.0	1.17	0.997	1.12	0.996	0.92	0.990	0.88	0.999	0.76	0.989	0.70	0.988	0.47	0.999	0.47	0.999
SFHRM 22.4	1.12	0.999	1.13	0.999	0.96	0.998	0.96	0.999	0.85	0.972	0.80	0.955	0.59	0.996	0.61	0.997
SFHRM 25.0	1.04	0.980	0.91	0.975	1.04	0.999	1.03	0.998	0.75	0.985	0.79	0.999	0.72	0.945	0.53	0.997
SFHRM 26.2	1.08	0.997	1.06	0.997	1.04	0.999	1.06	0.998	0.83	0.993	0.76	0.997	-	-	-	-
SFHRM 28.3	1.25	0.999	1.24	0.998	1.04	0.980	0.86	0.998	0.88	0.998	0.86	0.997	0.72	0.998	0.69	0.998
SFHRM 30.8	1.14	0.940	1.21	0.999	1.11	0.995	1.02	0.999	1.20	0.955	0.82	0.992	0.83	0.996	0.80	0.996
SFHRM 32.4	-	-	-	-	-	-	-	-	-	-	-	-	0.56	0.997	0.53	0.999
WRM 2.0	1.04	0.993	0.96	0.994	0.72	0.997	0.79	0.999	0.54	0.917	0.33	0.984	0.55	0.986	0.54	0.976
WRM 3.0	1.32	0.999	1.36	0.998	1.11	0.984	1.11	0.972	0.97	0.890	0.53	0.995	0.56	0.987	0.48	0.990
WRM 6.0	1.38	0.986	1.31	0.972	1.28	0.972	0.96	0.997	1.14	0.995	1.07	0.996	0.82	0.975	0.66	0.991
WRM 8.4	1.79	0.988	1.51	0.996	1.40	0.999	1.44	0.999	1.26	0.995	1.14	0.999	1.02	0.997	0.97	0.997
WRM 10.95	2.35	0.997	2.60	1.00	2.73	0.992	3.22	1.00	1.52	0.989	1.29	0.999	0.64	0.955	0.43	0.927
WRM 13.0	-	-	-	-	-	-	-	-	-	-	-	-	0.79	0.980	0.65	0.999

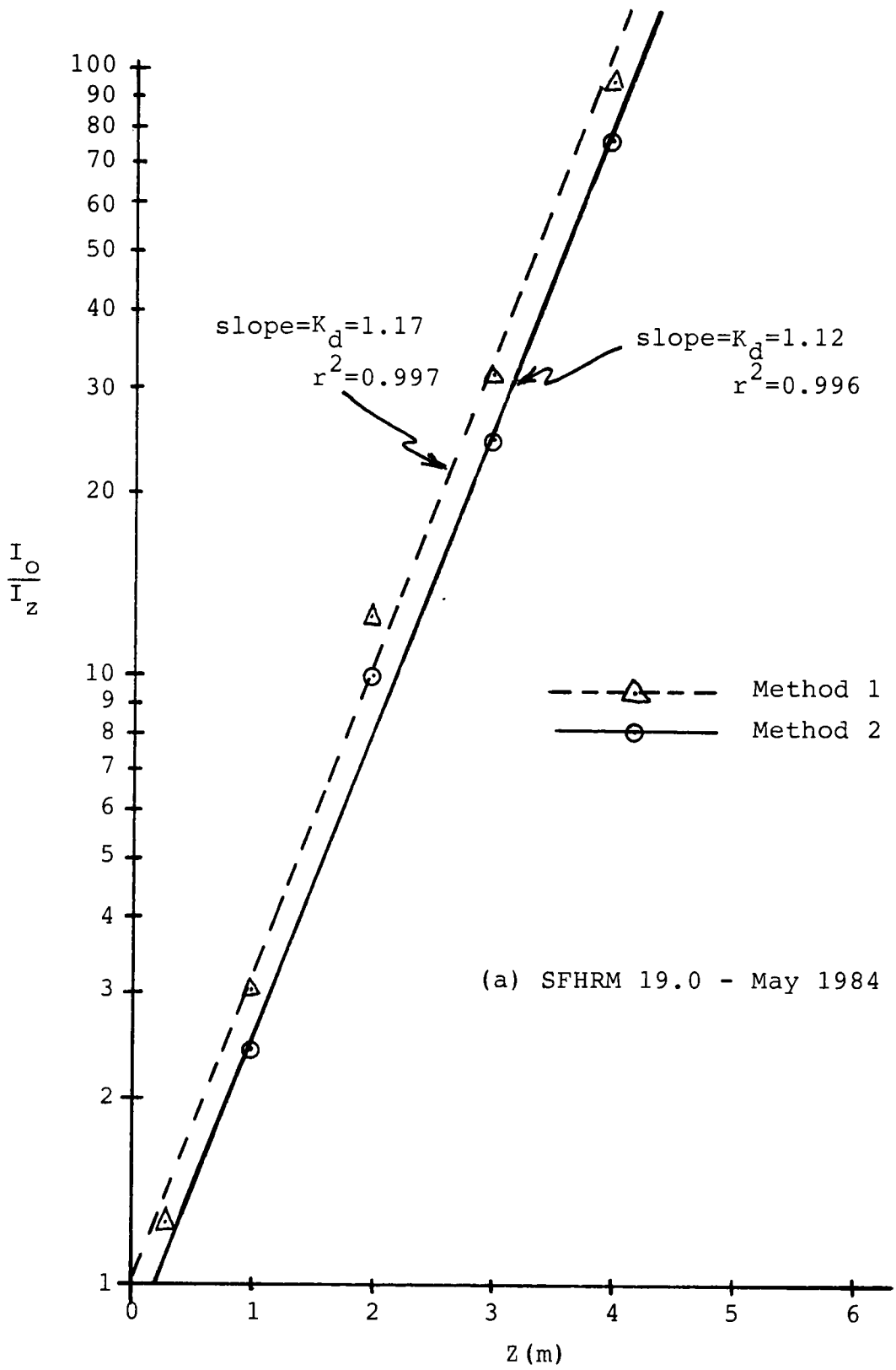

Figure 7. ln (I_o/I_z) Versus Depth (Z)

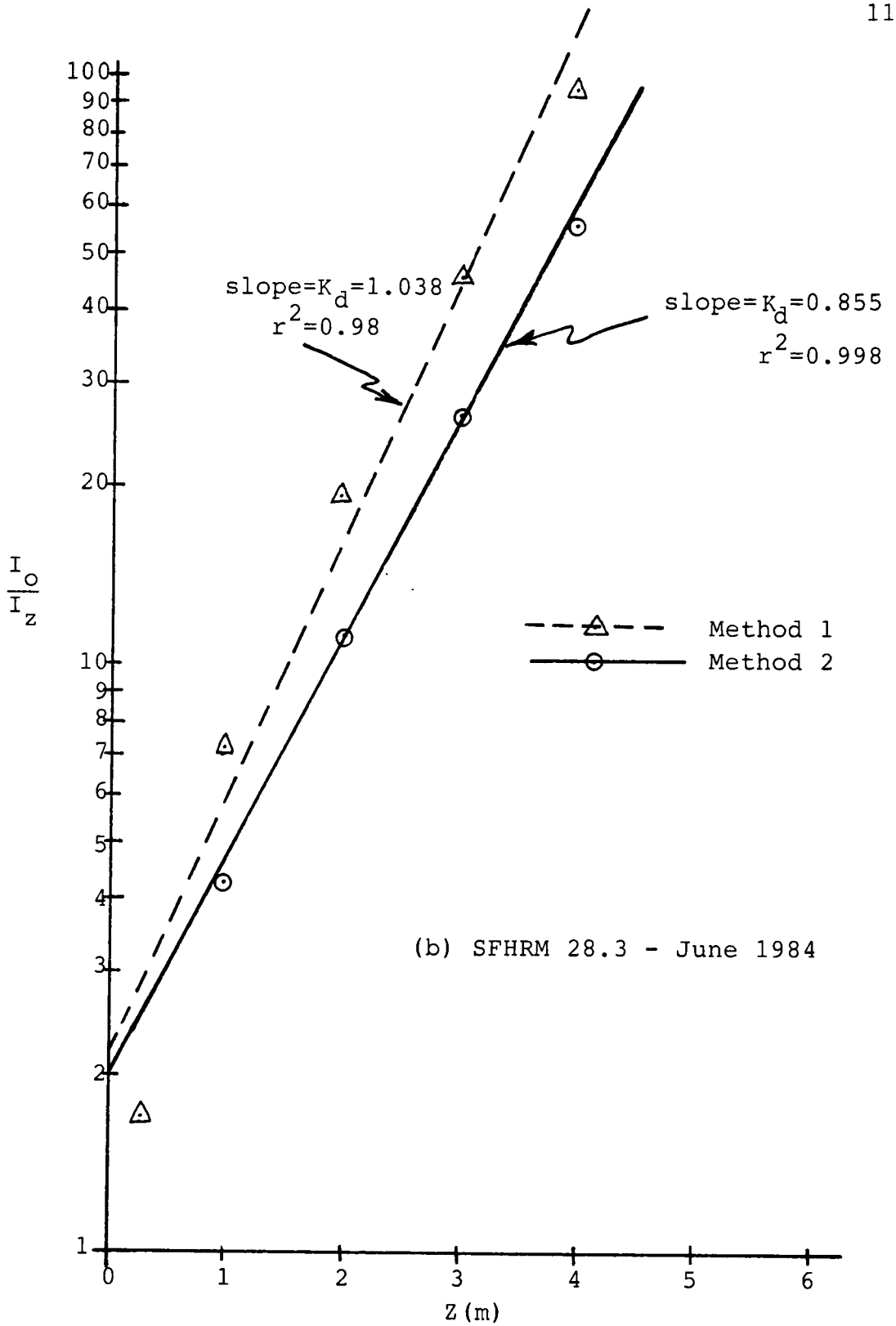

Figure 7 (Continued)

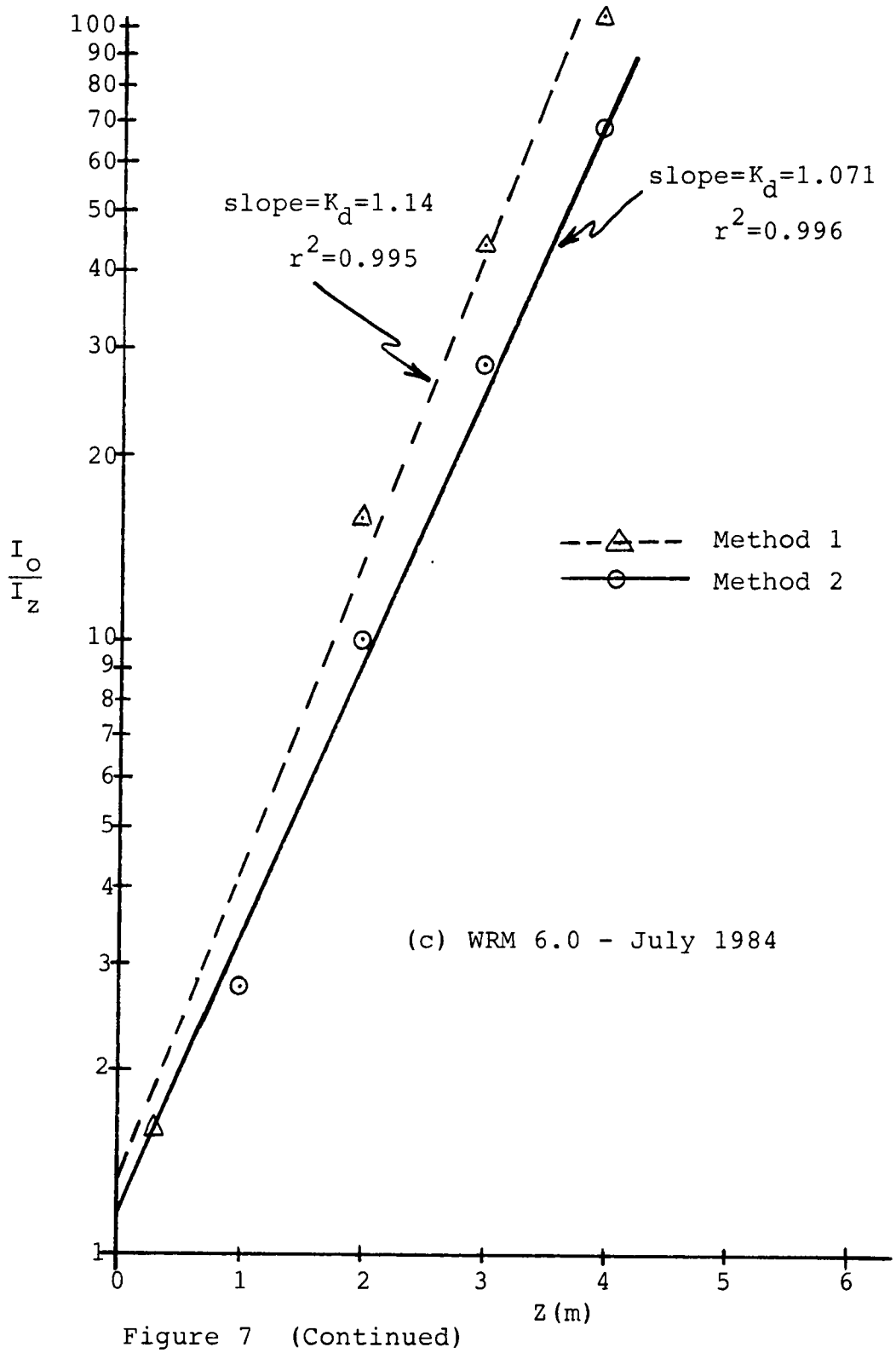

Figure 7 (Continued)

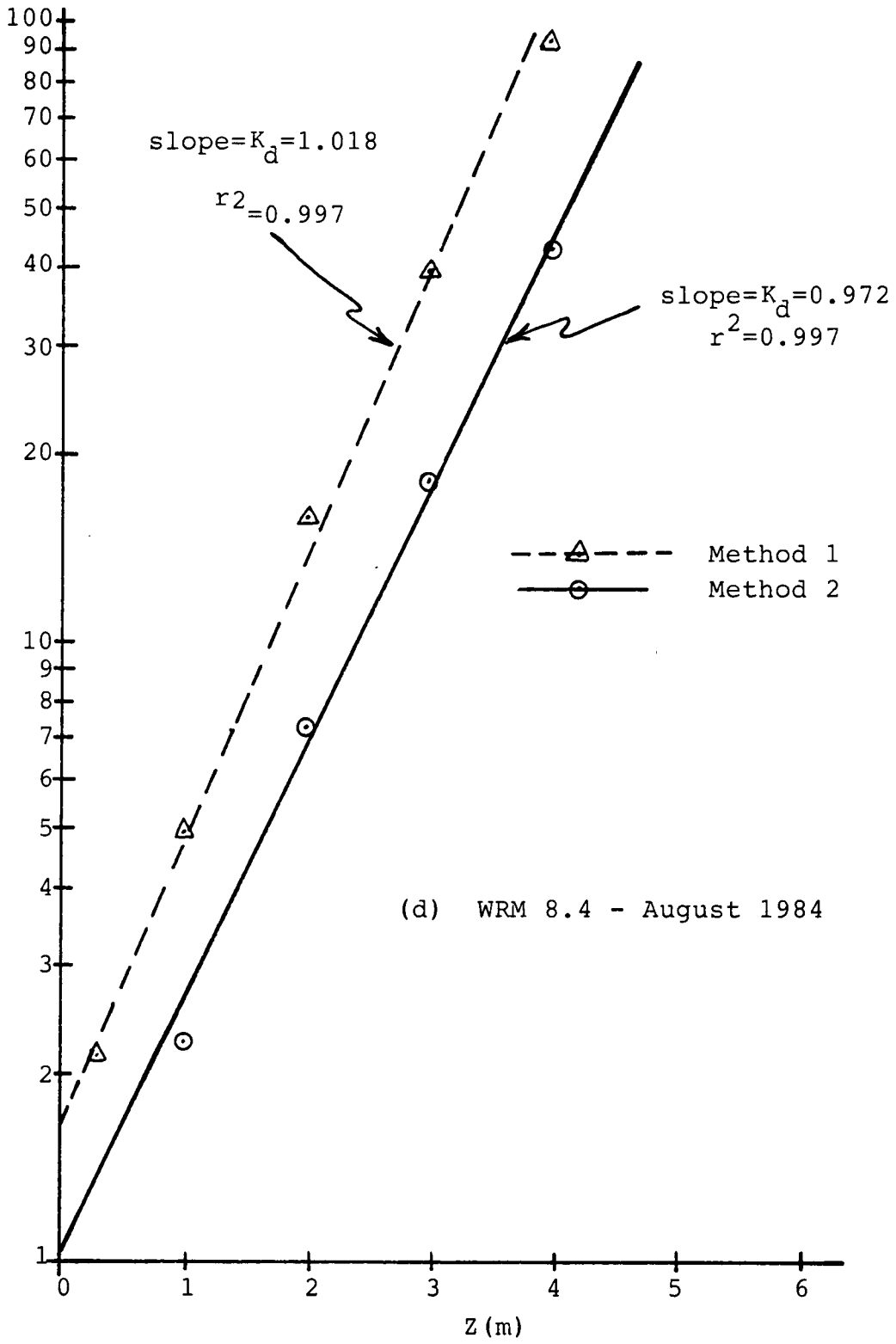

Figure 7 (Continued)

to changes in depth and less than 1% of the variability was due to random sampling error. Comparison of K_d values computed by either of the two methods described above show only small (<10%) differences in most cases.

As mentioned previously the K_d values given in Table 3 are the average values for the euphotic depth. The accuracy of using one K_d value to represent the attenuation of light over the entire euphotic depth may be evaluated approximately by obtaining the y-intercept of the regression of $\ln(I_o/I_z)$ versus depth. If optical properties in the euphotic zone are approximately uniform with depth then the regression line will cross the y-axis at or close to the origin (i.e. when depth is zero, I_o equals I_z) if random sampling error is low. If substantial variations in attenuating substances occur with depth, the attenuation coefficient, K_d, will be variable over small depths resulting in a y-intercept which does not pass through or near the origin (a proof of this statement is presented in Appendix I).

Inspection of the y-intercepts for $\ln(I_o/I_z)$ versus depth for Boone Reservoir (Table 4) reveals that in most cases there was substantial deviation of the y-intercept from the origin for both methods. This has significant implications in that it indicates the possibility of variations in light attenuating substances or optical

TABLE 4

Y-Intercepts of Linear Regression Analyses of $\ln(I_o/I_z)$ Versus Depth-Methods 1 and 2

	May		June		July		August	
Station	Method 1	Method 2	Method 1	Method 2	Method 1	Method 2	Method 1	Method 2
SFHRM 19.0	-0.024	0.21	0.23	0.180	0.35	0.39	1.90	2.14
SFHRM 22.4	0.031	-0.077	0.40	-0.028	0.31	0.35	1.37	-0.20
SFHRM 25.0	0.74	0.63	0.13	0.047	0.91	-0.50	1.23	1.37
SFHRM 26.2	0.43	0.13	0.33	-0.074	0.37	0.50	-	-
SFHRM 28.3	0.38	0.033	0.64	0.92	0.37	0.15	0.91	0.20
SFHRM 30.8	0.69	0.63	0.52	0.47	0.62	1.28	0.64	0.23
SFHRM 32.4	-	-	-	-	-	-	2.18	0.17
WRM 2.0	0.61	0.41	1.21	-0.24	2.46	1.01	1.93	0.082
WRM 3.0	-0.10	-0.16	0.41	-0.005	1.13	2.20	2.63	0.27
WRM 6.0	0.24	0.24	0.58	1.031	0.28	0.37	1.49	0.77
WRM 8.4	0.17	0.91	0.38	-0.0043	1.26	0.39	0.57	0.23
WRM 10.95	-0.04	-0.45	0.62	-0.902	0.55	0.76	1.70	0.79
WRM 13.0	-	-	-	-	-	-	1.62	0.71
Mean[1]	0.31	0.35	0.50	0.35	0.78	0.72	1.51	0.60

[1]Mean of absolute values of y-intercept

properties with depth. A better definition of the significance of these y-intercepts would require that the random sampling error and light instrument variability be reduced to a minimum so that any deviations from the origin could be attributed mainly to changes in optical properties with depth. This could be done by obtaining a larger number of observations of $\ln(I_o/I_z)$ versus depth.

The deviations of the y-intercept from the origin for the first method (i.e. I_o equals the ambient irradiance minus 10% reflectance) were generally greater than those of the second method. This is because the first method is based upon an assumed reflectance which may not be correct. Values of K_d computed by the second method will be used throughout the remainder of this report because they are based on observed irradiance values for I_o.

The K_d values in Table 3 represent mean values in the euphotic depth for the attenuation of irradiance in the 400-700 nm waveband. It can be seen that for a particular reservoir station K_d varies with time due to changes in the composition or relative percentages of light attenuating substances (algae, suspended solids, etc.). K_d also varies longitudinally along the reservoir arms on any particular date generally increasing in an upstream direction. This is likely due to increases in algal biomass which were usually higher in the upstream

reaches. K_d values for the study period (May to August) ranged from a minimum of 0.33 ln/m at WRM 2.0 in July to 3.22 ln/m at WRM 10.95 in June. Typical values of K_d reported in the literature are 0.9 to 5.67 ln/m for moderately turbid to very turbid Australian Lakes (19) and 0.04 to 0.1 ln/m for extremely clear Crater Lake, Oregon (23).

It is thus evident from the relatively high K_d values calculated in the preceding analyses that the transparency in Boone Reservoir is substantially impaired. To determine what substance or substances are primarily responsible for this reduction in transparency, the coefficient K_d must be partitioned in terms of the various attenuating substances which contribute to the total attenuation of light. This partitioning analysis will be conducted in section 4.1.2, but first one of the commonly used correlations in obtaining values for K_d (that of K_d versus secchi disc depth) will be evaluated for the case of Boone Reservoir.

4.1.1.1 K_d versus secchi disc depth

Figure 8 shows secchi disc depth versus K_d. This figure shows substantial data scatter and a poor correlation ($r^2 = 0.28$). This poor correlation probably occurred as a result of observer sighting variability and non-uniformity in the method of round-off when recording

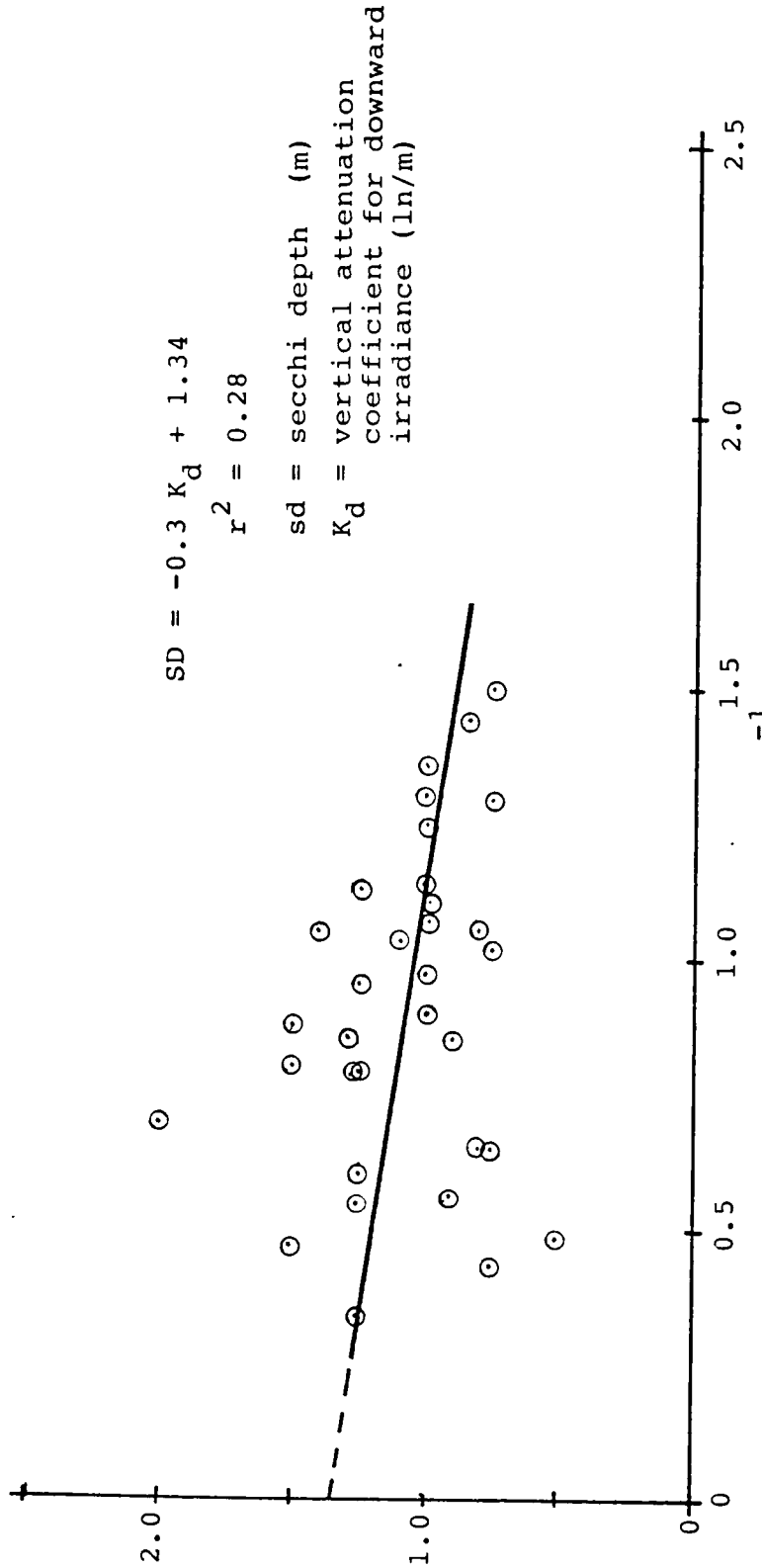

Figure 8. Secchi Disc Measurements Versus Vertical Attenuation Coefficients—Boone Reservoir, May to August, 1984.

secchi disk measurements. Since four different observers were used over the study period it is probable that variations in the visual response of each observer (e.g. depth perception, optical light gathering properties, contrast reception) resulted in significant data scatter. Also, since the secchi disc line was calibrated only in increments of one meter, observer variability in the method of round-off may have contributed to the poor correlation between K_d and secchi disc depth. Since the relationship between K_d and secchi disc is based on the premise that the visual sighting range of the disc corresponds to a fixed percentage of light attenuation (38), accurate (e.g. ± 0.1 meters) and consistent measurements of secchi disc depth in steep light gradient waters such as Boone Reservoir are essential. In these steep light gradient waters, observer dependent variations in measurement may result in significant variations in the corresponding irradiances and hence variations in the correlation between secchi disk depth and K_d. As an example consider a location with a K_d value of 1.5 (typical of some locations in Boone Reservoir), if two different observers record secchi disc depths of 0.8 meter and 0.5 meter for the same optical and lighting conditions, the corresponding variation in light attenuation is 17%.

The poor correlation between K_d and secchi disc depth for Boone Reservoir indicates that observer

variability may significantly impact the accuracy of secchi disc measurements. In future reservoir studies this variability may be reduced by using, to the greatest extent possible, the same observer for each secchi disc measurement. If this is not possible, it is recommended that the observer's initials be placed by each recorded measurement thus providing a means of tracing observer variability. Also, the secchi disc line should be calibrated in increments of at least 0.1 meter and readings should be recorded to the nearest 0.1 meter.

4.1.2 Partitioning of light attenuation coefficient, K_d

In this section, the coefficient K_d will be partitioned in terms of the various attenuating substances present in Boone Reservoir. The relative contributions of the processes of light absorption and scattering to the overall attenuation of light will also be investigated. Since this analysis will be particularly concerned with the fractional light attenuation associated with algae, a brief summary of the spatial and temporal distribution of algal groups within the reservoir is first warranted.

4.1.2.1 Identification and enumeration of algae

Appendix II presents group abundance, number of genera, and percent composition results for algal samples collected as 0 to 3 meter depth integrated composite

samples. Three major algal groups dominated at various times over the four survey sampling period (May to August), these included Bacillariophyta (a diatom), Chlorophyta (a green algae) and Cyanophyta (a blue-green algae). Figure 9 shows the temporal trends of both percentages of the total number of cells and of the number of cells per liter.

The general trend of algal dominance in the reservoir consisted of a period of blue-green (cyanophyta) algae and diatom (bacillariophyta) dominance in May, a period of green algae (chlorophyta) dominance in June or July, and back again to a period of blue-green and diatom dominance by August.

In May, the South Fork Holston arm of the reservoir was co-dominated by blue-green (cyanophyta) and diatoms (bacillariophyta), however cyanophyta comprised the greater percentage in most cases. On the Watauga arm, bacillariophyta and cyanophyta were also the major algal groups, however, the population of diatoms were significantly greater in all cases with increasing concentrations upstream. Chlorophyta populations in May were low for all reservoir sampling stations.

In June, the population of diatoms decreased substantially on both the South Fork Holston River and Watauga River arms. The green algae, chlorophyta, increased,

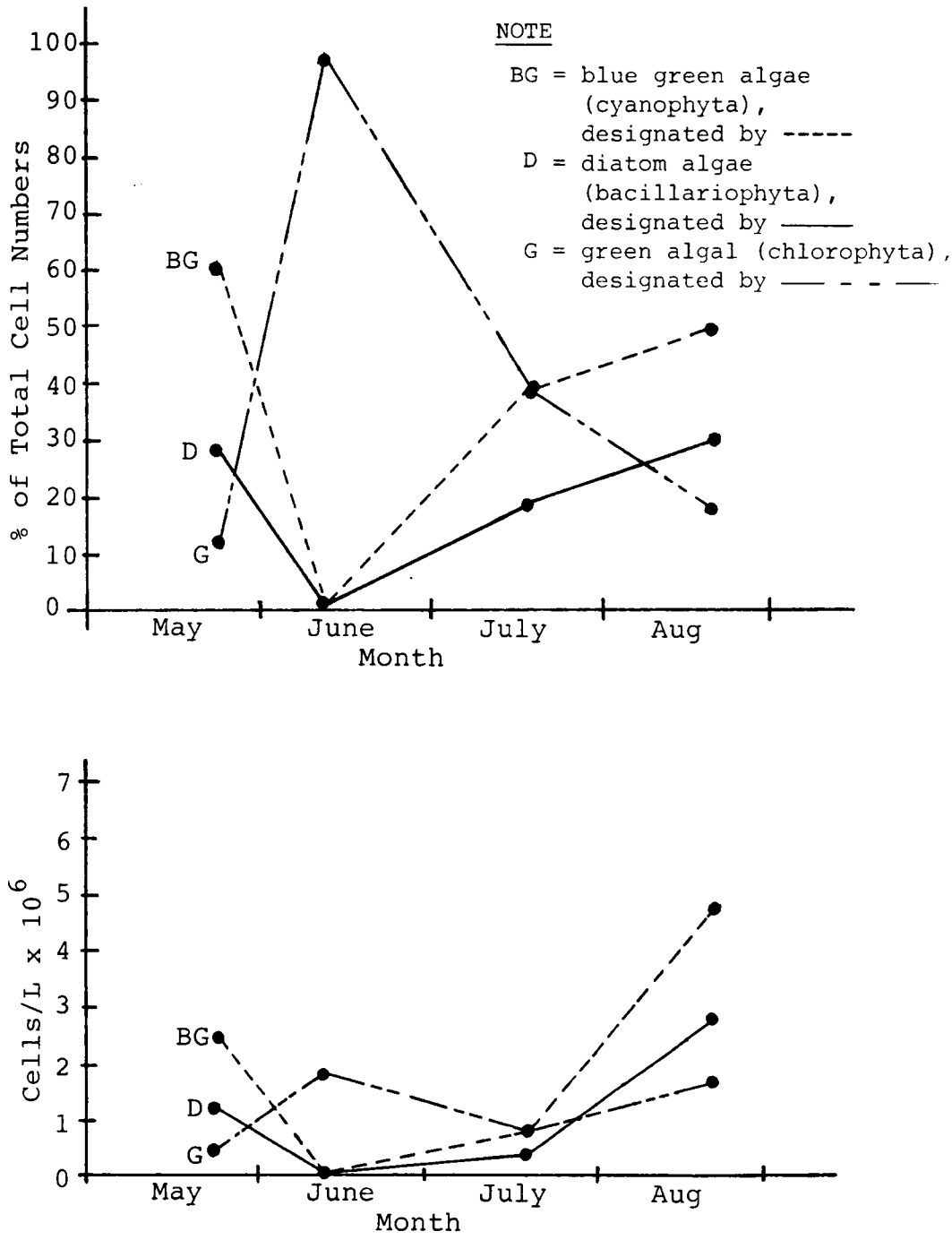

(A) SFHRM 19.0

Figure 9. Phytoplankton Abundance and Percent Composition for Major Algal Groups in Boone Reservoir — May to August, 1984.

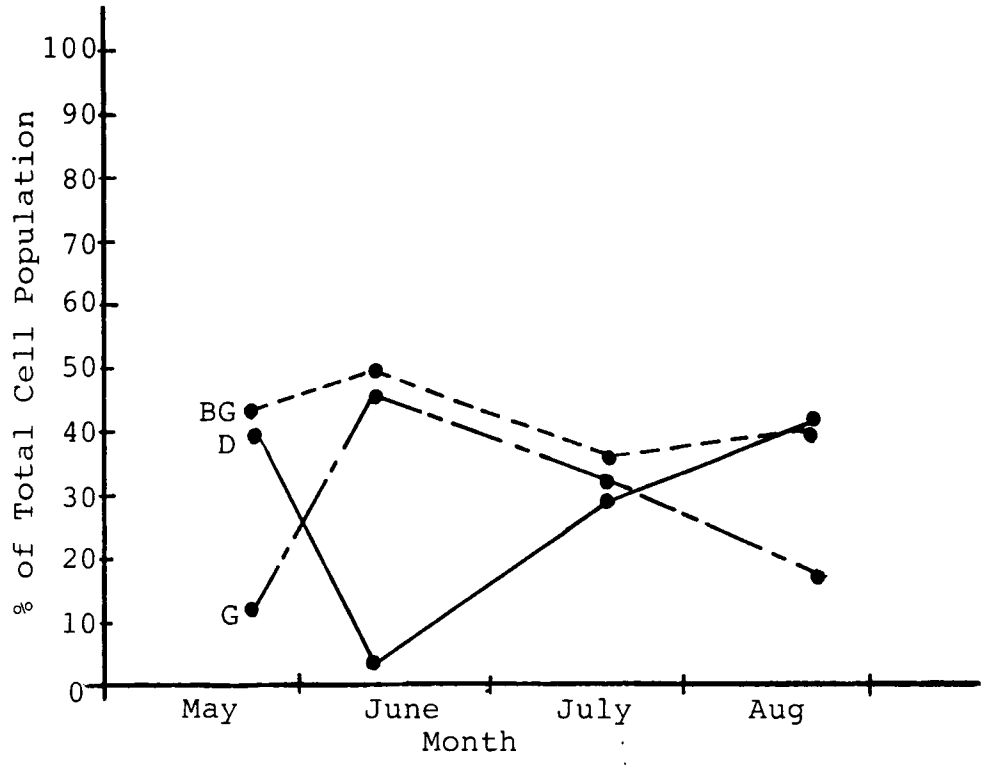

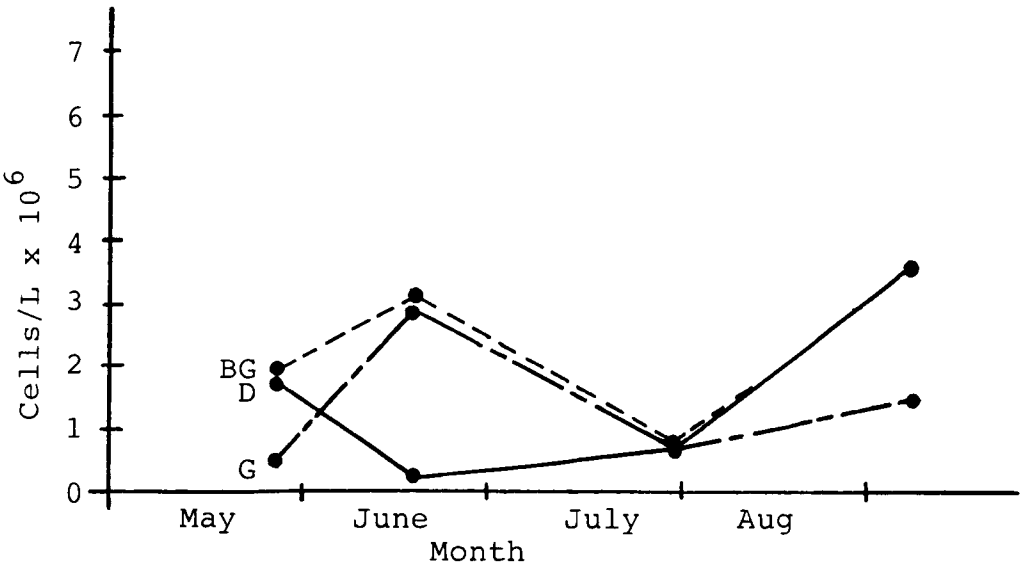

(B) SFHRM 26.2

Figure 9 (Continued)

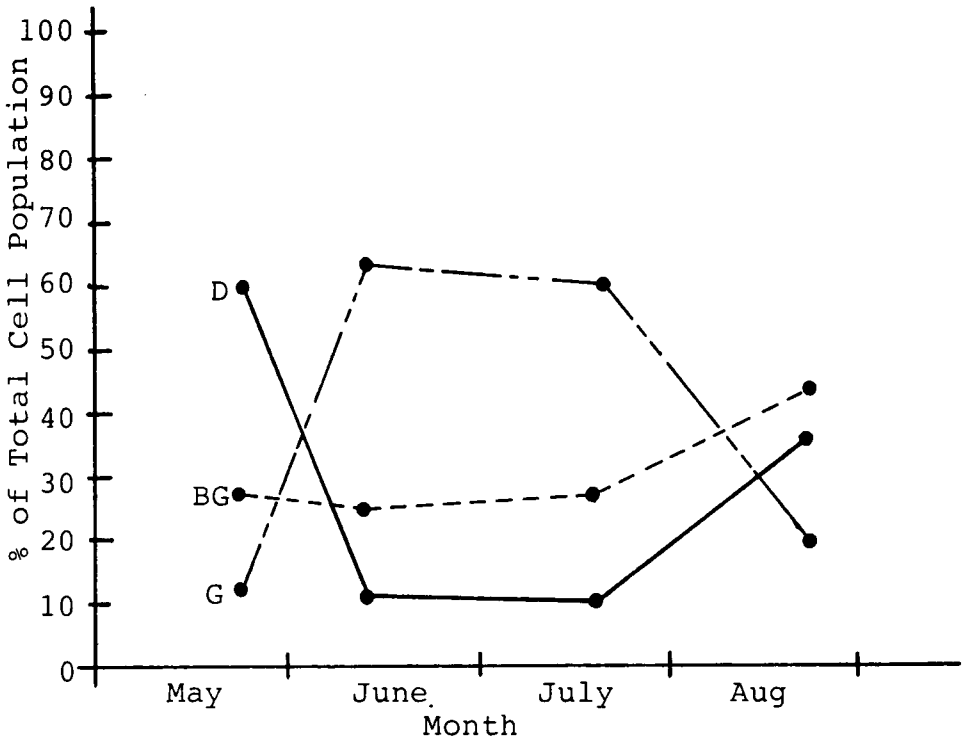

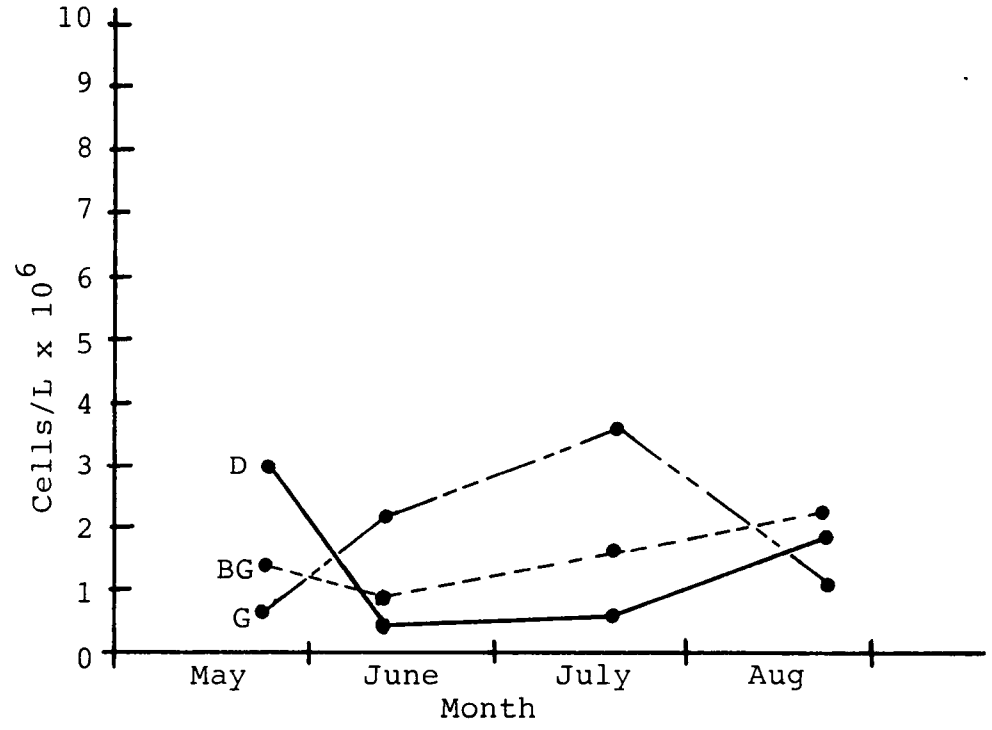

(C) WRM 2.0

Figure 9 (Continued)

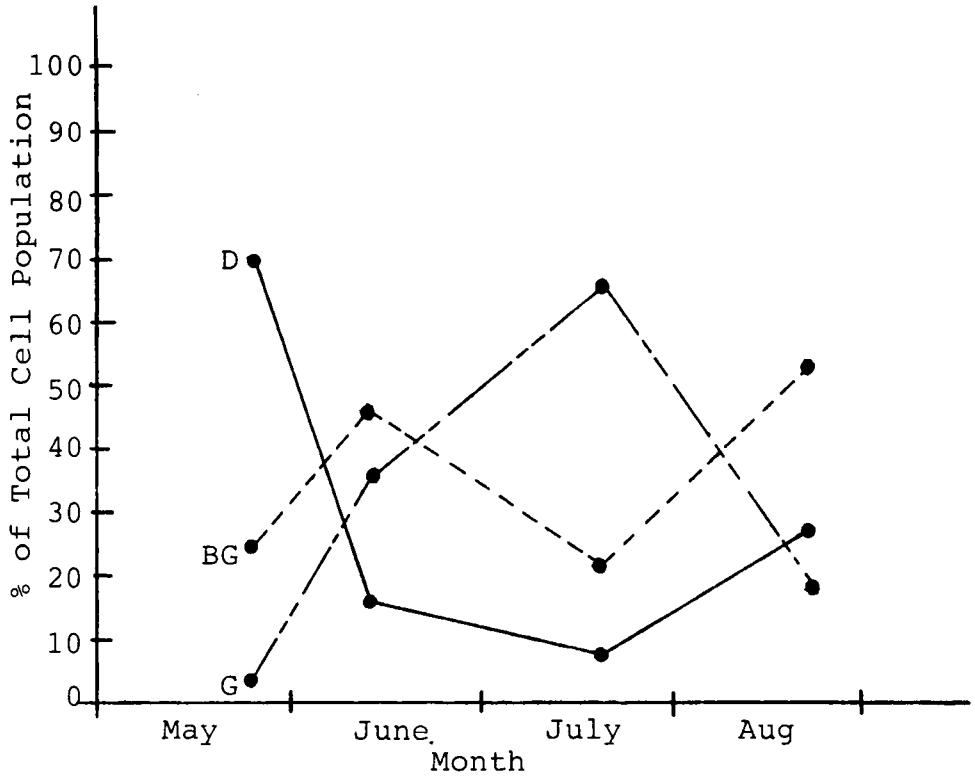

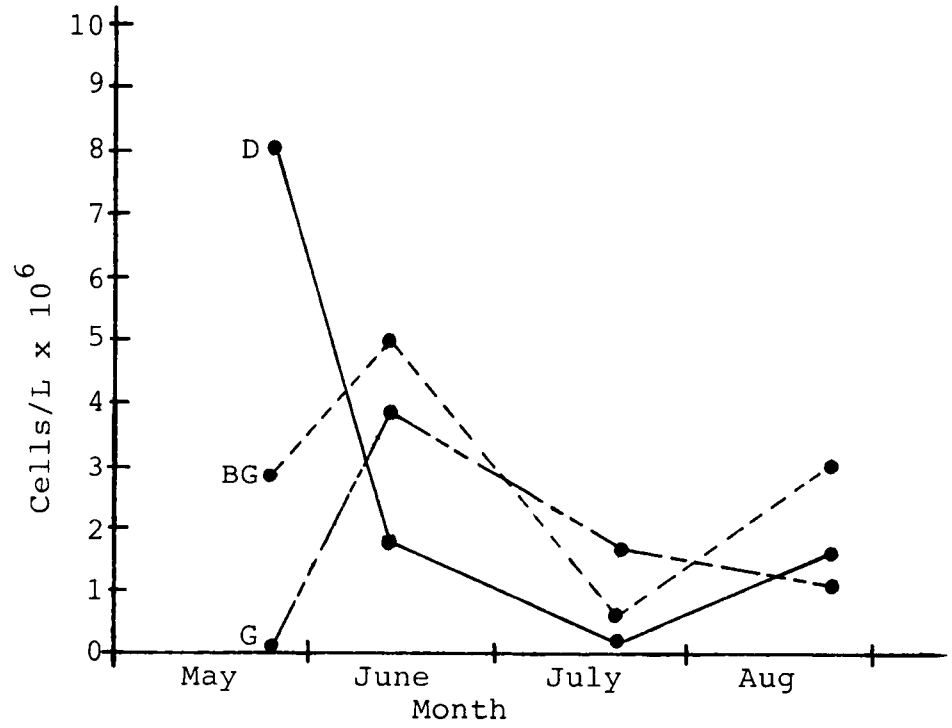

(D) WRM 6.0

Figure 9 (Continued)

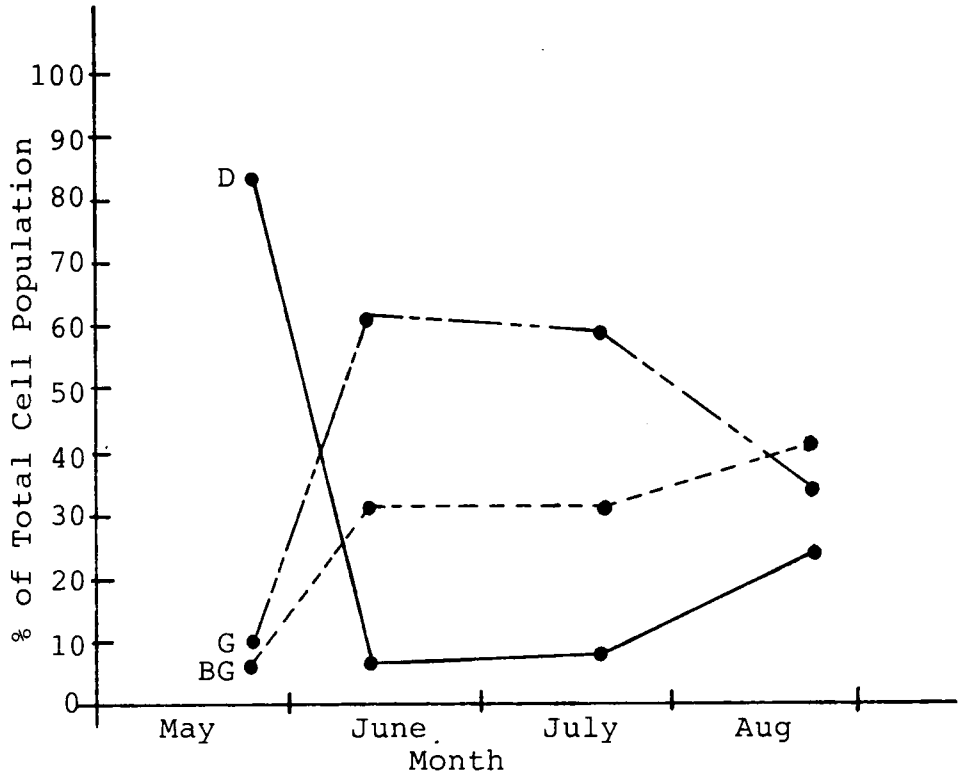

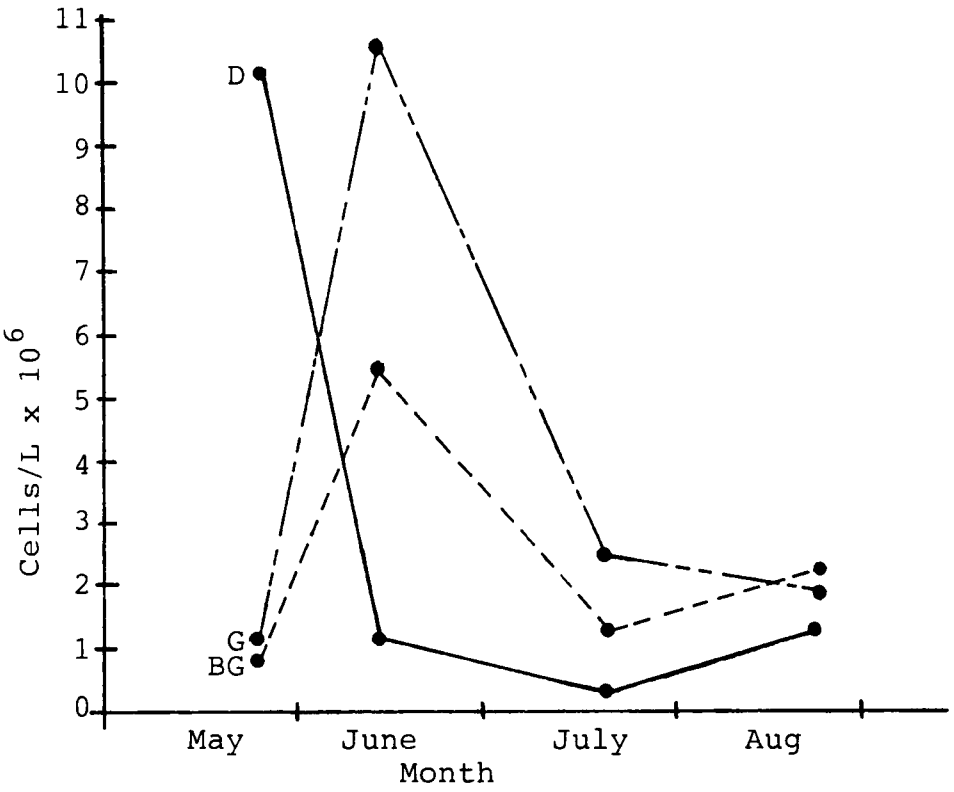

(E) WRM 10.95

Figure 9 (Continued)

however, at all sampled locations and was the dominant algal group at most locations on both the South Fork Holston and Watauga arms. Blue-green algae remained at co-dominant levels at the upstream locations on the South Fork Holston but decreased in the lower reach. On the Watauga, blue-greens either increased or remained at the same level at all stations.

Green and blue-green algae were again the major algal groups in July. On the South Fork Holston arm, these algae were generally lower than measured in June, however, both groups were co-dominant. On the Watauga arm, green and blue-green algae also decreased in population from the previous month but green algae remained the dominant algal group. Diatoms begin to rise in population on the South Fork Holston arm but continued to decrease at most locations on the Watauga arm.

In August, green algae decreased substantially at all sampling locations. Diatoms, however, increased in population at all locations. Blue-green algae also increased at all sampling locations. Blue-green algae and diatoms were co-dominant on both the South Fork Holston arm and the lower reach of the Watauga. In the upper reach of the Watauga arm, however, the blue-green algae were the dominant group.

Reasons for the temporal shifts in dominance include light, temperature, and nutrient variations with time.

The spring maximums of diatoms and blue-green algae consist of cells which fluorish in low light and low temperature conditions. As the ambient irradiance increases in June and July these cells begin to decline in numbers or move to lower depths where irradiance and temperature conditions are optimal. Diatoms may also decline due to limitations in ambient silica concentrations (a required nutrient for diatom growth). As ambient irradiance and temperature increase in June and July, the numbers of high light adapted green algae (chlorophyta) rise and become dominant. By August, conditions again become more favorable for blue-green and diatom dominance and the population of green algae begin to decline. Since ambient light conditions and temperature conditions in August are similar to those in July, the decline in chlorophyta dominance and the increase in blue-green and diatom populations may be associated with variations in nutrient availability.

4.1.2.2 Evaluation of K_c and K_w

The vertical attenuation coefficient, K_d, may be partitioned in terms of phytoplankton related and non-phytoplankton related attenuating substances as follows:

$$K_d = K_c C + K_w \qquad \text{(Equation 9)}$$

where K_c = light attenuation coefficient due to algae and algal degradation products (m^2/mg Chl a)

K_w = light attenuation coefficient due to non-phytoplankton substances (e.g. water, solids) (m^{-1})

C = Chl a (mg/m^3), average value for surface to 3 meters

In the application of this equation, it is assumed that light attenuation by algae is directly related to chlorophyll a content. Chlorophyll a, however, is not the only light attenuating component of an algal cell. Other pigments such as chlorophyll b, c, and carotenoids will also absorb light and contribute to the overall attenuation coefficient, K_d. Scattering by algal cells may also result in light attenuation. If the concentrations of these other pigments and the effects of algal light scattering vary in proportion to the chlorophyll a content of an algal population, then chlorophyll a may be used as a surrogate parameter which represents all attenuating components of the algal population. This proportional relationship may never actually exist in a natural environment but it can be approximately true for an algal population of a fixed species composition and adaptive state. For this reason, the coefficient of proportionality between light attenuation and chlorophyll a (i.e. K_c) will vary with changes in species composition and is applicable only for the algal species for which it was derived.

The determination of K_c involves the linear regression of K_d versus uncorrected chlorophyll a values. The slope of this regression is equivalent to K_c and the y-intercept is K_w.

For this study chlorophyll a and pheophytin were determined in the laboratory for surface to 3 meter depth-integrated samples collected at seven stations including SFHRM 19.0, 22.4, 26.2, and 30.8 and WRM 2.0, 6.0, and 10.95. Values of algal fluorescence were also determined at these stations. Appendix III, Part 1, presents the results of these analyses. At SFHRM 25.0 and 28.3 and WRM 3.0 and 8.4, only algal fluorescence values were determined; therefore, if K_c values were to be determined for these stations, the relationship between fluorescence and chlorophyll a had to be obtained. To determine this relationship the laboratory results of chlorophyll a and corrected chlorophyll a (Appendix III) were linearly regressed against corresponding field algal fluorescence values. This statistical analysis was performed for each specific survey date and on an overall basis aggregating all data. Poor correlations were obtained when all data was aggregated with a correlation coefficient (r^2) value of 0.0279 for chlorophyll a versus fluorescence and an r^2 value of 0.0381 for corrected chlorophyll a versus fluorescence. The data scatter exhibited by this analysis is shown in Figure 10 a and b. Analysis on an individual

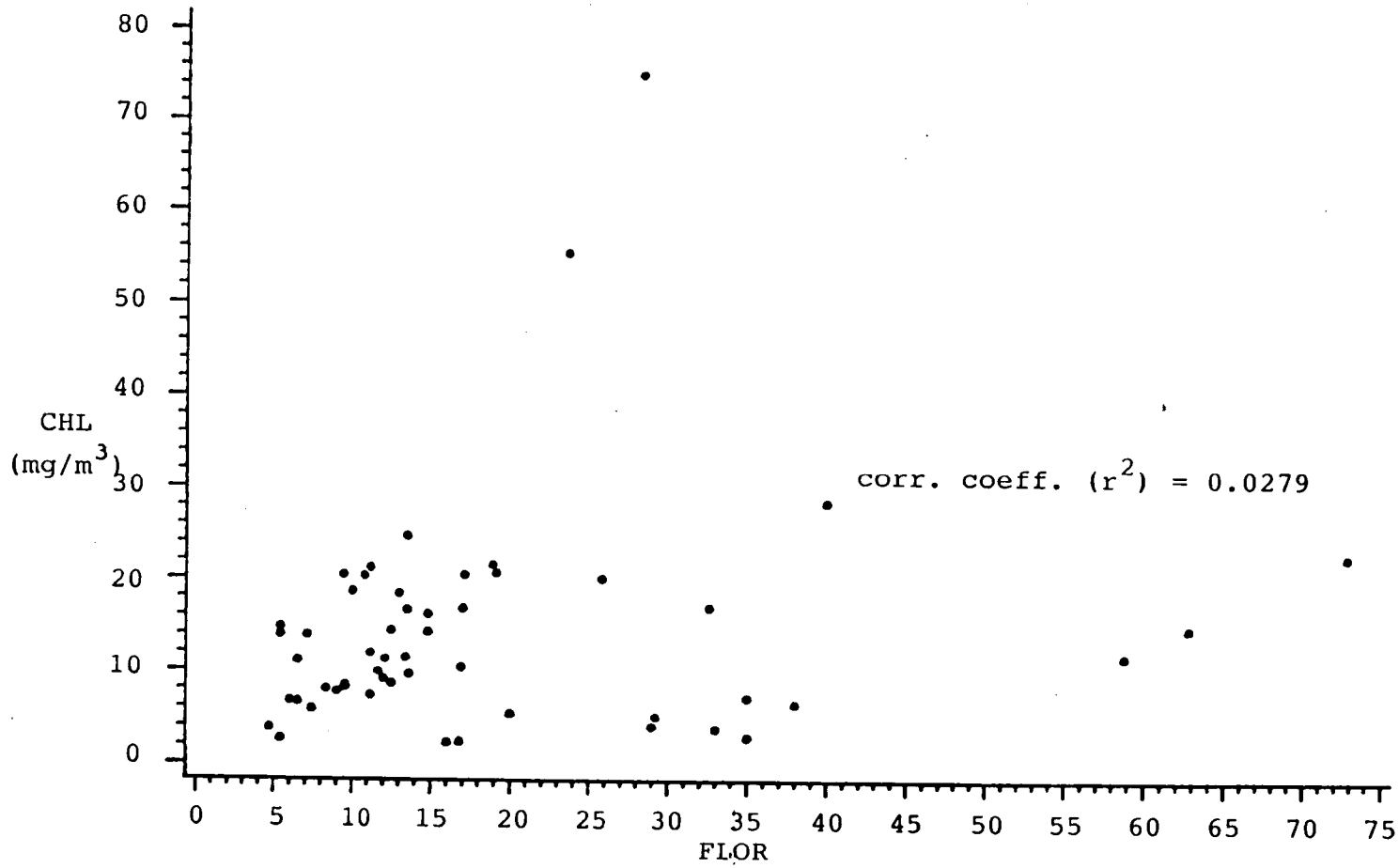

(a) Chlorophyll a (Uncorrected for Pheophytin) vs. Fluorescence.

Figure 10. Chlorophyll a versus Fluorescence--Aggregation of Monthly Data.

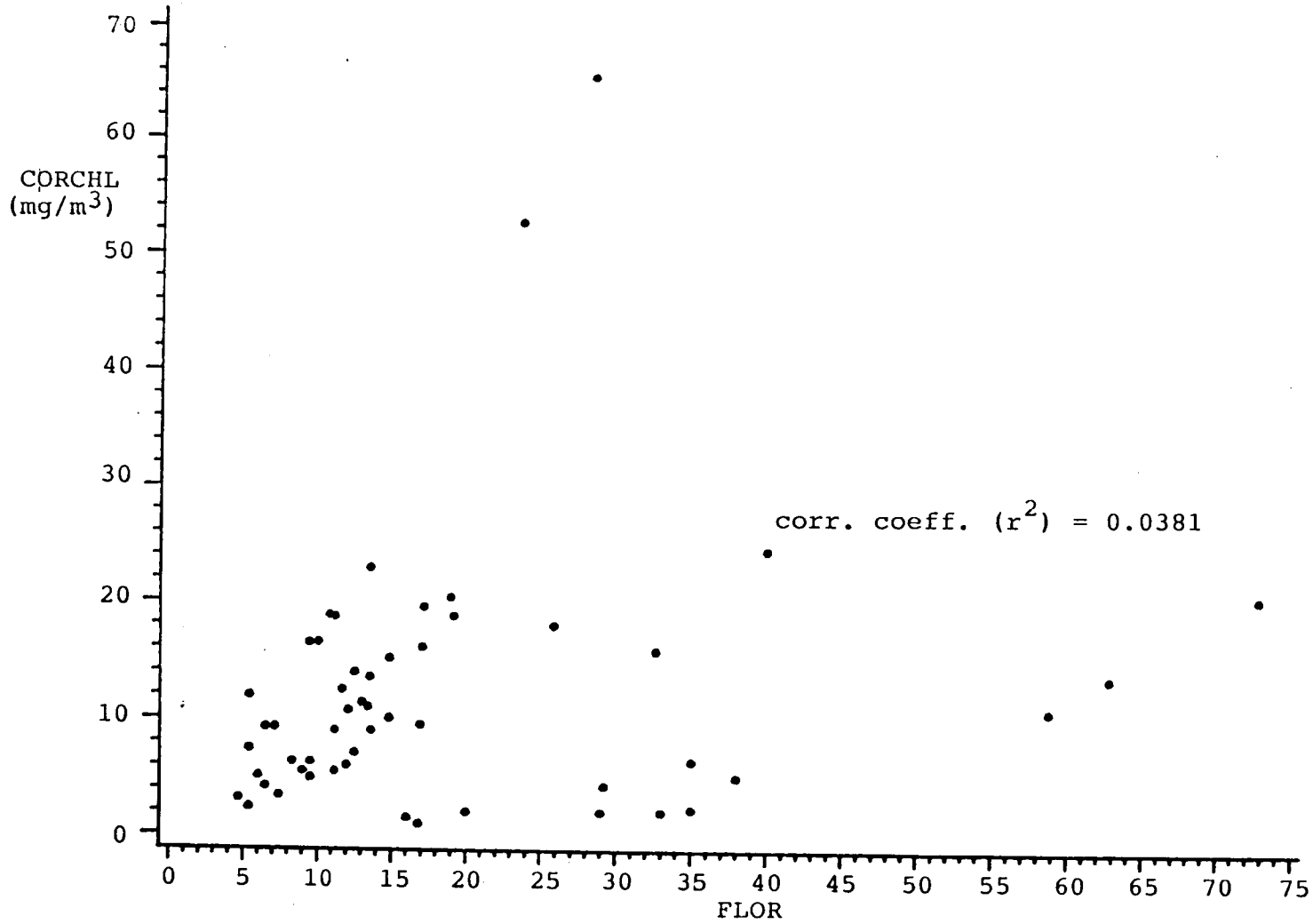

(b) Chlorophyll a (Corrected for Pheophytin) vs. Fluorescence.

survey basis, however, yielded much better results as variations in the relationship between algal fluorescence and cellular chlorophyll a content occurred with changes in species dominance. Table 5 lists the regression equations and correlation coefficients obtained for each survey date. Figure 11 a and b are plots of chlorophyll a and corrected chlorophyll a versus fluorescence for each survey and the corresponding linear regression lines. Also shown are the dominant algal groups occurring during each survey. It can be seen from these plots that there were significant variations with each survey in the relationship between fluorescence and chlorophyll (i.e. significant variations in slope).

The probable causes of these slope variations include changes in algal species dominance and changes in the adaptive and physiological condition of algae. It can be seen in Figure 11 that the least slope (i.e. greatest algal fluorescence per unit of chlorophyll a) was obtained when green algae were dominant. As populations of diatoms and blue-green algae increased the proportionality between algal fluorescence and chlorophyll a changed resulting in an increase in slope. While it is true that a unit of pure chlorophyll a isolated from one algal species will fluoresce in the same manner as that isolated from another algal species, the fluorescence of two differing algal

TABLE 5

Linear Regression Analyses Results--Chlorophyll a Versus Fluorescence--Monthly Data

Month	Chlorophyll a		Corrected Chlorophyll a	
	Linear Equation	Correlation r^2	Linear Equation	Correlation r^2
May	Chl a = 2.67(Flor)-7.14	0.9121	Cchl a = 2.52(Flor)-8.59	0.9334
June	Chl a = 0.306(Flor)-3.99	0.8516	Cchl a = 0.311(Flor)-5.50	0.8881
July	Chl a = 0.709(Flor)+1.71	0.8778	Cchl a = 0.677(Flor)+0.155	0.8422
August	Chl a = 1.286(Flor)-3.67	0.9736	Cchl a = 1.311(Flor)-4.04	0.9788

NOTE: Chl a = chlorophyll a

Cchl a = corrected chlorophyll a

Flor = insitu fluorescence

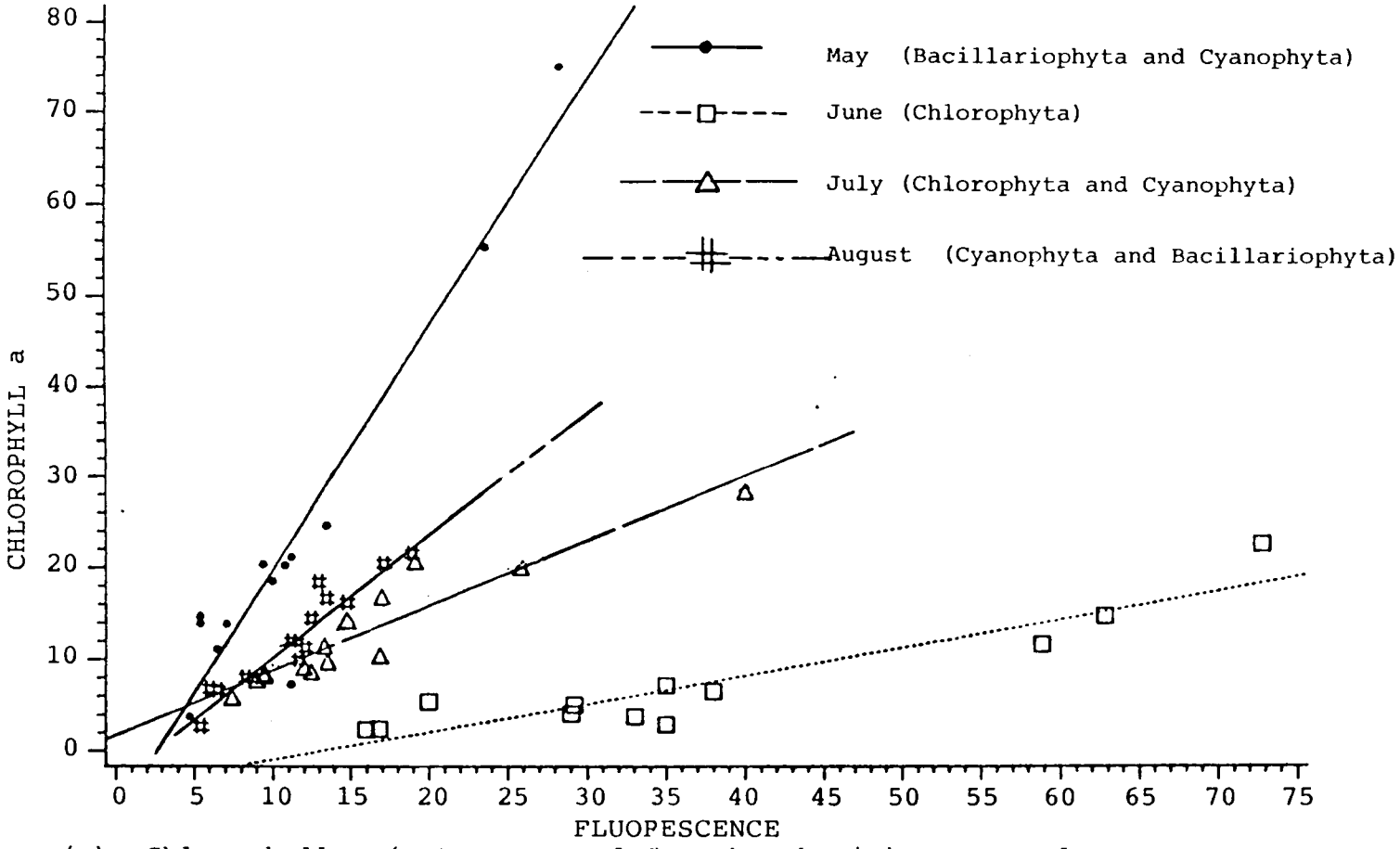

(a) Chlorophyll a (not corrected for pheophytin) Versus Fluorescence.

Figure 11. Laboratory Chlorophyll a Results Versus Fluorescence—Monthly Data with Corresponding Linear Regression Lines.

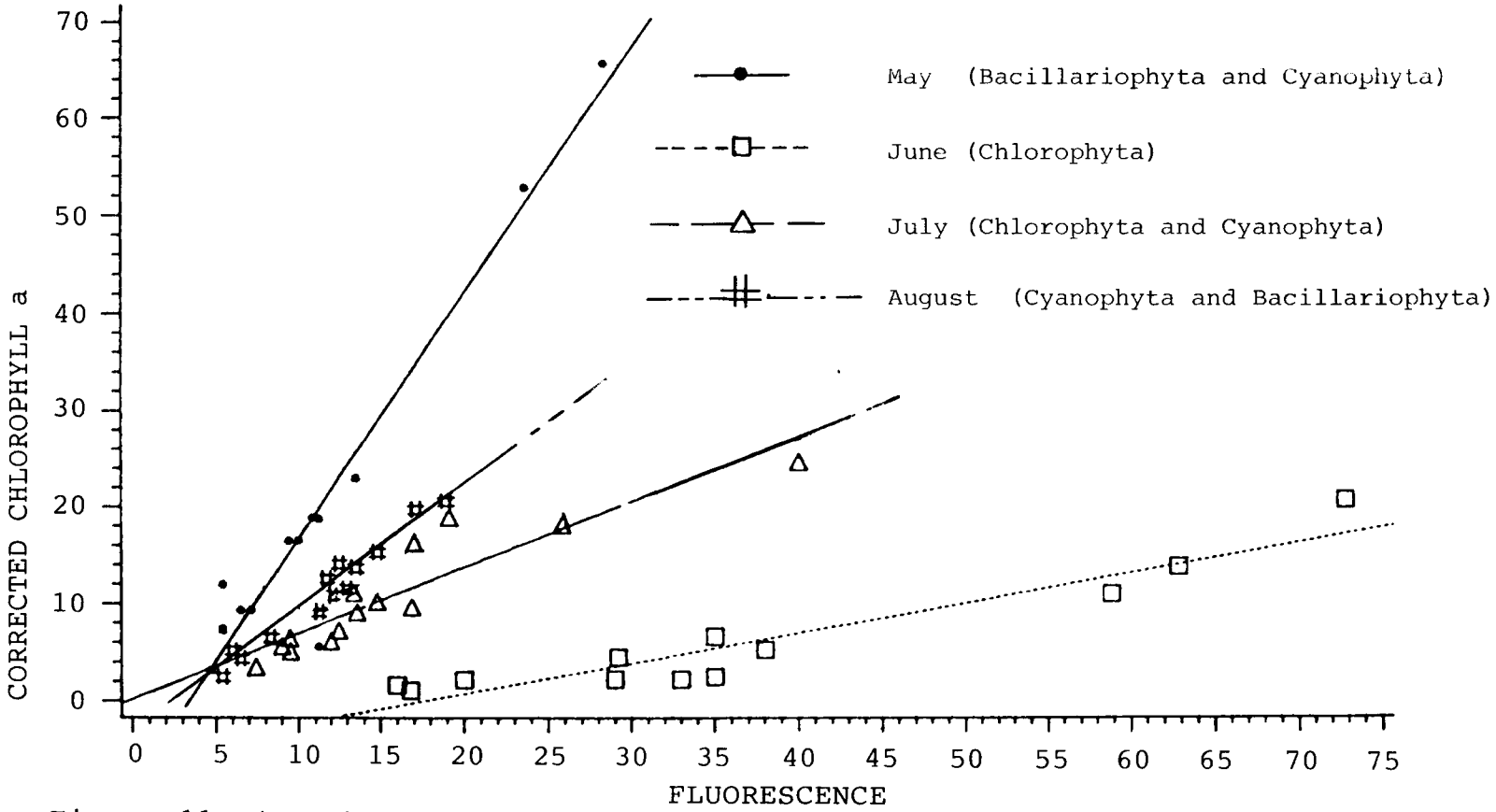

Figure 11 (Continued) (b) Corrected Chlorophyll a Versus Fluoresence.

species or groups measured in vivo (i.e. when the fluorescent material is within the cell) may be significantly different. This is because chlorophyll a is not the only pigment within an algal cell which fluoresces. Other pigments such as chlorophyll b, c, and carotenoids will also fluoresce and will contribute to the value of in vivo fluorescence. Variations in the relative proportion of these other pigments to the cellular chlorophyll a content will occur with variations, in algal group dominance. Hence, the slope of a plot of chlorophyll a versus algal fluorescence will vary with changes in algal group dominance. Variations in the manner in which the light attenuating pigments are packaged within a cell have been shown to influence the absorbance per unit pigment concentration (5), this "packaging effect" should also influence fluorescence and hence the slope of chlorophyll a versus algal fluorescence.

The slope variations in Figure 11 are significant for two reasons. First, since variations in dominant algal group resulted in variations in the proportionality between chlorophyll a and algal fluorescence, it can be expected that the proportionality between chlorophyll a and light attenuation by algae may also vary. This has significant implications in the modeling of algal light attenuation since chlorophyll a is used as a surrogate

parameter which represents all light attenuating algal components. If changes in algal group dominance result in variations in proportionality between chlorophyll a and algal light attenuation, then the coefficient of proportionality (K_c) will also change. Second, in future applications of the derived regression equations for prediction of chlorophyll a, one should ensure that the dominant algal groups which exist at the time of fluorescence measurements correspond to those which existed for the derived equation.

Appendix III, Part 2; lists the chlorophyll a and corrected chlorophyll a values predicted from fluorescence values for all stations including SFHRM 25.0 and 28.3 and WRM 3.0 and 8.4 for which no laboratory chlorophyll analyses were performed. Table 6 lists the K_d values determined previously along with uncorrected chlorophyll a values determined as weighted averages over the depths at which K_d was measured. Linear regression of K_d versus chlorphyll a yields estimates for K_c and K_w. This linear regression was performed for each separate survey date rather than an aggregation of all data since chlorophyll a versus fluorescence showed significant variations with each survey due to variations in algal group dominance. Figure 12 a through d show plots of K_d versus uncorrected chlorophyll a and the corresponding linear regression lines. Table 7 is a summary of the K_c and K_w values, the correlation

Table 6

Evaluation of K_c--Uncorrected Chlorophyll a Versus K_d

Station	May		June		July		August	
	K_d (ln/m)	Chl a (mg/m^3)	K_d (ln/m)	Chl a (mg/m^3)	K_d (ln/m)	Chl a (mg/m^3)	K_d (ln/m)	Chl a (mg/m^3)
SFHRM 19.0	1.12	31.19	0.88	5.60	0.70	10.99	0.47	12.23
SFHRM 22.4	1.13	33.64	0.96	7.24	0.80	11.86	0.59	13.04
SFHRM 25.0	0.91	25.58	1.03	13.32	0.79	14.66	0.72	17.13
SFHRM 26.2	1.06	20.79	1.06	12.39	0.76	15.08	-	13.90
SFHRM 28.3	1.24	24.05	0.86	17.23	0.86	15.02	0.72	13.85
SFHRM 30.8	1.21	24.69	1.02	13.77	0.82	20.68	0.83	16.19
WRM 2.0	0.96	32.93	0.79	6.58	0.33	11.47	0.55	18.58
WRM 3.0	1.36	49.83	1.11	11.34	0.53	17.93	0.56	21.26
WRM 6.0	1.31	55.21	0.96	22.63	1.07	17.33	0.82	18.70
WRM 8.4	1.51	63.95	1.44	15.93	1.14	22.67	1.02	17.33
WRM 10.95	2.60	74.85	3.22	43.00	1.29	28.35	0.64	13.85

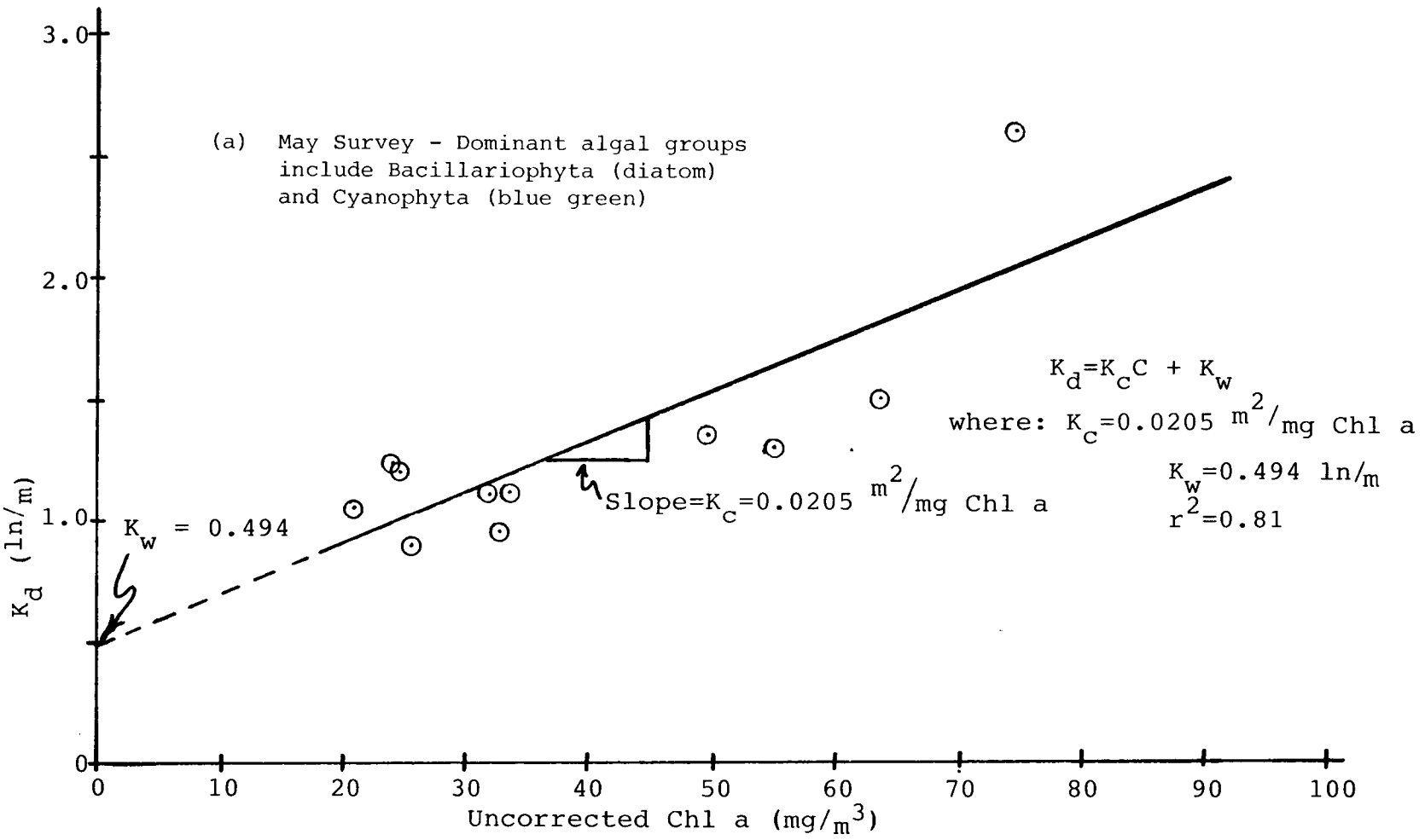

Figure 12. K_d Versus Uncorrected Chlorophyll a

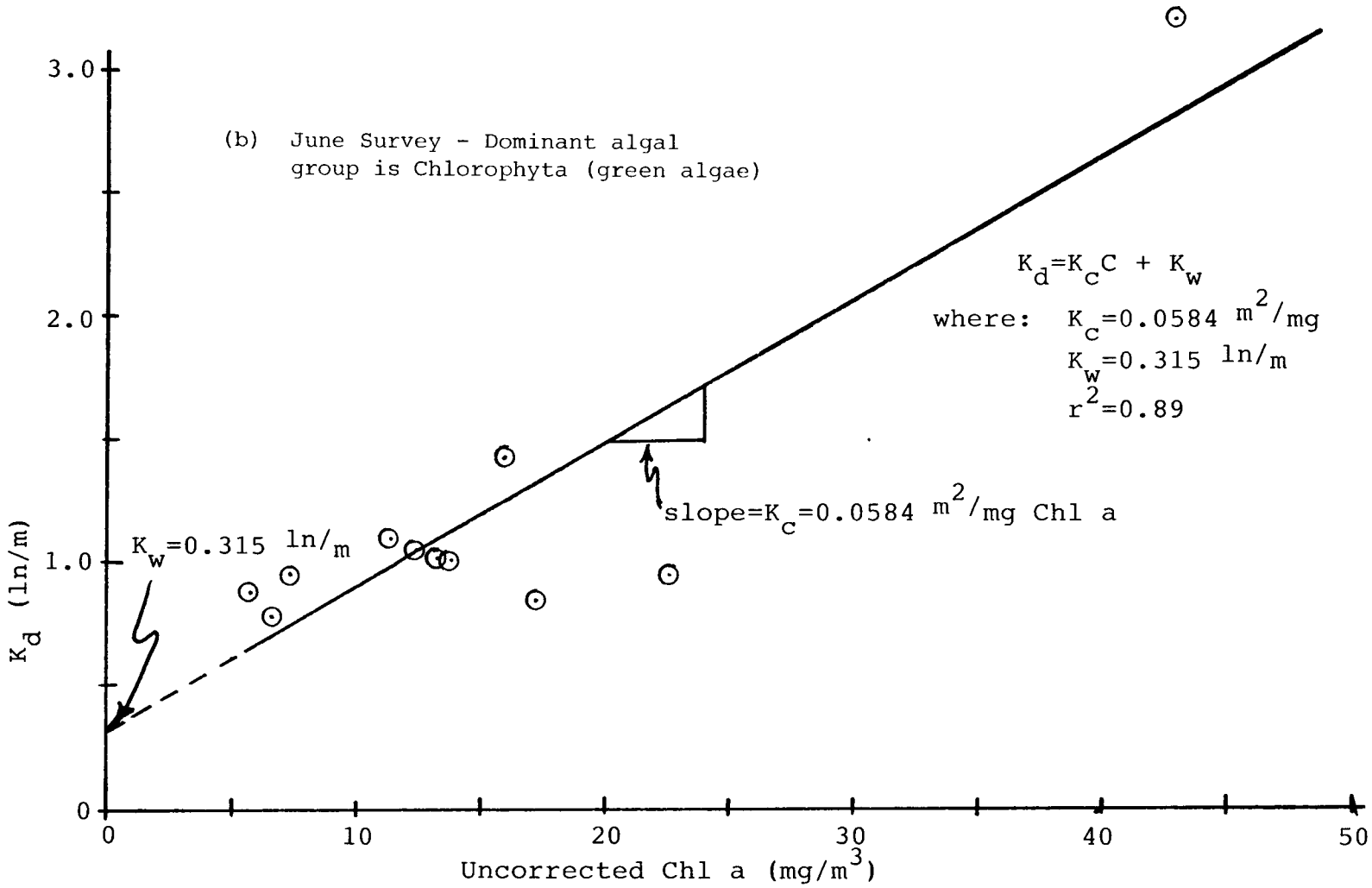

Figure 12 (Continued)

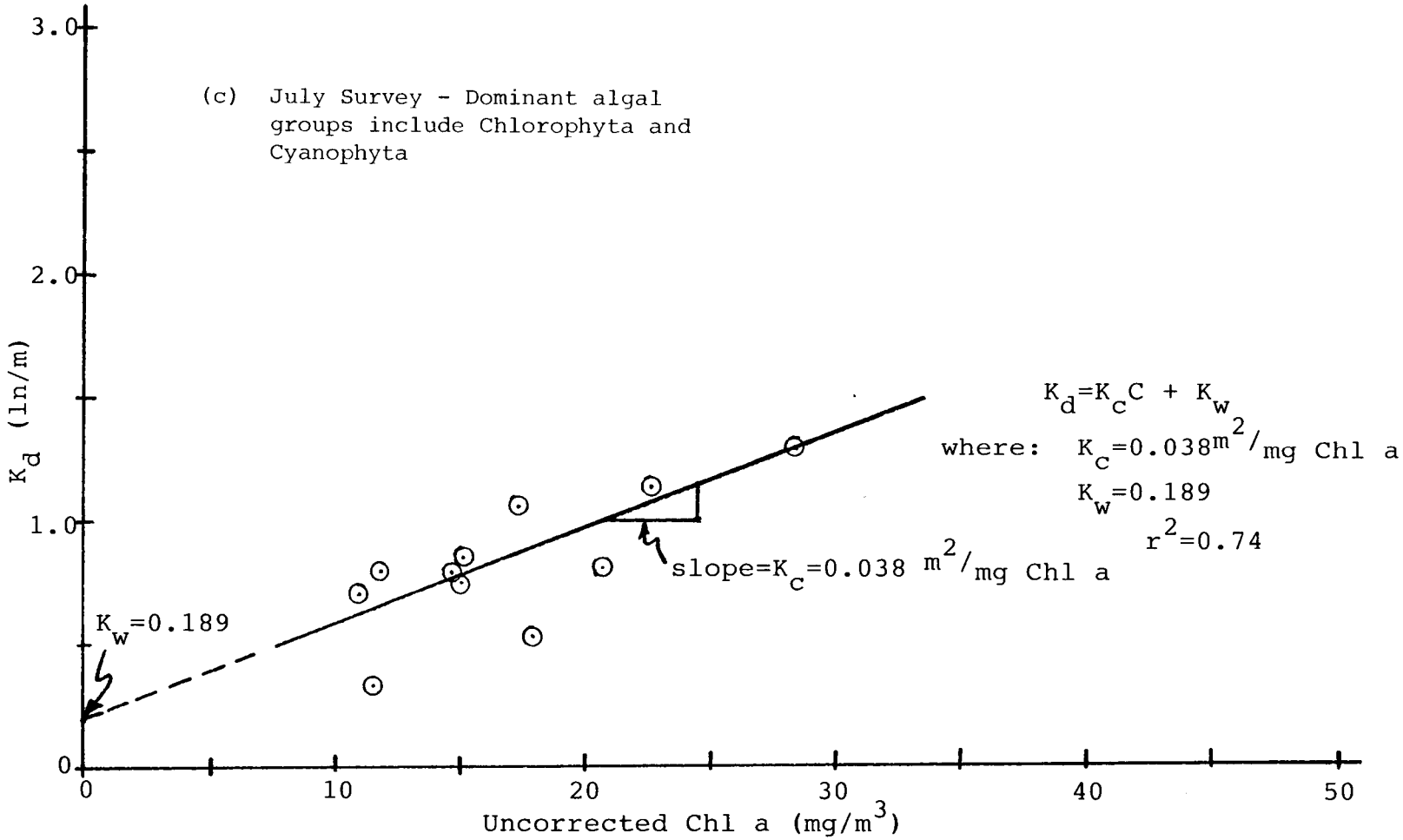

Figure 12 (Continued)

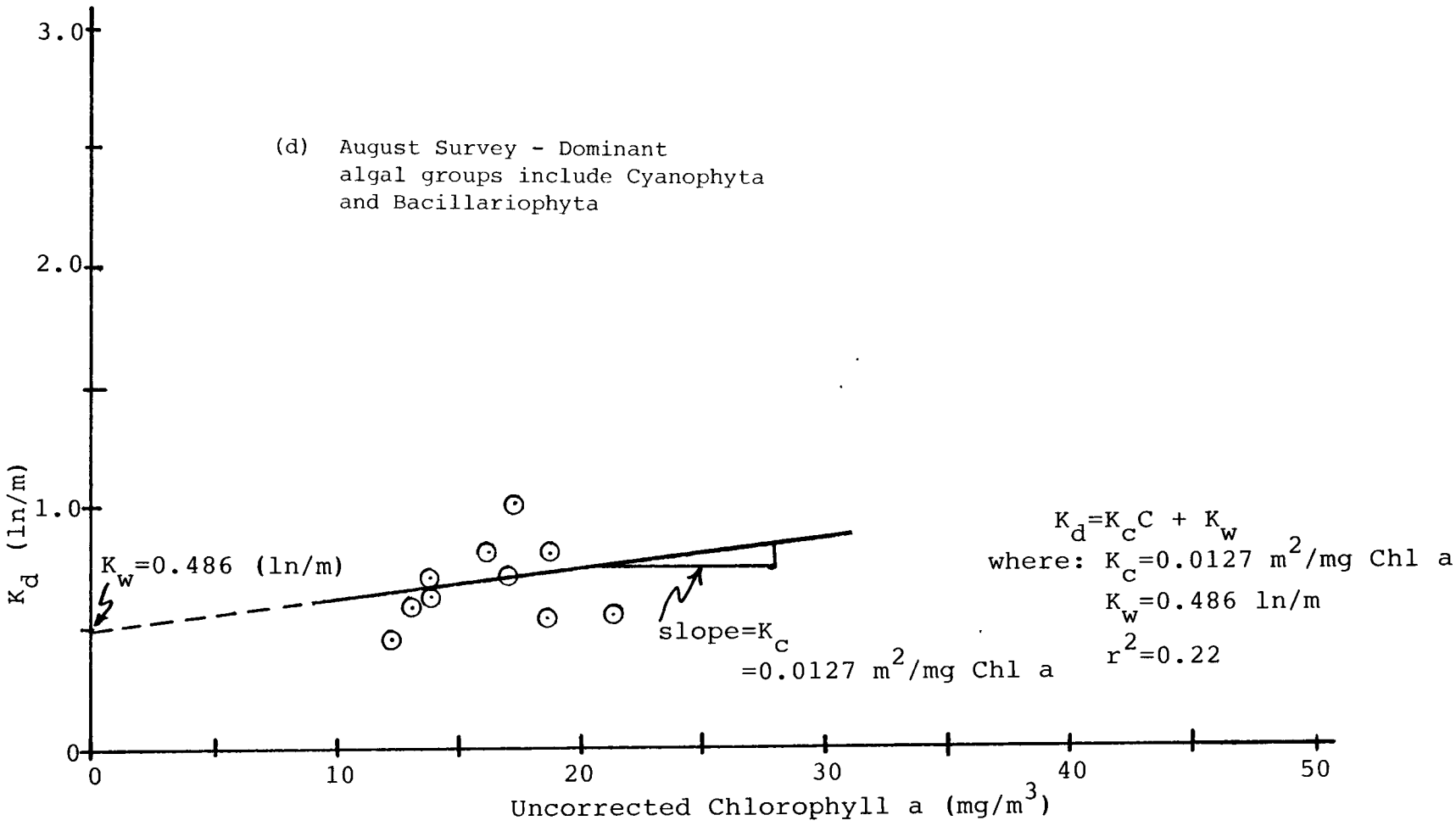

Figure 12 (Continued)

TABLE 7

Summary of K_c and K_w Coefficients for K_d Versus Uncorrected Chlorophyll a

Month	Dominant Algal Group	K_c (m^2/mg Chl a)	K_w (ln/m)	r^2
May	Bacillariophyta, Cyanophyta	0.0205	0.494	0.81
June	Chlorophyta	0.0584	0.315	0.89
July	Chlorophyta, Cyanophyta	0.038	0.189	0.74
August	Cyanophyta, Bacillariophyta	0.0127	0.486	0.22

coefficient values for each survey date, and the dominant algal groups which existed for each date. Reasonably good correlation was obtained between chlorophyll a and K_d for May through June with correlation coefficients of 0.76 to 0.96. The August data, however, yielded a poor correlation ($r^2 = 0.22$). For any particular survey date, a significant part of the variation between K_d and chlorophyll a may be due to variations at each station in the attenuation due to dissolved color and inanimate suspended solids and spatial variations in the relative numbers of dominant algal cells. Substantial variations in non-algal substances will cause greater data scatter and reduced correlation coefficients in the regression of K_d and chlorophyll a. This is because the linear equation $K_d = K_c C + K_w$ assumes that variations in K_d are due only to attenuation by algae and that K_w is a constant (i.e. the Y-intercept). K_w, however, may show strong spatial variations for any particular sampling date; therefore, the assumption of a constant K_w for any particular month may result in reduced correlation coefficients. Spatial variations in the relative number of dominating algal cells (e.g. a particular dominating algal group may comprise 60 percent of the total number of algal cells at one location while at another location it may comprise 90 percent of the total number) will cause variations in

K_d versus chlorophyll a because of spatial variations in the light absorbed per unit chlorophyll a.

Table 7 shows that the greatest K_c values were obtained when the green algal group chlorophyta was dominant or co-dominant (i.e. in June and July) with lesser values when diatoms and blue-green algae were dominant. Comparison of Table 7 with the values of algal fluorescence per unit chlorphyll (Table 4, page 114) indicates that the algal group with the greatest fluorescence per unit chlorophyll (i.e. chlorophyta) also had the greatest light attenuation per unit chlorophyll.

Comparison of K_c values in Table 7 with those reported in the literature (Table 1, page 38) show that the values reported in June and July in Boone Reservoir were higher than for other reservoirs. Values of K_c of 0.0584 and 0.038 m^2/mg Chl a for June and July exceed K_c values of 0.0067 to 0.030 m^2/mg K_c given in Table 1. K_c values for May and August were within the range of values reported in the literature.

Using the method described by Tilzer (37) K_c may be further partitioned into attenuation due to active biomass and attenuation due to pheophytin. The attenuation by pheophytin may be computed as follows:

$$K_p = K_c C \ (1 - p) \qquad (68)$$

where K_c = light attenuation coefficient due to chlorophyll a and pheophytin (m^2/mg Chl a)

K_p = light attenuation coefficient due to pheophytin (ln/m)

p = fraction of active chlorophyll in total pigments

$$= \frac{\text{Corrected Chlorophyll a}}{\text{Uncorrected Chlorophyll a}}$$

Now the coefficient of attenuation due to active chlorophyll a may be defined as K_c', where $K_c' = K_c C - K_p$.

K_w may be further partitioned into components of attenuation due to pure water and attenuation due to dissolved and suspended non-phytoplankton matter (i.e. inanimate suspended solids and dissolved color). This may be done by assuming an appropriate value of K for pure water from the literature. For this analysis, a K_{water} of 0.2 ln/m was assumed based on data presented by Effler (12). The attenuation coefficient due to inanimate particulates and dissolved color may now be computed as:

$$K_{pc} = K_w - K_{water} \tag{69}$$

where K_{pc} = Light attenuation coefficient due to inanimate particulates and dissolved color (ln/m)

K_w = Light attenuation coefficient due to all non-phytoplankton components (ln/m)

K_{water} = Light attenuation coefficient due to pure water (ln/m)

= 0.2/m

Table 8 provides values of K_d for each station and each month predicted using the K_c and K_w values given in Table 7 and the uncorrected chlorophyll a values (both observed and predicted) given in Appendix III, Parts 1 and 2. The partitioning of these predicted K_d values into components of K_cC; K_p; $K_{c'}$; K_{water} and K_{pc} (terms as defined above) is also shown in this table.

Table 8 shows that, in most cases, the greatest contribution to the overall attenuation of light during May to August is due to algal light attenuation as shown by the high K_cC and $K_{c'}$ values. The greatest light attenuation by algae occurred in May when bacillariophyta and cyanophyta were dominant and in June when chlorophyta were dominant. Although the K_c value (i.e. attenuation coefficient per unit chlorophyll a) for the bacillariophyta, cyanophyta dominated algal assemblage in May was significantly lower than the K_c value for the chlorophyta dominated algal assemblage in June, the total attenuation by algae (K_cC or $K_{c'}$) was as large or larger than that in June. This is because the cell counts and chlorophyll

TABLE 8

Predicted K_d Coefficients and Partitioning into Various Attenuation Components*

Station	Month	K_d (ln/m)	$K_c C$ (ln/m)	p	K_p (ln/m)	$K_{c'}$ (ln/m)	K_{water} (ln/m)	K_{pc} (ln/m)
SFHRM 19.0	May	1.13	0.639	0.90	0.064	0.575	0.20	0.294
	June	0.642	0.327	0.83	0.056	0.271	0.20	0.115
	July	0.607	0.418	0.96	0.017	0.401	0.20	0.0
	August	0.641	0.155	0.98	0.003	0.152	0.20	0.286
SFHRM 22.4	May	1.18	0.690	0.90	0.069	0.621	0.20	0.294
	June	0.738	0.423	0.82	0.076	0.347	0.20	0.115
	July	0.640	0.451	0.91	0.041	0.410	0.20	0.0
	August	0.652	0.166	0.98	0.003	0.163	0.20	0.286
SFHRM 25.0	May	1.02	0.524	0.83	0.089	0.435	0.20	0.294
	June	1.09	0.778	0.83	0.132	0.646	0.20	0.115
	July	0.746	0.557	0.85	0.084	0.473	0.20	0.0
	August	0.703	0.218	1.0	0.0	0.218	0.20	0.286

TABLE 8 (continued)

Station	Month	K_d (ln/m)	$K_c C$ (ln/m)	p	K_p (ln/m)	$K_{c'}$ (ln/m)	K_{water} (ln/m)	K_{pc} (ln/m)
SFHRM 26.2	May	0.920	0.426	0.96	0.017	0.409	0.20	0.294
	June	1.04	0.724	0.93	0.051	0.673	0.20	0.115
	July	0.762	0.573	0.92	0.046	0.527	0.20	0.0
	August	0.663	0.177	0.98	0.004	0.173	0.20	0.286
SFHRM 28.3	May	0.987	0.493	0.98	0.010	0.483	0.20	0.294
	June	1.32	1.01	0.93	0.071	0.939	0.20	0.115
	July	0.760	0.571	0.86	0.080	0.491	0.20	0.0
	August	0.662	0.176	1.0	0.0	0.176	0.20	0.286
SFHRM 30.8	May	1.00	0.506	0.93	0.036	0.470	0.20	0.294
	June	1.11	0.804	0.92	0.064	0.740	0.20	0.115
	July	0.975	0.786	0.95	0.039	0.747	0.20	0.0
	August	0.692	0.206	0.94	0.012	0.194	0.20	0.286
WRM 2.0	May	1.16	0.675	0.95	0.034	0.641	0.20	0.294
	June	0.70	0.384	0.88	0.046	0.338	0.20	0.115
	July	0.625	0.436	0.90	0.044	0.392	0.20	0.0
	August	0.722	0.236	0.97	0.007	0.229	0.20	0.286

TABLE 8 (continued)

Station	Month	K_d (ln/m)	$K_c C$ (ln/m)	p	K_p (ln/m)	$K_{c'}$ (ln/m)	K_{water} (ln/m)	K_{pc} (ln/m)
WRM 3.0	May	1.51	1.02	0.90	0.102	0.918	0.20	0.294
	June	0.977	0.662	0.89	0.073	0.589	0.20	0.115
	July	0.870	0.681	0.87	0.089	0.592	0.20	0.0
	August	0.756	0.270	0.96	0.011	0.259	0.20	0.286
WRM 6.0	May	1.62	1.13	0.95	0.060	1.07	0.20	0.294
	June	1.64	1.32	0.91	0.110	1.21	0.20	0.115
	July	0.848	0.659	0.88	0.079	0.580	0.20	0.0
	August	0.723	0.237	0.96	0.009	0.228	0.20	0.286
WRM 8.4	May	1.80	1.31	0.91	0.120	1.19	0.20	0.294
	June	1.25	0.93	0.93	0.065	0.865	0.20	0.115
	July	1.05	0.861	0.89	0.095	0.766	0.20	0.0
	August	0.706	0.220	1.0	0.0	0.220	0.20	0.286
WRM 10.95	May	2.02	1.53	0.87	0.200	1.33	0.20	0.294
	June	2.83	2.51	0.82	0.450	2.06	0.20	0.115
	July	1.27	1.08	0.87	0.140	0.940	0.20	0.0
	August	0.66	0.176	0.94	0.011	0.165	0.20	0.286

TABLE 8 (continued)

*K_d values predicted from uncorrected chlorophyll a results (Appendix III, using K_c and K_w values given in Table 7.

K_cC = attenuation coefficient for chlorophyll a and pheophytin

p = fraction of active chlorophyll a = Corrected Chl a/Uncorrected Chl a

K_p = attenuation coefficient due to pheophytin

$K_{c'}$ = attenuation coefficient due to active phytoplankton = $K_cC - K_p$

K_{water} = attenuation coefficient due to pure water = 0.20/m

K_{pc} = attenuation coefficient due to inanimate particulates and dissolved color = $K_w - K_{water}$

concentrations of the bacillariophyta, cyanophyta dominating assemblage were substantially greater at many locations than for the chlorophyta dominated assemblage of June thus offsetting the effect of the lower K_c value. The lowest values of light attenuation due to algae occurred during the August survey when bacillariophyta and cyanophyta were dominant. These low attenuation values are due to a combined effect of a low value for K_c and relatively low chlorophyll concentrations.

A comparison of predicted K_d values and measured K_d values is given in Table 9. Also shown are the means, standard deviations and correlation coefficients (r^2) for each month. Reasonably good correlation was obtained between predicted and observed results for the months of May, June and July with correlation coefficients (r^2) of 0.81, 0.89 and 0.74, respectively. Poor correlation ($r^2 = 0.22$), however, was obtained for the August data. Although substantial differences sometimes occurred between the predicted and measured values, the differences in the mean values for each month were insignificant.

Table 10 presents values of the fractional contribution of algae (expressed as chlorophyll a) to the total attenuation of underwater irradiance (i.e. $K_c,/K_w$). In most cases attenuation by algae exceeded 50 percent of the total attenuation (i.e. $K_c, > 0.5\ K_d$). Since

TABLE 9

Comparison of Predicted K_d Values With Measured K_d Values

	K_d (ln/m)							
	May		June		July		August	
Station	Predicted	Measured	Predicted	Measured	Predicted	Measured	Predicted	Measured
SFHRM 19.0	1.13	1.12	0.642	0.88	0.607	0.70	0.641	0.47
SFHRM 22.4	1.18	1.13	0.738	0.96	0.640	0.80	0.652	0.59
SFHRM 25.0	1.02	0.91	1.09	1.03	0.746	0.79	0.703	0.72
SFHRM 26.2	0.920	1.06	1.04	1.06	0.762	0.76	0.663	-
SFHRM 28.3	0.987	1.24	1.32	0.86	0.760	0.86	0.662	0.72
SFHRM 30.8	1.00	1.21	1.11	1.02	0.975	0.82	0.692	0.83
WRM 2.0	1.16	.96	0.700	0.79	0.625	0.33	0.722	0.55
WRM 3.0	1.51	1.36	0.977	1.11	0.870	0.53	0.756	0.56
WRM 6.0	1.62	1.31	1.64	0.96	0.848	1.07	0.723	0.82
WRM 8.4	1.80	1.51	1.25	1.44	1.05	1.14	0.706	1.02
WRM 10.95	2.02	2.60	2.83	3.22	1.27	1.29	0.660	0.64
Mean	1.30	1.31	1.21	1.21	0.832	0.826	0.689	0.692
Std. Dev.	0.373	0.462	0.611	0.68	0.202	0.270	0.036	0.165
Correlation (r^2)	(0.81)		(0.89)		(0.74)		(0.22)	

TABLE 10

Fractional Contribution of Algae to Overall Light Attenuation in Boone Reservoir

Station	Fractional Attenuation (K_c/K_d)			
	May	June	July	August
SFHRM 19.0	0.508	0.422	0.661	0.237
SFHRM 22.4	0.526	0.470	0.641	0.629
SFHRM 26.2	0.444	0.647	0.692	0.261
SFHRM 30.8	0.470	0.666	0.728	0.280
WRM 2.0	0.553	0.483	0.627	0.317
WRM 6.0	0.660	0.737	0.684	0.684
WRM 10.95	0.658	0.728	0.740	0.250

attenuation of light by algae is substantial in Boone Reservoir, it would be worthwhile to determine the fractional attenuation of each major algal group (bacillariophyta, chlorophyta, and cyanophyta). This may be done approximately by partitioning K_d as follows:

$$K_d = K_{BAC} N_{BAC} + K_{CHP} N_{CHP} + K_{CYN} N_{CYN} + K_W \quad (70)$$

where K_d = total light attenuation coefficient (m^{-1})

K_{BAC}, K_{CHP}, K_{CYN} = light attenuation coefficients due to bacillariophyta, chlorophyta, and cyanophyta, respectively. (m^2/cell)

N_{BAC}, N_{CHP}, N_{CYN} = number of cells/L for bacillariophyta, chlorophyta, and cyanophyta, respectively.

K_w = attenuation coefficient due to non algal components and pheophytin (m^{-1})

The above equation may be evaluated successfully only if the cell sizes and the amount of light attenuating pigments per cell are approximately constant for each algal group at varying locations in the reservoir or if the size distribution and distribution of light attenuating pigments per cell are constant from one location to the next for each algal group. The concentrations of non-algal light attenuating components which determine the y-intercept

(K_w) must also remain approximately constant for the relationship to be valid.

To obtain values for K_{BAC}, K_{CHP}, K_{CYN}, and K_w, multiple regression analyses were performed using the algal enumeration data given in Appendix II and the corresponding K_d values given in Table 3, page 108. These analyses were performed using an aggregation of all data and again for each specific month (to account for algal group dominance variations or adaptive changes with time). The results of these analyses are shown in Table 11. Also shown are the correlation coefficients for each analysis and the probabilities of a linear relationship between K_d and cell concentrations.

Table 11 shows that there is a wide variation in the values of the attenuation per cell concentration from month to month for any one algal group. Also there are several negative values for attenuation coefficients, a situation which is very unlikely in a natural environment. The probabilities of linear relationships between K_d and cell concentrations were also low for at least one algal group per analysis when regression analyses were performed for specific months. Because of these considerations, it is difficult to provide values for K_{BAC}, K_{CHP}, and K_{CYN} which can be used quantitatively in modeling studies.

TABLE 11

Summary of Multiple Regression Results of K_d Versus Cell Concentrations For Bacillariophyta, Chlorophyta, and Cyanophyta

		Bacillariophyta		Chlorophyta		Cyanophyta		
Month	Corr. Coeff.	K_{BAC} (m^2/cell x10^{-3})	Prob. of Linear Relation	K_{CHP} (m^2/cell x 10^{-3})	Prob. of Linear Relation	K_{CYN} (m^2/cell x 10^{-9})	Prob. of Linear Relation	(1/m)
All data	0.64	0.1520	0.99	0.25	0.99	-0.110	0.91	0.51
May	0.83	0.0620	0.78	1.34	0.68	0.012	0.05	0.14
June	0.99	-0.0517	0.36	0.32	0.99	-0.079	0.76	0.33
July	0.76	-2.3500	0.64	-0.21	0.33	0.640	0.33	1.58
August	0.53	-0.0503	0.30	-0.29	0.73	0.061	0.37	0.90

Two reasons may be given for the high variability and low statistical reliability of the results in Table 11. First, the amount of chlorophyll per cell for each algal group may vary from location to location on any given date and may also vary with time. Variations in chlorophyll a per cell will result in variations in light attenuation per cell for any given algal group. Second, variations in concentrations of non-algal light attenuating substances will adversely affect the regression analyses because the regression equation assumes that the light attenuation of these substances remains constant (i.e. K_w).

To assess the extent of the variability in chlorophyll a per cell, multiple regression analyses were performed of chlorophyll a versus cell concentration for bacillariophyta, chlorophyta, and cyanophyta. Because these algal groups generally compose 95 percent or greater of the total cell numbers, it was assumed that when all three groups have a cell concentration of zero, the total chlorophyll was zero (i.e. the y-intercept was forced through zero in the multiple regression). These analyses may be represented by the following equation:

$$(\text{Chl a})_{TOTAL} = \text{Chl}_{BAC} N_{BAC} + \text{Chl}_{CHP} N_{CHP} + \text{Chl}_{CYN} N_{CYN} \quad (71)$$

where $(\text{Chl a})_{TOTAL}$ = total corrected chlorophyll a for a 0 to 3 meter depth integrated sample (mg/m^3).

Values obtained from Appendix III, Part 1.

Chl_{BAC}, Chl_{CHP}, Chl_{CYN} = corrected Chl a per cell for bacillariophyta, chlorophyta, and cyanophyta, respectively (mg Chl a/cell).

N_{BAC}, N_{CHP}, N_{CYN} = cell concentrations of bacillariophyta, chlorophyta, and cyanophyta, respectively (cells/m^3).

The results of these analyses are given in Table 12. This table shows that the quantity of chlorophyll a per cell did actually vary from month to month which likely resulted in variations in attenuation per cell concentration. Low probabilities of linear relationships and negative values for chlorophyll a per cell were also a problem for the regression analyses for July, August, and the combined data set. This may be due to nonuniformity in the amount of chlorophyll per cell for any given algal group from one location to the next on any given sampling date.

Another reason for the variability in results and poor linear relationships between K_d or chlorophyll a and cell concentrations is analytical error. In obtaining cell counts, an analyst takes a small volume from a sample and identifies and counts all discernible cells within

TABLE 12

Summary of Multiple Regression Results for Total Corrected Chlorophyll a Versus Cell Concentrations for Bacillariophyta, Chlorophyta, and Cyanophyta

	(mg Chlorophyll a/cell) x 10^{-9}						
	Bacillariophyta			Chlorophyta		Cyanophyta	
Month	Corr. Coeff.	C_{BAC}	Prob. of Linear Relation	C_{CHP}	Prob. of Linear Relation	C_{CYN}	Prob. of Linear Relation
All data	0.65	3.61	0.99	8.85	0.99	-0.280	0.18
May	0.99	8.62	0.99	5.75	0.99	2.33	0.78
June	0.99	3.01	0.97	1.79	0.99	1.56	0.99
July	0.74	- 2.45	0.07	-5.23	0.12	21.53	0.32
August	0.83	10.01	0.13	-1.29	0.65	1.09	0.17

that volume using a microscope. The results of cell counts for this small volume are then scaled upward to determine the cell count per liter. The nature of this procedure allows for a significant amount of analyst variability if one analyst is less efficient in counting cells than another analyst or if detritus and turbidity in a sample make positive identification of cells difficult. The scaling up of results to a liter basis magnifies the analyst error.

Although the results of Tables 11 and 12 are inadequate for quantitative modeling they can be used to provide some qualitative insight into which algal groups are the greatest contributors to underwater light attenuation. Table 11 shows that for the months of May and June and when all data were combined, the green algae, chlorophyta, had the greatest attenuation per cell concentration. This supports earlier results of Table 7, page 143, which show that the K_c values for June and July (when chlorophyta populations are high) were the largest. Table 11 also shows that bacillariophyta and cyanophyta had substantially lower values for attenuation per cell concentration than chlorophyta for May, June, and the combined data set. This again supports the findings in Table 7 which show that when these groups were dominant (May and August), K_c values were lower than those when chlorophyta was dominant. The regressions for the months of July and

August show poor linear relationships between K_d and cell concentrations, therefore, qualitative assessments for these months cannot be satisfactorily made.

In summary, the preceding analyses have shown that the light attenuation coefficient, K_d, can be succussfully partitioned in terms of algal related (chlorophyll a and pheophytin) and non-algal related (water, inanimate particulates and dissolved color) components. When partitioned in this manner, the data show that algal related components were, in most cases, the greatest contributor to overall attenuation for the period of May to August. The green algae, chlorophyta, were shown to cause the greatest attenuation of light per unit chlorophyll and when dominant resulted in high K_d values. Although the attenuation per unit chlorophyll for periods of bacillariophyta and cyanophyta dominance were lower than that of chlorophyta, the strong dominance and high concentrations of these algal groups in May resulted in K_d values which were as large or larger than those obtained during periods of chlorophyta dominance. Attempts to partition K_d in terms of cell concentrations (cells/L) for the three major algal groups was of little quantitative success due to the high variability of the data, yet these results did qualitatively support findings that the group chlorophyta has the greatest potential for light attenuation.

4.1.2.3 Partitioning of K_d based on evaluation of inherent optical properties

Another method for partitioning K_d into various attenuating components involves establishing relationships between the inherent optical properties of water and the various attenuating substances (algae, water, inanimate particulates, etc.). The inherent properties may then be related to the apparent optical property, K_d, by using relationships derived by Kirk (12,19) from a Monte Carlo computer simulation of light penetration. This method has been successfully field tested by Kirk (20) and by Effler (12). Details of this method have been described previously in Section 2.5. The general procedure involved in this partitioning method involves three steps:

1. Estimation of the inherent optical properties a and b where "a" is the total absorption coefficient of a collimated beam of light and "b" is the total scattering coefficient of a collimated beam of light.
2. Evaluation of the relationship between a and b and the various attenuating substances. This may be done by linear regression of the concentrations of attenuating substances on a and b.

3. Calculation of K_d from measured or predicted values of a and b using the relationship developed by Kirk (19):

$$K_d = (a^2 + 0.256\ ab)^{1/2} \qquad \text{(Equation 19)}$$

The use of field transmissivity and turbidity data provides a convenient method for estimating values for the total absorption and scattering coefficients, a and b, and the beam attenuation coefficient, c, where c = a + b. Appendix IV provides a summary of the field transmissivity results (i.e. % transmittance) and corresponding field turbidity values. This data was collected only during the July and August surveys. In many instances, measurements of turbidity in the surface layer of water is omitted; this is due to interference of ambient light which is scattered into the photocell of the instrument.

The values of a and b were estimated using the Beer-Lambert equation for a beam of collimated light which may be written as:

$$\frac{I_z}{I_o} = e^{-cz} \qquad \text{(Equation 11)}$$

where I_o = initial intensity of collimated beam

I_z = remaining intensity of collimated beam after transversing a pathlength z

c = beam attenuation coefficient (ln/m)

= a + b

z = pathlength (m)

The percent transmittance values measured in the field may be expressed in terms of I_z/I_o by noting that:

$$100(I_z/I_o) = \%T \tag{72}$$

where T = transmittance (unitless)

Also, for the Montedoro Whitney Model TMU-1B instrument which was used for the measurement of transmissivity, the pathlength, z, was fixed at 1 meter. Thus the Beer-Lambert equation for beam attenuation measurements made on Boone Reservoir may be simplified to:

$$\frac{I_z}{I_o} = e^{-c(1)} = e^{-c} \tag{73}$$

or

$$\frac{\%T}{100} = e^{-c} = e^{-(a+b)} \tag{74}$$

Thus, values for the beam attenuation coefficient, c, may be obtained directly from the measurements of %T.

The value of the scattering coefficient, b, may be obtained by assuming b to be directly related to turbidity. This direct relationship between turbidity, expressed in NTU, and b has been demonstrated by Kirk for turbid Australian waters (20,22). To obtain the relationship between turbidity and light attenuation due to scattering, regression analyses were performed of -ln(%T/100), which is equivalent to c, versus turbidity. This regression yields an equation of the following form:

$$c = A + Bt \quad (75)$$

where B = slope of C versus turbidity

A = y-intercept of C versus trubidity

Since Bt represents the factor which explains the variation in c due to turbidity or scattering, it will be assumed that Bt is equivalent to the beam attenation coefficient due to scattering, b. The term A represents the fraction of c which does not vary with changes in turbidity, hence, it will be assumed that A is equivalent to the beam attenuation coefficient due to absorption, a.

The regression analyses described above were performed for the field turbidity and transmissivity data given in Appendix IV. As mentioned previously corresponding measurements of field turbidity and transmissivity were obtained only during the months of July and August, therefore regression analyses were performed only for these months. The values of a, b and c obtained for each station are given in Table 13.

The turbidity value used in the computation of b (i.e. b = Bt) was taken as the mean turbidity of the euphotic zone. Also shown are the correlation coefficients, r^2, for the regression of c versus turbidity. Figure 13 shows typical plots of c, expressed as ln(%T/100), versus turbidity. In most cases a high correlation was obtained between c and turbidity.

TABLE 13

Estimates of Inherent Optical Properties a, b, and c from Field Transmissometer Measurements

Station	July Survey					August Survey				
	a (ln/m)	Avg. Turbidity* (NTU)	b (ln/m)	c (ln/m)	Corr.** Coeff., r^2	a (ln/m)	Avg. Turbidity* (NTU)	b (ln/m)	c (ln/m)	Corr.** Coeff., r^2
SFHRM 19.0	0.314	1.8	0.414	0.728	0.92	0.30	1.4	0.27	0.57	0.91
SFHRM 22.4	0.269	2.2	0.460	0.729	0.96	0.27	2.0	0.42	0.69	0.96
SFHRM 25.0	0.367	3.6	0.612	0.979	0.79	0.0	2.2	0.92	0.92	0.77
SFHRM 26.2	0.366	2.8	0.560	0.926	0.96	0.23	2.1	0.48	0.71	0.99
SFHRM 28.3	0.428	3.7	0.703	1.130	0.83	0.22	2.1	0.48	0.70	0.99
SFHRM 30.8	1.350	4.1	0.0	1.350	0.02	0.65	2.8	0.34	0.99	0.60
WRM 2.0	0.320	2.0	0.42	0.74	0.54	0.25	2.2	0.46	0.71	0.94
WRM 3.0	0.470	2.4	0.38	0.85	0.45	0.20	2.3	0.53	0.73	0.98
WRM 6.0	0.560	3.0	0.54	1.10	0.91	0.41	2.7	0.57	0.98	0.98
WRM 8.4	0.85	3.1	0.62	1.47	0.98	0.69	2.5	0.33	1.02	0.98
WRM 10.95	2.14	3.4	0.07	2.21	0.89	1.27	4.1	0.10	1.27	0.01
WRM 13.0	1.79	7.4	0.52	2.31	0.82	-	-	-	-	-

*Average for the depth of the euphotic zone.

**Correlation coefficient for the regression of C versus turbidity.

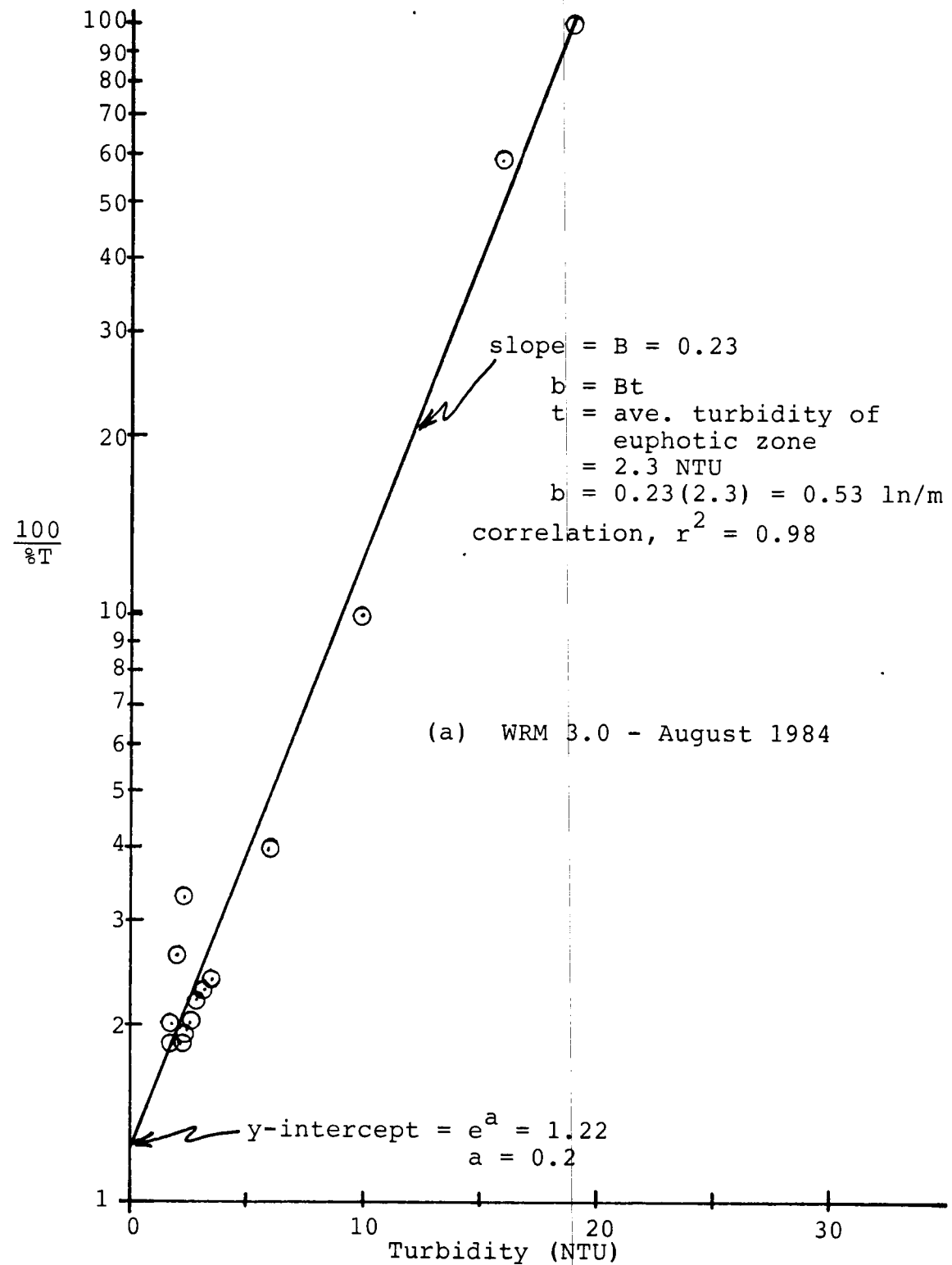

Figure 13. Regression Analysis of -ln(%T/100) vs. Turbidity for Determination of a, b, and c.

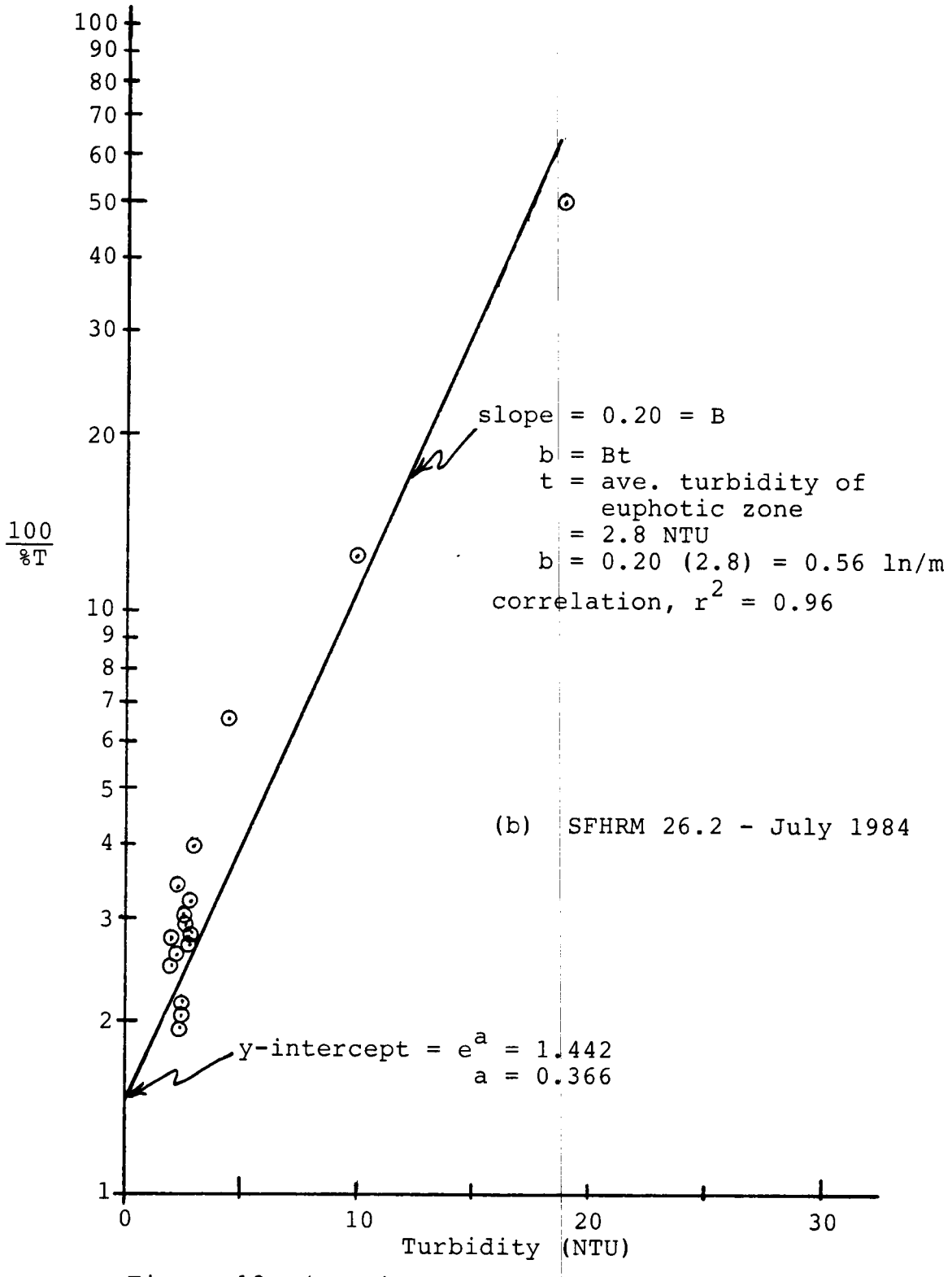

Figure 13 (Continued)

By linear regression with chlorophyll a, the coefficients a and b may be partitioned in terms of light attenuation due to phytoplankton. Figures 14 a and b show the results of this regression analyses. Poor correlation (r^2 less than 0.50) was obtained in most cases between chlorophyll a (uncorrected for pheophytin) and a and b. For the July data, however, a good correlation (r^2 = 0.91) was obtained between the absorption coefficient a and uncorrected chlorophyll a (see Figure 14-a). Because of the poor correlations obtained between a and b and chlorophyll a for the majority of the data, further partitioning of a and b into components of pheophytin, water, and non-phytoplankton dissolved and particulate substances was not performed.

An evaluation of the accuracy of using inherent optical properties to predict the apparent optical property, K_d, may be performed by comparing predicted K_d values with measured K_d values. Table 14 provides a comparison of the predicted values with the measured values. It can be seen from this table that the prediction method based on a and b significantly underestimated K_d in most cases. Correlation coefficients between predicted and observed values were not good with correlation coefficients of 0.66 and 0.36 for July and August, respectively. Using the t-test of paired comparisons the differences between the predicted and measured values were found to be significant at a 99% confidence level.

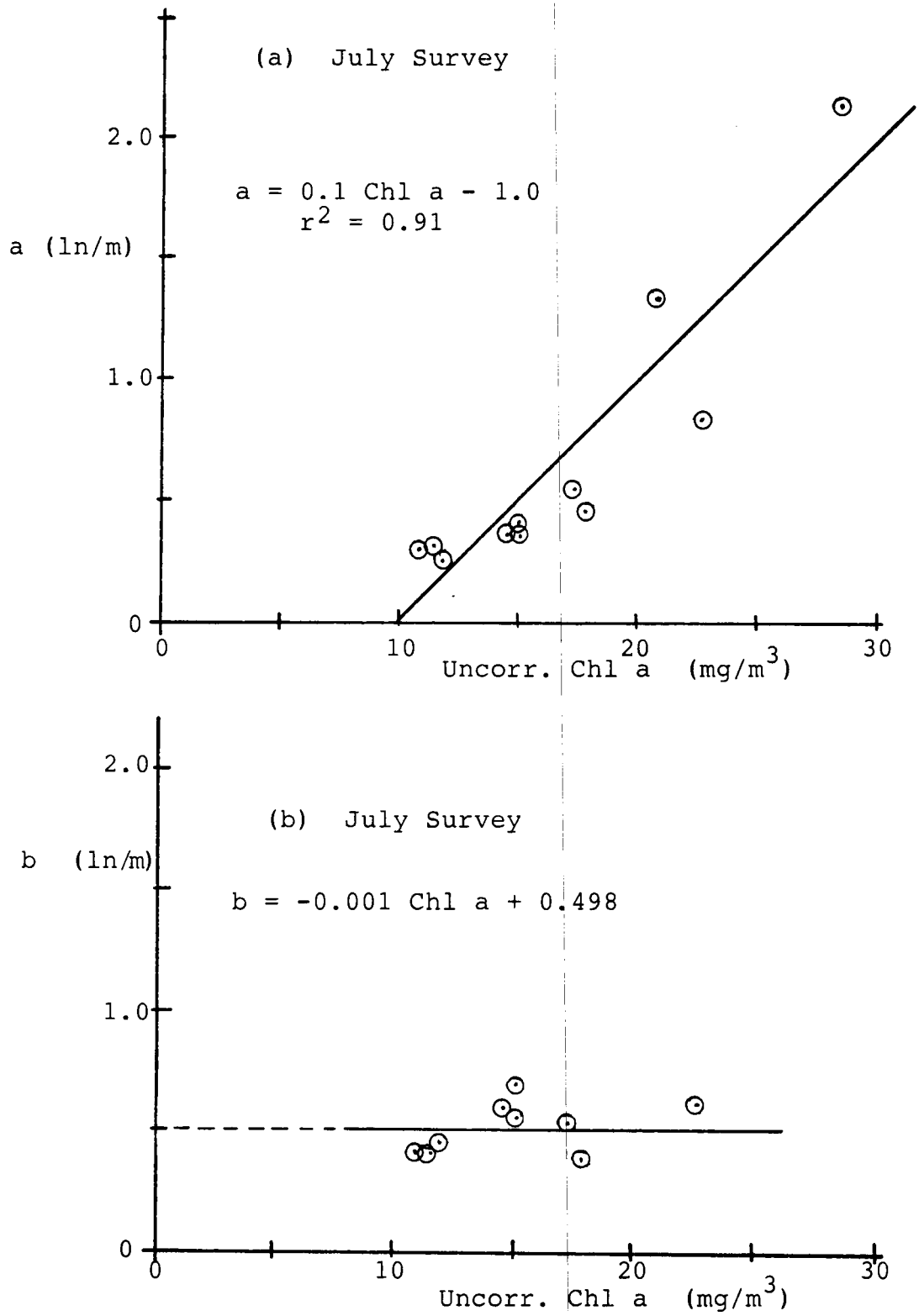

Figure 14. Correlation of Total Absorption Coefficients, a, and Total Scattering Coefficients, b, With Chlorophyll a.

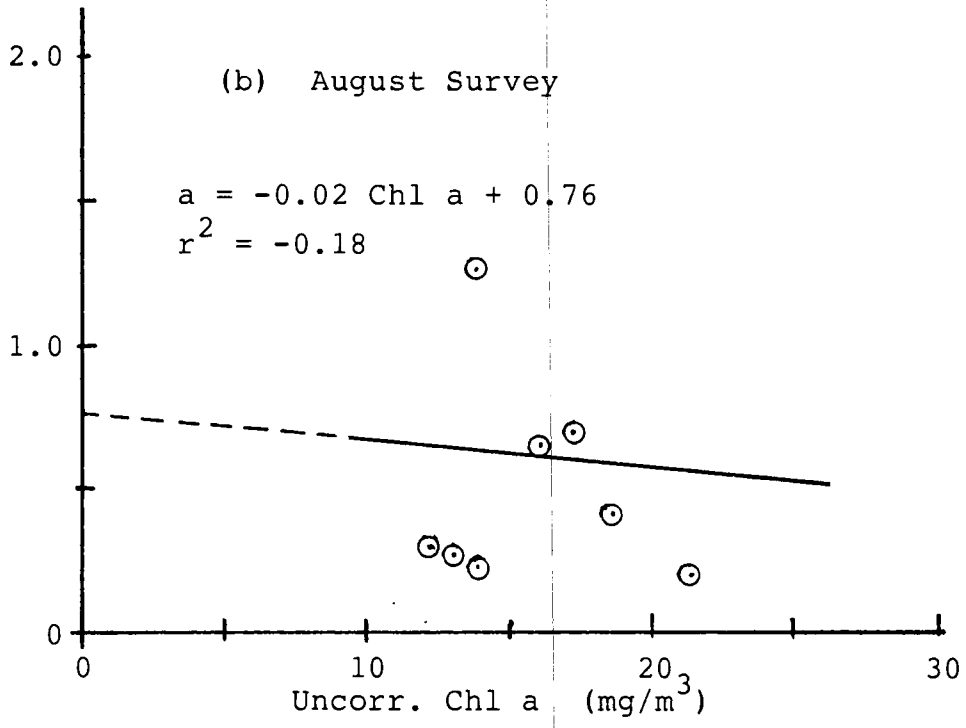

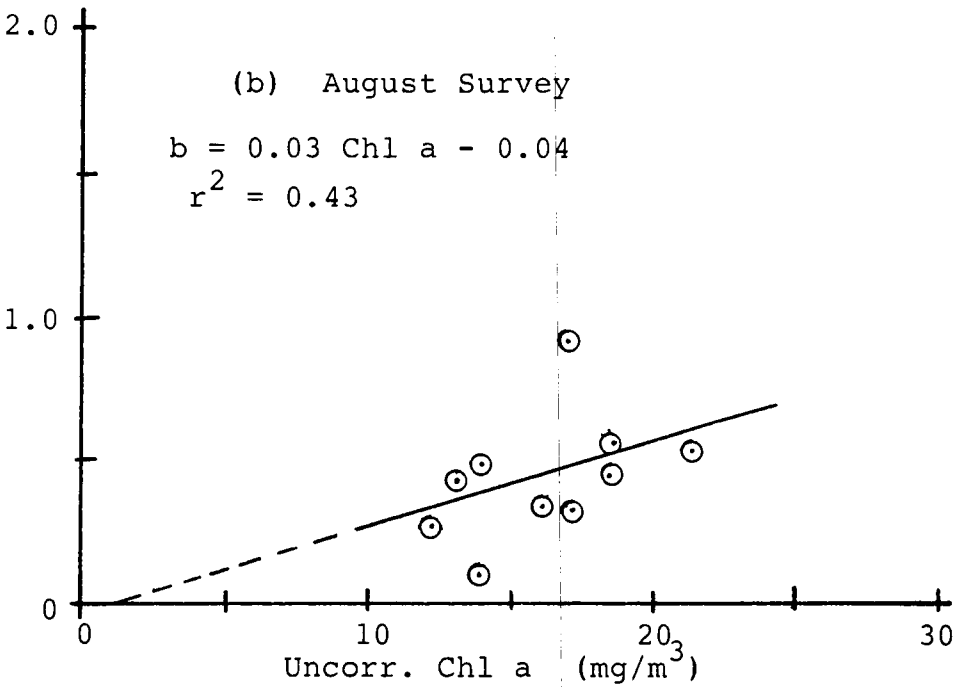

Figure 14 (Continued)

TABLE 14

Comparison of K_d Values Predicted from Inherent Optical Properties and K_d Values Measured in the Field

	July Survey		August Survey	
Station	Predicted K_d (ln/m)	Measured K_d (ln/m)	Predicted K_d (ln/m)	Measured K_d (ln/m)
SFHRM 19.0	0.363	0.70	0.332	0.47
SFHRM 22.4	0.323	0.80	0.319	0.59
SFHRM 25.0	0.438	0.79	-	0.72
SFHRM 26.2	0.431	0.76	0.280	-
SFHRM 28.3	0.510	0.86	0.275	0.72
SFHRM 30.8	1.35	0.82	0.692	0.83
WRM 2.0	0.370	0.33	0.303	0.55
WRM 3.0	0.516	0.53	0.259	0.56
WRM 6.0	0.625	1.07	0.477	0.82
WRM 8.4	0.926	1.14	0.73	1.02
WRM 10.95	2.15	1.29	1.28	0.64

Correlation Coefficient (r^2) = 0.66 for July
= 0.36 for August

NOTE: Predicted K_d value obtained by the equation developed by Kirk:

$$K_d = (a^2 + 0.256\ ab)^{0.5}$$

(a and b values obtained from Table 13)

Two possible reasons for the significant differences between the measured and predicted values are proposed. First the prediction method by Kirk is based on an assumed volume scattering function (19). Any significant deviations from this volume scattering function may result in losses in accuracy. The method was reported to work well in Australian waters for which light attenuation is predominantly due to turbidity and color derived from soil erosion (19). In Boone Reservoir, however, the light attenuation is controlled by phytoplankton and differences in the volume scattering function and hence significant losses of accuracy in the prediction method may be expected. The second possible source of error may be due to the use of transmissometer readings to represent the beam attenuation due to scattering and absorption. It was assumed that the percent transmittance measured by the transmissometer was the percent of the original collimated light beam intensity which was not scattered or absorbed. Thus it was assumed that the transmissometer photosensor measured only the percent intensity reduction of the collimated beam and did not respond to scattered light. It is probable, however, that some of the light scattered from the collimated beam was scattered into the photosensor resulting in higher than actual beam transmittance values. To completely exclude scattered light from entering the photosensor would require

that the acceptance angle of the photosensor be extremely small and directly in line with the path of the collimated beam.

Comparison of the two methods used in partitioning the overall light extinction coefficients for Boone Reservoir show that the highest correlations were obtained when the first method (regression of K_d on chlorophyll a concentration) was used. The value of the second method in computing K_d should not be overlooked, however. More work is needed in the definition of volume scattering functions and radiance distributions in reservoirs where light attenuation is dominated by algae. If this information is obtained, modeling studies similar to those by Kirk (19,20) may be used to develop equations relating the inherent optical properties, a and b, to the apparent optical properties, K_d. Once perfected, the use of this method becomes very desirable because laboratory measurements of the scattering and absorption coefficients, a and b, can be used to model the actual light attenuation in a reservoir.

The preceding analyses of light attenuation in Boone Reservoir have shown that algae were the major influence on reservoir transparency for the period investigated (May through August). It has been observed that severe metalimnetic sags in dissolved oxygen occur in Boone Reservoir during the period when algal biomass is the

greatest (i.e. spring and summer). It has been suggested that this is due to the death, settling, and aerobic decomposition of algal cells. Reductions in algal populations would thus be a worthy reservoir management goal for the reservoir. To assess the influences of various reservoir management strategies in obtaining algal population reductions, accurate models of algal dynamics should be developed. In the next section, the application of light-productivity models will be evaluated for Boone Reservoir in an attempt to obtain the light response parameters which are needed in the modeling of algal dynamics.

4.2 Light-Productivity Modeling

Measurements of primary productivity rates were made on Boone Reservoir in conjunction with measurements of chlorophyll a, light attenuation, and algal group composition. Table 15 presents the results of these measurements. Figure 15 shows typical photosynthetic profiles with depth for several locations. Table 15 shows that the lowest algal production rates generally occurred in May when cyanophyta and bacillariophyta were the dominant algal groups. Maximum production rates occurred during periods of chlorophyta dominance at four of the seven sampling locations, during cyanophyta dominance at two locations, and during bacillariophyta dominance at one location.

TABLE 15

Boone Reservoir--May to August, 1984,
Primary Productivity Results

Station	Date	Mean Corr. Chl a (mg/m^3)	Primary Production ($mg/ C/m^3/hr$) 0.5 Meter	1.0 Meter	2.0 Meter	3.0 Meter	Irradiance, I ($\mu W/cm^2$) x 10^{-3} 0.5 Meter	1.0 Meter	2.0 Meter	3.0 Meter
SFHRM 19.0	5/24/84	16.02	1.65	1.95	1.28	1.31	27.0	11.2	3.5	1.4
	6/12/84	4.01	9.81	10.39	9.69	5.62	31.0	15.0	5.7	2.4
	7/19/84	9.35	2.63	3.67	4.93	6.60	42.0	21.0	6.6	4.5
	8/21/84	9.34	5.79	5.75	5.27	3.32	39.0	3.3	2.1	1.4
SFHRM 22.4	5/24/84	19.09	4.47	5.76	3.00	1.68	41.0	18.8	7.0	2.3
	6/12/84	5.07	12.72	13.63	12.54	7.93	33.0	17.0	6.9	2.5
	7/19/84	10.95	12.30	12.13	11.83	10.23	44.0	18.0	12.0	1.9
	8/21/84	11.48	4.49	5.76	4.03	3.10	8.5	6.0	3.6	2.2
SFHRM 26.2	5/24/84	19.22	2.71	3.04	2.86	0.34	42.0	18.6	6.6	1.8
	6/12/84	10.68	7.53	7.82	6.26	1.65	33.0	16.0	6.6	2.1
	7/19/84	16.55	5.90	8.00	7.20	4.13	45.0	17.0	6.6	3.6
	8/21/84	14.69	7.18	6.58	6.69	2.32	-	-	-	-
SFHRM 30.8	5/24/84	23.76	3.46	3.68	2.72	0.95	41.0	9.5	2.7	0.82
	6/12/84	11.21	11.37	9.51	8.33	2.05	30.0	8.7	3.6	1.2
	7/19/84	20.56	13.63	1.97	1.60	7.30	38.0	5.7	3.0	1.1
	8/21/84	16.02	18.07	13.33	13.14	7.48	35.0	18.6	6.6	3.0

TABLE 15 (continued)

Station	Date	Mean Corr. Chl a (mg/m^3)	Primary Production ($mg/ C/m^3/hr$) 0.5 Meter	1.0 Meter	2.0 Meter	3.0 Meter	Irradiance, I ($\mu W/cm^2$) x 10^{-3} 0.5 Meter	1.0 Meter	2.0 Meter	3.0 Meter
WRM 2.0	5/25/84	17.49	2.71	3.75	1.92	0.51	22.0	6.6	3.4	1.2
	6/13/84	6.14	6.26	7.24	3.66	1.54	1.5	2.8	1.6	0.75
	7/20/84	9.35	10.38	10.68	7.13	3.03	5.4	1.5	1.3	0.9
	8/23/84	19.76	16.88	7.95	7.58	7.86	3.8	1.5	1.1	0.66
WRM 6.0	5/25/84	51.93	12.12	14.42	13.54	5.57	25.0	6.6	3.1	0.48
	6/13/84	20.29	15.99	20.11	12.12	7.03	20.0	3.9	1.3	0.57
	7/20/84	16.29	33.18	30.10	19.20	9.25	41.0	15.0	3.9	1.4
	8/23/84	21.36	11.11	16.39	11.95	4.61	9.9	3.0	1.4	0.71
WRM 10.95	5/25/84	70.36	61.77	59.71	13.09	1.51	26.1	6.4	0.46	-
	6/13/84	32.57	29.22	13.96	3.33	0.41	6.6	1.8	0.07	-
	7/20/84	24.83	55.80	39.98	22.45	6.20	13.0	2.4	0.63	0.17
	8/23/84	18.16	14.65	16.97	10.32	5.09	16.5	5.0	3.0	1.2

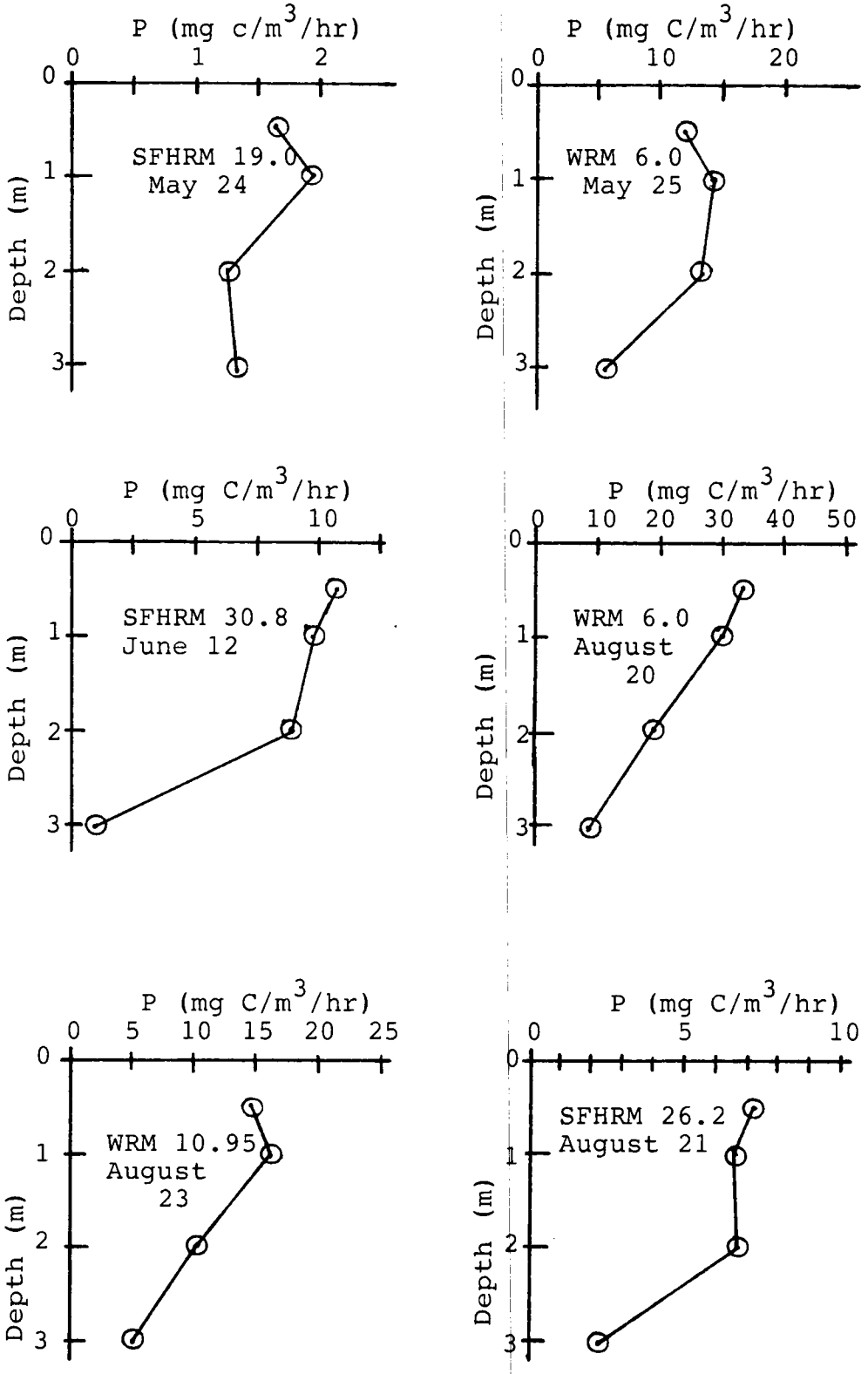

Figure 15. Typical Photosynthetic Rate Profiles—Boone Reservoir.

Table 15 also shows that photoinhibition was evident in 17 of the 28 photosynthetic profiles (i.e. production rates at 0.5 meters were less than one or more of the rates at lower depths). This, however, does not mean that only 17 cases exhibited surface inhibition, for inhibition may have occurred in the depth from 0 to 0.5 meters where no productivity measurements were made. Table 16 presents primary production rates per unit chlorophyll a (i.e. assimilation numbers). This table shows that the largest assimilation numbers generally occurred when chlorophyta was dominant.

As shown in section 2.6.3 the instantaneous volumetric production rate may be modeled as:

$$P = P_{max} F(I) \qquad \text{(Equation 19)}$$

or

$$\gamma = \gamma_{max} F(I) \qquad \text{(Equation 24)}$$

where P_{max} and γ_{max} = The light saturated production rate and assimilation number, respectively

$F(I)$ = A light curve relationship

The maximum light saturated production, maximum assimilation number, and the light intensity which saturates photosynthesis may be approximated from the data in Tables 15 and 16. This may be done by selecting

TABLE 16

Assimilation Numbers at Depths of Primary Production Measurements--Boone Reservoir

Station	Date	Assimilation Number, γ mg C/mg Chl a/hr 0.5 Meter	1.0 Meter	2.0 Meter	3.0 Meter
SFHRM 19.0	5/24/84	0.10	0.12	0.080	0.082
	6/12/84	2.45	2.59	2.42	1.40
	7/19/84	0.28	0.39	0.53	0.71
	8/21/84	0.62	0.62	0.56	0.36
SFHRM 22.4	5/24/84	0.23	0.30	0.16	0.09
	6/12/84	2.50	2.69	2.47	1.56
	7/19/84	1.12	1.11	1.08	0.93
	8/21/84	0.39	0.50	0.35	0.27
SFHRM 26.2	5/24/84	0.14	0.16	0.15	0.02
	6/12/84	0.71	0.73	0.59	0.15
	7/19/84	0.36	0.48	0.44	0.25
	8/21/84	0.49	0.45	0.46	0.16
SFHRM 30.8	5/24/84	0.15	0.15	0.11	0.040
	6/12/84	1.01	0.85	0.74	0.18
	7/19/84	0.66	0.096	0.078	0.36
	8/21/84	1.13	0.83	0.82	0.47
WRM 2.0	5/25/84	0.50	0.21	0.11	0.029
	6/13/84	1.02	1.18	0.60	0.25
	7/20/84	1.11	1.14	0.76	0.32
	8/23/84	0.85	0.40	0.38	0.40
WRM 6.0	5/25/84	0.23	0.28	0.26	0.11
	6/13/84	0.79	0.99	0.60	0.35
	7/20/84	2.04	1.85	1.18	0.57
	8/23/84	0.52	0.77	0.56	0.22
WRM 10.95	5/25/84	0.88	0.85	0.19	0.021
	6/13/84	0.90	0.43	0.10	0.013
	7/20/84	2.25	1.61	0.90	0.25
	8/23/84	0.81	0.93	0.57	0.28

the maximum rates which occur in each depth profile (P_{max} and γ_{max}) and the corresponding light intensity (I_{max}). Table 17 presents these values for the cases which exhibited surface photoinhibition. Only values for profiles which exhibited photoinhibition are listed because in these cases one can be more confident that the maximum value is the light saturated rate due to lower rate values both above and below. In cases where the rate at 0.5 meters is the greatest, it is possible that a higher rate may have been present somewhere between the surface and the 0.5 meter depth. The values in Table 17 were grouped by month and mean values of γ_{max} and I_p were obtained. Mean values of P_{max} were not obtained since this parameter varies significantly with chlorophyll a concentration. Aggregation of the total data set, irregardless of sampling date, and subsequent computation of mean values was avoided due to adaptive and species dominance variations which occur with time. Inspection of Table 17 shows that even for data collected during the same months there is substantial variation in the values for γ_{max} and I_{max}. Theory predicts that if the conditions for growth (nutrients, physiological state of algae, available carbon) are the same at each location then the values of γ_{max} and I_{max} should be similar. This is not so, however, for the data collected

on Boone Reservoir; possible explanations for the variance may include:

1. Differences in nutrient concentrations from location to location (i.e. differences in nutrient limitations)
2. Variations in the physiological or adaptive state of the algae at different locations
3. Algal group dominance variations at different locations
4. The sampling program was designed based on the assumption that the upper zone of the reservoir (i.e. the epilimnion) was well mixed and as such the algae within the euphotic zone are uniformly dispersed throughout. Based on this assumption all samples for production rate analyses were collected as 0 to 3 meter depth integrated samples. However, if wind mixing is not great enough, algal stratification may occur resulting in light-shade adaptive changes with depth and thus differing photosynthetic responses with depth. The collection of depth integrated composite samples in an algal stratified zone followed by incubation at different depths (i.e. different light levels) will cause cells which have adapted to low light levels to be subjected to higher (possibly

damaging) light levels and cells which have adapted to higher light levels to be subjected to lower light levels. This situation may result in erratic results. The possibility of optical stratification was demonstrated earlier in Section 4.1.1; thus variability in algal light response parameters (I_{max}, P_{max}, etc.) due to algal stratification is possible.

5. Experimental error

Using the mean values of γ_{max} and I_{max} given in Table 17 for each month, equations can be written for primary productivity using established light curve relationships. For this analysis the light curve equation of Steele (35) will be used first:

$$F(I) = (I/I_{max})e^{1-(I/I_{max})} \qquad \text{(Equation 22)}$$

This equation was selected because it includes photoinhibition, an occurrence which was observed in Boone Reservoir. Substituting the mean values given in Table 17 in the above equation yields productivity equations for each month as follows:

May $\gamma = 0.20(I/11.9)e^{1-(I/11.9)}$ (76)

June $\gamma = 1.64(I/10.9)e^{1-(I/10.9)}$ (77)

July $\gamma = 0.67(I/13.2)e^{1-(I/13.2)}$ (78)

TABLE 17

Light Saturated Values for Productivity (P_{max}), Assimilation Number (γ_{max}) and the Corresponding Irradiance (I_{max})--Boone Reservoir

Station	May 24, 1984			June 12, 1984			July 19, 1984			August 23, 1984		
	P_{max}	γ_{max}	I_{max}	P_{max}	γ_{max}	I_{max}	P_{max}	γ_{max}	I_{max}	P_{max}	γ_{max}	I_{max}
SFHRM 19.0	1.95	0.12	11.2	10.39	2.59	15.0	3.67	0.39	21.0	-	-	-
SFHRM 22.4	5.76	0.30	18.8	13.63	2.69	17.0	-	-	-	5.76	0.50	6.0
SFHRM 26.2	3.04	0.16	18.6	7.82	0.73	16.0	8.00	0.48	17.0	-	-	-
SFHRM 30.8	3.68	0.15	9.5	-	-	-	-	-	-	-	-	-
WRM 2.0	3.75	0.21	6.6	7.24	1.18	2.8	10.68	1.14	1.5	-	-	-
WRM 6.0	14.42	0.28	6.6	20.11	0.99	3.9	-	-	-	16.39	0.77	3.0
WRM 10.95	-	-	-	-	-	-	-	-	-	16.97	0.93	5.0
Mean	-	0.20	11.9	-	1.64	10.9	-	0.67	13.2	-	0.73	4.7
Std. Dev.	-	0.07	5.6	-	0.93	6.98	-	0.33	10.3	-	0.22	2.53

NOTE: Units for P_{max}, γ_{max}, and I_{max} are $mgC/m^3/hr.$, mg C/mg Chl a/hr. and $\mu W/cm^2 \times 10^{-3}$, respectively.

$$\underline{\text{August}} \quad \gamma = 0.73(I/4.7)e^{1-(I/4.7)} \qquad (79)$$

The applicability of these productivity equations in simulating actual observed data using measured irradiance data is shown in Table 18. The correlation between predicted and observed assimilation numbers was poor in each case with r^2 values of 0.33, 0.38, 0.24 and 0.11 for May, June, July and August, respectively. Figure 16 illustrates the correlation between the observed and predicted results for the months of May and August. In most all cases the effects of photoinhibition were overestimated.

Because of the poor fit obtained with the Steele equation and the overestimation of photoinhibition, the use of the Smith light curve equation was evaluated to determine if it provides a better fit. The equation was given previously as:

$$F(I) = \frac{I}{(I_p^m + I^m)^{1/m}} \qquad \text{(Equation 20)}$$

where m = 2.0

I_p = Light irradiance which produces 70-80% of the maximum light saturated rate

I = Light irradiance at depth of interest

Assuming that I_p is approximately 80% of I_{max} the equation for prediction of assimilation number may be expressed for each month as:

TABLE 18

Comparison of Measured Assimilation Numbers with Predicted Assimilation Numbers Using the Steele Light Curve Equation

		Assimilation Number (mg C/mg Chl a/hr)							
		0.5 m		1.0 m		2.0 m		3.0 m	
Month	Station	Predict.	Obs.	Predict.	Obs.	Predict.	Obs.	Predict.	Obs.
May	SFHRM 19.0	0.13	0.10	0.20	0.12	0.12	0.08	0.06	0.08
	SFHRM 22.4	0.06	0.23	0.18	0.30	0.18	0.16	0.09	0.09
	SFHRM 26.2	0.06	0.14	0.18	0.16	0.17	0.15	0.07	0.02
	SFHRM 30.8	0.06	0.15	0.20	0.15	0.10	0.11	0.03	0.04
	WRM 2.0	0.16	0.50	0.17	0.21	0.12	0.11	0.05	0.03
	WRM 6.0	0.14	0.23	0.17	0.28	0.11	0.26	0.02	0.11
	WRM 10.95	0.13	0.88	0.17	0.85	0.02	0.19	-	0.02
		(r^2 = 0.33 for May)							
June	SFHRM 19.0	0.10	2.45	1.55	2.59	1.38	2.42	0.79	1.40
	SFHRM 22.4	0.65	2.50	1.46	2.69	1.50	2.47	0.81	1.56
	SFHRM 26.2	0.65	0.71	1.51	0.73	1.47	0.59	0.71	0.15
	SFHRM 30.8	0.78	1.01	1.60	0.85	1.06	0.74	0.44	0.18
	WRM 2.0	0.53	1.02	0.89	1.18	0.57	0.60	0.29	0.25
	WRM 6.0	1.31	0.79	1.12	0.99	0.47	0.60	0.22	0.35
	WRM 10.95	1.47	0.90	0.62	0.43	0.03	0.10	-	0.01
		(r^2 = 0.38 for June)							

TABLE 18 (continued)

Month	Station	Assimilation Number (mg C/mg Chl a/hr)							
		0.5 m		1.0 m		2.0 m		3.0 m	
		Predict.	Obs.	Predict.	Obs.	Predict.	Obs.	Predict.	Obs.
July	SFHRM 19.0	0.36	0.28	0.57	0.39	0.55	0.53	0.44	0.71
	SFHRM 22.4	0.22	1.12	0.64	1.11	0.67	1.08	0.23	0.93
	SFHRM 26.2	0.21	0.36	0.65	0.48	0.55	0.44	0.38	0.25
	SFHRM 30.8	0.29	0.66	0.51	0.10	0.33	0.08	0.14	0.36
	WRM 2.0	0.49	1.11	0.18	1.14	0.16	0.76	0.12	0.32
	WRM 6.0	0.25	2.04	0.66	1.85	0.40	1.18	0.17	0.57
	WRM 10.95	0.67	2.25	0.28	1.61	0.08	0.90	0.02	0.25
		(r^2 = 0.24 for July)							
August	SFHRM 19.0	0.28	0.62	0.69	0.62	0.57	0.56	0.44	0.36
	SFHRM 22.4	0.59	0.39	0.71	0.50	0.71	0.35	0.58	0.27
	SFHRM 26.2	-	0.49	-	0.45	-	0.46	-	0.16
	SFHRM 30.8	0.01	1.13	0.15	0.83	0.68	0.82	0.67	0.47
	WRM 2.0	0.71	0.85	0.46	0.40	0.37	0.38	0.24	0.40
	WRM 6.0	0.51	0.52	0.67	0.77	0.44	0.56	0.26	0.22
	WRM 10.95	0.21	0.81	0.73	0.93	0.67	0.57	0.39	0.28
		(r^2 = .11 for August)							

NOTE: Predicted values were obtained using Steele's light curve equation which includes photoinhibition.

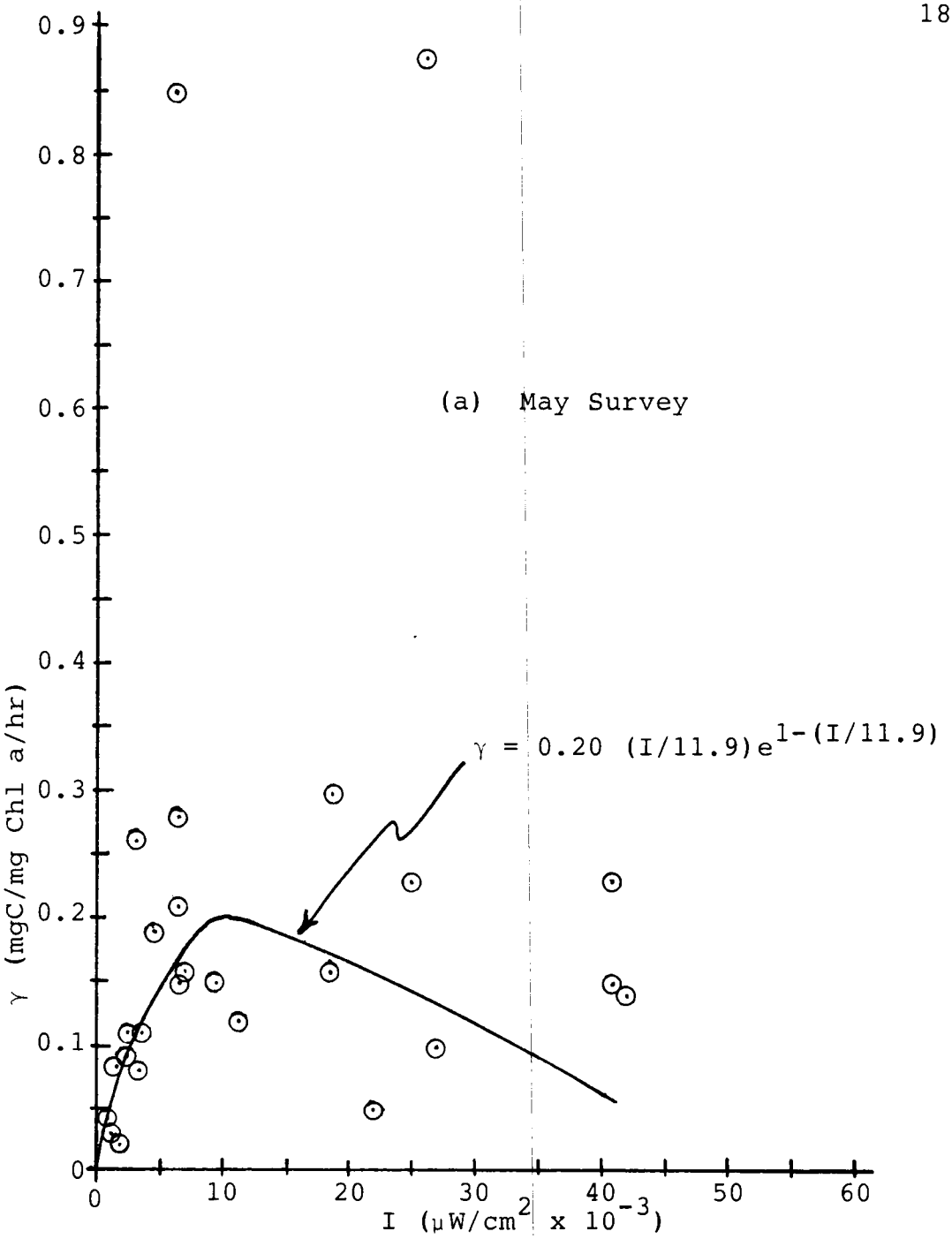

Figure 16. Assimilation Number (γ) vs. Irradiance (I)——Observed Values and Values Predicted Using Steele Light Curve Equation——Boone Reservoir.

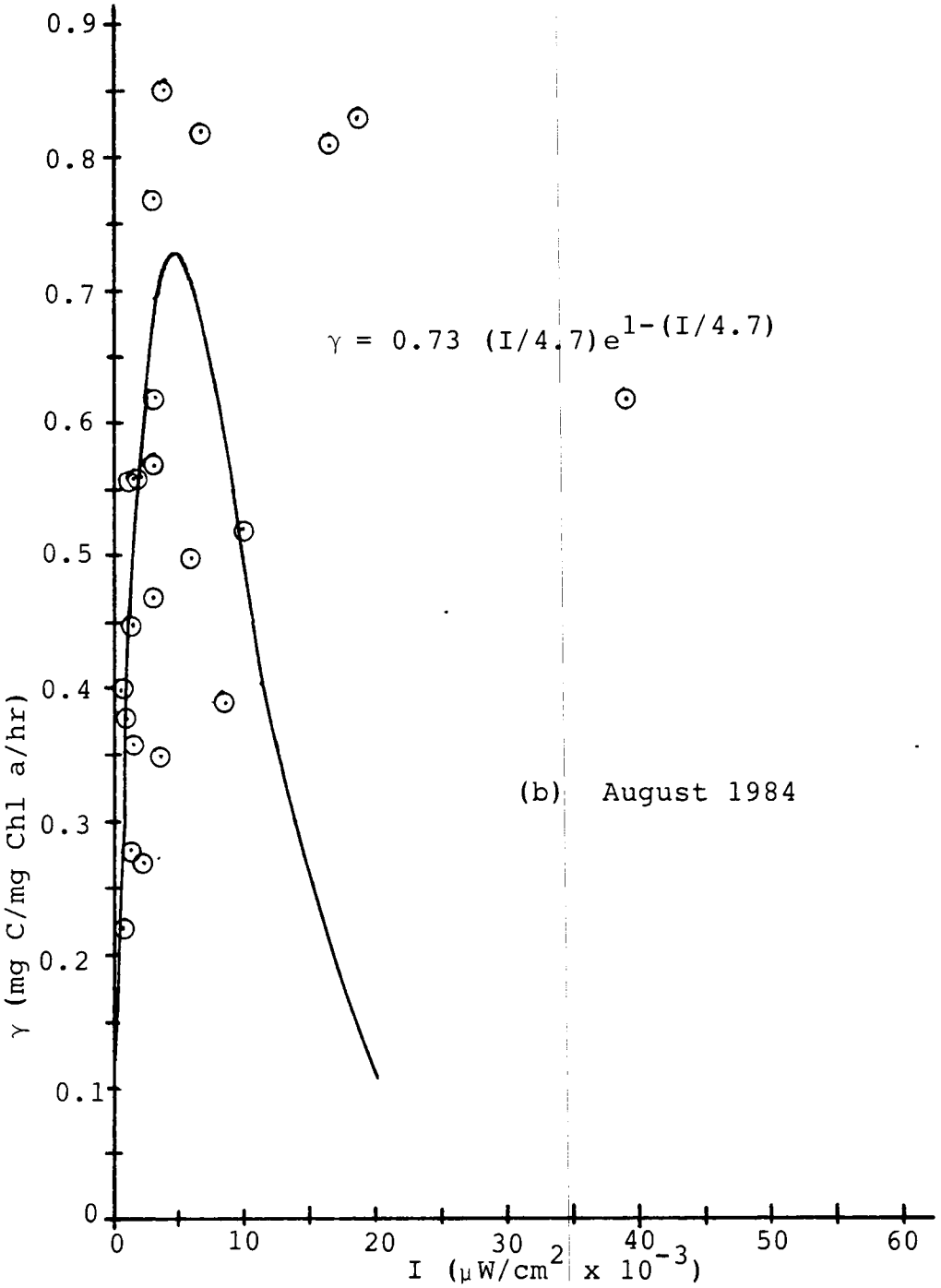

Figure 16 (Continued)

$$\underline{\text{May}}\ \gamma = 0.20 \frac{I}{[(9.5)^2 + I^2]^{1/2}} \quad (80)$$

$$\underline{\text{June}}\ \gamma = 1.64 \frac{I}{[(8.7)^2 + I^2]^{1/2}} \quad (81)$$

$$\underline{\text{July}}\ \gamma = 0.67 \frac{I}{[(10.6)^2 + I^2]^{1/2}} \quad (82)$$

$$\underline{\text{August}}\ \gamma = 0.73 \frac{I}{[(3.8)^2 + I^2]^{1/2}} \quad (83)$$

Table 19 shows the applicability of the above equation in simulating observed assimilation numbers. Again low correlations were obtained between predicted and observed values with correlation coefficients (r^2) of 0.38, 0.57, 0.25, and 0.66 for May, June, July, and August, respectively. The correlations obtained with the Smith equation were higher, however, than those obtained previously using the Steele equation. Figure 17 illustrates the correlation between observed values and those predicted by the Smith equation for the months of May and August. The low correlations between the observed data and the predicted data for both the Steele and Smith equations were due primarily to the high variability in γ_{max} and I_{max} for different stations.

Due to the poor fit of the light-productivity models and the large variation in I_{max}, γ_{max} and I_p from station

TABLE 19

Comparison of Measured Assimilation Numbers with Predicted Assimilation Numbers Using the Smith Light Curve Equation

		Assimilation Number (mg C/mg Chl a/hr)							
		0.5 m		1.0 m		2.0 m		3.0 m	
Month	Station	Predict.	Obs.	Predict.	Obs.	Predict.	Obs.	Predict.	Obs.
May	SFHRM 19.0	0.19	0.10	0.15	0.12	0.07	0.08	0.03	0.08
	SFHRM 22.4	0.19	0.23	0.18	0.30	0.12	0.16	0.05	0.09
	SFHRM 26.2	0.20	0.14	0.18	0.16	0.11	0.15	0.04	0.02
	SFHRM 30.8	0.19	0.15	0.14	0.15	0.05	0.11	0.02	0.04
	WRM 2.0	0.18	0.50	0.11	0.21	0.07	0.11	0.03	0.03
	WRM 6.0	0.19	0.23	0.11	0.28	0.06	0.26	0.01	0.11
	WRM 10.95	0.19	0.88	0.11	0.85	0.01	0.19	-	0.02
		(r^2 = 0.38 for May)							
June	SFHRM 19.0	1.58	2.45	1.42	2.59	0.90	2.42	0.44	1.40
	SFHRM 22.4	1.59	2.50	1.46	2.69	1.02	2.47	0.45	1.56
	SFHRM 26.2	1.59	0.71	1.44	0.73	0.99	0.59	0.38	0.15
	SFHRM 30.8	1.58	1.01	1.16	0.85	0.63	0.74	0.22	0.18
	WRM 2.0	0.27	1.02	0.50	1.18	0.30	0.60	0.14	0.25
	WRM 6.0	1.50	0.79	0.67	0.99	0.24	0.60	0.11	0.35
	WRM 10.95	0.99	0.90	0.33	0.43	0.01	0.10	-	0.01
		(r^2 = 0.57 for June)							

TABLE 19 (continued)

Month	Station	Assimilation Number (mg C/mg Chl a/hr)							
		0.5 m		1.0 m		2.0 m		3.0 m	
		Predict.	Obs.	Predict.	Obs.	Predict.	Obs.	Predict.	Obs.
July	SFHRM 19.0	0.65	0.28	0.60	0.39	0.35	0.53	0.26	0.71
	SFHRM 22.4	0.65	1.12	0.58	0.11	0.50	1.08	0.12	0.93
	SFHRM 26.2	0.65	0.36	0.57	0.48	0.35	0.44	0.22	0.25
	SFHRM 30.8	0.64	0.66	0.32	0.10	0.18	0.08	0.07	0.36
	WRM 2.0	0.30	1.11	0.09	1.14	0.08	0.76	0.06	0.32
	WRM 6.0	0.65	2.04	0.55	1.85	0.23	1.18	0.09	0.57
	WRM 10.95	0.52	2.25	0.15	1.61	0.04	0.90	0.01	0.25
		(r^2 = 0.25 for July)							
August	SFHRM 19.0	0.72	0.62	0.48	0.62	0.35	0.56	0.25	0.36
	SFHRM 22.4	0.67	0.39	0.62	0.50	0.50	0.35	0.37	0.27
	SFHRM 26.2	-	0.49	-	0.45	-	0.46	-	0.16
	SFHRM 30.8	0.73	1.13	0.72	0.83	0.63	0.82	0.45	0.47
	WRM 2.0	0.52	0.85	0.27	0.40	0.20	0.38	0.12	0.40
	WRM 6.0	0.68	0.52	0.45	0.77	0.25	0.56	0.13	0.22
	WRM 10.95	0.71	0.81	0.58	0.93	0.45	0.57	0.22	0.28
		(r^2 = 0.66 for August)							

NOTE: Predicted values were obtained using E. L. Smith's light curve equation which does not include photoinhibition.

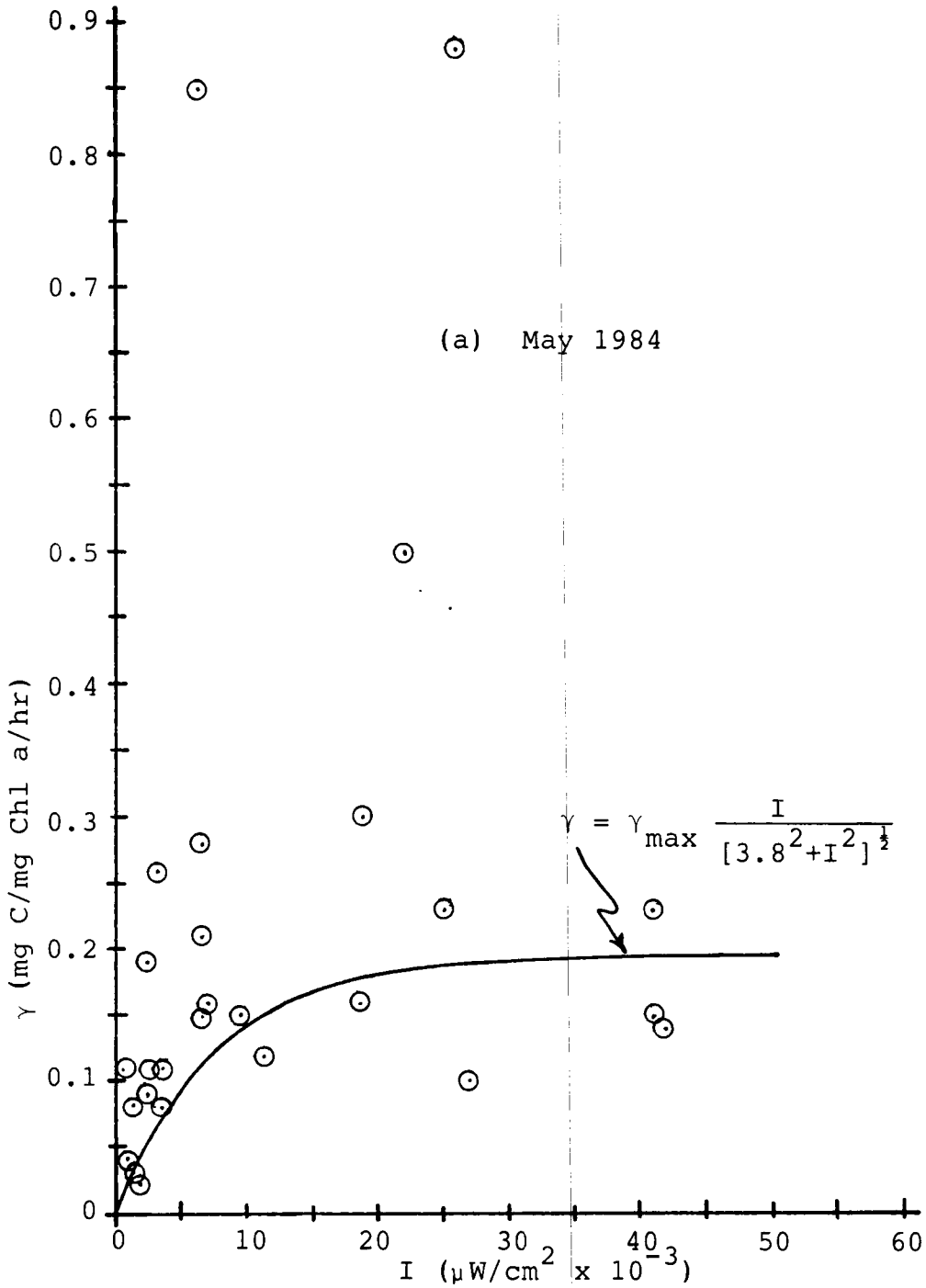

Figure 17. Assimilation Number (γ) vs. Irradiance (I)——Observed Values and Values Predicted Using Smith Light Curve Equation—— Boone Reservoir.

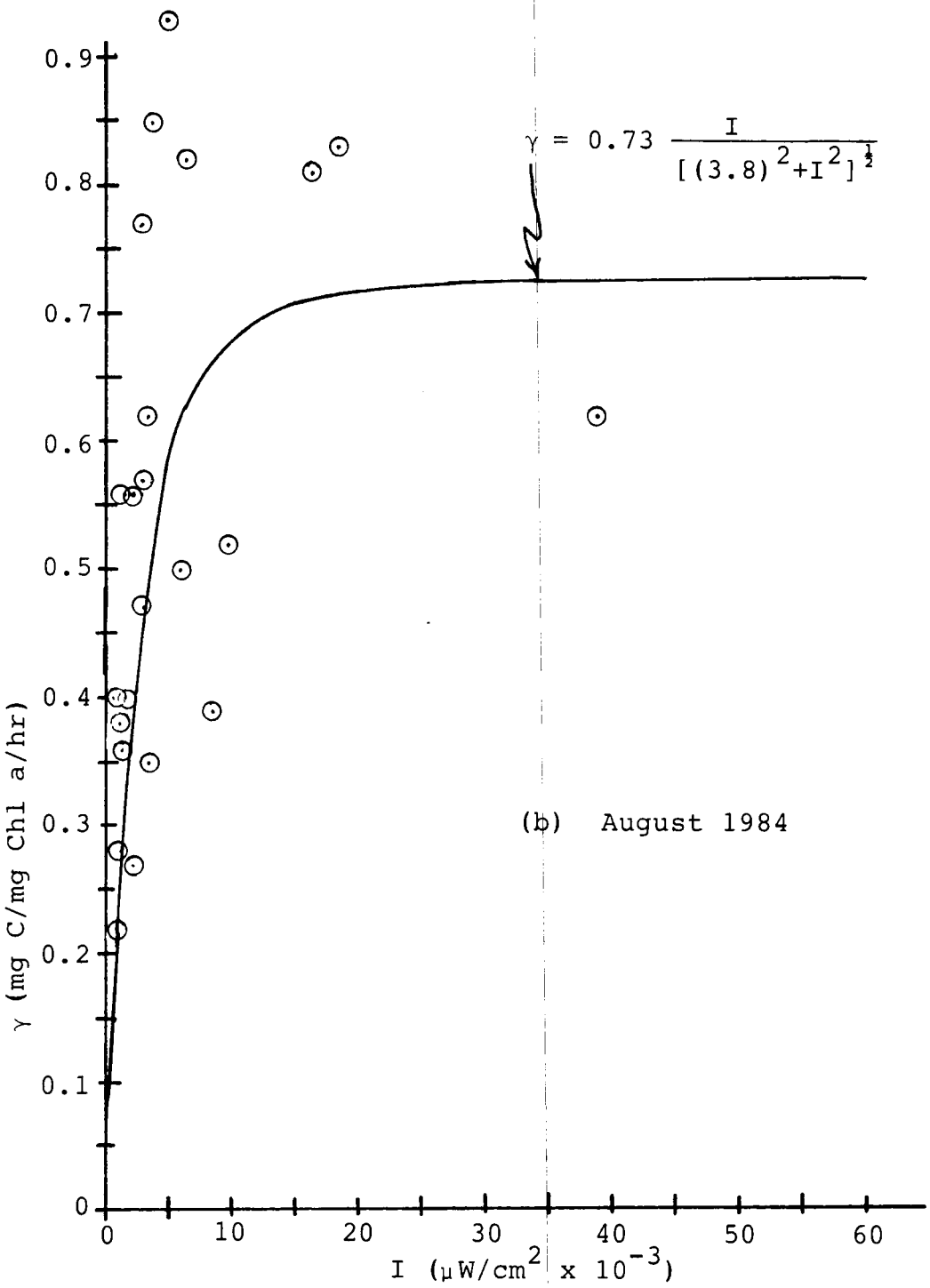

Figure 17 (Continued)

to station, additional measurements of productivity should be conducted to establish accurate values for these parameters. If algal modeling techniques are to be successful in predicting the benefits derived from reservoir management strategies, accurate light curve equations must be developed to explain the response of algae to light.

The daily integral rate of photosynthesis (i.e. primary productivity) may be predicted using the simplified Bannister equation (1) if the algal concentration and the light attenuation coefficients due to algal and non-algal components are known. The equation developed by Bannister (1) for daily integral production is:

$$\pi = \Psi \frac{K_c C}{K_w + K_c C} \qquad \text{(Equation 42)}$$

where π = Daily integral production rate (mg $C/m^2/day$ or mg $O_2/m^2/day$

Ψ = Theoretical upper limit to production which would be attained if all incident light were absorbed by algae (mg $C/m^2/day$)

K_w = Light attenuation coeffiicent due to nonalgal components (ln/m)

$K_c C$ = Light attenuation coefficent due to algae (ln/m)

C = Chlorophyll a concentration (mg/m^3)

Thus the daily production rate is a function of the fractional attenuation of light by algae.

Daily integral production rates, π, were obtained for each date and each station on Boone Reservoir by summing the volumetric rates at each depth, multiplying this sum by the time of incubation in hours, and then multiplying by the ratio of total incident radiation during the incubation period to the total incident radiation for the entire day. Since measurements of chlorophyll a and light attenuation were also made at each station, all data necessary for an evaluation of the Bannister model are available. Table 20 is a summary of the daily integral production rates obtained on Boone Reservoir during May through August. Also given in this table are values of fractional light attenuation by algae as given previously in Table 10, page 154. This table shows that the greatest daily integral production rates generally occurred in June and July when chlorophyta were the dominant algal group, however, the highest single rate (906.8 mg $C/m^2/day$) occurred in May at WRM 10.95 when bacillariophyta populations were very extensive. The lowest daily integral rates were obtained in May (with the exception of WRM 10.95) when bacillariophyta and cyanophyta were co-dominant.

To evaluate the term, Ψ, the Bannister equation as rearranged by Megard (27) will be used. In this form

TABLE 20

Daily Integral Production Rates and Algal Fractional Attenuation Values--Boone Reservoir

Month	Station	π (mg C/m^2/day)	Fractional Attenuation* $\left(\frac{K_c'}{K_d}\right)$
May	SFHRM 19.0	43.7	0.508
	SFHRM 22.4	100.7	0.526
	SFHRM 26.2	73.5	0.444
	SFHRM 30.8	88.8	0.470
	WRM 2.0	56.62	0.553
	WRM 6.0	287.9	0.660
	WRM 10.95	906.8	0.658
June	SFHRM 19.0	255.2	0.422
	SFHRM 22.4	300.8	0.470
	SFHRM 26.2	158.5	0.647
	SFHRM 30.8	217.1	0.666
	WRM 2.0	152.0	0.483
	WRM 6.0	419.6	0.737
	WRM 10.95	369.1	0.728
July	SFHRM 19.0	175.5	0.661
	SFHRM 22.4	386.7	0.641
	SFHRM 26.2	217.2	0.692
	SFHRM 30.8	185.2	0.728
	WRM 2.0	238.8	0.627
	WRM 6.0	707.8	0.684
	WRM 10.95	848.3	0.74
August	SFHRM 19.0	179.1	0.237
	SFHRM 22.4	151.9	0.629
	SFHRM 26.2	191.3	0.261
	SFHRM 30.8	455.1	0.280
	WRM 2.0	275.8	0.317
	WRM 6.0	272.8	0.684
	WRM 10.95	289.4	0.250

*Fractional light attenuation values are from Table 10.

the equation may be expressed in a manner similar to the Michaelis-Menten equation:

$$\pi = \Psi \frac{C}{(K_w/K_c) + C} \qquad \text{(Equation 44)}$$

where K_w/K_c = The algal concentration at which π equals half the maximum rate

Tilzer (37) also incorporated the light attenuation due to pheophytin into the K_w term since pheophytin absorbs light but does not participate in photosynthesis. Thus the above equation may be written as:

$$\pi = \Psi \frac{C}{((K_w + K_p)/K_c) + C} \qquad (84)$$

where C = Chlorophyll a corrected for pheophytin

K_w = Light attenuation coefficient due to nonalgal components

K_c = Light attenuation coefficient due to algae

K_p = Light attenuation coefficient due to pheophytin

Expressing this equation in a form similar to the Lineweaver-Burk form of the Michaelis-Menten equation will allow interpretation of the coefficient Ψ from available data:

$$1/\pi = 1/\Psi + [((K_w + K_p)/K_c)/\Psi](1/C) \qquad (85)$$

Using values of corrected chlorophyll a (weighted averages over the depth of the euphotic zone) obtained from Appendix III, Part 1, and π values given in Table 20, the above equation was evaluated graphically. By plotting $1/\pi$ versus 1/Corr. Chl a, Ψ can be found as 1/y-intercept. Figure 18 shows plots of this type for each survey. This graphical analysis yielded poor results in all cases. For May and August Ψ values were undefined by this method due to negative y-intercept values. For June, when a positive y-intercept was determined, the resulting Ψ value of 297 mg C/m^2/day was much lower than the maximum measured rate of 419.6 mg C/m^2/day; this condition is highly improbable. The analyses of the July data yielded a Ψ value of 909 mg C/m^2/day which was greater than the maximum measured rate of 848.3 mg C/m^2/day, yet the correlation coefficient for this analysis was only 0.34.

The poor fit of the Bannister model may be attributed to the same factors that resulted in poor fits of the Smith and Steele light-productivity equations. These factors include high variability in the parameters γ_{max} and I_{max} from station to station, possibly due to variations in nutrient concentrations, physiological or adaptive state, species dominance, light-shade adaptation, and experimental error.

The fractional light attenuation by algae in the euphotic zone (Table 20) was high in most cases with

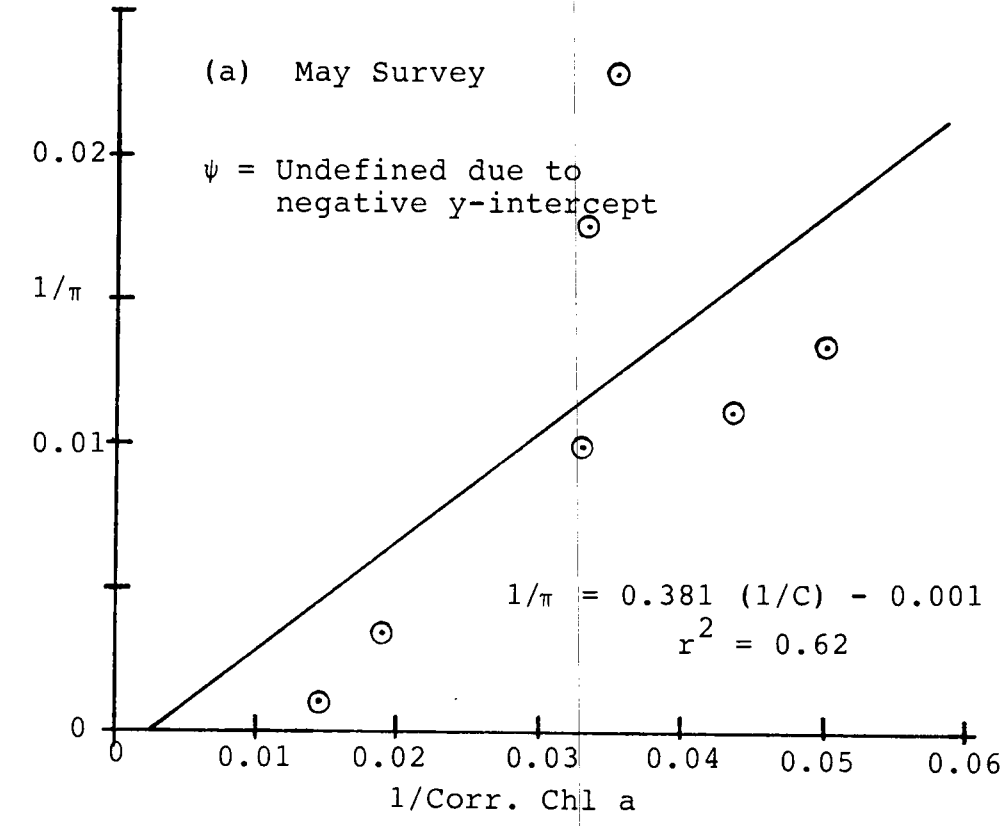

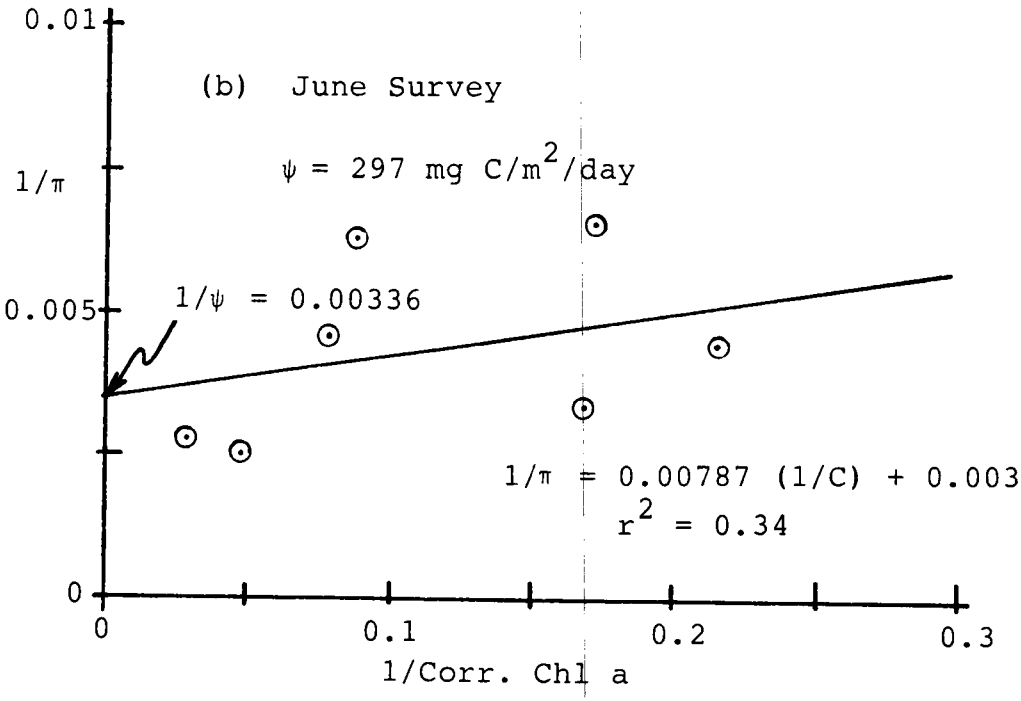

Figure 18. Graphical Evaluation of the Linear Form of the Bannister Model for Daily Integral Algae Production.

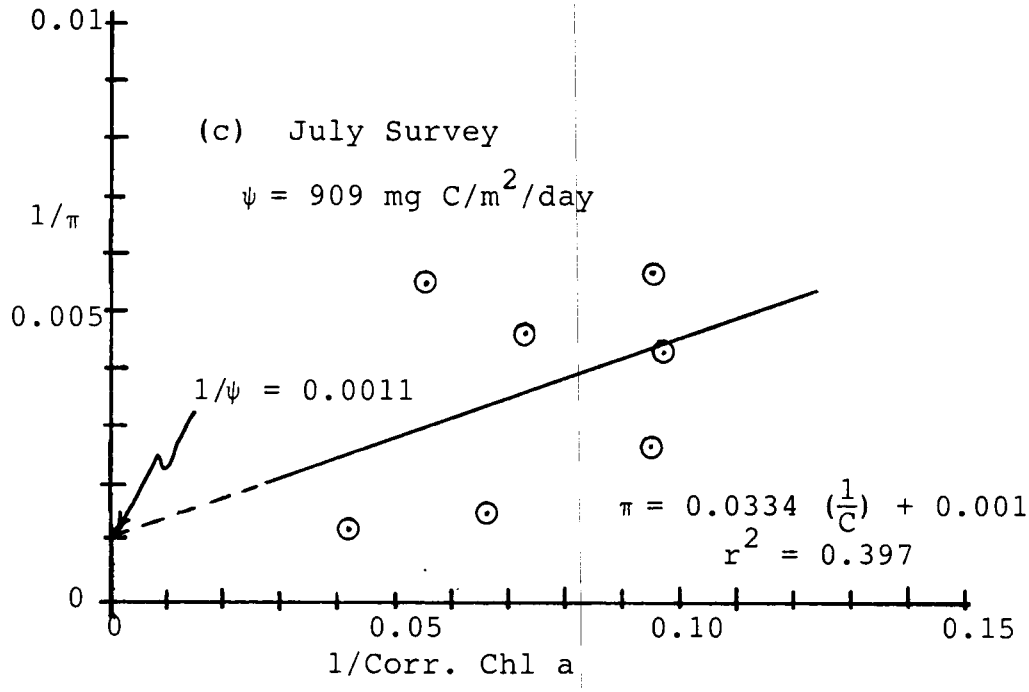

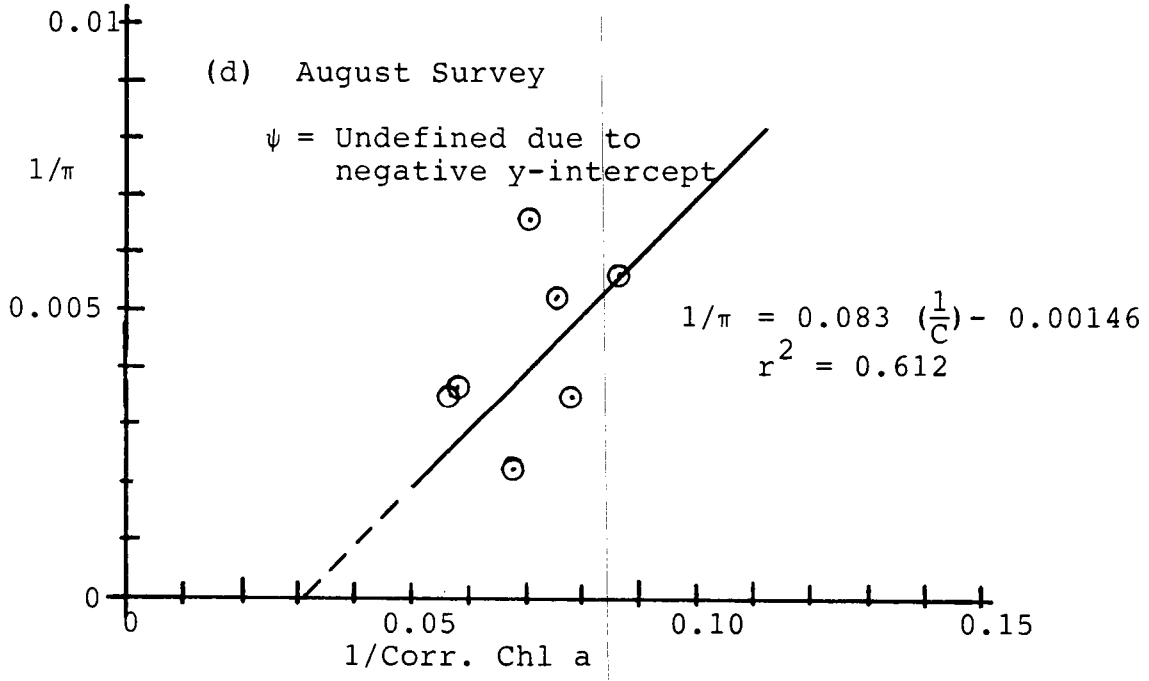

Figure 18 (Continued)

values greater than 50 percent in all cases. Increases in fractional light attenuation from station to station for any particular month did not always result in increases in algal production. This contradicts the Bannister model which predicts that algal production is directly proportional to fractional light attenuation by algae.

Comparison of daily integral production rates obtained in Boone Reservoir with those of other eutrophic reservoirs gives some contradicting results. Wetzel (39) presented mean annual values of daily integral production for seven different eutrophic lakes located in the United States and abroad. These values ranged from 820 mg $C/m^2/day$ to 1750 mg $C/m^2/day$. The daily integral production rates in Boone Reservoir, however, ranged from 44 to 907 mg $C/m^2/day$ (Table 20) with a mean value of 286 mg $C/m^2/day$, significantly lower than the range presented by Wetzel. The biomass present in Boone Reservoir (measured as Chlorophyll a concentration) was, however, similar to that reported by Megard (26) for eutrophic Lake Minnetonka, Minnesota. In Lake Minnetonka, chlorophyll a concentrations in the euphotic zone measured during the algal growing season ranged from 3 to 56 mg Chl a/m^3 with a mean value of 21 mg Chl a/m^3. Chlorophyll a concentrations in Boone Reservoir were similar with

values ranging from 6 to 70 mg Chl a/m^3 with a mean value of 19 mg Chl a/m^3. A discrepancy therefore exists in Boone Reservoir between chlorophyll values which are indicative of eutrophic conditions and productivity values which were much less than those in eutrophic lakes. Three possible explanations exist for the unusually low productivity measurements on Boone Reservoir:

1. Samples for production measurements were generally collected and incubated within ± 2 hours of noon. It is possible that a dense algal assemblage with ample supplies of nutrients may have undergone an intense period of photosynthetic activity in the early morning hours before sample collection. Thus at the time of sample collection the algae may have been experiencing end product inhibition due to an accumulation of internal carbon stores (24). The algae may also have been affected by carbon limitation due to rapid removal of dissolved CO_2 early in the morning. In fact high carbon dioxide removal was indicated by high pH measurements during the study which often exceeded 10.

2. As mentioned previously, the samples for production rate measurements were taken as 0 to 3 meter depth integrated composites. For stations at which algae were stratified into varying light adapted layers, the compositing of cells with varying light response characteristics followed by incubation at various depth may result

in lower than expected production measurements. This is because algal cells which are adapted to a certain light level are placed in a light environment to which they are not adapted thus resulting in non-optimal photosynthetic response or photoinhibition.

3. Sampling error may have resulted in loss of fixed radioactive carbon (i.e. the quantity which is measured to determine carbon uptake). After the end of the incubation period, the sample bottles were removed from the incubation location in the reservoir and placed in an opaque box. This box was then transported to another location where the biomass was filtered from sample bottles, preserved, and shipped to the laboratory for determination of radiological C-14 activity. Because of the remote locations of some of the sampling sites, it was often two or three hours before the samples in the opaque box could be filtered and preserved. It is possible that during the time the algal samples were in the dark (i.e. in the opaque box) a significant quantity of the fixed radioactive carbon was respired resulting in a net carbon loss and erroneously low productivity measurements. One solution to this problem would have been to chemically preserve the samples (e.g. with formaldehyde) immediately before placing them in the opaque box. However, past experiences with other

productivity measurements has shown that preservation before filtration may result in cell rupture and loss of internal dissolved carbon stores which passes out with the filtrate during filtration causing erroneously low productivity measurements. The ultimate answer to the problem is to make provisions for filtration of samples in the boat immediately after incubation.

It is evident from the preceding discussion and analyses that additional data are required to develop a predictive model for determining the effects of light, nutrients, and other environmental variables on the photosynthetic production and growth of algae in Boone Reservoir. These data should include production rate measurements which are made using discrete samples which are collected at single depths and incubated at the depths at which they are collected. Data should also include productivity measurements over the entire daylight period rather than over a set time interval in late morning and early afternoon. This will allow the assessment of end product inhibition or carbon limitation, if these processes occur. Limiting nutrient studies should also be conducted to determine whether nutrient saturation exists or non-optimal nutrient limitation is present. The use of oxygen production as a complement to carbon-14 uptake measurements should also be considered. Since measurement of oxygen

production involves a less detailed experimental method (only Winkler DO tests are required) than C-14 analyses, it should be subject to less experimental error. Finally the use of a quantum scalar irradiameter should be considered as a replacement for the flat plate cosine irradiameter. This type of instrument should provide measurements which are more representative of the total reception of light by an algal cell which receives light from all directions.

CHAPTER 5

CONCLUSION

The preceding discussion and analyses have demonstrated the applicability and importance of light attenuation partitioning methods and light-productivity models in defining the factors affecting the transparency and algal production in Boone Reservoir. By partitioning of the light attenuation coefficient, K_d, it was shown that algae are the major contributor to transparency reduction in Boone Reservoir during the period May to August which coincides with the peak recreational use period for the reservoir. Additional measurements are needed to determine the factor controlling the reservoir transparency during September through April, however, it is expected that the attenuation contribution by algae is small during periods of low temperature and incident irradiance (late fall, winter).

In most cases light attenuation by algae, presented as K_cC, was greater than 50 percent of the total light attenuation. The major algal groups responsible for light attenuation include bacillariophyta (a diatom), chlorophyta (a green algae), and cyanophyta (a blue-green algae). The greatest attenuation contribution was due to chlorophyta. This has important implications in support of

reservoir management strategies directed at reduction in algal populations. Currently, the major wastewater discharges to Boone Reservoir are providing secondary treatment only and agricultural drainage is substantial. Significant reductions in algal populations resulting from nutrient removal strategies (e.g. tertiary treatment and nonpoint source control) would produce significant increases in reservoir transparency. Using the values of K_c determined in this report, the effects of decreases in algal populations on the reservoir can be assessed.

The partitioning of light attenuation in terms of K_c; $K_{c'}$; K_w; K_{water}; and K_{pc} (all terms defined previously) provided much better results than the inherent/apparent optical properties partitioning method and is thus recommended for future modeling studies of the reservoir. The principal difficulty in the latter approach is that it relies on the use of the volume scattering function and the underwater radiance distribution, which are not readily measured in the field. Formulations developed by Kirk (19, 20) based on assumed volume scattering functions and simulated radiance distributions provided poor results in most cases for Boone Reservoir. Partitioning of light attenuation in terms of the cell concentrations of major algal groups (bacillariophyta, chlorophyta, and cyanophyta) was of limited quantitative success, however,

it did show that the algal group chlorophyta had the greatest potential for transparency reduction.

Due to the substantial impairment of reservoir transparency by algae and other algal associated problems (e.g. algae are believed to be responsible for metalimnetic dissolved oxygen reduction and increased sediment oxygen demand), algal population reductions in Boone Reservoir are strongly recommended. Implementation of nutrient reduction and control strategies for algae reductions are, however, expensive and the costs must be generally financed by the public sector. The use of algal dynamics models will permit an assessment of the benefits of nutrient control before the investment of funds in such strategies.

Knowledge of the amount of sunlight available for algal production at any given depth and the photosynthetic response of algae to absorbed light are necessary components of algal dynamics models. Using K_c and K_d values given in this report, the intensity of photosynthetically available radiation (PAR) and the fractional attenuation by algae can be predicted for inclusion in algal models. The prediction of the growth response of algae to available solar radiation requires the use of light-productivity models which include light curve parameters γ_{max}, I_{max}, I_p, and Ψ. The use of light-productivity models

such as those of Steele, Smith, and Bannister did not accurately describe the observed algal production measurements in Boone Reservoir. The primary reason for the poor fit of these models was the significant variation in light curve parameters at different sampling stations and the variable response of productivity to fractional algal light attenuation. These variations in algal light response may be due to variations at different reservoir locations in nutrient limitations and availability, light-shade adaptation, species variations, and variations in physiological and adaptive states of the algae. There were also concerns about errors associated with the use of depth-integrated samples to represent a possibly stratified euphotic layer and about experimental errors in the C-14 method used to measure primary production.

In summary, light penetration in Boone Reservoir during the study period (May through August) was affected to a large extent by algae. During this period light attenuation by algae were generally responsible for greater than 50 percent of the total light attenuation with depth. Thus reservoir management programs directed at algal control by reductions in nutrient loadings will likely result in improvements in the transparency of the reservoir during the algal growing season.

In the analyses and data interpretation of this study there were several instances where additional data

or changes in sampling methodologies would have permitted a better interpretation of results and stronger conclusions. The following changes are recommended for future light attenuation and algal production studies on Boone Reservoir to provide results which can be viewed with greater confidence:

1. To provide a thorough description of the temporal trends in light attenuation in Boone Reservoir, measurements of light attenuation and the concentrations of attenuating substance should be made on at least one occasion during each month of the year. This will allow an assessment of the factors controlling reservoir transparency during the periods when algal populations are low.

2. Since optical stratification apparently existed in the epilimnion during the study period with steep light attenuation gradients, future measurements of underwater irradiance should be made at several more intermediate depths within the euphotic zone to provide a better definition of K_d.

3. To provide a better evaluation of the relationship between K_d and the depth of secchi disc visibility, it is recommended that one observer be used to the extent possible in obtaining depths of secchi disc visibility. If this is not possible all secchi disc measurements should be followed by the observer's initials to allow

observer variability to be tracked. Provisions should also be made to allow accurate measurement of secchi disc depth to the nearest 0.1 meter. This will redice the error associated with round off.

4. To provide a better definition of the distribution of algae and other light attenuating substances within the euphotic zone, the use of depth integrated composite samples should be avoided. Samples should be collected at specific depths (e.g. every 0.5 or 1 meter). This will provide a determination of the extent of algal stratification and will permit the evaluation of changes in the slope of the light attenuation gradient (i.e. $\ln(I_o/I_z)/Z$) with depth. Measurement of concentrations of attenuating substances other than algae (dissolved color, sediment, etc.) should also be made to determine their fractional contribution to overall light attenuation. This will permit a multiple regression of the concentrations of all attenuating substances against K_d and will reduce the variability of the y-intercept (K_w) thus providing a more reliable linear model.

5. Future measurements of algal production should be made using samples collected and incubated at specific depths rather than the incubation of depth integrated samples at specific depths. This will prevent the exposure of light-adapted algal cells to a light environment

to which they are not accustomed. Also, provisions should be made for immediate filtration and preservation of algal samples following incubation; this will reduce the possibility of algal respiration and loss of carbon stores during sample storage.

6. If future attempts are to be made using inherent optical properties to predict apparent optical properties for Boone Reservoir, measurements of the complete volume scattering function should be made and specific mathematical relationships for prediction of apparent optical properties should be developed using computer simulations (e.g. Monte Carlo simulations).

7. A strict program of quality control should be implemented for all laboratory and field measurements. While all laboratory chlorophyll a measurements were obtained in duplicate for this study, many measurements such as fluorescence, underwater irradiance, and algal enumeration and identification were performed as single analyses. If duplicates of these measurements had been made periodically an idea of the analytical and natural variability of the measured parameter could have been obtained.

LIST OF REFERENCES

LIST OF REFERENCES

1. Bannister, T. T., "Production Equations in Terms of Chlorophyll Concentration, Quantum Yield, and Upper Limit to Production," Limnology and Oceanography, Vol. 19, 1974, pp. 1-12.

2. Bannister, T. T., "A General Theory of Steady-State Phytoplankton Growth in a Nutrient Saturated Mixed Layer," Limnology and Oceanography, Vol. 19, 1974, pp. 13-30.

3. Bannister, T. T., "Quantitative Description of Steady State, Nutrient-Saturated Algal Growth Including Adaptation," Limnology and Oceanography, Vol. 24, 1979, pp. 76-96.

4. Booth, C. R., "The Design and Evaluation of a Measurement System for Photosynthetically Active Quantum Scalar Irradiance," Limnology and Oceanography, Vol. 21, 1976, pp. 326-336.

5. Bricaud, A., Morel, A., and Prieur, L., "Optical Efficiency Factors of Some Phytoplankters," Limnology and Oceanography, Vol. 28, 1983, pp. 816-832.

6. Brown, R., "Relationships Between Suspended Solids, Turbidity, Light Attenuation, and Algal Productivity," Proceedings of the Third Annual Conference of the North American Lake Management Society, US EPA Publication 440/5/84-001, 1984.

7. Brown, R., Hauser,G., McKinnon, M. K., Shao, M., "Two Dimensional Modeling of Fort Loudoun Reservoir Water Quality," Tennessee Valley Authority, Technical Report No. WR 28-1-10-100, February 1985.

8. Brown, R., McKinnon, M. K., Shao, M., "Water Quality Modeling of Pickwick Reservoir," Tennessee Valley Authority, Technical Report No. WR 28-1-4-111, 1985.

9. Dubinsky, Z., Berman, T., "Seasonal Changes in the Spectral Composition of Downwelling Irradiance in Lake Kinneret (Israel)," Limnology and Oceanography, Vol. 24, 1979, pp. 652-653.

10. Duntley, S. Q., "Light in the Sea," Journal of the Optical Society of America, Vol. 53, 1963, pp. 214-233.

11. Effler, S. W., Field, S. D., Meyer, M. A., and Sze, P., "Response of Onondaga Lake to Restoration Efforts," Journal of the Environmental Engineering Division, ASCE, Vol. 108, No. EE1, February 1981, pp. 191-210.

12. Effler, S. W., Wodka, M. C., and Field, S. D., "Scattering and Absorption of Light in Onondaga Lake," Journal of the Environmental Engineering Division, ASCE, Vol. 110, No. 6, December 1984, pp. 1134-1145.

13. Field, S. D., and Effler, S. W., "Photosynthesis--Light Mathematical Formulations," JEE, ASCE, Vol. 108, No. EE1, February 1982, pp. 199-203.

14. Field, S. D., and Effler, S. W., "Light-Productivity Model for Onondaga Lake NY," Journal of the Environmental Engineering Division, ASCE, Vol 109, No. 4, August 1983, pp. 830-844.

15. Gaudy, A. F., and Gaudy, E. T., Microbiology for Environmental Scientists and Engineers, McGraw-Hill Book Co., 1980.

16. Gulliver, J. S., and Stefan, H. G., "Lake Phyto plankton Model With Destratification," Journal of the Environmental Engineering Division, ASCE, Vol. 108, No. 5, October 1983, pp. 864-882.

17. Jassby, A. D., and Platt, T., "Mathematical Formulation of the Relationship Between Photosynthesis and Light For Phytoplankton," Limnology and Oceanography, Vol. 21, 1976, pp. 540-547.

18. Kahl Scientific Instrument Corp., "Underwater Irradiameters, Photometers, Temperature, and Depth Meters," Bulletin WAP-0277.

19. Kirk, J. T. O., "Monte Carlo Study of the Nature of the Underwater Light Field in, and the Relationship Between Optical Properties of, Turbid Yellow Waters," Australian Jcurnal of Marine and Freshwater Research, Vol. 32, 1981, pp. 517-532.

20. Kirk, J. T. O., "Estimation of the Scattering Coefficient of Natural Waters Using Underwater Irradiance Measurements," Australian Journal of Marine and Freshwater Research, Vol. 32, 1981, pp. 533-539.

21. Kirk, J. T. O., "Spectral Absorption Properties of Natural Waters: Contribution of the Soluble and Particulate Fractions to Light Absorption in Some Inland Waters of South-eastern Australia," Australian Journal of Marine and Freshwater Research, Vol. 31, 1980, pp. 287-296.

22. Kirk, J. T. O., "Relationship Between Nephelometric Turbidity and the Scattering Coefficients in Certain Australian Waters," Australian Journal of Marine and Freshwater Research, Vol. 31, 1980, pp. 1-12.

23. Larson, D. W., "Temperature, Transparency, and Phytoplankton Productivity in Crater Lake, Oregon," Limnology and Oceanography, Vol. 17, 1972, pp. 410-417.

24. Lehman, J. T., Botkin, D. B., and Likens, G. E., "The Assumptions and Rationales of a Computer Model of Phytoplankton Population Dynamics," Limnology and Oceanography, Vol. 20, 1975, pp. 343-364.

25. Lorenzen, M. W., "Use of Chlorophyll-Secchi Disk Relationships," Limnology and Oceanography, Vol. 25, 1980, pp. 371-372.

26. Megard, R. O., "Phytoplankton, Photosynthesis, and Phosphorus in Lake Minnetonka, Minnesota," Limnology and Oceanography, Vol. 17, 1972, pp. 68-87.

27. Megard, R. O., Combs, W. S., Smith, P. D., and Knoll, A. S., "Attenuation of Light and Daily Integral Rates of Photosynthesis Attained by Planktonic Algae," Limnology and Oceanography, Vol 24, 1979, pp. 1038-1050.

28. Montedoro-Whitney Corporation, Instruction and Maintenance Manual for the Illuminance Meter Model LMT-8B.

29. Morel, A., and Smith, R. C., "Relation Between Total Quanta and Total Energy for Aquatic Photosynthesis," Limnology and Oceanography, Vol. 19, 1974, pp. 591-600.

30. Placke, J. F., "Trophic Status Evaluation of TVA Reservoirs," TVA Technical Report Series, Report No. TVA/ONR/WR-8317, October 1983.

31. Rates, Constants, and Kinetics Formulations in Surface Water Quality Modeling, United States Environmental Protection Agency, Report No. EPA-600-3-78-105, December 1978.

32. Smith, E. L., "Photosynthesis in Relation to Light and Carbon Dioxide," Proceedings of the National Academy of Science, Vol 22, 1936, pp. 504-511.

33. Smith, R. C., and Tyler, J. E., "Optical Properties of Clear Natural Water," Journal of the Optical Society of America, Vol. 57, 1967, pp. 589-595.

34. Standard Methods for the Examination of Water and Wastewater, AWWA-APHA, 15th Edition, 1980.

35. Steele, J. H., "Environmental Control of Photosynthesis in the Sea," Limnology and Oceanography, Vol. 7, 1962, pp. 137-150.

36. Thomas, W. H., and Dodson, A. N., "On Nitrogen Deficiency in Tropical Pacific Oceanic Phytoplankton," Limnology and Oceanography, Vol. 17, 1972, pp. 515-523.

37. Tilzer, M. M., "The Importance of Fractional Light Absorption by Photosynthetic Pigments for Phytoplankton Productivity in Lake Constance," Limnology and Oceanography, Vol. 28, 1983, pp. 833-846.

38. Tyler, J. E., "The Secchi Disc," Limnology and Oceanography, Vol. 13, 1968, pp. 1-6.

39. Wetzel, R. G., Limnology, W. B. Saunders Company, 1975.

40. Wofsy, S. C., "A Simple Model to Predict Extinction Coefficients and Phytoplankton Biomass in Eutrophic Waters," Limnology and Oceanography, Vol. 28, 1983, pp. 1144-1155.

APPENDIXES

APPENDIX I

BOONE RESERVOIR IRRADIANCE AND SECCHI DISC MEASUREMENTS

Boone Reservoir Irradiance and Secchi Disc Measurements

Station	Date	Time (EDT)	% Horiz	Secchi Disc Depth (m)	LIGHT PENETRATION OF EUPHOTIC ZONE			
					Depth (m)	Ambient Light ($\mu W/cm^2$)	Underwater Light ($\mu W/cm^2$)	% Available Light
SFHRM 19.0	5/24/84	0919	50	0.9	0.3	37,800	27,000	71.4
					1.0	38,000	11,200	29.5
					2.0	49,000	3,500	7.1
					3.0	49,000	1,440	2.9
					4.0	49,000	460	0.9
	6/12/84	0957	50	1.5	0.3	53,000	31,000	58.5
					1.0	54,000	15,000	27.8
					2.0	54,000	5,700	10.6
					3.0	54,000	2,400	4.4
					4.0	54,000	1,000	1.9
					5.0	55,000	450	0.8
	7/19/84	1016	50	2.0	0.3	68,000	42,000	61.8
					1.0	68,000	21,000	30.9
					2.0	69,000	6,600	9.6
					3.0	71,000	4,500	6.3
					4.0	70,000	2,400	3.4
					5.0	71,000	1,100	1.5
	8/21/84	0938	50	1.5	0.3	39,000	39,000	100.0
					1.0	40,000	3,300	8.2
					2.0	40,000	2,100	5.2
					3.0	41,000	1,410	3.4
					4.0	41,000	870	2.1
					5.0	41,000	510	1.2
SFHRM 22.4	5/24/84	1107	75	1.25	0.3	68,000	41,000	60.3
					1.0	68,000	18,750	27.6
					2.0	69,000	7,000	10.1
					3.0	70,000	2,280	3.3
					4.0	71,000	655	0.9
	6/12/84	1104	75	1.0	0.3	74,000	33,000	44.6
					1.0	74,000	17,000	33.0
					2.0	74,000	6,900	9.3
					3.0	75,000	2,500	3.3
					4.0	76,000	1,000	1.3
	7/19/84	1130	75	1.5	0.3	72,000	44,000	61.1
					1.0	71,000	18,000	25.4
					2.0	73,000	12,000	16.4
					3.0	73,000	1,900	2.7
					4.0	73,000	1,600	2.2
					5.0	74,000	930	1.3
	8/21/84	1050	75	1.25	0.3	49,000	8,500	17.3
					1.0	46,000	6,000	13.0
					2.0	49,000	3,600	7.3
					3.0	48,000	2,150	4.5
					4.0	48,000	1,110	2.3
					5.0	47,000	510	1.1

Station	Date	Time (EDT)	% Horiz	Secchi Disc Depth (m)	LIGHT PENETRATION OF EUPHOTIC ZONE			
					Depth (m)	Ambient Light ($\mu W/cm^2$)	Underwater Light ($\mu W/cm^2$)	% Available Light
SFHRM 25.0	5/24/84	1504	25	1.0	0.3	84,000	35,000	41.7
					1.0	83,000	12,600	15.2
					2.0	84,000	2,800	3.3
					3.0	84,000	1,476	1.8
					4.0	83,000	740	0.9
	6/12/84	1458	60	1.1	0.3	54,000	32,000	59.3
					1.0	59,000	15,000	25.4
					2.0	63,000	6,600	10.5
					3.0	63,000	2,400	3.8
					4.0	63,000	720	1.1
	7/19/84	1441	25	1.25	0.3	74,000	15,000	20.3
					1.0	75,000	18,300	24.4
					2.0	75,000	6,600	8.8
					3.0	77,000	2,900	3.8
					4.0	76,000	1,400	1.8
					5.0	76,000	600	0.8
	8/21/84	1435	25	-	0.3	83,000	36,000	43.4
					1.0	84,000	6,000	7.1
					2.0	85,000	3,900	4.6
					3.0	84,000	2,400	2.9
					4.0	80,000	1,320	1.7
					5.0	81,000	700	0.9
SFHRM 26.2	5/24/84	1159	25	-	0.3	93,000	42,000	45.2
					1.0	93,000	18,600	20.0
					2.0	93,000	6,550	7.0
					3.0	92,800	1,830	2.0
					4.0	93,000	660	0.7
					5.0	93,000	300	
	6/12/84	1135	25	0.8	0.3	72,000	33,000	45.8
					1.0	73,000	16,000	21.9
					2.0	73,000	6,600	9.0
					3.0	73,000	2,100	2.9
					4.0	73,000	690	0.9
	7/19/84	1211	25	1.4	0.3	72,000	45,000	62.5
					1.0	72,000	17,000	23.6
					2.0	72,000	6,600	8.3
					3.0	72,000	3,600	5.0
					4.0	72,000	1,800	2.5
					5.0	72,000	720	1.0

Station	Date	Time (EDT)	% Horiz	Secchi Disc Depth (m)	LIGHT PENETRATION OF EUPHOTIC ZONE			
					Depth (m)	Ambient Light ($\mu W/cm^2$)	Underwater Light ($\mu W/cm^2$)	% Available Light
SFHRM 28.3	5/24/84	1558	60	1.0	0.3	73,000	31,000	42.5
					1.0	73,500	13,200	18.0
					2.0	74,000	3,400	4.6
					3.0	74,000	1,110	1.5
	6/12/84	1425	60	0.9	0.3	72,000	38,000	52.8
					1.0	71,000	8,700	12.3
					2.0	71,000	3,300	4.6
					3.0	71,000	1,400	2.0
					4.0	70,000	660	0.9
	7/19/84	1412	60	1.3	0.3	74,000	38,000	51.4
					1.0	75,000	20,000	26.7
					2.0	76,000	7,800	10.3
					3.0	76,000	2,900	3.9
					4.0	76,000	1,300	1.7
					5.0	74,000	660	0.9
	8/21/84	1404	60	-	0.3	24,000	7,800	32.5
					1.0	25,000	4,400	17.6
					2.0	25,000	1,950	7.8
					3.0	26,000	990	3.8
					4.0	26,000	560	2.2
					5.0	26,000	280	1.1
SFHRM 30.8	5/24/84	1329	25	-	0.3	96,000	41,000	42.7
					1.0	96,000	9,450	9.8
					2.0	96,000	2,700	2.8
					3.0	94,500	825	0.9
	6/12/84	1230	25	0.75	0.3	63,000	30,000	7.6
					1.0	63,000	8,700	13.8
					2.0	63,000	3,600	5.7
					3.0	63,000	1,200	1.9
					4.0	63,000	420	0.7
	7/19/84	1326	25	-	0.3	72,000	38,000	52.8
					1.0	71,000	5,700	8.0
					2.0	71,000	3,000	4.2
					3.0	71,000	1,100	1.5
	8/21/84	1307	25	-	0.3	82,500	35,000	42.4
					1.0	87,500	18,600	21.3
					2.0	88,000	6,600	7.5
					3.0	87,500	3,000	3.4
					4.0	87,000	1,500	1.7
					5.0	87,000	720	0.8

Station	Date	Time (EDT)	% Horiz	Secchi Disc Depth (m)	LIGHT PENETRATION OF EUPHOTIC ZONE			
					Depth (m)	Ambient Light ($\mu W/cm^2$)	Underwater Light ($\mu W/cm^2$)	% Available Light
SFHRM 32.4	8/21/84	1325	50	-	0.3	87,000	8,100	9.3
					1.0	86,000	4,800	5.6
					2.0	87,000	2,700	3.1
					3.0	86,000	1,650	1.9
					4.0	87,000	990	1.1
WRM 2.0	5/25/84	0951	50	1.25	0.3	51,000	22,000	43.1
					1.0	51,000	6,600	12.9
					2.0	51,000	3,350	6.6
					3.0	50,000	1,170	2.3
					4.0	49,000	370	0.8
	5/25/84	0945	50	1.25	0.3	51,000	22,000	43.1
					1.0	51,000	6,600	12.9
					2.0	51,000	3,350	6.6
					3.0	50,000	1,170	2.3
					4.0	49,000	370	0.8
	6/13/84	0900	50	1.3	0.3	23,000	1,500	32.6
					1.0	23,000	2,800	12.2
					2.0	23,000	1,600	7.0
					3.0	23,000	750	3.3
					4.0	23,000	330	1.4
WRM 2.0	7/20/84	0935	50	1.25	0.3	52,000	5,400	10.4
					1.0	54,000	1,500	2.8
					2.0	54,000	1,260	2.3
					3.0	56,000	900	1.6
					4.0	55,000	570	1.1
	8/22/84	0906	50	-	0.3	33,000	3,800	11.5
					1.0	23,000	1,500	6.5
					2.0	23,400	1,080	4.6
					3.0	22,000	660	3.0
					4.0	21,300	270	1.3
WRM 3.0	5/25/84	1345	25	1.0	0.3	65,000	40,000	61.5
					1.0	66,000	17,000	25.8
					2.0	66,000	5,100	7.7
					3.0	67,000	1,400	2.1
					4.0	69,000	300	0.4
	6/13/84	1243	25	1.0	0.3	42,000	18,000	42.9
					1.0	40,000	11,000	27.5
					2.0	39,000	1,700	4.4
					3.0	37,000	690	1.9
					4.0	35,000	320	0.9
	7/20/84	1351	25	1.25	0.3	82,000	48,000	58.5
					1.0	82,000	3,900	4.8
					2.0	82,000	2,000	2.4
					3.0	82,000	1,200	1.5
					4.0	82,000	780	1.0
	8/23/84	1300	25	0.5	0.3	96,000	5,800	6.0
					1.0	96,000	3,300	3.4
					2.0	95,000	1,800	1.9
					3.0	94,000	1,245	1.3

Station	Date	Time (EDT)	% Horiz	Secchi Disc Depth (m)	LIGHT PENETRATION OF EUPHOTIC ZONE			
					Depth (m)	Ambient Light ($\mu W/cm^2$)	Underwater Light ($\mu W/cm^2$)	% Available Light
WRM 6.0	5/25/84	1116	50	1.0	0.3	49,000	25,000	51.0
					1.0	49,000	6,600	13.5
					2.0	49,000	3,100	6.3
					3.0	48,500	480	1.0
	6/13/84	1000	50	-	0.3	40,000	20,000	50.0
					1.0	41,000	3,900	9.5
					2.0	41,000	1,300	4.0
					3.0	41,000	570	1.4
	7/20/84	1102	50	1.0	0.3	72,000	41,000	56.9
					1.0	72,000	15,000	20.8
					2.0	69,000	3,900	5.7
					3.0	69,000	1,400	2.0
					4.0	68,000	570	0.8
	8/23/84	1028	50	0.8	0.3	44,000	9,900	22.5
					1.0	41,000	3,000	7.3
					2.0	48,000	1,410	2.9
					3.0	43,000	710	1.7
					4.0	45,000	440	1.0
WRM 8.4	5/25/84	1305	25	0.75	0.3	60,000	37,000	61.7
					1.0	58,000	5,400	9.3
					2.0	61,000	1,000	1.6
					3.0	62,000	280	0.5
	6/13/84	1127	25	0.84	0.3	51,000	21,000	41.2
					1.0	51,000	7,800	15.3
					2.0	49,000	1,700	4.0
					3.0	44,000	420	1.0
	7/20/84	1307	25	1.0	0.3	45,000	21,000	46.7
					1.0	43,000	6,300	14.7
					2.0	42,000	1,800	4.3
					3.0	42,000	630	1.5
	8/23/84	1226	25	-	0.3	94,000	39,000	46.4
					1.0	96,000	17,500	18.2
					2.0	92,000	5,200	5.7
					3.0	92,000	2,100	2.3
					4.0	90,000	870	1.0

Station	Date	Time (EDT)	% Horiz	Secchi Disc Depth (m)	LIGHT PENETRATION OF EUPHOTIC ZONE			
					Depth (m)	Ambient Light ($\mu W/cm^2$)	Underwater Light ($\mu W/cm^2$)	% Available Light
WRM 10.95	5/25/84	1208	90	-	0.3	62,000	26,100	42.1
					1.0	60,000	6,400	10.7
					2.0	58,000	460	0.8
	6/13/84	1050	90	0.60	0.3	38,000	6,600	17.4
					1.0	40,000	1,800	4.5
					2.0	40,000	72	0.2
	7/20/84	1142	90	0.75	0.3	30,000	13,000	43.3
					1.0	29,000	2,400	8.3
					2.0	28,000	630	2.2
					3.0	27,000	170	0.6
	8/23/84	1127	90	0.75	0.3	85,000	16,500	19.4
					1.0	75,000	5,000	6.7
					2.0	86,000	3,000	3.5
					3.0	33,000	1,230	3.7
					4.0	32,000	490	1.5
WRM 13.0	8/23/84	1156	50	0.75	0.3	31,000	6,000	19.4
					1.0	27,000	1,700	6.3
					2.0	27,000	800	3.0
					3.0	27,000	440	1.6
					4.0	26,500	230	0.9

Part 2

Discussion of the Significance of Optical Uniformity in the Evaluation of K_d

In the discussion given below, the importance of optical uniformity in the evaluation of the average attenuation coefficient over a given depth will be presented. First, an example of an optically uniform layer will be presented and the average attenuation coefficient $(K_d)_{ave.}$ over the depth of the layer will be computed. Next, an optically stratified layer will be considered and $(K_d)_{ave.}$ will be computed. In both cases the reliability of using the average coefficient to represent light attenuation over the entire depth of the layer will be evaluated.

I. Example 1: Optically Uniform Water

Consider an optically uniform layer (e.g. a well-mixed layer or a clear, turbidity-free layer) of depth 3 meters.

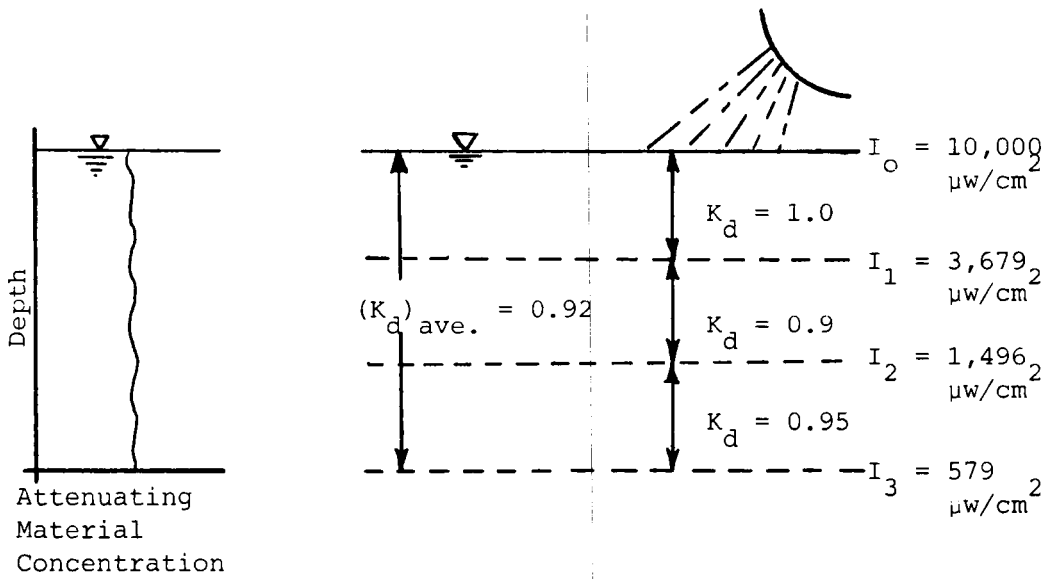

Small scale variations in K_d with depth are not significant.

$(K_d)_{ave.}$ may be computed from slope of plot of $\ln(I_o/I_z)$ versus depth.

$$I_z = I_o\, e^{-K_d z}$$

Depth (m)	$\ln(I_o/I_z)$
1	0.999
2	1.8998
3	2.8490

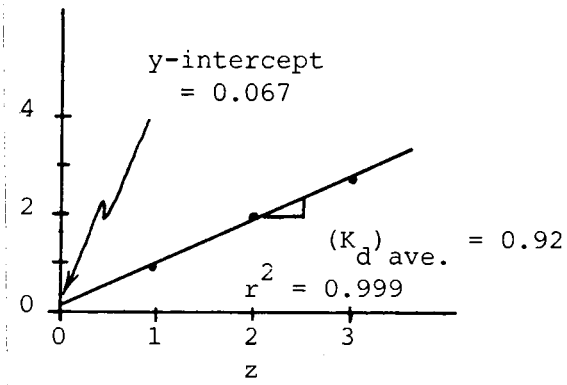

Differential Form of Beer's Law

$$dI = I_o K_d(z)\,dz$$

For optically uniform waters the function $K_d(z)$ which specifies the variation of K_d with depth may be considered to be approximately constant. Hence,

$$I = I_o \int_{z_o}^{z} K_d(z)\,dz = I_o K_d \int_{z_o}^{z} dz$$

and $$I = I_o K_d (z - z_o)$$

However, for a non-optically uniform water $K_d(z)$ cannot be assumed to be constant with depth.

II. Example 2:

Consider an optically stratified layer with variations in concentrations of attenuating substances with depth (e.g. a layer in which algae are stratified into layers of light seeking groups and shade seeking groups).

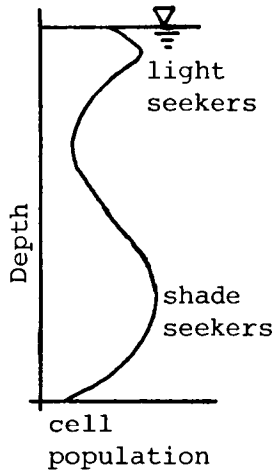

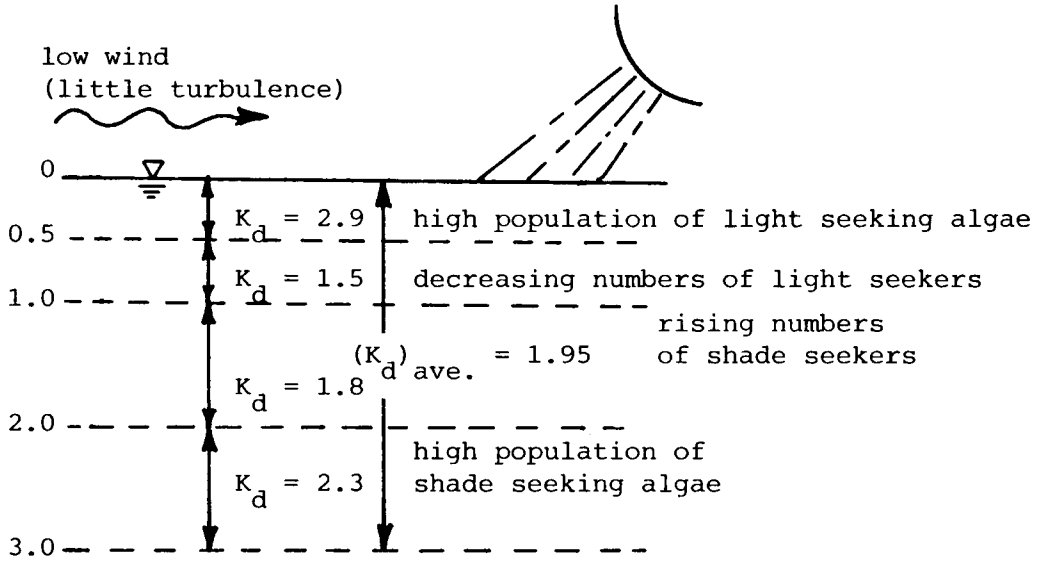

z	$\ln(I_o/I_z)$
0.5	1.450
1.0	2.199
2.0	4.001
3.0	6.320

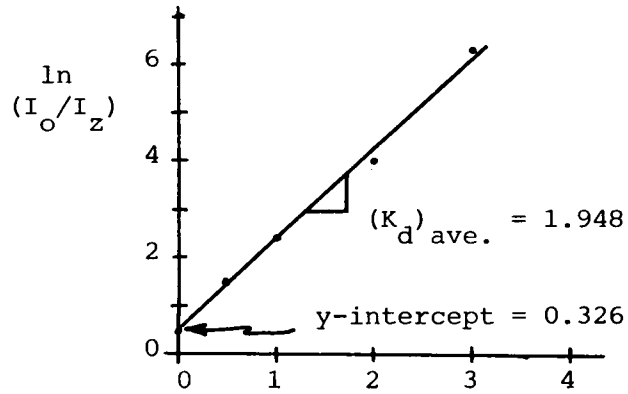

III. Observations

1. The use of $(K_d)_{ave.}$ in an optically uniform layer provides results which are representative of actual optical conditions, whereas $(K_d)_{ave.}$ for a non-optically uniform layer is representative only of the composite behavior of light attenuation with depth. The accuracy of using one $(K_d)_{ave.}$ value to represent attenuation over the total layer may be evaluated by inspection of the y-intercept. If the calculated $(K_d)_{ave.}$ value is truly representative of light attenuation over the entire layer, the y-intercept of the equation

$\ln(I_o/I_z) = (K_d)_{ave.}\ z$ should pass through the origin of the semilog plot. This is because at a depth of zero, the irradiance I_z should equal I_o or $\ln(I_o/I_z) = 0$ if the light attenuation gradient represented by $(K_d)_{ave.}$ is accurate. In the previous examples, it was shown that the optically uniform water had a y-intercept near the origin whereas the non-optically uniform water had a y-intercept which significantly departed from the origin. The use of the y-intercept as a proof of non-optical uniformity

is applicable only if the statistical variability of the y-intercept is small (e.g. a narrow 95% confidence interval for the y-intercept).

2. The coefficient of correlation, r^2, is relatively insensitive to significant variations in K_d over small depths (i.e. r^2 only from 0.999 to 0.996 when going from optically uniform to non-optically uniform waters, respectively).
3. $(K_d)_{ave.}$ for a given layer expresses the <u>composite</u> behavior of the exponential decay of light with depth in that layer.

IV. Conclusion

Modeling studies generally employ an average K_d value which represents both areal and depthwise variations in optical clarity. In non-optically uniform waters such as those of a non well-mixed euphotic reservoir this $(K_d)_{ave.}$ value will represent a greater variability of optical attenuation coefficients. For this type of reservoir the modeling results obtained using this $(K_d)_{ave.}$ value should be viewed with discretion keeping in mind that $(K_d)_{ave.}$ is representative only of the composite behavior of the light field.

V. Proposed Monitoring and Modeling Methods for Non-Optically Uniform Water

The following steps present a proposed scheme for modeling the attenuation of light in a layer which is optically stratified.

1. Obtain a continuous profile of irradiance with depth. This may be done by installing a chart recorder to the irradiameter and slowly lowering the light sensor until light extinction is near complete.
2. Inspect irradiance depth profile and divide into regions of similar optical properties.
3. At same time of irradiance measurements obtain samples for chlorophyll a analyses and algal species identification (maybe also get samples for suspended solids (non volatile) and dissolved color). Take these samples at numerous discrete depths. Take enough samples to adequately define depthwise variations over the euphotic zone.
4. For each optical region determined in step #1, partition the corresponding K_d according to chlorophyll a and species type, suspended solids, dissolved color, etc.
5. By this method you will arrive at a set of depth specific equations by which K_d may be predicted

in terms of attenuating substances. These equations however, are only good for a specific location and time. By conducting these measurements at several locations and several dates of the year, a detailed light attenuation model should be able to be developed which reflects seasonal and areal light attenuation patterns.

APPENDIX II

BOONE RESERVOIR PHYTOPLANKTON DATA

1984 Boone Reservoir Phytoplankton Data

Group Abundance, Number of Genera, Percent Composition
0-3 Meter Integrated Depth

WRM 2.0 — May 25, 1984

Group	Cells/L x 10^6	No. of Genera	Percent of Total
Chlorophyta	0.66	3	13.0
Bacillariophyta	2.98	2	59.6
Cryptophyta	0	0	0
Cyanophyta	1.36	4	27.2
Euglenophyta	0.02	1	0.2
Pyrrhophyta	0	0	0
Total	5.02	10	100

WRM 2.0 — August 23, 1984

Group	Cells/L x 10^6	No. of Genera	Percent of Total
Chlorophyta	1.03	18	20.0
Bacillariophyta	1.85	4	35.8
Cryptophyta	0.01	1	0.2
Cyanophyta	2.23	4	43.3
Euglenophyta	0.01	1	0.2
Pyrrhophyta	0.02	1	0.3
Total	5.15	29	100

WRM 2.0 — June 13, 1984

Group	Cells/L x 10^6	No. of Genera	Percent of Total
Chlorophyta	2.17	5	63.5
Bacillariophyta	0.39	2	11.4
Cryptophyta	0	0	0
Cyanophyta	0.86	2	25.1
Euglenophyta	<0.01	1	1.0
Pyrrhophyta	0	0	0
Total	3.42	10	100

WRM 6.0 — May 25, 1984

Group	Cells/L x 10^6	No. of Genera	Percent of Total
Chlorophyta	0.59	4	5.0
Bacillariophyta	8.04	2	69.2
Cryptophyta	0	0	0
Cyanophyta	2.93	3	25.2
Euglenophyta	0.07	2	0.5
Pyrrhophyta	0	0	0
Total	11.62	11	100

WRM 2.0 — July 20, 1984

Group	Cells/L x 10^6	No. of Genera	Percent of Total
Chlorophyta	3.58	17	60.7
Bacillariophyta	0.61	4	10.3
Cryptophyta	0	0	0
Cyanophyta	1.61	4	27.4
Euglenophyta	0.05	2	0.8
Pyrrhophyta	0.04	2	0.6
Total	5.88	29	100

WRM 6.0 — June 13, 1984

Group	Cells/L x 10^6	No. of Genera	Percent of Total
Chlorophyta	3.83	7	35.8
Bacillariophyta	1.81	2	16.9
Cryptophyta	0.01	1	<0.1
Cyanophyta	5.00	4	46.7
Euglenophyta	0.06	2	0.5
Pyrrhophyta	0	0	0
Total	10.71	16	100

1984 Boone Reservoir Phytoplankton Data

(Continued)

Group Abundance, Number of Genera, Percent Composition
0-3 Meter Integrated Depth

WRM 6.0
July 20, 1984

Group	Cells/L x 10^6	No. of Genera	Percent of Total
Chlorophyta	1.71	11	65.9
Bacillariophyta	0.21	4	8.0
Cryptophyta	0.01	1	0.4
Cyanophyta	0.57	4	21.8
Euglenophyta	0.04	2	1.4
Pyrrhophyta	0.06	2	2.4
Total	2.60	24	100

WRM 10.95
June 13, 1984

Group	Cells/L x 10^6	No. of Genera	Percent of Total
Chlorophyta	10.62	8	61.1
Bacillariophyta	1.22	4	7.0
Cryptophyta	0.02	1	<0.1
Cyanophyta	5.40	3	31.1
Euglenophyta	0.10	2	<0.6
Pyrrhophyta	0.01	1	<0.1
Total	17.37	19	100

WRM 6.0
August 23, 1984

Group	Cells/L x 10^6	No. of Genera	Percent of Total
Chlorophyta	1.13	18	19.5
Bacillariophyta	1.61	4	27.6
Cryptophyta	0.01	1	0.2
Cyanophyta	3.02	4	52.1
Euglenophyta	0.03	2	0.5
Pyrrhophyta	0.01	1	0.1
Total	5.81	30	100

WRN 10.95
July 20, 1984

Group	Cells/L x 10^6	No. of Genera	Percent of Total
Chlorophyta	2.49	12	58.4
Bacillariophyta	0.32	5	7.5
Cryptophyta	0.02	1	0.6
Cyanophyta	1.30	3	30.7
Euglenophyta	0.05	2	1.2
Pyrrhophyta	0.07	2	1.5
Total	4.25	25	100

WRM 10.95
May 25, 1984

Group	Cells/L x 10^6	No. of Genera	Percent of Total
Chlorophyta	1.20	3	9.8
Bacillariophyta	10.19	1	82.9
Cryptophyta	0	0	0
Cyanophyta	0.80	1	6.5
Euglenophyta	0.09	1	0.7
Pyrrhophyta	0	0	0
Total	12.28	6	100

WRM 10.95
August 23, 1984

Group	Cells/L x 10^6	No. of Genera	Percent of Total
Chlorophyta	1.93	16	34.5
Bacillariophyta	1.32	5	23.6
Cryptophyta	0.03	1	0.6
Cyanophyta	2.27	3	40.5
Euglenophyta	0.03	2	0.6
Pyrrhophyta	0.02	2	0.3
Total	5.59	29	100

1984 Boone Reservoir Phytoplankton Data

(Continued)

Group Abundance, Number of Genera, Percent Composition
0-3 Meter Integrated Depth

SFHRM 19.0
May 24, 1984

Group	Cells/L x 10^6	No. of Genera	Percent of Total
Chlorophyta	0.50	1	11.9
Bacillariophyta	1.19	2	28.2
Cryptophyta	0	0	0
Cyanophyta	2.48	2	60.0
Euglenophyta	0.04	2	0.9
Pyrrhophyta	0	0	0
Total	4.20	7	100

SFHRM 19.0
August 21, 1984

Group	Cells/L x 10^6	No. of Genera	Percent of Total
Chlorophyta	1.70	20	18.0
Bacillariophyta	2.84	4	30.1
Cryptophyta	0.02	1	0.2
Cyanophyta	4.80	4	50.1
Euglenophyta	0.05	2	0.6
Pyrrhophyta	0.02	2	0.3
Total	9.43	33	100

SFHRM 19.0
June 12, 1984

Group	Cells/L x 10^6	No. of Genera	Percent of Total
Chlorophyta	1.83	3	97.5
Bacillariophyta	0.02	1	1.0
Cryptophyta	0	0	0
Cyanophyta	0.01	1	0.6
Euglenophyta	0.02	2	0.8
Pyrrhophyta	0	0	0
Total	1.87	8	100

SFHRM 22.4
May 24, 1984

Group	Cells/L x 10^6	No. of Genera	Percent of Total
Chlorophyta	0.83	4	15.0
Bacillariophyta	2.56	2	46.2
Cryptophyta	0	0	0
Cyanophyta	2.08	3	37.5
Euglenophyta	0.07	1	1.3
Pyrrhophyta	0	0	0
Total	5.53	10	100

SFHRM 19.0
July 19, 1984

Group	Cells/L x 10^6	No. of Genera	Percent of Total
Chlorophyta	0.81	11	39.1
Bacillariophyta	0.41	3	19.9
Cryptophyta	0.01	1	0.3
Cyanophyta	0.80	4	38.7
Euglenophyta	0	0	0
Pyrrhophyta	0.04	2	2.0
Total	2.06	21	100

SFHRM 22.4
June 12, 1984

Group	Cells/L x 10^6	No. of Genera	Percent of Total
Chlorophyta	1.95	4	89.6
Bacillariophyta	0.01	1	0.6
Cryptophyta	0	0	0
Cyanophyta	0.21	2	9.7
Euglenophyta	<0.01	1	0.1
Pyrrhophyta	0	0	0
Total	2.18	10	100

1984 Boone Reservoir Phytoplankton Data

(Continued)

Group Abundance, Number of Genera, Percent Composition
0-3 Meter Integrated Depth

SFHRM 19.0
May 24, 1984

Group	Cells/L x 10^6	No. of Genera	Percent of Total
Chlorophyta	0.50	1	11.9
Bacillariophyta	1.19	2	28.2
Cryptophyta	0	0	0
Cyanophyta	2.48	2	60.0
Euglenophyta	0.04	2	0.9
Pyrrhophyta	0	0	0
Total	4.20	7	100

SFHRM 19.0
August 21, 1984

Group	Cells/L x 10^6	No. of Genera	Percent of Total
Chlorophyta	1.70	20	18.0
Bacillariophyta	2.84	4	30.1
Cryptophyta	0.02	1	0.2
Cyanophyta	4.80	4	50.1
Euglenophyta	0.05	2	0.6
Pyrrhophyta	0.02	2	0.3
Total	9.43	33	100

SFHRM 19.0
June 12, 1984

Group	Cells/L x 10^6	No. of Genera	Percent of Total
Chlorophyta	1.83	3	97.5
Bacillariophyta	0.02	1	1.0
Cryptophyta	0	0	0
Cyanophyta	0.01	1	0.6
Euglenophyta	0.02	2	0.8
Pyrrhophyta	0	0	0
Total	1.87	8	100

SFHRM 22.4
May 24, 1984

Group	Cells/L x 10^6	No. of Genera	Percent of Total
Chlorophyta	0.83	4	15.0
Bacillariophyta	2.56	2	46.2
Cryptophyta	0	0	0
Cyanophyta	2.08	3	37.5
Euglenophyta	0.07	1	1.3
Pyrrhophyta	0	0	0
Total	5.53	10	100

SFHRM 19.0
July 19, 1984

Group	Cells/L x 10^6	No. of Genera	Percent of Total
Chlorophyta	0.81	11	39.1
Bacillariophyta	0.41	3	19.9
Cryptophyta	0.01	1	0.3
Cyanophyta	0.80	4	38.7
Euglenophyta	0	0	0
Pyrrhophyta	0.04	2	2.0
Total	2.06	21	100

SFHRM 22.4
June 12, 1984

Group	Cells/L x 10^6	No. of Genera	Percent of Total
Chlorophyta	1.95	4	89.6
Bacillariophyta	0.01	1	0.6
Cryptophyta	0	0	0
Cyanophyta	0.21	2	9.7
Euglenophyta	<0.01	1	0.1
Pyrrhophyta	0	0	0
Total	2.18	10	100

1984 Boone Reservoir Phytoplankton Data

(Continued)

Group Abundance, Number of Genera, Percent Composition
0-3 Meter Integrated Depth

SFHRM 22.4
July 19, 1984

Group	Cells/L x 10^6	No. of Genera	Percent of Total
Chlorophyta	-	-	-
Bacillariophyta	-	-	-
Cryptophyta	-	-	-
Cyanophyta	-	-	-
Euglenophyta	-	-	-
Pyrrhophyta	-	-	-
Total			

SFHRM 26.2
June 12, 1984

Group	Cells/L x 10^6	No. of Genera	Percent of Total
Chlorophyta	2.53	4	46.1
Bacillariophyta	0.17	2	3.2
Cryptophyta	0	0	0
Cyanophyta	2.74	4	49.8
Euglenophyta	0.05	2	0.9
Pyrrhophyta	0	0	0
Total	5.50	12	100

SFHRM 22.4
August 21, 1984

Group	Cells/L x 10^6	No. of Genera	Percent of Total
Chlorophyta	1.41	13	14.5
Bacillariophyta	3.96	5	40.6
Cryptophyta	0.01	1	0.1
Cyanophyta	4.29	4	44.0
Euglenophyta	0.05	2	0.5
Pyrrhophyta	0.02	2	0.3
Total	9.76	27	100

SFHRM 26.2
July 19, 1984

Group	Cells/L x 10^6	No. of Genera	Percent of Total
Chlorophyta	0.63	9	32.6
Bacillariophyta	0.56	3	29.2
Cryptophyta	0.01	1	0.3
Cyanophyta	0.70	3	36.3
Euglenophyta	0.01	1	0.3
Pyrrhophyta	0.02	3	1.3
Total	1.92	20	100

SFHRM 26.2
May 24, 1984

Group	Cells/L x 10^6	No. of Genera	Percent of Total
Chlorophyta	0.48	4	12.7
Bacillariophyta	1.49	2	39.5
Cryptophyta	0	0	0
Cyanophyta	1.65	3	43.6
Euglenophyta	0.16	1	4.2
Pyrrhophyta	0	0	0
Total	3.78	10	100

SFHRM 26.2
August 21, 1984

Group	Cells/L x 10^6	No. of Genera	Percent of Total
Chlorophyta	1.30	16	17.3
Bacillariophyta	3.13	4	41.7
Cryptophyta	0	0	0
Cyanophyta	3.07	3	40.8
Euglenophyta	0.01	2	0.1
Pyrrhophyta	0	0	0
Total	7.51	25	100

1984 Boone Reservoir Phytoplankton Data

(Continued)

Group Abundance, Number of Genera, Percent Composition
0-3 Meter Integrated Depth

SFHRM 30.8
May 24, 1984

Group	Cells/L x 10^6	No. of Genera	Percent of Total
Chlorophyta	0.60	3	11.0
Bacillariophyta	1.30	2	23.9
Cryptophyta	0	0	0
Cyanophyta	3.43	4	63.0
Euglenophyta	0.12	1	2.1
Pyrrhophyta	0	0	0
Total	5.44	10	100

SFHRM 30.8
July 19, 1984

Group	Cells/L x 10^6	No. of Genera	Percent of Total
Chlorophyta	-	-	-
Bacillariophyta	-	-	-
Cryptophyta	-	-	-
Cyanophyta	-	-	-
Euglenophyta	-	-	-
Pyrrhophyta	-	-	-
Total			

SFHRM 30.8
June 12, 1984

Group	Cells/L x 10^6	No. of Genera	Percent of Total
Chlorophyta	2.67	7	52.5
Bacillariophyta	1.87	2	3.7
Cryptophyta	0.01	1	0.1
Cyanophyta	2.15	3	42.4
Euglenophyta	0.06	2	1.1
Pyrrhophyta	0.01	1	0.2
Total	5.08	16	100

SFHRM 30.8
August 21, 1984

Group	Cells/L x 10^6	No. of Genera	Percent of Total
Chlorophyta	1.21	15	19.9
Bacillariophyta	1.70	4	27.9
Cryptophyta	0.01	1	0.2
Cyanophyta	3.15	4	51.6
Euglenophyta	0.01	2	0.2
Pyrrhophyta	0.02	1	0.3
Total	6.09	27	100

APPENDIX III

MEASURED AND PREDICTED CHLOROPHYLL CONCENTRATIONS AND CORRESPONDING INSITU ALGAL FLUORESCENCE MEASUREMENTS BOONE RESERVOIR

Part 1

Chlorophyll Analyses Results and Corresponding In Situ Fluorescence Measurements--Boone Reservoir, May to August, 1984

Station	Date	Time (EDT)	Depth (meters)	% Horiz	CHLOROPHYLL Chl a (mg/m^3)	Corrected Chl a (mg/m^3)	Pheophytin a (mg/m^3)	Pheophytin Index	Chl b (mg/m^3)	Chl c (mg/m^3)	In Situ Fluorescence[1] (no units)
SFHRM 19.0	5/24/84	0907	0-3	50	18.09	16.02	2.48	1.61	0.24	3.09	10.0
				(dup.)	19.19	17.09	2.54	1.61	0.64	3.52	
			6	50	40.42	32.84	10.33	1.53	-1.48	7.46	-
	6/12/84	0914	0-3	50	4.86	4.01	1.23	1.54	0.58	0.35	29.2
				(dup.)	5.32	4.81	0.61	1.62	0.55	0.45	
			6	50	2.44	1.05	2.26	1.22	0.35	0.25	16.8
	7/19/84	0928	0-3	50	9.84	9.35	0.37	1.67	0.68	2.72	13.6
				(dup.)	9.64	8.81	0.91	1.63	0.45	2.17	
			6	50	14.31	10.15	6.30	1.43	0.64	1.55	14.8
	8/21/84	0944	0-3	50	10.08	9.34	0.37	1.67	0.60	2.44	11.7
				(dup.)	9.85	15.75	3.50	1.57	0.79	1.74	
			6	50	18.40	11.48	-0.08	1.70	0.79	2.08	13.0
SFHRM 22.4	5/24/84	1017	0-3	75	21.90	19.09	2.50	1.62	1.20	3.02	11.2
				(dup.)	20.52	18.42	2.51	1.62	1.25	2.87	
			6	75	7.40	5.61	2.62	1.48	0.07	1.15	11.2
	6/12/84	1035	0-3	75	6.08	5.07	1.47	1.54	0.90	1.01	38.0
				(dup.)	6.89	5.34	2.32	1.49	0.76	0.57	
			6	75	4.09	2.14	3.10	1.29	0.20	0.03	29.0
	7/19/84	1113	0-3	75	11.23	10.95	-0.11	1.71	0.45	2.37	13.4
				(dup.)	11.79	11.21	0.37	1.68	0.57	2.38	
			6	75	9.20	6.14	4.70	1.40	0.38	1.16	12.0
	8/21/84	1054	0-3	75	11.78	11.48	-0.08	1.70	0.81	2.05	12.1
				(dup.)	10.86	10.15	0.69	1.66	0.85	2.09	
			6	75	16.65	13.62	4.33	1.53	1.23	1.99	13.5
SFHRM 26.2	5/24/84	1150	0-3	25	21.01	19.22	1.90	1.64	0.85	2.63	10.8
				(dup.)	19.64	18.56	1.91	1.63	0.88	2.60	
			6	25	13.94	9.34	6.92	1.40	-0.11	1.26	7.1
	6/12/84	1124	0-3	25	11.17	10.68	0.35	1.68	1.40	1.08	58.8
				(dup.)	12.28	11.21	1.31	1.63	1.85	1.02	
			6	25	3.82	2.14	2.72	1.31	0.70	0.16	33.0
	7/19/84	1212	0-3	25	17.46	16.55	0.64	1.67	0.91	3.27	17.3
				(dup.)	16.22	15.75	-0.05	1.70	0.71	3.26	
			6	25	8.25	5.87	3.66	1.43	0.84	1.05	
				(dup.)	7.35	5.34	3.07	1.44	0.70	0.92	9.0
	8/21/84	1156	0-3	25	15.09	14.69	-0.11	1.71	0.76	2.43	12.5
				(dup.)	13.83	13.35	0.11	1.69	0.78	2.35	
			6	25	11.96	9.08	4.38	1.47	1.57	1.47	11.2

Station	Date	Time (EDT)	Depth (meters)	% Horiz	CHLOROPHYLL Chl a [3] (mg/m^3)	Corrected Chl a [3] (mg/m^3)	Pheophytin a [3] (mg/m^3)	Pheophytin Index	Chl b [3] (mg/m^3)	Chl c [3] (mg/m^3)	In Situ Fluorescence [1] (no units)
SFHRM 30.8	5/24/84	1250	0-3	25	25.42	23.76	1.47	1.66	1.17	3.69	13.5
				(dup.)	23.96	22.16	1.76	1.65	0.94	3.31	
			6	25	3.85	3.20	0.91	1.55	0.23	0.80	4.7
	6/12/84	1213	0-3	25	12.09	11.21	0.93	1.65	1.33	1.29	62.8
				(dup.)	17.49	16.29	1.47	1.64	3.77	1.92	
			6	25	2.92	2.40	0.77	1.53	0.53	0.28	35.0
	7/19/84	1307	0-3	25	22.50	20.56	2.24	1.63	2.22	3.28	19.1
				(dup.)	18.86	17.09	2.16	1.62	2.01	3.10	
			6	25	8.71	7.21	2.14	1.54	0.81	1.15	12.5
	8/21/84	1234	0-3	25	16.53	16.02	0.05	1.70	1.26	2.25	14.8
				(dup.)	15.85	14.42	1.66	1.63	1.17	2.50	
			6	25	8.01	6.41	2.38	1.51	0.92	1.33	8.3
WRM 2.0	5/24/84	0929	0-3	50	22.47	17.49	4.00	1.55	0.90	3.60	9.4
				(dup.)	18.40	15.49	3.95	1.56	0.68	3.06	
			6	50	14.03	7.48	10.28	1.29	-0.19	1.49	5.4
	6/13/84	0900	0-3	50	7.15	6.14	1.34	1.57	0.47	0.37	35.0
				(dup.)	7.12	6.94	-0.03	1.70	0.83	0.71	
			6	50	2.36	1.60	1.20	1.40	0.41	0.27	16.0
	7/20/84	0951	0-3	50	10.07	9.35	0.75	1.65	0.84	2.12	16.9
				(dup.)	10.88	9.88	1.15	1.63	0.61	2.42	
			6	50	8.47	5.07	5.39	1.34	0.97	0.69	9.5
	8/23/84	0910	0-3	50	20.86	19.76	0.80	1.67	1.19	3.72	17.1
				(dup.)	20.01	19.49	-0.24	1.71	0.50	3.09	
			6	50	6.78	5.61	1.68	1.54	0.79	0.83	6.0
WRM 6.0	5/25/84	1101	0-3	50	52.95	51.93	2.36	1.68	0.08	10.98	23.6
				(dup.)	57.46	53.40	3.60	1.66	0.32	11.46	
			6	50	14.81	12.01	3.87	1.53	-0.13	2.86	5.4
	6/13/84	0947	0-3	50	22.63	20.29	2.70	1.62	0.75	1.92	72.8
				(dup.)	22.62	21.09	1.34	1.66	0.70	2.42	
			6	50	5.43	2.14	5.34	1.20	0.49	0.43	20.0
	7/20/84	1046	0-3	50	18.38	16.29	2.59	1.60	0.89	2.98	25.8
				(dup.)	21.73	19.76	2.30	1.63	1.70	4.19	
			6	50	5.89	3.47	3.82	1.33	0.49	0.29	7.4
	8/23/84	1006	0-3	50	22.38	21.36	0.51	1.68	0.67	3.67	18.9
				(dup.)	20.68	19.49	0.88	1.67	0.49	3.81	
			6	50	6.66	4.27	3.76	1.37	0.87	0.61	6.5

Station	Date	Time (EDT)	Depth (meters)	% Horiz	CHLOROPHYLL Chl a (mg/m^3)	Corrected Chl a (mg/m^3)	Pheophytin a (mg/m^3)	Pheophytin Index	Chl b (mg/m^3)	Chl c (mg/m^3)	In Situ Fluorescence[1] (no units)
WRM 10.95	5/25/84	1144	0-3	90	84.18	70.36	3.84	1.68	4.36	15.78	28.3
				(dup.)	65.51	60.61	5.37	1.64	6.49	14.52	
			6	90	11.20	9.34	2.62	1.55	0.82	2.70	6.5
	6/13/84	1042	0-3	90	40.41	32.57	11.53	1.52	5.25	3.00	
				(dup.)	45.60	37.65	11.51	1.54	5.85	3.47	
			6	90	6.63	4.27	3.76	1.37	1.29	0.45	
	7/20/84	1149	0-3	90	28.97	24.83	5.45	1.57	0.91	5.02	40.0
				(dup.)	27.73	24.30	4.30	1.59	0.69	5.26	
			6	90	8.25	6.41	2.75	1.49	0.79	1.54	9.5
	8/23/84	1108	0-3	90	19.13	18.16	0.72	1.67	1.56	2.48	
				(dup.)	14.84	13.62	1.33	1.64	1.13	1.90	
			6	90	2.68	2.40	0.40	1.60	0.61	0.56	

[1] In situ fluorescence values for the 0 to 3 meter depth water column were computed as the mean of the fluorescence values at 0.3, 1.0, 2.0, and 3.0 meters.

Part 2

Measured In Situ Fluorescence Results and Corresponding Predicted Chlorophyll Values

May Survey[2]

Depth (m)	SFHRM 19.0 Fluor (no units)	SFHRM 19.0 Chl a (mg/m)	SFHRM 19.0 Cchl a (mg/m)	SFHRM 22.4 Fluor (no units)	SFHRM 22.4 Chl a (mg/m)	SFHRM 22.4 Cchl a (mg/m)
0.3	7.6	13.18	10.55	11.2	22.81	19.61
0.5	8.0	14.25	11.56	8.5	15.59	12.81
1.0	8.8	16.39	13.57	8.2	14.79	12.06
2.0	10.2	20.14	17.10	11.5	23.61	20.37
3.0	15.6	34.58	30.69	16.6	37.25	33.21
4.0	28.4	68.82	62.93	29.2	70.96	64.95
5.0	-	-	-	18.3	41.80	37.49
6.0	-	-	-	11.2	22.81	19.61
7.0	3.70	2.75	0.73	8.4	15.32	12.56
8.0	3.32	1.73	-	6.0	8.90	6.52
9.0	3.15	1.28	-	5.5	7.57	5.26
10.0	3.05	1.01	-	5.2	6.76	4.50
11.0	2.90	0.61	-	5.2	6.75	4.50
12.0	2.32	-	-	5.5	7.57	5.26

Depth (m)	SFHRM 25.0 Fluor (no units)	SFHRM 25.0 Chl a (mg/m)	SFHRM 25.0 Cchl a (mg/m)	SFHRM 26.2 Fluor (no units)	SFHRM 26.2 Chl a (mg/m)	SFHRM 26.2 Cchl a (mg/m)
0.3	6.9	11.31	8.78	8.0	14.25	11.56
0.5	8.0	14.25	11.56	8.3	15.05	12.31
1.0	11.7	24.15	20.87	11.2	22.81	19.61
2.0	12.2	24.49	22.13	13.9	30.03	26.41
3.0	14.0	30.30	26.67	12.8	27.09	23.64
4.0	13.6	29.23	25.66	10.6	21.21	18.10
5.0	15.0	32.98	29.18	10.8	21.74	18.61
6.0	8.1	14.52	11.81	7.1	11.85	9.29
7.0	6.9	11.31	8.78	6.8	11.04	8.53
8.0	6.1	9.17	6.77	6.2	9.44	7.02
9.0	6.5	10.24	7.78	6.0	8.90	6.52
10.0	7.1	11.85	9.29	5.8	8.37	6.01
11.0	6.8	11.04	8.53	5.5	7.57	5.26
12.0	6.6	10.51	8.03	5.3	7.03	4.76

May Survey[2]

Depth (m)	SFHRM 19.0 Fluor (no units)	SFHRM 19.0 Chl a (mg/m)	SFHRM 19.0 Cchl a (mg/m)	SFHRM 22.4 Fluor (no units)	SFHRM 22.4 Chl a (mg/m)	SFHRM 22.4 Cchl a (mg/m)
0.3	7.6	13.18	10.55	11.2	22.81	19.61
0.5	8.0	14.25	11.56	8.5	15.59	12.81
1.0	8.8	16.39	13.57	8.2	14.79	12.06
2.0	10.2	20.14	17.10	11.5	23.61	20.37
3.0	15.6	34.58	30.69	16.6	37.25	33.21
4.0	28.4	68.82	62.93	29.2	70.96	64.95
5.0	-	-	-	18.3	41.80	37.49
6.0	-	-	-	11.2	22.81	19.61
7.0	3.70	2.75	0.73	8.4	15.32	12.56
8.0	3.32	1.73	-	6.0	8.90	6.52
9.0	3.15	1.28	-	5.5	7.57	5.26
10.0	3.05	1.01	-	5.2	6.76	4.50
11.0	2.90	0.61	-	5.2	6.75	4.50
12.0	2.32	-	-	5.5	7.57	5.26

Depth (m)	SFHRM 25.0 Fluor (no units)	SFHRM 25.0 Chl a (mg/m)	SFHRM 25.0 Cchl a (mg/m)	SFHRM 26.2 Fluor (no units)	SFHRM 26.2 Chl a (mg/m)	SFHRM 26.2 Cchl a (mg/m)
0.3	6.9	11.31	8.78	8.0	14.25	11.56
0.5	8.0	14.25	11.56	8.3	15.05	12.31
1.0	11.7	24.15	20.87	11.2	22.81	19.61
2.0	12.2	24.49	22.13	13.9	30.03	26.41
3.0	14.0	30.30	26.67	12.8	27.09	23.64
4.0	13.6	29.23	25.66	10.6	21.21	18.10
5.0	15.0	32.98	29.18	10.8	21.74	18.61
6.0	8.1	14.52	11.81	7.1	11.85	9.29
7.0	6.9	11.31	8.78	6.8	11.04	8.53
8.0	6.1	9.17	6.77	6.2	9.44	7.02
9.0	6.5	10.24	7.78	6.0	8.90	6.52
10.0	7.1	11.85	9.29	5.8	8.37	6.01
11.0	6.8	11.04	8.53	5.5	7.57	5.26
12.0	6.6	10.51	8.03	5.3	7.03	4.76

May Survey[2]

Depth (m)	SFHRM 28.3 Fluor (no units)	SFHRM 28.3 Chl a (mg/m)	SFHRM 28.3 Cchl a (mg/m)	SFHRM 30.8 Fluor (no units)	SFHRM 30.8 Chl a (mg/m)	SFHRM 30.8 Cchl a (mg/m)
0.3	8.5	15.6	12.81	11.6	23.88	20.62
0.5	10.0	19.6	16.59	11.6	23.88	20.61
1.0	11.9	24.68	21.38	13.8	29.77	26.16
2.0	15.2	33.51	29.69	15.5	34.31	30.44
3.0	12.5	26.29	22.89	14.8	32.44	28.68
4.0	8.0	14.25	11.56	14.8	32.44	28.68
5.0	7.5	12.92	10.30	5.5	7.57	5.26
6.0	8.1	14.52	11.81	4.7	5.43	3.24
7.0	7.3	12.38	9.79	4.6	5.16	2.99
8.0	6.5	10.24	7.78	4.4	4.62	2.49
9.0	5.6	7.83	5.51	4.3	4.36	2.24
10.0	6.00	8.90	6.52	4.0	3.55	1.48
11.0	4.90	5.96	3.75	4.0	3.55	1.48
12.0	4.90	5.96	3.75	-	-	-

Depth (m)	WRM 2.0 Fluor (no units)	WRM 2.0 Chl a (mg/m)	WRM 2.0 Cchl a (mg/m)	WRM 3.0 Fluor (no units)	WRM 3.0 Chl a (mg/m)	WRM 3.0 Cchl a (mg/m)
0.3	6.4	9.97	7.53	5.8	8.37	6.01
0.5	6.4	9.97	7.53	6.8	11.04	8.53
1.0	7.8	13.72	11.05	8.2	14.79	12.06
2.0	10.9	22.01	18.86	10.0	19.60	16.59
3.0	15.5	34.31	30.44	30.0	73.10	66.96
4.0	29.0	70.42	64.44	38.0	94.49	87.11
5.0	22.0	51.70	46.81	11.0	22.28	19.11
6.0	5.4	7.30	5.01	5.0	6.23	4.00
7.0	5.4	7.30	5.01	4.4	4.62	2.49
8.0	3.8	3.02	0.98	3.9	3.29	1.23
9.0	3.1	1.15	-	3.7	2.75	0.73
10.0	2.8	0.34	-	3.4	1.95	-
11.0	2.4	-	-	3.2	1.41	-
12.0	2.00	-	-	3.1	1.15	-

May Survey[2]

Depth (m)	WRM 6.0 Fluor (no units)	WRM 6.0 Chl a (mg/m)	WRM 6.0 Cchl a (mg/m)	WRM 8.4 Fluor (no units)	WRM 8.4 Chl a (mg/m)	WRM 8.4 Cchl a (mg/m)
0.3	7.2	12.11	9.54	8.0	14.25	11.56
0.5	8.4	15.32	12.56	9.2	17.46	14.58
1.0	31.0	75.77	69.48	25.0	59.72	54.37
2.0	20.6	47.95	43.29	40.0	99.84	92.14
3.0	51.0	129.26	119.85	23.0	54.37	49.33
4.0	29.0	70.42	64.44	18.0	41.0	36.74
5.0	13.0	27.63	24.15	9.8	19.10	16.09
6.0	5.4	7.30	5.01	6.0	8.90	6.52
7.0	4.2	4.09	1.99	4.6	5.16	2.99
8.0	3.6	2.48	0.47	4.2	4.09	1.99
9.0	3.3	1.68	-	3.8	3.02	0.98
10.0	3.0	0.88	-	3.6	2.48	0.47
11.0	3.0	0.88	-	3.4	1.95	-
12.0	3.0	0.88	-	3.2	1.41	-

Depth (m)	WRM 10.95 Fluor (no units)	WRM 10.95 Chl a (mg/m)	WRM 10.95 Cchl a (mg/m)
0.3	16.0	35.65	31.70
0.5	23.5	55.71	50.59
1.0	33.0	81.12	74.51
2.0	47.0	118.56	109.77
3.0	22.0	51.70	46.81
4.0	9.0	16.93	14.07
5.0	7.0	11.58	9.04
6.0	6.5	10.24	7.78
7.0	5.4	7.30	5.01
8.0	4.6	5.16	2.99
9.0	4.0	3.55	1.48
10.0	-	-	-
11.0	-	-	-
12.0	-	-	-

June Survey[2]

Depth (m)	SFHRM 19.0 Fluor (no units)	Chl a (mg/m)	Cchl a (mg/m)	SFHRM 22.4 Fluor (no units)	Chl a (mg/m)	Cchl a (mg/m)
0.3	22.0	2.75	1.35	27.0	4.28	2.91
0.5	24.0	3.36	1.97	27.0	4.28	2.91
1.0	24.0	3.36	1.97	28.0	4.59	3.22
2.0	28.0	10.72	9.45	54.0	12.55	11.31
3.0	48.0	10.72	9.45	54.0	12.55	11.31
4.0	42.0	8.88	7.58	44.0	9.49	8.20
5.0	25.5	3.82	2.44	34.0	6.43	5.09
6.0	16.8	1.16	-	29.0	4.90	3.53
7.0	15.5	0.76	-	27.0	4.28	2.91
8.0	15.5	0.76	-	26.0	3.98	2.60
9.0	16.5	1.07	-	26.0	3.98	2.60
10.0	17.5	1.37	-	26.0	3.98	2.60
11.0	18.2	1.59	0.20	25.0	3.67	2.28
12.0	18.0	1.53	0.10	25.0	3.67	2.28

Depth (m)	SFHRM 25.0 Fluor (no units)	Chl a (mg/m)	Cchl a (mg/m)	SFHRM 26.2 Fluor (no units)	Chl a (mg/m)	Cchl a (mg/m)
0.3	38.0	7.65	6.33	46.0	10.10	8.82
0.5	39.0	7.96	6.64	46.0	10.10	8.82
1.0	42.0	8.88	7.58	54.0	12.55	11.32
2.0	54.0	12.55	11.32	62.0	15.00	13.81
3.0	70.0	17.46	16.30	86.0	22.36	21.28
4.0	48.0	10.72	9.45	60.0	14.39	13.18
5.0	37.0	7.35	6.02	40.0	8.27	6.96
6.0	30.0	5.20	3.84	33.0	6.12	4.78
7.0	26.0	3.98	2.60	29.0	4.90	3.53
8.0	24.0	3.36	1.97	27.0	4.28	2.91
9.0	24.0	3.36	1.97	26.0	3.98	2.60
10.0	25.0	3.67	2.28	26.0	3.98	2.60
11.0	26.0	3.98	2.60	27.0	4.28	2.91
12.0	27.0	4.28	2.91	27.5	4.44	3.06

June Survey[2]

Depth (m)	SFHRM 28.3 Fluor (no units)	SFHRM 28.3 Chl a (mg/m)	SFHRM 28.3 Cchl a (mg/m)	SFHRM 30.8 Fluor (no units)	SFHRM 30.8 Chl a (mg/m)	SFHRM 30.8 Cchl a (mg/m)
0.3	36.0	7.04	5.71	54.0	12.55	11.32
0.5	44.0	9.49	8.20	59.0	14.09	12.87
1.0	63.0	15.31	14.12	61.0	14.70	13.50
2.0	89.0	23.28	22.22	76.0	19.29	18.17
3.0	80.0	20.52	19.41	64.0	15.62	14.43
4.0	57.0	13.47	12.25	48.0	10.72	9.45
5.0	56.0	13.17	11.94	37.0	7.35	6.02
6.0	49.0	11.02	9.76	35.0	6.73	5.40
7.0	50.0	11.33	10.07	30.0	5.20	3.84
8.0	46.0	10.10	8.82	29.0	4.90	3.53
9.0	46.0	10.10	8.82	28.0	4.59	3.22
10.0	44.0	9.49	8.20	28.0	4.59	3.22
11.0	41.0	8.57	7.27	28.0	4.59	3.22
12.0	38.0	7.65	6.33	-	-	-

Depth (m)	WRM 2.0 Fluor (no units)	WRM 2.0 Chl a (mg/m)	WRM 2.0 Cchl a (mg/m)	WRM 3.0 Fluor (no units)	WRM 3.0 Chl a (mg/m)	WRM 3.0 Cchl a (mg/m)
0.3	33.0	6.12	4.78	34.0	6.43	5.09
0.5	37.0	7.35	6.02	40.0	8.26	6.96
1.0	37.0	7.35	6.02	44.0	9.49	8.20
2.0	33.0	6.12	4.78	59.0	14.08	12.87
3.0	35.0	6.73	5.40	57.0	13.47	12.25
4.0	29.0	4.90	3.53	44.0	9.49	8.20
5.0	19.5	1.98	0.57	27.5	4.44	3.06
6.0	16.0	0.91	-	22.5	2.90	1.51
7.0	13.5	0.15	-	20.5	2.29	0.88
8.0	13.0	-	-	20.5	2.29	0.88
9.0	12.7	-	-	23.5	3.21	1.82
10.0	12.7	-	-	24.5	3.52	2.13
11.0	12.2	-	-	24.5	3.52	2.13
12.0	12.0	-	-	24.5	3.52	2.13

June Survey[2]

Depth (m)	WRM 6.0 Fluor (no units)	WRM 6.0 Chl a (mg/m)	WRM 6.0 Cchl a (mg/m)	WRM 8.4 Fluor (no units)	WRM 8.4 Chl a (mg/m)	WRM 8.4 Cchl a (mg/m)
0.3	73.0	18.38	17.23	58.0	13.78	12.56
0.5	74.0	18.68	17.54	66.0	16.23	15.05
1.0	75.0	18.99	17.86	89.0	23.28	22.22
2.0	87.0	22.66	21.59	10.0	-	-
3.0	55.0	12.86	11.63	60.0	14.39	13.18
4.0	31.0	5.51	4.15	42.0	8.88	7.58
5.0	25.0	3.67	2.28	31.0	5.51	4.15
6.0	20.0	2.14	0.73	32.0	5.81	4.46
7.0	19.5	1.98	0.57	29.0	4.90	3.53
8.0	11.5	-	-	24.0	3.36	1.97
9.0	11.5	-	-	22.0	2.75	1.35
10.0	12.0	-	-	24.0	3.36	1.97
11.0	12.0	-	-	25.0	3.67	2.28
12.0	11.8	-	-	28.0	4.59	3.22

Depth (m)	WRM 10.95 Fluor (no units)	WRM 10.95 Chl a (mg/m)	WRM 10.95 Cchl a (mg/m)
0.3	220.0	63.40	63.01
0.5	230.0	66.48	66.13
1.0	270.0	78.73	78.59
2.0	190.0	54.22	53.67
3.0	132.0	36.45	35.61
4.0	120.0	32.78	31.87
5.0	50.0	11.33	10.07
6.0	32.0	5.81	4.46
7.0	32.0	5.81	4.46
8.0	-	-	-
9.0	-	-	-
10.0	-	-	-
11.0	-	-	-
12.0	-	-	-

July Survey[2]

Depth (m)	SFHRM 19.0 Fluor (no units)	SFHRM 19.0 Chl a (mg/m)	SFHRM 19.0 Cchl a (mg/m)	SFHRM 22.4 Fluor (no units)	SFHRM 22.4 Chl a (mg/m)	SFHRM 22.4 Cchl a (mg/m)
0.3	10.3	9.01	7.12	10.0	8.80	6.92
0.5	12.0	10.22	8.27	11.0	9.51	7.60
1.0	14.0	11.64	9.63	14.0	11.64	9.63
2.0	15.5	12.70	10.64	15.0	12.34	10.30
3.0	16.0	13.05	10.98	16.5	13.41	11.32
4.0	15.0	12.34	10.30	16.9	13.69	11.59
5.0	16.5	13.41	11.32	13.2	11.07	9.09
6.0	14.8	12.20	10.17	12.0	10.22	8.27
7.0	17.1	13.83	11.73	10.5	9.16	7.26
8.0	11.5	9.86	7.94	10.5	9.16	7.26
9.0	8.0	7.38	5.57	10.0	8.80	6.92
10.0	8.0	7.38	5.57	7.2	6.82	5.03
11.0	6.9	6.60	4.82	7.0	6.68	4.89
12.0	6.1	6.04	4.28	7.0	6.68	4.89

Depth (m)	SFHRM 25.0 Fluor (no units)	SFHRM 25.0 Chl a (mg/m)	SFHRM 25.0 Cchl a (mg/m)	SFHRM 26.2 Fluor (no units)	SFHRM 26.2 Chl a (mg/m)	SFHRM 26.2 Cchl a (mg/m)
0.3	9.0	8.09	6.24	14.5	11.99	9.97
0.5	13.0	10.93	8.95	14.5	11.99	9.97
1.0	16.0	13.05	10.98	16.0	13.05	10.98
2.0	24.5	19.08	16.73	20.5	16.24	14.03
3.0	23.5	18.37	16.06	21.0	16.60	14.36
4.0	19.0	15.18	13.01	17.8	14.33	12.20
5.0	11.0	9.51	7.60	12.5	10.57	8.61
6.0	9.0	8.09	6.24	9.0	8.09	6.24
7.0	7.5	7.03	5.23	7.5	7.03	5.23
8.0	7.0	6.68	4.89	7.5	7.03	5.23
9.0	6.5	6.32	4.55	7.0	6.68	4.89
10.0	6.5	6.32	4.55	7.0	6.68	4.89
11.0	7.0	6.68	4.89	7.5	7.03	5.23
12.0	6.5	6.32	4.55	-	-	-

July Survey[2]

Depth (m)	SFHRM 28.3 Fluor (no units)	SFHRM 28.3 Chl a (mg/m)	SFHRM 28.3 Cchl a (mg/m)	SFHRM 30.8 Fluor (no units)	SFHRM 30.8 Chl a (mg/m)	SFHRM 30.8 Cchl a (mg/m)
0.3	13.0	10.93	8.95	16.0	13.05	10.98
0.5	17.5	14.12	12.00	16.0	13.05	10.98
1.0	21.0	16.60	14.36	18.0	14.47	12.33
2.0	25.0	19.43	17.07	24.5	19.08	16.73
3.0	23.0	18.01	15.72	21.0	16.60	14.36
4.0	18.0	14.47	12.33	16.0	13.05	10.98
5.0	10.0	8.80	6.92	12.0	10.22	8.27
6.0	9.0	8.09	6.24	12.5	10.57	8.61
7.0	9.0	8.09	6.24	12.0	10.22	8.27
8.0	9.0	8.09	6.24	7.0	6.68	4.89
9.0	9.0	8.09	6.24	7.0	6.68	4.89
10.0	11.0	9.51	7.60	7.0	6.68	4.89
11.0	11.0	9.51	7.60	-	-	-
12.0	11.0	9.51	7.60	-	-	-

Depth (m)	WRM 2.0 Fluor (no units)	WRM 2.0 Chl a (mg/m)	WRM 2.0 Cchl a (mg/m)	WRM 3.0 Fluor (no units)	WRM 3.0 Chl a (mg/m)	WRM 3.0 Cchl a (mg/m)
0.3	15.5	12.70	10.64	16.0	13.05	10.98
0.5	16.0	13.05	10.98	18.5	14.83	12.67
1.0	17.0	13.76	11.66	20.0	15.89	13.69
2.0	18.5	14.83	12.67	28.0	21.56	19.10
3.0	17.5	14.12	12.00	28.0	21.56	19.10
4.0	18.0	14.47	12.33	17.0	13.76	11.66
5.0	19.0	15.18	13.01	9.0	8.09	6.24
6.0	9.5	8.45	6.58	6.3	6.18	4.42
7.0	7.8	7.24	5.43	6.1	6.04	4.28
8.0	7.0	6.68	4.89	7.3	6.89	5.09
9.0	6.5	6.32	4.55	6.9	6.60	4.82
10.0	5.6	5.68	3.94	7.3	6.89	5.09
11.0	5.2	5.40	3.67	7.4	6.96	5.16
12.0	-	-	-	7.2	6.82	5.03

July Survey[2]

Depth (m)	WRM 6.0 Fluor (no units)	WRM 6.0 Chl a (mg/m)	WRM 6.0 Cchl a (mg/m)	WRM 8.4 Fluor (no units)	WRM 8.4 Chl a (mg/m)	WRM 8.4 Cchl a (mg/m)
0.3	22.0	17.31	15.04	27.0	20.85	18.42
0.5	24.0	18.72	16.39	33.0	25.10	22.48
1.0	30.0	22.97	20.45	38.0	28.64	25.87
2.0	36.0	27.23	24.51	42.0	31.48	28.57
3.0	17.0	13.76	11.66	13.0	10.93	8.95
4.0	10.5	9.16	7.26	10.0	8.80	6.92
5.0	6.2	6.11	4.35	9.5	8.45	6.58
6.0	7.4	6.96	5.16	9.5	8.45	6.58
7.0	8.2	7.53	5.70	10.5	9.16	7.26
8.0	8.0	7.38	5.57	10.5	9.16	7.26
9.0	6.8	6.53	4.76	10.5	9.16	7.26
10.0	6.4	6.25	4.49	11.0	9.51	7.60
11.0	6.8	6.53	4.76	-	-	-
12.0	6.9	6.60	4.82	-	-	-

Depth (m)	WRM 10.95 Fluor (no units)	WRM 10.95 Chl a (mg/m)	WRM 10.95 Cchl a (mg/m)
0.3	42.0	31.48	28.57
0.5	42.0	31.48	28.57
1.0	46.0	34.31	31.28
2.0	46.0	34.31	31.28
3.0	24.0	18.72	16.39
4.0	24.0	18.72	16.39
5.0	13.0	10.93	8.95
6.0	9.5	8.45	6.58
7.0	7.5	7.03	5.23
8.0	7.5	7.03	5.23
9.0	7.5	7.03	5.23
10.0	9.0	8.09	8.09
11.0	-	-	-
12.0	-	-	-

August Survey[2]

Depth (m)	SFHRM 19.0 Fluor (no units)	Chl a (mg/m)	Cchl a (mg/m)	SFHRM 22.4 Fluor (no units)	Chl a (mg/m)	Cchl a (mg/m)
0.3	11.5	11.12	11.04	9.0	7.90	7.76
0.5	11.5	11.12	11.04	10.5	9.83	9.73
1.0	11.5	11.12	11.04	12.0	11.76	11.69
2.0	11.8	11.50	11.43	14.2	14.59	14.58
3.0	12.0	11.76	11.69	15.0	15.62	15.63
4.0	15.0	15.62	15.63	16.0	16.91	16.94
5.0	15.0	15.62	15.63	14.0	14.33	14.31
6.0	13.0	13.05	13.00	13.5	13.69	13.66
7.0	11.5	11.12	11.04	9.0	7.90	7.76
8.0	8.0	6.62	6.45	6.6	4.82	4.61
9.0	5.3	3.15	2.91	6.4	4.56	4.35
10.0	4.7	2.37	2.12	5.9	3.92	3.69
11.0	3.5	0.83	0.55	5.4	3.27	3.04
12.0	3.2	0.45	0.16	5.0	1.47	1.20

Depth (m)	SFHRM 25.0 Fluor (no units)	Chl a (mg/m)	Cchl a (mg/m)	SFHRM 26.2 Fluor (no units)	Chl a (mg/m)	Cchl a (mg/m)
0.3	11.5	11.12	11.04	10.2	9.45	9.33
0.5	10.6	9.96	9.86	9.5	8.55	8.41
1.0	14.0	14.33	14.31	11.5	11.12	11.04
2.0	16.0	16.91	16.94	15.0	15.62	15.63
3.0	19.0	20.76	20.87	16.2	17.16	17.20
4.0	17.8	19.22	19.30	15.0	15.62	15.63
5.0	15.5	16.26	16.28	11.0	10.48	10.38
6.0	12.2	12.02	11.95	11.2	10.73	10.64
7.0	8.5	7.26	7.10	9.0	7.90	7.76
8.0	7.0	5.33	5.14	7.2	5.59	5.40
9.0	6.1	4.17	3.96	6.0	4.05	3.83
10.0	5.6	3.53	3.30	4.3	1.86	1.60
11.0	4.3	1.86	1.60	4.1	1.60	1.34
12.0	4.4	1.99	1.73	4.0	1.47	1.20

August Survey[2]

Depth (m)	SFHRM 28.3 Fluor (no units)	Chl a (mg/m)	Cchl a (mg/m)	SFHRM 30.8 Fluor (no units)	Chl a (mg/m)	Cchl a (mg/m)
0.3	12.0	11.76	11.69	12.5	12.41	12.35
0.5	12.0	11.76	11.69	14.0	14.33	14.31
1.0	14.0	14.33	14.31	15.0	15.62	15.63
2.0	19.2	21.02	21.13	17.0	18.19	18.25
3.0	19.2	21.02	21.13	15.5	16.26	16.28
4.0	9.2	8.16	8.02	10.0	9.19	9.07
5.0	7.5	5.98	5.79	8.3	7.00	6.84
6.0	6.4	4.56	4.35	8.3	7.00	6.84
7.0	5.7	3.66	3.43	8.0	6.62	6.45
8.0	5.5	3.40	3.17	5.5	3.40	3.17
9.0	4.9	2.63	2.38	6.4	4.56	4.35
10.0	4.9	2.63	2.38	6.6	4.82	4.61
11.0	6.3	4.43	4.22	-	-	-
12.0	7.8	6.36	6.19	-	-	-

Depth (m)	SFHRM 32.4 Fluor (no units)	Chl a (mg/m)	Cchl a (mg/m)
0.3	12.0	11.76	11.69
0.5	12.5	12.41	12.35
1.0	13.8	14.08	14.05
2.0	15.8	16.65	16.67
3.0	16.4	17.42	17.46
4.0	13.0	13.05	13.00
5.0	10.2	9.45	9.33
6.0	5.8	3.79	3.56
7.0	6.2	4.30	4.09
8.0	-	-	-
9.0	-	-	-
10.0	-	-	-
11.0	-	-	-
12.0	-	-	-

August Survey[2]

Depth (m)	SFHRM 34.4 Fluor (no units)	SFHRM 34.4 Chl a (mg/m)	SFHRM 34.4 Cchl a (mg/m)	WRM 2.0 Fluor (no units)	WRM 2.0 Chl a (mg/m)	WRM 2.0 Cchl a (mg/m)
0.3	12.0	11.76	11.69	15.0	15.62	15.63
0.5	10.0	9.19	9.07	15.8	16.65	16.67
1.0	12.5	12.41	12.35	16.9	18.06	18.12
2.0	9.0	7.90	7.76	17.5	18.84	18.90
3.0	4.0	1.47	1.20	20.2	22.31	22.44
4.0	4.6	2.25	1.99	13.0	13.05	13.00
5.0	-	-	-	9.0	7.90	7.76
6.0	-	-	-	6.0	4.05	3.83
7.0	-	-	-	5.3	3.15	2.91
8.0	-	-	-	4.9	2.63	2.38
9.0	-	-	-	4.6	2.25	1.99
10.0	-	-	-	4.6	2.25	1.99
11.0	-	-	-	4.6	2.25	1.99
12.0	-	-	-	4.5	2.12	1.86

Depth (m)	WRM 3.0 Fluor (no units)	WRM 3.0 Chl a (mg/m)	WRM 3.0 Cchl a (mg/m)	WRM 6.0 Fluor (no units)	WRM 6.0 Chl a (mg/m)	WRM 6.0 Cchl a (mg/m)
0.3	10.0	9.19	9.07	16.5	17.55	17.59
0.5	10.5	9.83	9.73	19.2	21.02	21.13
1.0	15.1	15.75	15.76	20.0	22.05	22.18
2.0	20.0	22.05	22.18	20.0	22.05	22.18
3.0	25.5	29.12	29.39	18.8	20.51	20.61
4.0	16.5	17.55	17.59	10.8	10.22	10.12
5.0	8.1	6.75	6.58	8.0	6.62	6.45
6.0	6.8	5.07	4.87	6.5	4.69	4.48
7.0	5.6	3.53	3.30	6.5	4.69	4.48
8.0	5.5	3.40	3.17	6.5	4.69	4.48
9.0	5.5	3.40	3.17	7.0	5.33	5.14
10.0	5.6	3.53	3.30	7.1	5.46	5.27
11.0	5.8	3.79	3.56	7.4	5.85	5.66
12.0	6.4	4.56	4.35	7.4	5.85	5.66

August Survey[2]

Depth (m)	WRM 8.4 Fluor (no units)	WRM 8.4 Chl a (mg/m)	WRM 8.4 Cchl a (mg/m)	WRM 10.95 Fluor (no units)	WRM 10.95 Chl a (mg/m)	WRM 10.95 Cchl a (mg/m)
0.3	18.9	20.64	20.74	57.0	69.63	70.69
0.5	19.2	21.02	21.13	59.0	72.20	73.31
1.0	19.0	20.76	20.87	19.5	21.41	21.52
2.0	17.0	18.19	18.25	16.8	17.93	17.98
3.0	17.0	18.19	18.25	10.8	10.22	10.12
4.0	12.3	12.15	12.09	6.3	4.43	4.22
5.0	10.0	9.19	9.07	5.4	3.27	3.04
6.0	9.2	8.16	8.02	5.2	3.02	2.78
7.0	9.2	8.16	8.02	5.6	3.53	3.30
8.0	10.0	9.19	9.07	5.9	3.92	3.69
9.0	8.4	7.13	6.97	-	-	-
10.0	7.4	5.85	5.66	-	-	-
11.0	7.4	5.85	5.66	-	-	-
12.0	-	-	-	-	-	-

Depth (m)	WRM 13.0 Fluor (no units)	WRM 13.0 Chl a (mg/m)	WRM 13.0 Cchl a (mg/m)
0.3	16.0	16.91	16.94
0.5	16.5	17.55	17.59
1.0	15.7	16.52	16.54
2.0	7.0	5.33	5.14
3.0	4.0	1.47	1.20
4.0	4.4	1.99	1.73
5.0	4.6	2.25	1.99
6.0	-	-	-
7.0	-	-	-
8.0	-	-	-
9.0	-	-	-
10.0	-	-	-
11.0	-	-	-
12.0	-	-	-

[1]See Table 5 for the linear equations used for chlorophyll predictions.

[2]For specific dates and times in which fluorescence values were obtained, see Appendix 3, Part 2, chlorophyll results.

APPENDIX IV

FIELD TRANSMISSIVITY AND TURBIDITY DATA

BOONE RESERVOIR

% Light Transmittance and Turbidity Results--July and August Surveys

Station	Date	% Horiz	Time (EDT)	Depth (m)	% Light Trans. (%T)	TURBIDITY Field (NTU)	TURBIDITY Lab (NTU)
SFHRM 19.0	7/19/84	50	1016	0.3	46	1.6	-
				1.0	44	1.7	-
				2.0	42	1.8	-
				3.0	42	1.8	2.3[1]
				4.0	42	1.8	-
				5.0	43	1.8	-
				6.0	46	1.5	1.4
				7.0	48	1.6	-
				8.0	51	1.3	-
				9.0	57	1.3	-
				10.0	60	1.2	-
				11.0	62	1.2	-
				12.0	62	1.2	1.2
				15.0	56	1.6	-
				18.0	52	2.0	1.4
				21.0	46	2.6	-
				24.0	44	2.8	-
				27.0	34	4.2	-
				30.0	22	5.8	3.9
				33.0	9	8.4	-
	8/21/84	50	0950	0.3	48	-	-
				1.0	48	-	-
				2.0	49	-	-
				3.0	49	1.2	1.4[1]
				4.0	47	1.6	-

Station	Date	% Horiz	Time (EDT)	Depth (m)	% Light Trans. (%T)	TURBIDITY Field (NTU)	TURBIDITY Lab (NTU)
SFHRM 19.0	8/21/84	50	0950	5.0	49	1.5	-
				6.0	51	1.4	1.4
				7.0	53	1.3	-
				8.0	55	1.3	-
				9.0	61	1.2	-
				10.0	69	1.0	-
				11.0	70	1.0	-
				12.0	69	1.1	0.43
				15.0	65	1.4	-
				18.0	61	1.7	1.5
				21.0	50	2.0	-
				24.0	48	2.2	-
				27.0	41	3.2	-
				30.0	30	4.4	3.5
				33.0	16	8.2	-
SFHRM 22.4	7/19/84	75	1110	0.3	41	2.3	-
				1.0	40	2.3	-
				2.0	38	2.3	-
				3.0	38	2.3	2.8[1]
				4.0	37	2.2	-
				5.0	41	2.1	-
				6.0	50	1.8	1.4
				7.0	51	1.8	-
				8.0	52	1.9	-
				9.0	53	1.8	-

Station	Date	% Horiz	Time (EDT)	Depth (m)	% Light Trans. (%T)	TURBIDITY Field (NTU)	TURBIDITY Lab (NTU)
SFHRM 22.4	7/19/84	75	1110	10.0	59	1.7	-
				11.0	55	2.0	-
				12.0	51	2.4	1.8
				15.0	51	2.5	-
				18.0	48	2.7	2.1
				21.0	45	3.7	-
				24.0	38	3.9	-
				27.0	18	6.2	-
				30.0	8	12.0	-
	8/21/84	75	1049	0.3	44	-	-
				0.5	44	-	-
				1.0	45	-	-
				2.0	43	2.0	-
				3.0	43	2.0	2.1[1]
				4.0	43	2.0	-
				5.0	44	2.0	-
				6.0	48	1.7	1.6
				7.0	53	1.5	-
				8.0	60	1.4	-
				9.0	60	1.4	-
				10.0	62	1.3	-
				11.0	65	1.2	-
				12.0	70	1.1	0.4
				15.0	54	1.9	-
				18.0	51	2.2	1.2
				21.0	48	2.6	-
				24.0	38	3.9	-
				26.0	6	12.0	-

Station	Date	% Horiz	Time (EDT)	Depth (m)	% Light Trans. (%T)	TURBIDITY Field (NTU)	TURBIDITY Lab (NTU)
SFHRM 25.0	7/19/84	25	1441	0.5	30	6.0	-
				1.0	31	4.0	-
				2.0	32	3.0	-
				3.0	29	3.2	-
				4.0	30	3.4	-
				5.0	35	3.2	-
				6.0	40	3.2	-
				7.0	45	3.0	-
				8.0	48	3.0	-
				9.0	49	2.8	-
				10.0	50	2.8	-
				11.0	48	3.1	-
				12.0	31	3.6	-
				15.0	34	5.0	-
				18.0	18	6.8	-
				21.0	12	10.0	-
	8/21/84	25	1439	0.3	40	-	-
				0.5	40	-	-
				1.0	40	-	-
				2.0	39	2.1	-
				3.0	38	2.3	-
				4.0	40	2.2	-
				5.0	42	2.0	-
				6.0	47	1.8	-
				7.0	50	1.7	-
				8.0	58	1.5	-
				9.0	62	1.5	-
				10.0	69	1.0	-
				11.0	71	1.1	-
				12.0	64	1.4	-
				15.0	49	2.5	-

Station	Date	% Horiz	Time (EDT)	Depth (m)	% Light Trans. (%T)	TURBIDITY Field (NTU)	TURBIDITY Lab (NTU)
SFHRM 26.2	7/19/84	25	1208	0.3	33	2.6	-
				1.0	34	2.7	-
				2.0	31	2.8	-
				3.0	31	2.8	3.3
				4.0	35	2.8	-
				5.0	37	2.8	-
				6.0	46	2.6	1.9
				7.0	49	2.5	-
				8.0	51	2.4	-
				9.0	50	2.5	-
				10.0	47	2.8	-
				11.0	43	3.4	-
				12.0	33	4.0	3.3
				15.0	22	6.6	-
				18.0	8	10.0	-
				21.0	2	18.0	6.2
				23.0	0.05	30.0	-
	8/21/84	25	1152	0.3	43	-	-
				0.5	44	-	-
				1.0	44	-	-
				2.0	41	-	-
				3.0	39	2.3	1.9[1]
				4.0	41	2.1	-
				5.0	44	2.0	-
				6.0	48	1.8	1.6
				7.0	52	1.6	-
				8.0	56	1.6	-
				9.0	61	1.4	-

Station	Date	% Horiz	Time (EDT)	Depth (m)	% Light Trans. (%T)	TURBIDITY Field (NTU)	TURBIDITY Lab (NTU)
SFHRM 26.2	8/21/84	25	1152	10.0	66	1.2	-
				11.0	70	1.2	-
				12.0	67	1.4	0.7
				15.0	64	1.5	-
				18.0	31	3.9	1.1
				21.0	1.2	18.0	-
SFHRM 28.3	7/19/84	60	1415	0.5	28	3.2	-
				1.0	26	3.8	-
				2.0	22	4.0	-
				3.0	23	4.0	-
				4.0	33	3.6	-
				5.0	38	3.2	-
				6.0	40	3.3	-
				7.0	40	3.7	-
				8.0	40	3.8	-
				9.0	34	4.6	-
				10.0	27	5.3	-
				11.0	21	6.6	-
				12.0	20	7.2	-
				15.0	6	12.0	-
	8/21/84	60	1411	0.3	42	-	-
				0.5	41	-	-
				1.0	39	-	-
				2.0	36	-	-
				3.0	36	2.3	-
				4.0	43	2.1	-
				5.0	49	2.1	-

Station	Date	% Horiz	Time (EDT)	Depth (m)	% Light Trans. (%T)	TURBIDITY Field (NTU)	TURBIDITY Lab (NTU)
SFHRM 28.3	8/21/84	60	1411	6.0	48	2.4	-
				7.0	49	2.4	-
				8.0	50	2.3	-
				9.0	53	2.0	-
				10.0	44	3.3	-
				11.0	28	4.6	-
				12.0	15	7.5	-
				15.0	0.39	23.0	-
SFHRM 30.8	7/19/84	25	1300	0.3	28	3.8	-
				1.0	26	4.0	-
				2.0	25	4.2	-
				3.0	27	4.2	3.9[1]
				4.0	28	4.6	-
				5.0	27	4.6	-
				6.0	23	5.6	7.2
				7.0	26	5.5	-
				8.0	29	5.4	-
				9.0	28	6.0	-
				10.0	28	7.8	16.0
	8/21/84	25	1226	0.3	34	-	-
				0.5	33	-	-
				1.0	33	2.9	-
				2.0	33	2.9	-
				3.0	36	2.8	2.2[1]
				4.0	44	2.5	-
				5.0	45	2.9	-
				6.0	31	4.1	2.4
				7.0	28	4.4	-
				8.0	29	4.5	-
				9.0	28	6.0	7.2

Station	Date	% Horiz	Time (EDT)	Depth (m)	% Light Trans. (%T)	TURBIDITY Field (NTU)	TURBIDITY Lab (NTU)
WRM 2.0	7/20/84	50	0945	0.3	44	2.2	-
				0.5	41	1.7	-
				1.0	40	1.8	-
				2.0	40	1.8	-
				3.0	40	2.0	3.4[1]
				4.0	38	2.2	-
				5.0	44	2.2	-
				6.0	45	2.2	2.2
				7.0	50	2.2	-
				8.0	50	2.0	-
				9.0	56	1.7	-
				10.0	60	1.8	-
				11.0	62	2.0	-
				12.0	60	2.4	0.93
				15.0	52	3.4	-
				18.0	42	2.6	2.2
				21.0	25	3.8	-
				24.0	20	5.8	-
	8/23/84	50	0906	0.3	42	-	-
				0.5	41	-	-
				1.0	41	-	-
				2.0	41	-	-
				3.0	39	2.2	1.3[1]
				4.0	39	2.1	-
				5.0	49	1.8	-
				6.0	55	1.6	0.61
				7.0	60	1.5	-
				8.0	61	1.5	-
				9.0	54	2.0	-

Station	Date	% Horiz	Time (EDT)	Depth (m)	% Light Trans. (%T)	TURBIDITY Field (NTU)	TURBIDITY Lab (NTU)
WRM 2.0	8/23/84	50	0945	10.0	49	2.4	-
				11.0	46	2.7	-
				12.0	45	2.8	1.3
				15.0	42	3.4	-
				18.0	39	3.8	2.8
				21.0	28	5.2	-
				24.0	15	7.8	-
				25.0	13	7.9	-
WRM 3.0	7/20/84	25	1422	0.3	-	-	-
				0.5	36	1.2	-
				1.0	34	2.5	-
				2.0	30	2.4	-
				3.0	31	2.4	-
				4.0	34	2.4	-
				5.0	42	2.4	-
				6.0	42	2.6	-
				7.0	45	2.8	-
				8.0	45	2.7	-
				9.0	50	2.6	-
				10.0	55	2.0	-
				11.0	60	1.8	-
				12.0	60	1.8	-
				15.0	54	1.8	-
				18.0	48	2.4	-
				21.0	30	4.2	-
				24.0	22	6.4	-

Station	Date	% Horiz	Time (EDT)	Depth (m)	% Light Trans. (%T)	TURBIDITY Field (NTU)	TURBIDITY Lab (NTU)
WRM 3.0	8/23/84	25	1257	0.3	34	-	-
				0.5	33	-	-
				1.0	33	-	-
				2.0	31	-	-
				3.0	30	2.3	-
				4.0	38	2.0	-
				5.0	50	1.8	-
				6.0	54	1.8	-
				7.0	54	2.0	-
				8.0	51	2.4	-
				9.0	49	2.6	-
				10.0	46	2.8	-
				11.0	43	3.2	-
				12.0	41	3.2	-
				15.0	42	3.5	-
				18.0	42	3.5	-
				21.0	25	5.9	-
				24.0	10	10.0	-
				27.0	1.7	16.0	-
				28.0	1.0	19.0	-
WRM 6.0	7/20/84	50		0.5	30	2.6	-
				1.0	26	2.8	-
				2.0	24	2.9	-
				3.0	35	2.9	4.2[1]
				4.0	35	3.4	-
				5.0	30	3.8	-
				6.0	26	6.1	8.4
				7.0	8	11.0	-
				8.0	7	12.0	11.0
				9.0	18	8.0	-

Station	Date	% Horiz	Time (EDT)	Depth (m)	% Light Trans. (%T)	TURBIDITY Field (NTU)	TURBIDITY Lab (NTU)
WRM 6.0	7/20/84	50		10.0	22	5.8	-
				11.0	26	5.4	-
				12.0	30	5.0	7.4
				15.0	22	6.0	-
				18.0	8	10.0	12.0
				21.0	4	14.0	-
	8/23/84	50	1000	0.3	31	-	-
				0.5	32	-	-
				1.0	32	2.7	-
				2.0	31	2.8	-
				3.0	32	2.7	1.0[1]
				4.0	39	2.5	-
				5.0	45	2.2	-
				6.0	48	2.3	0.79
				7.0	43	2.8	-
				8.0	41	2.9	-
				9.0	35	3.4	-
				10.0	20	5.8	-
				11.0	16	6.8	-
				12.0	14	7.8	4.8
				15.0	8	10.0	-
				18.0	8	10.0	9.8
				21.0	6	12.0	-
WRM 8.4	7/20/84	25	1300	0.5	25	2.7	-
				1.0	19	3.3	-
				2.0	19	3.2	-
				3.0	24	3.0	-
				4.0	25	4.3	-
				5.0	6.1	8.9	-

Station	Date	% Horiz	Time (EDT)	Depth (m)	% Light Trans. (%T)	TURBIDITY Field (NTU)	TURBIDITY Lab (NTU)
WRM 8.4	7/20/84	25	1300	6.0	1.7	20.0	-
				7.0	0.31	23.0	-
				8.0	0.26	26.0	-
				9.0	0.12	29.0	-
				10.0	0.11	30.0	-
	8/23/84	25	1230	0.3	30.0	-	-
				0.5	30.0	-	-
				1.0	30.0	-	-
				2.0	32.0	2.6	-
				3.0	34.0	2.4	-
				4.0	40.0	2.5	-
				5.0	36.0	3.3	-
				6.0	32.0	3.8	-
				7.0	30.0	4.2	-
				8.0	27.0	4.8	-
				9.0	20.0	6.6	-
				10.0	15.0	10.0	-
				11.0	10.0	13.0	-
				12.0	7.0	15.0	-
WRM 10.95	7/20/84	95	1140	0.3	16.0	-	-
				0.5	16.0	3.3	-
				1.0	16.0	3.2	-
				2.0	16.0	3.4	-
				3.0	16.0	3.6	5.5[1]
				4.0	0.6	110.0	-
				5.0	0.24	140.0	-
				6.0	0.22	-	18.0
				7.0	0.11	180.0	-
				8.0	0.06	330.0	-

Station	Date	% Horiz	Time (EDT)	Depth (m)	% Light Trans. (%T)	TURBIDITY Field (NTU)	TURBIDITY Lab (NTU)
WRM 10.95	8/23/84	95	1104	0.3	28	-	-
				0.5	27	3.2	-
				1.0	27	3.2	-
				2.0	25	4.2	-
				3.0	26	4.2	1.5[1]
				4.0	32	4.7	-
				5.0	35	4.5	-
				6.0	38	4.6	2.4
				7.0	35	5.4	-
				8.0	28	6.2	-
				9.0	26	6.8	-
WRM 13.0	7/20/84	50	1234	0.5	12	4.4	-
				1.0	11	4.5	-
				2.0	11	4.7	-
				3.0	13	8.4	-
				4.0	6.7	12.0	-
				5.0	4.8	17.0	-
	8/23/84	50	1154	0.3	24	-	-
				0.5	22	-	-
				1.0	23	-	-
				2.0	38	4.0	-
				3.0	43	4.2	-
				4.0	43	3.9	-
				5.0	43	4.0	-

[1]Turbidity value of surface to 3-meter depth integrated sample.

VITA

David Michael Carden was born July 9, 1957, in Oak Ridge, Tennessee. He attended elementary and junior high school in Cleveland, Tennessee and Greenville, Kentucky and high school in Jackson, Tennessee. Immediately following high school graduation in May 1975, he entered Jackson State Community College in Jackson, Tennessee and in fall 1977 transferred to The University of Tennessee, Knoxville. In June 1979, he received a Bachelor of Science degree in Civil Engineering from The University of Tennessee, Knoxville.

In July 1979, he was employed as a civil engineer at Duke Power Company, an electric utility located in Charlotte, North Carolina. After one year of service with Duke Power Company, he began work as an environmental engineer with the Tennessee Valley Authority in Knoxville, Tennessee, where he is presently employed. In September 1980, he was enrolled at The Graduate School of The University of Tennessee, Knoxville where he is currently pursuing a Master of Science degree with a major in Environmental Engineering.

The author is a member of Chi Epsilon and Tau Beta Pi engineering honor societies, the Water Pollution Control Federation, and the American Society of Civil Engineers.